R-06-52

Near-surface hydrogeological model of Forsmark

Open repository and solute transport applications – Forsmark 1.2

Emma Bosson, Sten Berglund
Svensk Kärnbränslehantering AB

December 2006

Svensk Kärnbränslehantering AB
Swedish Nuclear Fuel
and Waste Management Co
Box 5864
SE-102 40 Stockholm Sweden
Tel 08-459 84 00
+46 8 459 84 00
Fax 08-661 57 19
+46 8 661 57 19

ISSN 1402-3091
SKB Rapport R-06-52

Near-surface hydrogeological model of Forsmark

Open repository and solute transport applications – Forsmark 1.2

Emma Bosson, Sten Berglund
Svensk Kärnbränslehantering AB

December 2006

Summary

The Swedish Nuclear Fuel and Waste Management Company (SKB) is currently performing site investigations at two potential sites for a final repository for spent nuclear fuel. This report presents results of water flow and solute transport modelling of the Forsmark site. The modelling reported in this document focused on the near-surface groundwater, i.e. groundwater in Quaternary deposits (QD) and shallow rock, and surface water systems, and was performed using the MIKE SHE tool. The site data providing the basis for the modelling were delivered in the Forsmark 1.2 dataset (data freeze in July, 2004).

The modelling presented in this report involved an update and analysis of the basic flow model for the present, "undisturbed" conditions. In addition, specific flow and transport modelling activities were performed to test model capabilities and provide results for use in connection with Safety Assessment (SA), i.e. the SR-Can assessment, and Environmental Impact Assessment (EIA). The present work can be subdivided into the following four parts:

1. Update of the numerical flow model (with the previous model presented in the Forsmark 1.2 site description as the starting point).
2. Hydrological analysis of present-day, "undisturbed" conditions.
3. Analysis of the hydrological effects of an open repository.
4. Analysis of solute transport from sources at large depth in the rock.

During the construction and operation of the repository, there will be atmospheric pressure in the open tunnels and shafts in the repository, including the access tunnel from ground surface. This will cause disturbances in the pressure field around the subsurface constructions, and inflow of groundwater. The size of this inflow and its possible effects on surrounding groundwater and surface water systems need to be quantified. The modelling of flow under open repository conditions produces results to be used within both SA and EIA.

Modelling of radionuclide transport from the repository is an important part of the analyses performed in support of SA. In the actual safety assessment calculations, the transport modelling is usually focused on the transport through the rock, whereas the transport in the uppermost part of the system is handled in a simplified manner. However, such model simplifications must be supported, possibly by modelling, and methods and tools useful for performing this kind of modelling must be studied.

In addition to an extension of the model area, the main updates relative to the previous near-surface hydrogeology and surface hydrology model of Forsmark concerned the hydraulic properties of the QD and the bedrock, and the meteorological input data. The annual precipitation in the updated model, based on locally measured meteorological data from 2003–2004, is 597 mm, which is 77 mm less than that reported in the Forsmark 1.2 site description. This resulted in a significant decrease in the calculated runoff; the average annual runoff was calculated to 144 mm (4.6 $Ls^{-1} km^{-2}$) in the present model.

A sensitivity analysis was performed with the main objective of investigating the sensitivity to the vertical extent of the model and the hydraulic properties of the QD. The first part, the investigation of the sensitivity to the vertical extent, showed no large differences in the modelling results if the model was extended to 450 m below sea level, instead of 135 m below sea level as in the base case. Similarly, no large effects were obtained when the bottom boundary condition was changed at these depths, from a head boundary condition to a no-flow boundary condition. This can probably be explained by the very low hydraulic conductivities of the bedrock at these depths. Conversely, the modelling results were highly sensitive to a decrease in the vertical extent of the model. When the bottom boundary was set at 20 m below sea level almost all precipitation left the model volume as surface runoff (i.e. very small groundwater recharge).

For the sensitivity cases testing the hydraulic properties of the QD, a comparison of the results for topographic high and low points showed that the largest absolute differences between the sensitivity cases were obtained for the topographic high, which also showed the largest temporal variations. Among the parameters tested, the model was found to be most sensitive to changes in the horizontal hydraulic conductivity. The overall water balance was not affected by the tested variations in the hydraulic parameters of the QD.

It was concluded that the changes in the overall water balance (relative to the Forsmark 1.2 site descriptive model) could be explained by changes in the meteorological data. However, there were also large changes in the distribution of the total evapotranspiration upon its different components. Specifically, the transpiration has increased considerably, whereas the evaporation from ponded water decreased by almost the same amount. The calculated specific discharge from the catchments of the three largest lakes in the model area varied between 5.4 and 6.5 $Ls^{-1}km^{-2}$. The discharge in the studied water course was highly transient during the year, with several peaks and periods of zero or very low flow rates between the peaks.

A first comparison between calculated and measured hydraulic heads was performed as a part of the present work. The results for the nine monitoring wells included in the study showed that the mean differences between the results obtained with the present, uncalibrated model and the field data varied between 0.3 m and 1.4 m. In terms of mean differences, the model consistently overpredicted the measured heads. However, in three of the wells periods of alternating positive and negative deviations could be observed. Discharge data from measurements in the water courses were not available when the modelling presented in this report was performed. Such data will constitute the basis for the calibration of forthcoming hydrological-hydrogeological models; also the measured head data will be used in the calibration procedure.

The results of the open repository calculations showed that most of the inflow to the access ramp occurred in the upper c. 50 m of the ramp. Below 50 m below sea level only very small inflows were recorded, due to the low hydraulic conductivity of the bedrock. In this model, which was based on the Forsmark 1.2 site description, the upper parts of the ramp were not intersected by high-conductive fracture zones. This leads to a comparatively small calculated inflow also in this part of the ramp. The model-calculated inflow was found to be highly dependent on the hydraulic conductivity of the bedrock in the vicinity of the access ramp, which implies that the results may be different when an updated bedrock model is used in forthcoming modelling studies. The modelling also showed that the inflow to the shafts was insignificant compared to the inflow to the access ramp.

The calculated groundwater level drawdown and the size of its influence area (here defined as the area with drawdown ≥ 0.3 m) depended strongly on the extent of grouting. In a "worst case scenario" without grouting, the largest model-calculated drawdown of the groundwater level was 25 m, occurring above the access tunnel (which is shaped like a spiral that covers a certain horizontal area). Even in this (hypothetical) "worst case", the results did not indicate any effects on surface water levels or discharges. It was found that the repository had only a minor impact on the overall water balance of the land part of the model area. However, the impact was larger when considering that the effects would be concentrated to the influence area of the groundwater level drawdown. In the (hypothetical) "worst case" without grouting, the inflow to the ramp and shafts corresponded to a specific discharge of 400 mm within the (small) influence area.

Generally, the differences in the inflow and drawdown results from boundary case 1 (deep parts of repository not included) and boundary case 2 (those parts included) were small. Case 2 produced a somewhat smaller inflow, and a slightly larger influence area of the groundwater level drawdown. Boundary case 2 considered also the deep parts of the repository (i.e. parts located below the bottom boundary of the surface/near-surface model), by using a "disturbed" boundary condition obtained from a deep rock model that included the repository.

The solute transport modelling presented in this report included particle tracking (PT) and advection-dispersion (AD) simulations. In particular, the modelling was focused on solute transport from sources at depth, i.e. from a hypothetical solute release in a nuclear waste repository in the deep rock. All simulations were performed with solute injections at 135 m below sea level i.e. at a depth well below the thickest QD in the area but also some distance above repository depth. The main objectives of the transport modelling were to develop and illustrate model capabilities, and to provide the SR-Can safety assessment with supporting modelling results.

The PT results for an injection below the whole on-shore part of the model area showed that most particles had their exit points within the surface water catchment below which they were injected. This indicated that the horizontal transport distances were relatively small. However, a non-negligible fraction of the particles went from below land to discharge into the sea. The intake channel for water to the nuclear power plant received the largest fraction of the particles that went to the sea.

Also in the second type of PT simulation, where particles were injected along flow paths from the deep rock, particles appeared to be transported more or less vertically in the upper rock and the QD. The flow paths used to identify starting positions for the near-surface PT simulations were calculated in connection with the SR-Can safety assessment, using canister positions within the planned repository as injection points for particles in similar model calculations with a large-scale, deep rock groundwater flow model. Since most of the starting positions at 135 m below sea level extracted from the deep rock modelling results were located below the sea, the majority of the particles injected there in the near-surface model discharged into the sea. No major differences were observed when comparing the exit points calculated in the near-surface modelling with those obtained from the deep rock model.

AD simulations were performed for two different point source locations, one from which most of the injected solute mass went to the sea and the other with mass discharge mainly to the unsaturated zone on land. In both cases, a continuous, constant-concentration source was considered. The AD results emphasise the importance of the parameters describing the physical properties of the different calculation layers. Variability in porosity and hydraulic conductivity along and among the flow paths resulted in significant differences in the spreading patterns of the solutes. These differences concerned both advective transport and dilution, and the solute retardation associated with sorption. Furthermore, both the PT and the AD results clearly illustrate the importance of a proper selection of source locations (i.e. locations of individual sources or patterns of multiple sources) for the results to represent the transport problem of interest.

The last chapter of the report summarises the uncertainties and conclusions of the work. It is emphasised that the modelling is based on the version 1.2 dataset (with a data freeze in July, 2004), which implies that much more site data will be available for forthcoming model versions. Most importantly, longer time series of data from meteorological, hydrological and hydrogeological measurements, primarily the main meteorological parameters (precipitation and potential evapotranspiration) and water levels and surface water discharges, can be used in the next model version. This is important both for the comparison between model results and field data, and for the direct meteorological input to the model. Also the database of hydrogeological properties parameters has been improved by additional measurements, although to less extent than the time series dataset.

The general impression from the relatively crude evaluations performed so far is that reasonable results were obtained in the flow and transport simulations. However, much more work is required to analyse the agreement, or lack thereof, between model and reality, and, if necessary, improve the models. Consequently, the uncertainties related to the limited use of site data for testing and calibrating the flow model are judged to be the most important ones at the present stage of the Forsmark model development. Additional sensitivity studies and an efficient calibration methodology are important for improving this aspect of the modelling. Activities intended to provide these inputs have been initiated.

Sammanfattning

Svensk Kärnbränslehantering AB (SKB) genomför för närvarande platsundersökningar inom två potentiella områden för lokalisering av ett slutförvar för utbränt kärnbränsle. Denna rapport presenterar resultat av vattenflödes- och transportmodellering av Forsmarksområdet. Modelleringen som redovisas i denna rapport är fokuserad på det ytnära grundvattnet, dvs grundvattnet i jordlagren och i den övre delen av berget, och ytvattensystemet. Den genomfördes med modelleringsverktyget MIKE SHE. De platsdata som användes vid modelleringen ingick i datamängden Forsmark 1.2 (med s k datafrys i juli 2004).

De modelleringsaktiviteter som beskrivs här innefattar en uppdatering av den grundläggande modellen som beskriver vattenflöden under nuvarande ”ostörda” förhållanden. Dessutom genomfördes andra modelleringar för att testa specifika modelltillämpningar och för att förse Säkerhetsanalys (SA), särskilt den nyligen slutförda analysen SR-Can, och Miljökonsekvensbeskrivning (MKB) med beräkningsresultat. De genomförda modelleringsarbetena kan delas in i följande fyra delar:

1. Uppdatering av den numeriska flödesmodellen (med den föregående modellen i platsbeskrivningen Forsmark 1.2 som utgångspunkt).
2. Hydrologisk analys av flöden under nuvarande ”ostörda” förhållanden.
3. Analys av de hydrologiska effekterna av ett öppet förvar.
4. Analys av transport av lösta ämnen från källor i det djupa berget.

Under perioden av byggande och drift av slutförvaret kommer atmosfärstryck att råda i tunnlar och schakt i det öppna förvaret, inklusive tunneln mellan markytan och deponeringsområdet. Detta kommer att medföra förändringar i grundvattnets tryck runt undermarkskonstruktionerna och grundvatteninflöde till förvaret. Inläckagets storlek och effekterna på omgivande grund- och ytvattensystem behöver kvantifieras. Modelleringen av flöden under ”störda” förhållanden i och kring det öppna förvaret producerar resultat som används inom både SA och MKB.

Modelleringen av radionuklidtransport från förvaret är en väsentlig del av de analyser som görs till stöd för SA. Säkerhetsanalysens transportmodellering är vanligen fokuserad på transporten genom berget, medan transporten i den övre delen av systemet hanteras med förenklade metoder. Sådana förenklingar måste dock underbyggas, vilket möjligen innefattar modelleringar; metoder och verktyg för att genomföra sådana modelleringar måste därför undersökas.

Förutom att modellområdet utökats, utgörs de viktigaste uppdateringarna av modellen för ythydrologi och ytnära hydrogeologi i Forsmark jämfört med platsbeskrivning version 1.2 av förändringar i beskrivningarna av jordlagrens och bergets hydrauliska egenskaper och i meteorologiska indata. Den årliga nederbörden i den uppdaterade modellen, som bygger på lokala mätningar under 2003–2004, är 597 mm, vilket är 77 mm mindre än den som rapporterades i platsbeskrivning Forsmark 1.2. Detta resulterade i en avsevärd minskning av den beräknade avrinningen; den genomsnittliga specifika avrinningen för hela landdelen av modellområdet beräknades till 144 mm/år (ca 4.6 $Ls^{-1} km^{-2}$) i den uppdaterade modellen.

En känslighetsanalys genomfördes i syfte att undersöka känsligheten för modellens utsträckning i vertikalled och jordlagrens hydrauliska egenskaper. Undersökningen av känsligheten för modellens djupgående visade på små skillnader när bottenranden placerades på nivån 450 m under havet, istället 135 m under havet i basfallet. Inga större effekter kunde heller konstateras om randvillkoret på dessa djup förändrades från ett tryckrandvillkor till en tät rand. Detta beror antagligen på bergets mycket låga hydrauliska konduktiviteter på dessa djup. Modellresultaten var däremot mycket känsliga för en minskning av modellens vertikala utsträckning. När bottenranden placerades på nivån 20 m under havet lämnade nästan hela nederbörden modellvolymen i form av ytavrinning (endast mycket liten grundvattenbildning skedde).

I känslighetsfallen som testade jordlagrens hydrauliska egenskaper, visade en jämförelse av resultaten för punkter i höjdlägen och i låglänta områden att de största absoluta skillnaderna mellan känslighetsfallen uppkom i höjdlägena, vilka också uppvisade de största tidsmässiga variationerna. Av de parametrar som testades, befanns modellresultaten vara mest känsliga för ändringar i den horisontella hydrauliska konduktiviteten. Den övergripande vattenbalansen påverkades inte av de undersökta variationerna i jordlagrens hydrauliska egenskaper.

Det konstaterades att förändringarna i vattenbalansens huvudkomponenter (jämfört med platsbeskrivning Forsmark 1.2) kunde förklaras av förändringar i meteorologiska indata. Stora förändringar i evapotranspirationens fördelning på olika komponenter kunde emellertid också noteras. Transpirationen hade ökat avsevärt, samtidigt som avdunstningen från öppna vattenytor hade minskat ungefär lika mycket. Den beräknade specifika avrinningen inom avrinningsområdena för de tre största sjöarna i området varierade mellan 5.4 och 6.5 $Ls^{-1}km^{-2}$. Den beräknade avrinningen i det vattendrag som studerades uppvisade stora tidsmässiga variationer under året, varvid avrinningen var koncentrerad till ett antal flödestoppar med perioder av inget eller mycket litet flöde däremellan.

En första jämförelse mellan beräknade och uppmätta grundvattennivåer genomfördes i samband med det aktuella arbetet. Resultaten för de nio grundvattenrör som ingick i jämförelsen visade att medeldifferenserna (över hela mätperioden) mellan den okalibrerade modellen och resultaten från fältmätningarna varierade mellan 0,3 m och 1,4 m. I termer av medeldifferenser överskattade modellen konsekvent grundvattennivåerna. I tre av grundvattenrören kunde dock perioder av alternerande positiva och negativa differenser observeras.

Resultaten av beräkningarna med ett öppet förvar visade att större delen av inflödet till tillfartstunneln skedde i de översta ca 50 m av tunneln. Under nivån 50 m under havet noterades endast mycket små inflöden, vilket beror på bergets låga hydrauliska konduktivitet. I denna modell, som alltså baserades på version 1.2 av platsbeskrivningen av Forsmark, korsades tillfartstunnelns övre del inte av starkt vattenförande deformationszoner. Detta medförde att inflödet även i detta avsnitt av tunneln var relativt litet. Det beräknade inflödet befanns vara starkt beroende av bergets hydrauliska konduktivitet i närheten av tillfartstunneln, vilket innebär att resultaten kan komma att förändras när en uppdaterad bergmodell används i kommande modellversioner. Modelleringen visade också att schaktens inverkan var obetydlig jämfört med inflödet till tillfartstunneln.

Den beräknade avsänkningen av grundvattenytan och storleken på påverkansområdet (här definierat som området med avsänkning $\geq 0{,}3$ m) var starkt beroende av tätningsnivån i förvaret, dvs av hur mycket injektering som antogs göras i tunnelväggarna. I ett ”värsta fall” utan tätning beräknades den största avsänkningen av grundvattenytan till 25 m, vilken uppnåddes i området ovanför tillfartstunneln (som är spiralformad och därför täcker en viss horisontell area). Inte ens i detta (hypotetiska) ”värsta fall” visade resultaten på någon inverkan på ytvattenflöden eller vattennivåer i sjöar. Resultaten visade att förvaret hade liten inverkan på vattenbalansen för modellområdet som helhet. Inverkan var dock större om det beaktades att effekterna var koncentrerade till påverkansområdet. I det (hypotetiska) ”värsta fallet” utan tätning av berget motsvarade inflödet till tillfartstunnel och schakt en specifik avrinning av 400 mm/år inom påverkansområdet.

Simuleringar genomfördes med två alternativa bottenrandvillkor, randvillkor 1 där inverkan av förvarets djupare delar inte beaktades (bottenrandvillkoret på nivån 135 m under havet gavs av tryck erhållna från en storskalig/djupgående modell för ostörda förhållanden) och randvillkor 2 där även förvarets delar på större djup beaktades (genom att randvillkoret hämtades ur en storskalig modellering där hela förvaret ingick). Skillnaderna mellan resultaten för de två randvillkoren var små. Randvillkor 2 resulterade i ett något mindre inflöde till förvaret och ett något större område med avsänkt grundvattenyta.

Transportmodelleringen som redovisas i denna rapport innefattar simuleringar med MIKE SHE-rutinerna för partikelspårning och advektions-dispersionsmodellering (AD), i det senare fallet med linjär jämviktssorption. Modelleringen fokuserades på transporten av lösta ämnen från

källor i det djupa berget uppåt mot markytan, eftersom avsikten var att undersöka spridningen efter hypotetiska utsläpp från ett slutförvar på stort djup. Alla simuleringar genomfördes med källor placerade på nivån 135 m under havet, dvs på ett djup som avsevärt översteg de mäktigaste avlagringarna i området men samtidigt låg ett stycke ovanför den tilltänkta förvarsnivån (400–700 m). De viktigaste syftena med transportmodelleringen var att utveckla och illustrera modellernas användningsområden, och att förse säkerhetsanalysen SR-Can med stödjande modellresultat.

Resultaten av partikelspårning från källor jämnt fördelade inom hela landdelen av modellområdet visade att flertalet partiklar hade sina utströmningspunkter från den mättade grundvattenzonen inom samma ytavrinningsområden som de injicerades i. Detta indikerade att partiklarnas horisontella transportsträckor var relativt korta. En icke försumbar andel av partiklarna gick dock från startpunkter under landområdet till havet. Intagskanalen för kylvatten till kärnkraftverket mottog den största andelen av de partiklar som transporterades till havet.

Också i den andra typen av partikelspårning som gjordes, där partiklar injicerades längs flödesvägar från det djupa berget, föreföll partiklarna transporteras mer eller mindre vertikalt uppåt i den övre delen av berget och jordlagren. De flödesvägar som användes för att identifiera startpunkter för partiklar i den ytnära modellen hämtades från liknande beräkningar utförda i samband med säkerhetsanalysen SR-Can. Där användes en grundvattenflödesmodell som innefattade det djupa berget med en detaljerad beskrivning av förvaret, varvid partikelspårning utfördes från enskilda kapselpositioner i förvaret. Eftersom flertalet av de startpunkter som erhölls från den djupa modellen låg under havet, hamnade majoriteten av partiklarna i den ytnära modellen i havet. Inga större skillnader kunde observeras vid en jämförelse mellan utströmningspunkternas lägen vid markytan/havsbotten i de två modellerna.

AD-simuleringar utfördes för två olika punktkällor, en från vilken transporten huvudsakligen gick till havet och en där den tillförda massan till största delen gick till den omättade zonen på land. I båda fallen modellerades transporten från en kontinuerlig källa med konstant koncentration. Resultaten visar på betydelsen av de fysikaliska parametrar som ansattes i modellens olika beräkningslager. Variationer i porositet och hydraulisk konduktivitet längs och mellan flödesvägar resulterade i avsevärda skillnader i de lösta ämnenas spridningsmönster. Dessa skillnader gällde såväl advektion och utspädning som fördröjning orsakad av sorption. Både partikelspårnings- och AD-resultaten visade också på vikten av att välja källornas lägen (dvs enskilda punktkällor eller mönster av många källor) så att resultaten blir representativa för det scenario som skall studeras.

Rapportens sista kapitel summerar de huvudsakliga osäkerheter som är förknippade med modelleringen, och slutsatserna av arbetet. Där framhålls att modelleringen baseras på den datamängd som levererades redan till modellversion 1.2 (med datafrys i juli 2004), vilket innebär att betydligt mer platsdata kommer att vara tillgängliga för nästkommande modellversioner. Mest betydelsefullt är att längre tidsserier av data från meteorologiska, hydrologiska och hydrogeologiska mätningar, främst meteorologiska parametrar som nederbörd och potentiell evapotranspiration, vattennivåer och ytvattenflöden, kommer att kunna användas i nästa modellversion. Detta är viktigt både för jämförelsen mellan modellresultat och fältdata, och för att få en bättre direkt input av meteorologidata till modellen. Även databasen för de hydrogeologiska egenskapsparametrarna har förbättrats genom ytterligare mätningar, dock i mindre omfattning än för tidsserierna.

Det generella intrycket från de relativt grova utvärderingar som hittills genomförts är att resultaten av flödes- och transportsimuleringarna är rimliga. Mycket arbete behöver dock göras för att analysera överensstämmelsen, eller avsaknaden av sådan, mellan modell och verklighet, och vid behov förbättra modellerna. Följdriktigt bedöms osäkerheter förknippade med den begränsade användningen av fältdata för tester och kalibrering av modeller vara de viktigaste i detta skede av modelleringsarbetet med Forsmark. Ytterligare känslighetsanalyser och utvecklingen av en effektiv kalibreringsmetodik är viktiga för att förbättra modellerna i detta hänseende. Aktiviteter som syftar till att tillföra dessa komponenter har igångsatts.

Contents

1 Introduction

1.1 Background

The Swedish Nuclear Fuel and Waste Management Company (SKB) is performing site investigations at two different locations in Sweden, referred to as the Forsmark and Simpevarp areas, with the objective of siting a final repository for high-level radioactive waste. Data from the site investigations are used in a variety of modelling activities, the results of which are presented within the frameworks of Site Descriptive Models (SDM), Safety Assessment (SA), and Environmental Impact Assessment (EIA). Numerical modelling of flow and solute transport is one of the modelling activities performed in support of SDM, SA and EIA. This report presents model development and results of numerical flow and transport modelling of surface water and near-surface groundwater at the Forsmark site.

The SDM provides a description of the present conditions at the site, which is used as a basis for developing models intended to describe the future conditions in the area. In particular, model predictions of the effects of the construction, operation and long-term waste storage are of interest. The latest version of the Forsmark SDM, version 1.2 (SDM F1.2, for short), is presented in /SKB 2005/. In a background report to SDM F1.2, /Johansson et al. 2005/ describe the modelling of surface hydrology and near-surface hydrogeology that was performed using the Forsmark 1.2 dataset. This description is used as a starting point for the modelling presented herein, which comprises hydrological analyses of undisturbed and open repository conditions (i.e. for “natural” conditions and during the construction and operation phases, respectively), as well as solute transport applications.

During the construction and operation phases, there will be atmospheric pressure in the open tunnels and shafts in the repository. This will cause disturbances in the pressure field around the subsurface constructions and inflow of groundwater. The size of this inflow and its possible effects on surrounding groundwater and surface systems need to be quantified. The issues related to the effects of the open repository concern both the conditions in the repository (inflows and hydrochemical conditions) and in the surrounding environment (effects of groundwater drawdown). Thus, the open repository modelling will deliver results to both SA and EIA. The modelling presented in this report is focused on the effects on the surface hydrology and near-surface hydrogeology, i.e. on the surrounding environment.

Modelling of radionuclide transport from the repository is an important part of the analyses performed in order to support SA. This modelling is usually focused on the transport through the rock, whereas the transport in the uppermost part of the system (the upper rock and the Quaternary deposits) is handled in a simplified manner. However, such model simplifications must be supported by (at least) model studies of some selected “representative” cases focusing on the near-surface system. For some applications, primarily related to the SA biosphere modelling, detailed modelling of the near-surface system may be needed to provide direct quantitative input to the modelling work. This report presents solute transport applications based on both particle tracking simulations and, for the first time in this context, advection-dispersion calculations.

1.2 Objectives and scope

For reasons related to the timing relative to other activities and the time effectively available for performing the work, the modelling performed in connection with SDM F1.2 /Johansson et al. 2005/ did not make full use of all the site data available at the time or included important model development activities such as sensitivity analysis. Therefore, the modelling presented in this document involves an update and analysis of the basic flow model for the present, "undisturbed" conditions, in addition to the analyses of solute transport and open repository conditions performed in support of SA and EIA (cf. above).

With the previous SDM F1.2 as starting point, the present work can be subdivided into the following four parts:

1. Update of the numerical flow model (enlargement of the model area and inclusion of additional site data in the model).
2. Hydrological analysis of "undisturbed" conditions (sensitivity analysis and detailed analysis of the selected base case).
3. Analysis of the hydrological effects of an open repository (effects on surface hydrology and the hydrogeological conditions in the Quaternary deposits and the upper rock).
4. Analysis of solute transport from sources at large depth in the rock into and within the near-surface system.

The general objectives of the present modelling are the following:

- Develop and present an updated flow model that makes full use of the Forsmark 1.2 dataset.
- Improve our understanding of the present conditions in the Forsmark area.
- Develop and demonstrate modelling tools needed for hydrological and solute transport applications within SA and EIA.
- Provide qualitative and quantitative results to be used in current SA (SR-Can) and EIA (evaluation of open repository effects) activities, and in the planning of forthcoming modelling work.

The specific objectives of parts 2–4 above are presented in the beginning of their respective chapters in this report (cf. below).

1.3 Setting

The Forsmark area is located approximately 150 km north of Stockholm, in northern Uppland within the municipality of Östhammar. Figure 1-1 shows the regional model area and candidate area considered by the site investigation and within the site descriptive modelling, and also some lakes and other objects of importance for the hydrological modelling.

The candidate area is the area initially prioritised for potentially hosting the geological repository, which means that the repository possibly could be built somewhere within this area, not that it would occupy the whole area. This implies that more detailed investigations have been performed within the candidate area, at least for that some of the site investigation disciplines, see /SKB 2005/ for details. The candidate area is situated in the immediate vicinity of the Forsmark nuclear power plant and the underground repository for low- and medium-active nuclear waste, SFR. It is located along the shoreline of Öresundsgrepen (a part of the Baltic), and extends from the nuclear power plant and the access road to the SFR facility in the northwest to the Kallrigafjärden bay in the southeast. The candidate area is approximately 6 km long and 2 km wide.

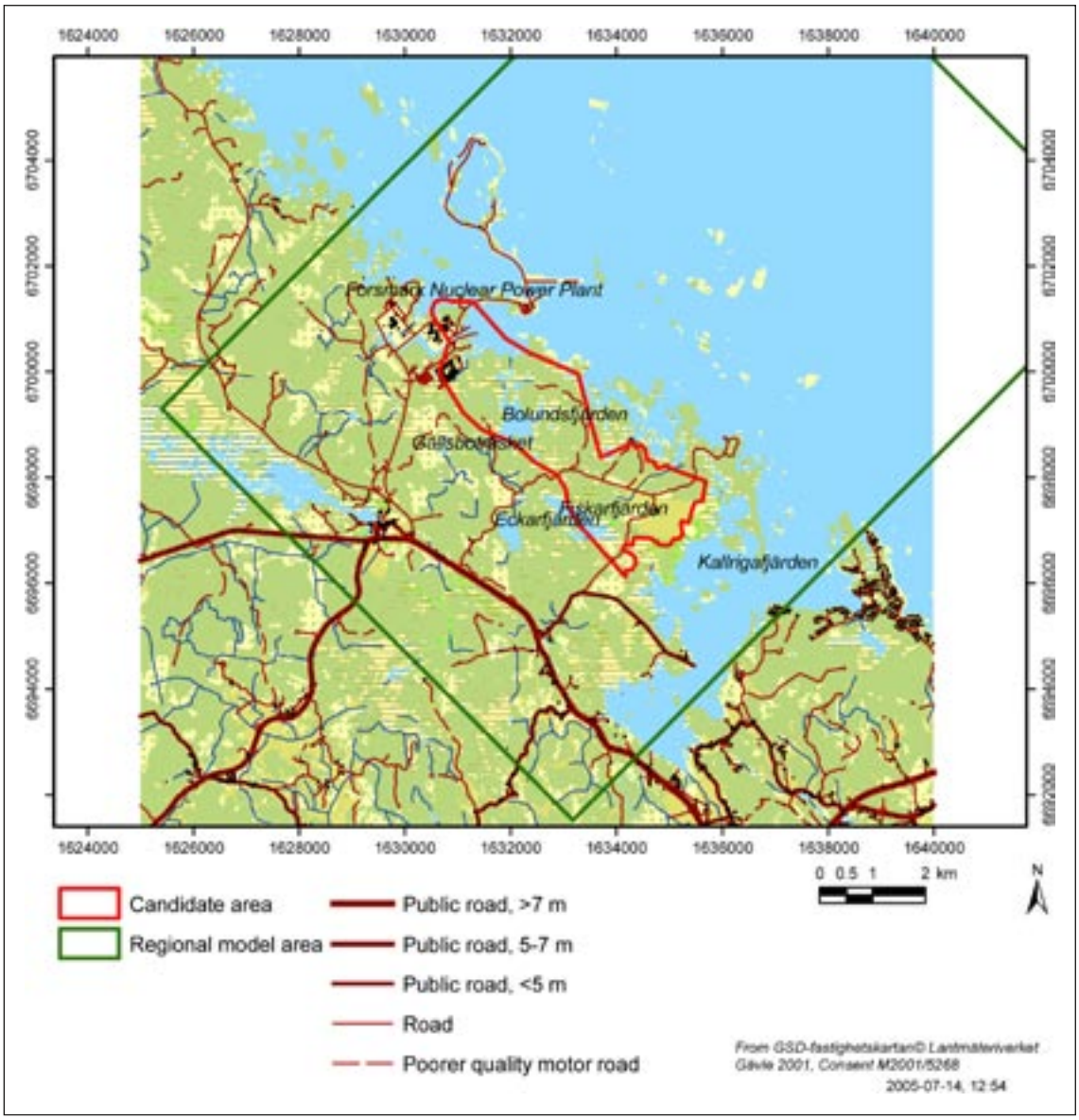

Figure 1-1. *Detailed map of the land part of the regional model area and some objects of particular interest for the hydrological modelling.*

As a result of the investigations and modelling performed, a further prioritisation and focusing of (some of) the investigations has been made during the course of the site investigation. Specifically, the current open repository and SA modelling uses a repository layout where the repository is located in the north-western part of the candidate area, see Chapter 4. A description of the climate, and the hydrological and hydrogeological conditions in the Forsmark area is presented in /Johansson et al. 2005/. /Lindborg 2005/ gives a description of the whole surface and near-surface system, including the most current models of, e.g. the topography and the Quaternary deposits. The site characteristics and parameters considered in the present work are summarised and described in Chapter 2.

1.4 Related modelling activities

Several modelling activities have provided the various external input data and models required for the present modelling and the preceding SDM F1.2 modelling. Whereas most of these inputs are described in some detail in Chapter 2 and in /Johansson et al. 2005/, we discuss here briefly the interactions with the hydrogeological activities that consider flow modelling of the integrated rock-overburden system.

The work described in this report is focused on the surface systems, i.e. on the overburden and the upper part of the bedrock. The numerical model was developed using the MIKE SHE tool, and has a vertical extent from the ground surface to 135 m below sea level. For applications involving the repository at c. 500 m below sea level as a source of either a hydraulic disturbance (open repository) or dissolved substances (solute transport applications), this means that the boundary condition at the bottom of the near-surface model preferably should be obtained from a model that includes the repository. Conversely, the larger-scale models that go down to repository depth (about twice as deep, actually) can use information from the more detailed near-surface model as a basis for setting the upper boundary condition.

The hydrogeological modelling activities that provided inputs to the various parts of this work can be summarised as follows:

- SDM F1.2 hydrogeological modelling preformed with the DarcyTools modelling tool /Svensson et al. 2004/ delivered the hydrogeological properties of the rock and the bottom boundary condition used in the modelling of the undisturbed hydrological conditions and solute transport /Follin et al. 2005/.
- Open repository modelling Forsmark 1.2, which also was performed with DarcyTools /Svensson 2005/, provided the “disturbed” bottom boundary condition used in the MIKE SHE open repository simulations (the boundary condition for undisturbed conditions was also used). There was also a data exchange in the opposite direction; the groundwater recharge calculated in the MIKE SHE model was delivered to the DarcyTools model and used in a sensitivity case.
- SA groundwater flow and solute transport modelling performed for the SR-Can assessment using the ConnectFlow code /Hartley et al. 2006/ presented calculated flow paths from the repository, which were used as starting points for particles in the near-surface model.

The relation between the MIKE SHE model described in the present report and the DarcyTools open repository model /Svensson 2005/ is illustrated in Figure 1-2. In particular, the figure indicates the boundaries of the MIKE SHE model, which are described using data from the DarcyTools model. It can also be seen that the DarcyTools model covers a larger depth interval including the deep repository, whereas the MIKE SHE model contains the upper parts of the access tunnel and shafts. Conversely, the DarcyTools model does not include the uppermost parts of access tunnel and shafts.

1.5 This report

This report provides an integrated presentation of the modelling activities listed as parts 1–4 in Section 1.2. Chapter 2 describes the modelling tools and the input data (part 1), with emphasis on the changes since the previously reported SDM F1.2 modelling /Johansson et al. 2005/. In Chapter 3, the hydrological analysis of the undisturbed situation is reported (part 2). Chapter 4 describes the open repository simulations (part 3), whereas Chapter 5 presents the results of the solute transport modelling (part 4). Finally, Chapter 6 contains a discussion of the results, including an uncertainty evaluation, and the conclusions of the work.

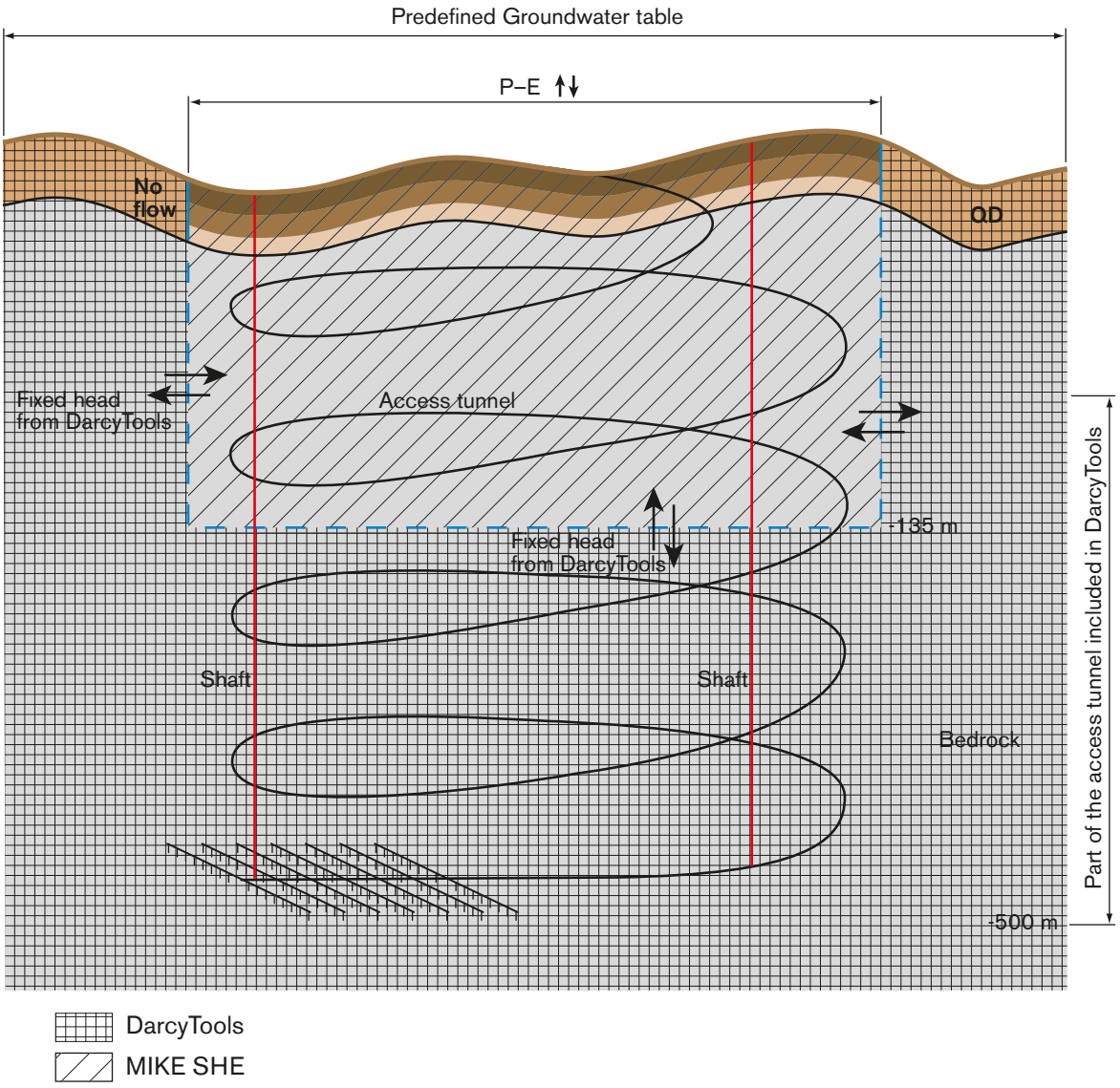

Figure 1-2. *Sketch of depth intervals and parts of the repository covered by the MIKE SHE and DarcyTools models used in the Forsmark open repository modelling. Boundaries for which data are exchanged between the models are also indicated. Note that the DarcyTools model extends from the ground surface to below repository depth, but that the uppermost parts of the ramp and shafts are not represented in that model.*

2 Modelling tools and input data

This chapter describes the modelling tools used in the hydrological/hydrogeological model development and simulations. In particular, the novel integration of MIKE SHE-MIKE 11 and the MOUSE-SHE code, which was developed within the present project, is described in some detail. Furthermore, the input data are described, with focus on the changes relative to the SDM F1.2 model; the main data updates concern the meteorological data (site data are used in the present model), and the hydrogeological properties of the rock and the Quaternary deposits (in both cases, the data have been updated to reflect the SDM F1.2 description).

2.1 Overview of modelling tools

2.1.1 MIKE SHE – groundwater and surface water flow

MIKE SHE (SHE = Système Hydrologique Europeen) is a physically based, distributed model that simulates water flows from rainfall to river flow. It is a commercial code, developed by the Danish Hydraulic Institute (DHI). This subsection summarises the basic components of the MIKE SHE tool. For a more detailed description, see the MIKE SHE user's guide and technical reference /DHI Software 2004a/.

MIKE SHE considers all the main processes in the land phase of the hydrological cycle; the modelled processes are illustrated in Figure 2-1. The precipitation can either be intercepted by leaves or fall to the ground. The water on the ground surface can infiltrate, evaporate or form overland flow. Once the water has infiltrated into the soil, it enters the unsaturated zone. In the unsaturated zone, the water can either be extracted by roots and leave the system as transpiration, or it can percolate down to the saturated zone (Figure 2-1). MIKE SHE is fully integrated with a channel-flow code, MIKE 11. The exchange of water between the two modelling tools takes place during the whole simulation, i.e. the two programs run simultaneously.

The MIKE SHE tool was developed primarily for modelling of groundwater flow in porous media, and uses a conventional continuum description of the hydraulic properties of the subsurface. This implies that the fractured rock included in the present MIKE SHE model must be handled as a continuum, i.e. by way of an Equivalent porous medium (EPM) or Continuum porous medium (CPM) representation, see /Hartley et al. 2006/.

The MIKE SHE model consists of the following five compartments:

- Overland flow (OL).
- Evapotranspiration (ET).
- Unsaturated zone (UZ).
- Saturated zone (SZ).
- Channel flow (MIKE 11, M11).

The water flow is calculated in different ways in each compartment. In addition to the different compartments, there is a frame component that runs simultaneously with the other components of the model; this component controls the exchange of water between all the other compartments. For a detailed description of the each compartment, including the governing equations, the methods used to solve them, and the associated parameters, see /Werner et al. 2005/ and /DHI Software 2004a/.

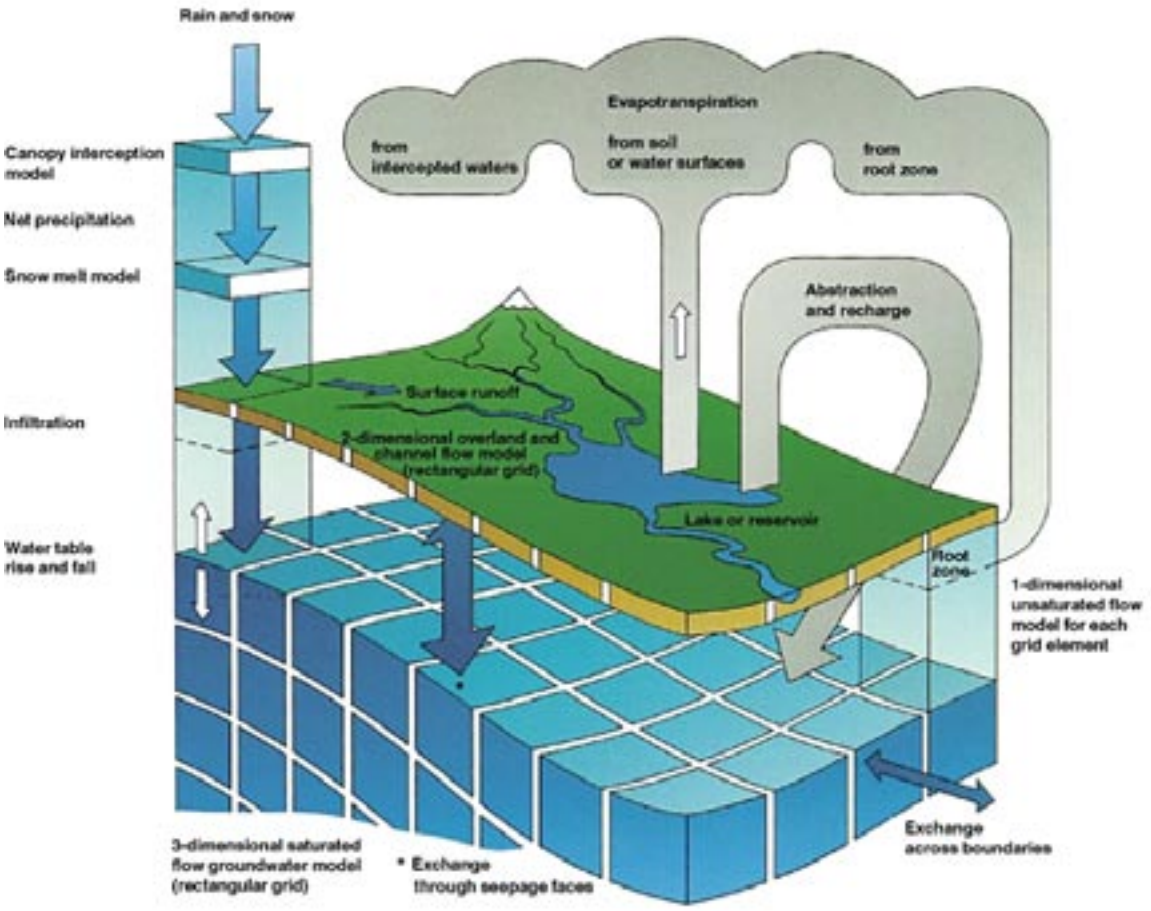

Figure 2-1. *Overview of the processes considered in the MIKE SHE model /DHI Sverige and VBB VIAK 1998/.*

2.1.2 Modelling of tunnel and shafts

MOUSE-SHE – inflow to the tunnel (ramp)

Even though the model used in the open repository modelling presented in this report does not include the deep, main part of the repository (i.e. deposition tunnels and other constructions at depth), there are some parts of it that need to be represented explicitly in the model. Specifically, the ramp and a number of shafts pass through the model volume, which implies that their hydraulic interactions with the surrounding aquifer must be modelled. These interactions involve inflow to open (air-filled) vertical shafts and a tunnel that also goes through the whole vertical extent of the model.

In the open repository modelling, the MOUSE-SHE code /DHI Software 2004b/ has been used for modelling the inflow to the tunnel (ramp). MOUSE-SHE is a modelling tool developed for urban hydrology. It is primarily used for calculating groundwater inflows to sewers. In the present work, the tunnel to the deep part of the repository has been described as a number of water pipes in MOUSE. The code has been further developed within the present project, in order to integrate MOUSE and MIKE SHE for the tunnel application at hand. The novel, integrated code calculates the flow of water between the MIKE SHE groundwater flow model and the MOUSE model, i.e. the inflow of water to the tunnel.

When calculating the exchange of water between the groundwater flow model and MOUSE, the properties of both the “pipe”, including the effect of grouting, and the aquifer are taken into consideration. The flow from/to a MIKE SHE groundwater cell to/from a MOUSE pipe intersecting the cell is calculated as:

$Q_{cell} = dh \cdot L \cdot P \cdot LC$

where:

Q_{cell} leakage flow from the grid cell to the tunnel [m^3s^{-1}]

dh head difference between aquifer and pipe [m]

L length of the section of the pipe intersecting the cell [m]

P wet perimeter [m] (P_{inner} – if flow from pipe to cell, P_{outer} – if flow from cell to pipe, see Figure 2-2)

LC leakage coefficient [s^{-1}]

The LC value is calculated as a combination of the pipe leakage coefficient, $LC_{p,}$ and the "average leakage coefficient" of the aquifer grid cell in MIKE SHE, LC_{aq}. Specifically, the combined leakage coefficient is evaluated as the harmonic mean of these "pipe" and "aquifer" contributions, as:

$$\frac{1}{LC} = \frac{1}{LC_p} + \frac{1}{LC_{aq}}$$

This concept and the related parameters are illustrated in Figure 2-2.

LC_{aq} is calculated under the assumption that the water taking part in the exchange between the aquifer and the pipe flows to/from the centre of the grid cell as horizontal and/or vertical flow. However, the current implementation of the MOUSE-SHE coupling does not involve a detailed geometric calculation in the quantification of the flow resistance between the aquifer and the tunnel. Although the MOUSE pipe can have any location in a grid cell, an approximation in the form of an average flow length is used. This assumed average flow length is 0.25 times the grid cell length, i.e. 0.25 times the horizontal length, denoted dx, for horizontal flow and 0.25 times the cell height, dz, for vertical flow. Thus, the leakage coefficient of the grid cell is calculated using the equation:

$$LC_{aq} = LC_{aq(h)} + LC_{aq_{(v)}} = \frac{K_h}{0.25 \cdot dx} + \frac{K_v}{0.25 \cdot dz}$$

where:

dx horizontal cell size [m]

dz vertical cell size [m]

K_h horizontal hydraulic conductivity [ms^{-1}]

K_v vertical hydraulic conductivity [ms^{-1}]

LC_p is calculated on the basis of a known level of grouting, expressed as a hydraulic conductivity of the grouted rock, divided by the thickness of the grouted layer, i.e. as:

$$LC_p = \frac{K_g}{d_g}$$

where:

K_g hydraulic conductivity of the grouted rock [ms^{-1}]

d_g thickness of grouted zone in the rock [m].

The application of these equations is demonstrated in Chapter 4.

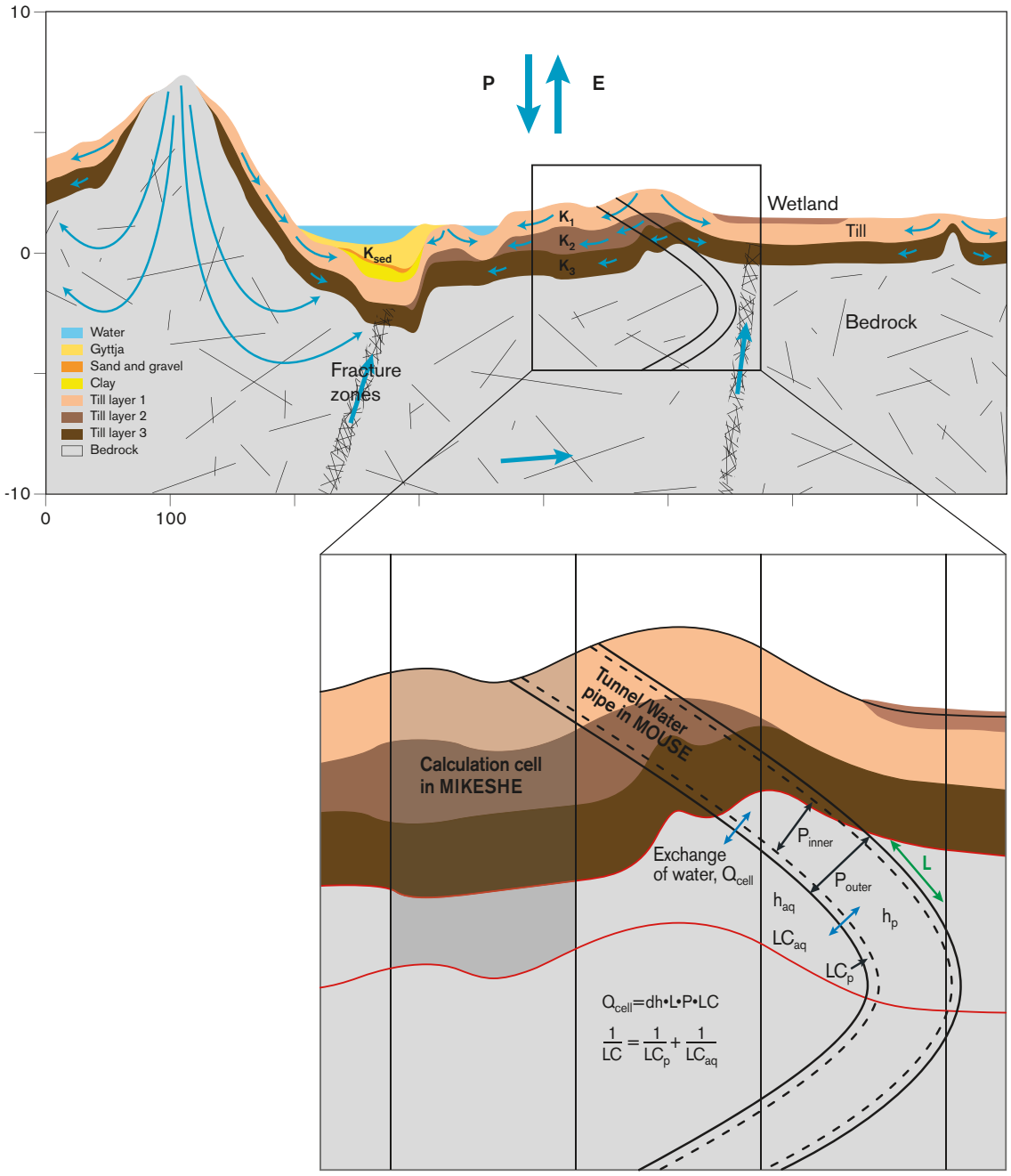

Figure 2-2. *Illustration of the model and parameters used in the calculation of the exchange of water between MOUSE and MIKE SHE. The hydraulic heads in the aquifer and the tunnel are denoted as h_{aq} and h_p, respectively; dh is the difference between these head values.*

Modelling of inflow to shafts in MIKE SHE

The shafts are described in MIKE SHE as cells with atmospheric pressure characterised hydraulically by a conductance values that takes the grouting of the rock into consideration. The total conductance used in the modelling of the inflow of groundwater from the aquifer to the shafts is calculated as:

$C = LC_s \cdot \Delta z \cdot 2 \cdot r \cdot \pi$

where:

C total conductance [$m^2 s^{-1}$]

LC_s total leakage coefficient [s^{-1}]

Δz height of calculation layer [m]

r radius of the shaft [m]

Similar to the MOUSE-SHE tunnel modelling described above, the total leakage coefficient is calculated by combining leakage coefficients representing the aquifer and the grouted zone in the rock, as:

$$\frac{1}{LC_s} = \frac{1}{LC_{aq,s}} + \frac{1}{LC_s}; \qquad LC_{aq,s} = \frac{K_h}{\Delta x}; \qquad LC_s = \frac{K_{g,s}}{d_{g,s}}$$

where:

$LC_{aq,s}$ leakage coefficient of the aquifer cell [s^{-1}]

LC_s leakage coefficient of the grouted zone [s^{-1}]

K_h horizontal hydraulic conductivity [ms^{-1}]

Δx horizontal grid size [m]

$K_{g,s}$ hydraulic conductivity of the grouted rock [ms^{-1}]

$d_{g,s}$ thickness of the grouted zone in the rock [m]

2.1.3 Transport modelling tools

Particle tracking simulations

In a particle tracking simulation, a collection of hypothetical “water parcels” or “particles” are released in the water flow field. The particles travel with the flow, from their starting positions towards internal sinks and boundaries, whereby various quantities of interest for characterising flow and advective transport (i.e. transport with the water flow) can be obtained. For example, the flow paths can be “tagged” and visualised, such that the analysis provides information on the locations of discharge areas, and transport can be quantified in terms of travel times between selected sources and compliance boundaries.

The calculated, three-dimensional flow field is the basis for the movement of the particles. The particles are transported according to the local groundwater velocity, which in MIKE SHE is calculated in the “Water movement” module. Additional input data required for the particle tracking simulations (as compared to flow simulations) are the effective porosity, the number of particles introduced and the starting point of each particle. Furthermore, the input data may include specifications of internal “control planes”, areas or volumes, if the transport to such objects is to be evaluated.

In the present simulations, the effective porosity of the bedrock is imported from the Forsmark 1.2 groundwater flow simulations with DarcyTools /Follin et al. 2005/, whereas the effective porosity of each overburden (unconsolidated) material is assumed equal to the specific yield of that material. In the current version of MIKE SHE, particle tracking can be performed in the saturated groundwater zone only; particles that leave the saturated zone are not traced further. This means that, if such transport takes place, the continued transport with overland or unsaturated flow, or in the water courses must be modelled by means of other tools. However, it is possible to identify what kind of sinks the particles have moved to, i.e. water courses, the unsaturated zone, model boundaries, or wells.

MIKE SHE uses so-called “registration zones” to identify internal boundaries at which particle transport is monitored. This means that if, e.g. a catchment area or a lake is defined as a registration zone, then the number of particles reaching that object, and the associated particle travel times, are calculated. Furthermore, the monitoring in the registration zones can provide information on the starting positions of the particles, enabling analyses of recharge-discharge patterns (provided the starting positions are selected to facilitate such analyses).

Advection-dispersion calculations

In advection-dispersion calculations (AD, for brevity), as implemented here, transport is modelled by numerical solution of the well-known advection-dispersion equation, e.g. /Domenico and Schwartz 1998/. This implies that mass balance equations are formulated and solved for each cell in the numerical model. Whereas discrete mass entities, particles, are considered in the particle tracking simulations, the solute mass in a cell in the AD model is assumed to be fully mixed within that cell; this implies that the concentration is constant throughout the cell but differs from cell to cell. The results are given in terms of (dissolved) concentrations, which can be obtained as functions of time for each cell in the numerical grid.

Similar to the particle tracking calculations, the calculated, three-dimensional flow field is an important basic input to the AD solute transport calculations. In addition to the advective transport, mass transport between cells takes place also by dispersion. Dispersive transport is modelled as a diffusion process, commonly using field-scale "dispersivities" in place of the diffusivities. In such cases, dispersion is thought to represent the "smearing" of breakthrough curves that occurs due to velocity variations on various scales. As compared to "pure" flow simulations, the additional input data required for AD calculations include the effective porosity, the longitudinal and transverse dispersivities, and the strength and location of the solute source (i.e the transport boundary condition).

The MIKE SHE Advection-dispersion module consists of four components, each describing solute transport in one subsystem within the hydrological cycle /DHI Software 2005/. The four components of the Advection-dispersion module are Overland flow transport, Channel flow transport, Unsaturated flow transport and Saturated flow transport. Thus, solute transport can in principle be modelled throughout the whole groundwater-surface water system, which implies extended modelling capabilities relative to the particle tracking. However, in the present application solute transport has been modelled in the saturated zone only.

In this work, the same effective porosities were used in the AD modelling as in the particle tracking simulations. The dispersivities were set to zero in all the cases. However, some "artificial" numerical dispersion could still be observed in the results (cf. Chapter 5). Also sorption processes can be modelled with the MIKE SHE Advection-dispersion module. The current modelling includes linear equilibrium sorption, where an additional parameter, the K_d value, quantifies the sorption and hence the associated retardation of solute transport.

2.2 Meteorological, hydrological and hydrogeological input data

The input data to the MIKE SHE model include data on topography, land use, geology, hydrogeology and meteorology. In addition, MIKE 11 (the Channel flow component describing flow in the water courses) requires information on the stream network within the model area. At the time of modelling, site-specific data were not available on all the input parameters in the model. Most of the site-specific data included in the present model were available already at the time of the Forsmark 1.2 data freeze (July, 2004).

However, as mentioned in Section 1.2, all site data could not be used in the flow modelling performed in connection with SDM F1.2 /Johansson et al. 2005/. Therefore, the input data to the present modelling have been updated relative to the SDM F1.2 model; the most important changes concern the hydrogeological properties of rock and overburden, and the meteorological data. The summary of input data given below is focused on the data updates in this work, and is not a complete description of the input data to the modelling. Data types and parameter values not described here are the same as in SDM F1.2, and are presented in /Johansson et al. 2005/.

Also the conceptual model providing the basis for the present MIKE SHE flow modelling is described in /Johansson et al. 2005/. Thus, the conceptual model is the same as in the previous work; the model updates concern parameter values. The hydrological analysis of the present, undisturbed conditions consists of a (initial) base case definition, a sensitivity analysis, and an evaluation and detailed analysis of the base case. The data presented in the following comprise the dataset used in the (initial) base case. This base case was used as a starting point for identifying the parameter ranges considered in the sensitivity analysis.

2.2.1 Meteorology

The meteorological input data are taken from two local meteorological stations established by SKB within the site investigation program; the locations of these stations are shown in Figure 2-3. Data on temperature, precipitation and potential evapotranspiration are used in the MIKE SHE modelling. The potential evapotranspiration is calculated with the Penman-Monteith equation with data from the local station "Högmasten" in Forsmark /Gustafsson et al. 2006/.

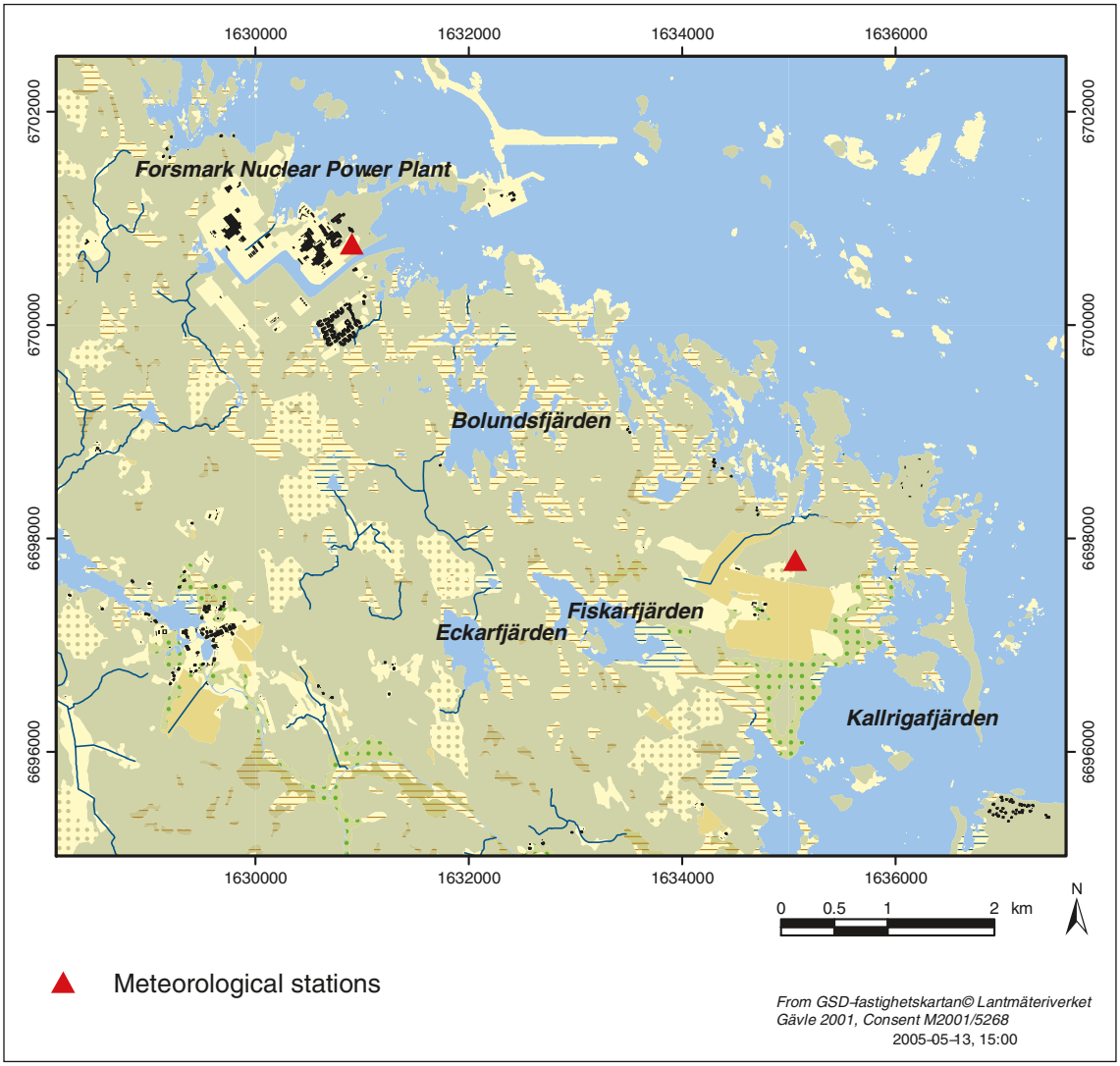

Figure 2-3. *Meteorological stations in Forsmark; the northwestern station is referred to as "Högmasten" and the southwestern one is "Storskäret".*

The annual (corrected) precipitation for the simulation period, May, 2003–May, 2004, is 597 mm and the total potential evapotranspiration during this period is calculated to 435 mm.

2.2.2 Hydrogeology

The conceptual model for the near-surface hydrogeology consists of three main units, the Quaternary deposits (QD), the lake sediments, and the bedrock. As described below, the numerical flow model consists of 11 layers, of which three layers consist of QD and eight layers are in the bedrock. Below the lakes and a fen in the model area, the geological layers are complemented by geological lenses. The lenses have hydraulic properties that differ from those of the surrounding materials. For a detailed description of the conceptual near-surface hydrogeological model, i.e. the layers in the QD, see /Johansson et al. 2005/. The conceptual and numerical modelling of the rock hydrogeology in Forsmark is summarised in /SKB 2005/.

Bedrock

The part of the MIKE SHE model that consists of rock is parameterised using data taken from the Forsmark 1.2 hydrogeological modelling performed with the Darcy Tools code /Follin et al. 2005, SKB 2005/. Data on the hydrogeological properties of the rock were taken from eight different levels in the DarcyTools CPM model, ranging from 135 m below sea level up to the bedrock surface. The bedrock is described in terms of its vertical and horizontal hydraulic conductivity; the hydraulic conductivity in a horizontal plane at 135 m below sea level is shown in Figure 2-4.

The specific yield of the bedrock is assumed to be equal to the effective porosity. The storage coefficient, S_s [m^{-1}], is calculated according to an empirical relationship between the hydraulic conductivity and the storage coefficient, provided by the DarcyTools modelling team:

$$S_S = a \cdot K^b$$

where S_s is the storage coefficient [m^{-1}], and the dimensionless parameters a and b are assigned the values $a = 6.037 \cdot 10^{-5}$ and $b = 0.2312$ based on experimental data from earlier studies at Äspö /Rhén et al. 1997/.

In addition, the calculated head at 135 m below sea level was used as a boundary condition at the bottom boundary of the MIKE SHE model, Figure 2-5. Thus, the groundwater flow models of the near-surface system and the large-scale, integrated rock-overburden system are equivalent in term of head at this boundary and also in terms of the hydrogeological properties of the part of the rock where the two models overlap.

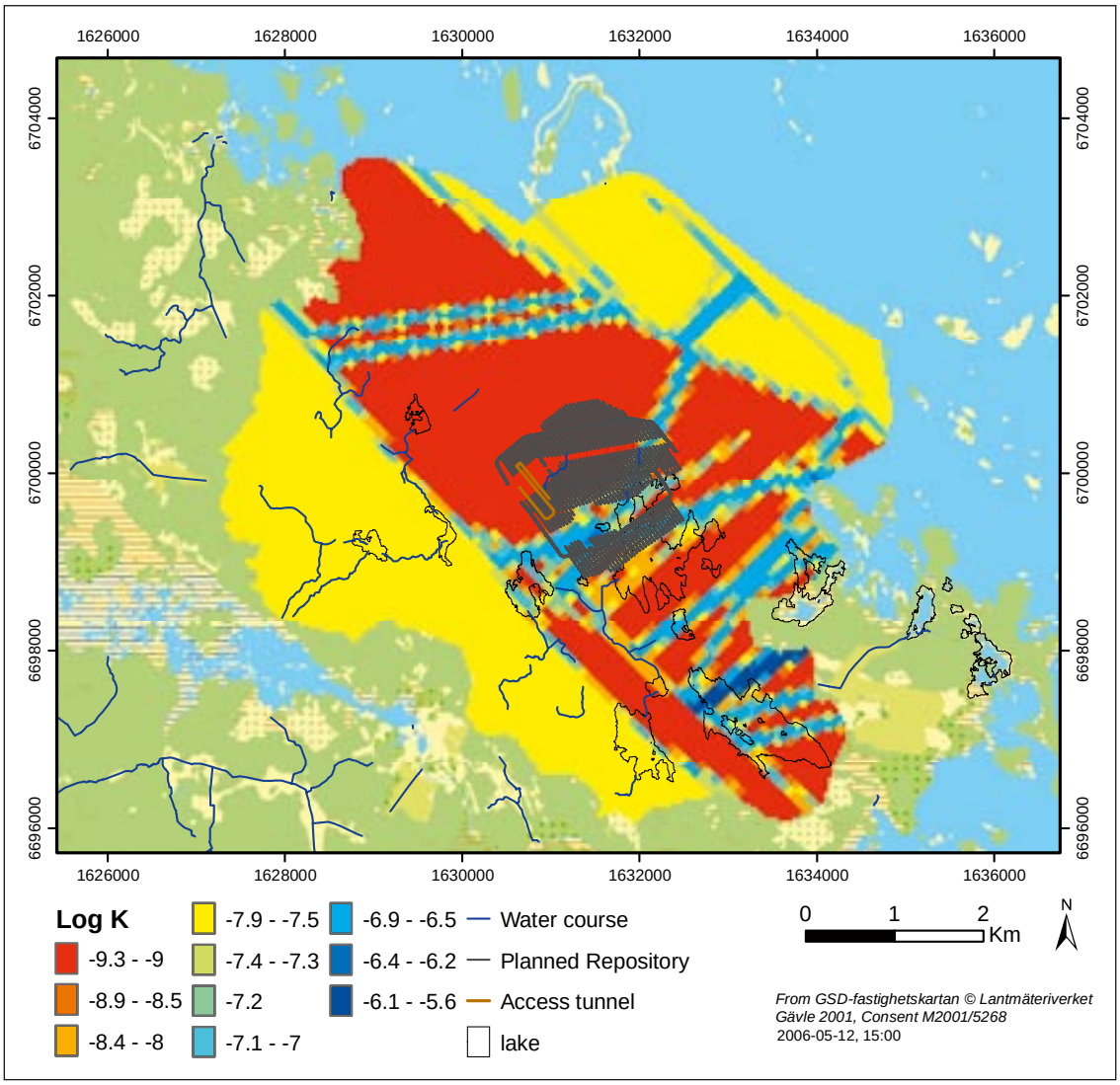

Figure 2-4. *Horizontal hydraulic conductivity (Log(K_{xy})) at 135 m below sea level in the model area (data imported from DarcyTools). The lakes in the area, the planned repository and the access tunnel are also shown in the figure. Note that the legend is applicable within the model area only.*

Quaternary deposits

The geological modelling of the QD was performed by use of the GIS-extension GeoEditor, see /Vikström 2005/ for a detailed description of the tool and the modelling procedure. Since its hydraulic properties are changing within the stratigraphical profile, the till is divided into three layers, which are denoted Z1, Z2 and Z3 (see Figure 2-6). In the geological model, these layers are described geometrically, i.e. in terms of their respective thicknesses at each location within the model area, based on the topographic model, an interpolated rock surface level, and a set of "rules".

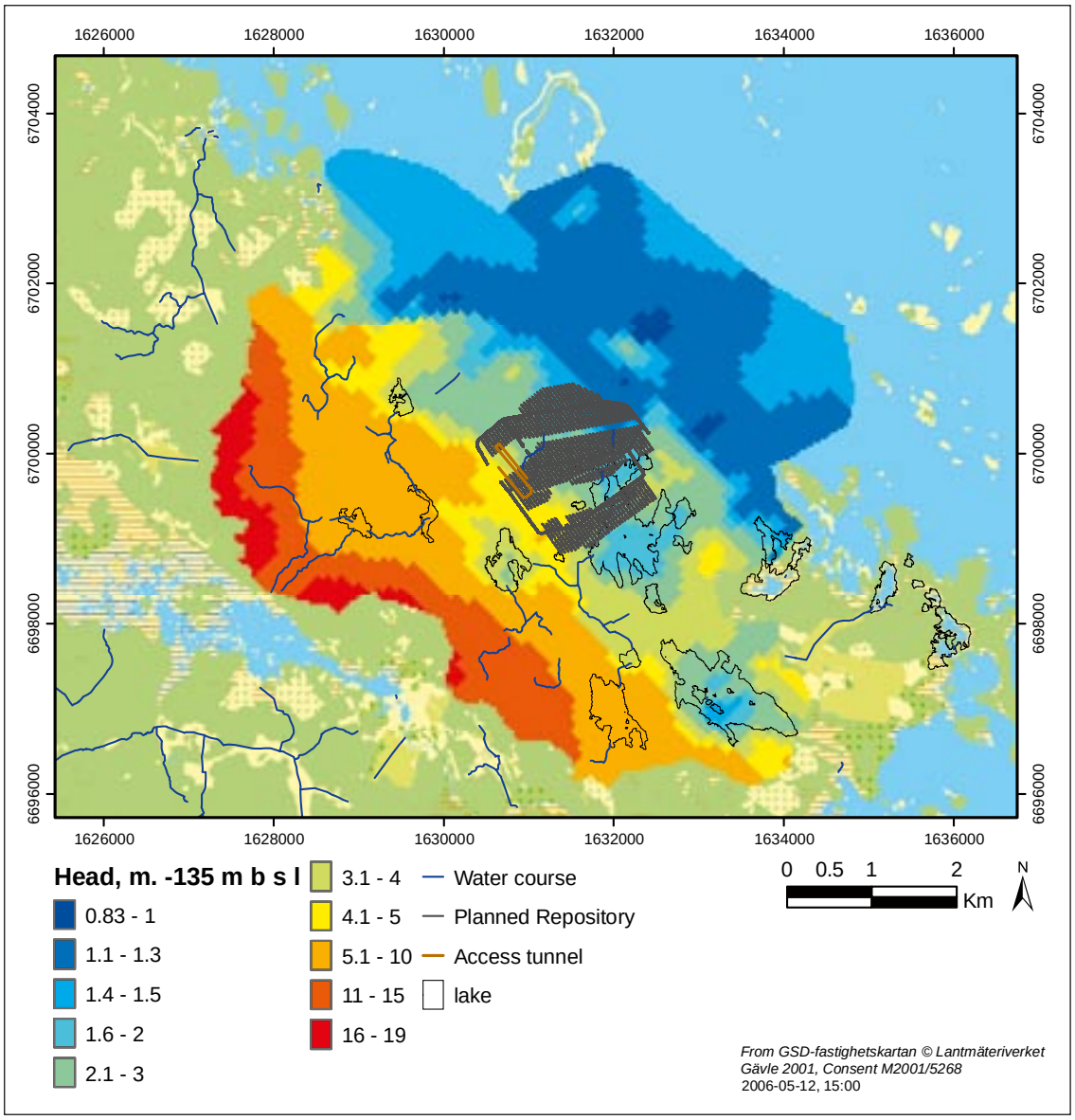

Figure 2-5. *Calculated head (m) at 135 m below sea level in the model area (data imported from DarcyTools). The lakes in the area, the planned repository and the access tunnel are also shown in the figure. Note that the legend is applicable within the model area only.*

The hydraulic properties of the top layer, Z1, are affected by plant roots and bioturbation. In general, the hydraulic conductivity can be assumed to be higher in this zone than in the underlying parts of the QD /Johansson et al. 2005/. This relatively high-permeable layer is followed by a more compact, less conductive layer, Z2. The third and deepest layer, Z3, represents the more high-conductive (as compared to Z2) soil/rock contact zone indicated by the hydraulic test results /Johansson et al. 2005/. Below wetlands and lakes this three-layer principle is complemented by geological lenses. These lenses have hydraulic properties that differ from those of the surrounding till materials.

The thickness of each layer in the model (Figure 2-6) depends on the total thickness of the QD, i.e. the difference between the ground surface level (GSL) and the rock surface level (RSL). In the present model, it is assumed that layers Z1 and Z3 have thicknesses of 0.5 m and 1 m, respectively, if the total thickness of the QD exceeds 1.5 m. With this basic assumption, there are three possible cases to be considered when determining the levels of the internal interfaces; the top surface levels of Z2 and Z3 are referred to as TSL_{Z2} and TSL_{Z3}, respectively, and the thicknesses of the layers are denoted D_{Z1}, D_{Z2} and D_{Z3}.

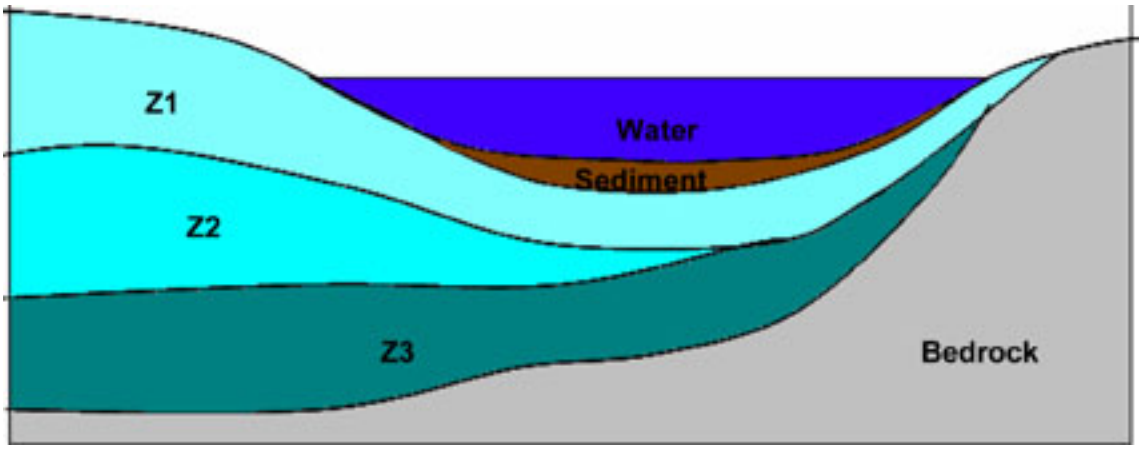

Figure 2-6. *Geological model illustrating the three-layer principle adopted for the till deposits and a sediment lens under a lake.*

Based on these assumptions or rules, the three possible cases can be summarised as follows:

1. The total thickness of the QD is larger than 1.5 m (GSL–RSL > 1.5 m)

   ⇒ three till layers (Z1, Z2 and Z3):

   TSL_{Z2} = GSL–0.5 m

   TSL_{Z3} = RSL+1.0 m

   D_{Z1} = 0.5 m

   D_{Z2} = TSL_{Z2}–TSL_{Z3}

   D_{Z3} = 1.0 m

2. The total thickness of the QD is between 0.5 m and 1.5 m (0.5 m ≤ GSL–RSL < 1.5 m)
   ⇒ two till layers (Z1 and Z3):

   TSL_{Z3} = GSL–0.5 m

   D_{Z1} = 0.5 m

   D_{Z2} = 0

   D_{Z3} = TSL_{Z3}–RSL

3. The total thickness of the QD is less than 0.5 m (GSL–RSL ≤ 0.5 m)
   ⇒ one till layer (Z1):

   D_{Z1} = GSL–RSL

   D_{Z2} = 0

   D_{Z3} = 0

The spatial distribution of the QD in layer Z1 is based on the detailed map of QD presented in /Sohlenius et al. 2004/. The uppermost layer has been divided into seven classes, including bedrock outcrops. Layer Z2 and Z3 are assumed to consist of sandy till, clayey till, or sand only, depending on the overlying QD in layer Z1. The assignment of QD to the different layers, which is also the basis for the assignment of hydraulic parameters, is shown in Table 2-1. The hydraulic properties of the overburden vary within the model area, as determined by the spatial distribution of QD. As shown in Table 2-2, each class has been assigned a material-specific set of parameters. Unless otherwise stated, the properties for each class are taken from the SDM F1.2 descriptive model reported in /Johansson et al. 2005/.

Table 2-1. Quaternary deposit in Z1, Z2 and Z3.

Z1	Z2	Z3
Sandy till	Sandy till	Sandy till
Clayey till	Clayey till	Sandy till
Peat	Sandy till	Sandy till
Clay	Sandy till	Sandy till
Gyttja	Sandy till	Sandy till
Sand	Sand	Sand
Bedrock	Bedrock	Bedrock

Table 2-2. Hydraulic properties for the QD in Z1, Z2 and Z3.

	K [m s^{-1}]	Sy [–]	S [m^{-1}]
Sandy till, Z1	$1.5 \cdot 10^{-5}$	0.15	0.001
Sandy till, Z2	$1.5 \cdot 10^{-6}$	0.05	0.001
Sandy till, Z3	$1.5 \cdot 10^{-5}$	0.05	0.001
Clayey till Z1	$1.5 \cdot 10^{-6}$	0.15	0.001
Clayey till Z2	$1.5 \cdot 10^{-7}$	0.05	0.001
Clay	$1.5 \cdot 10^{-8}$	0.03	0.006
Peat	$1.5 \cdot 10^{-5}$	0.24[1]	0.005[1]
Gyttja	$1.5 \cdot 10^{-7}$	0.03	0.006
Sand/gravel Z1, Z2, Z3	$1.0 \cdot 10^{-4}$	0.25[3]	0.025[2]

[1] Generic data from the literature /Kellner 2003/.

[2] Assigned a value equal to 1/10 of S_Y.

[3] Generic data from the literature /Domenico and Schwartz 1998/.

The lake sediments are divided into three layers. The uppermost layer consists of gyttja, which is underlain by sand. The deepest layer is a clay layer. The sediments are introduced in the model as geological lenses. The parameters assigned to the lake sediments are listed in Table 2-2. The lenses under the wetland areas in the model are not divided into layers; instead, they are all assumed to consist of peat.

The parameters for unsaturated flow are taken from the database in the MIKE SHE program. Generic data from /Domenico and Schwartz 1998/ are used for the specific yield (Table 2-3). The values for “Till, sand”, “Till, silt”, “Sand, coarse”, “Clay” and “Peat” are used in the model. There is no variation of these properties of the till with depth since unsaturated flow is calculated with the full Richard’s equation in the uppermost calculation layer only. The storage coefficient of the QD is set to 0.001 m^{-1} in the whole model area; this value is taken from /DHI Sverige and VBB VIAK 1998/.

2.2.3 Water courses and lakes

The MIKE 11 (stream network) model requires geometrical information on the water courses, including their positions in the horizontal plane, bottom levels, and cross-sections. A description of the main water courses in the Forsmark area was presented by /Brydsten and Strömgren 2005/. The locations where the cross-sections of the water courses and the lake thresholds have been measured are presented in Figure 2-7. The cross-sections in the water courses were measured every 100 m and the elevation of the river bed was measured every 20 m. The water courses for which no measurement results are available are assumed to have a triangular shape with a width of 2 m and a maximum depth of 1 m.

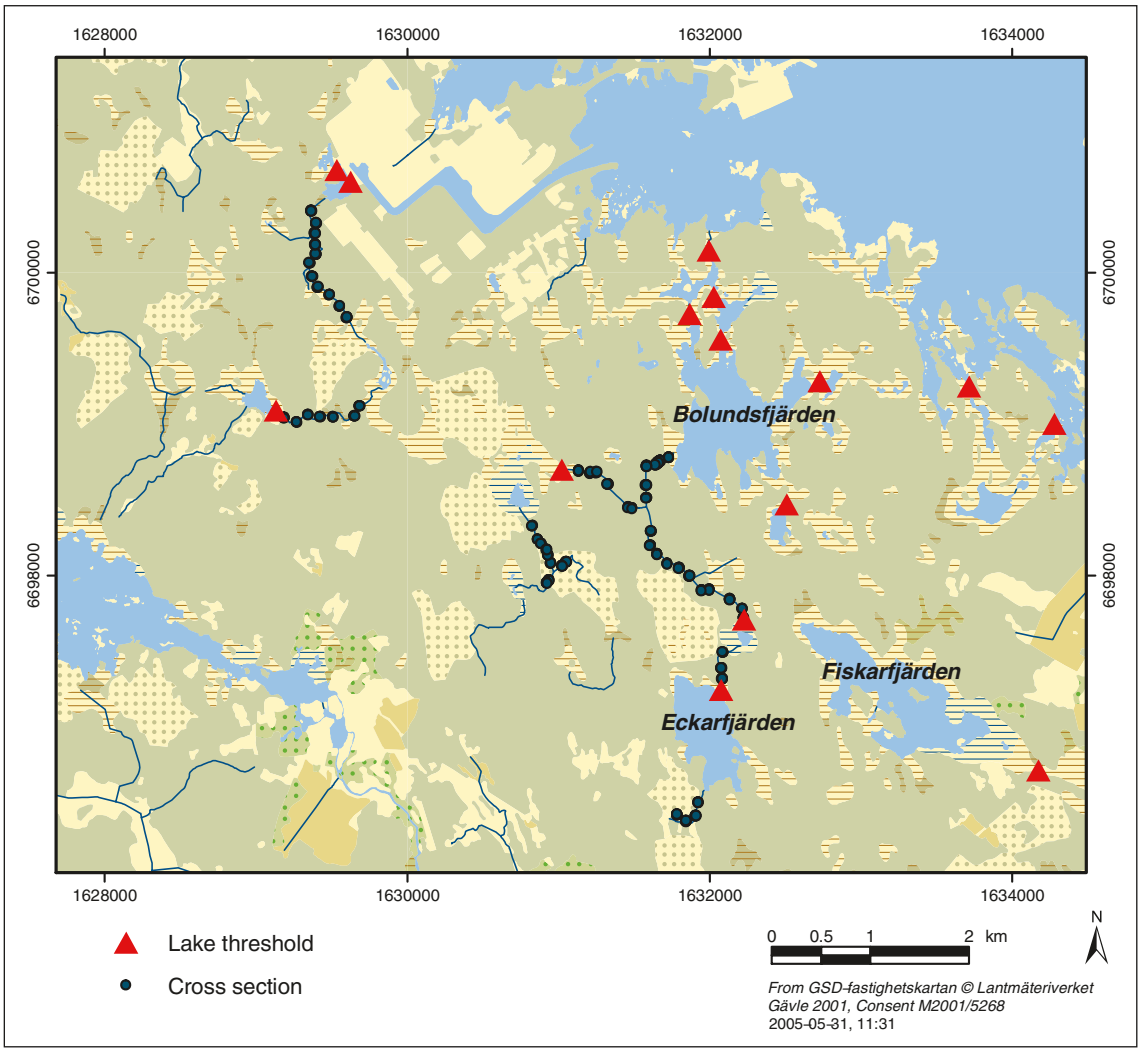

Figure 2-7. *Locations for field measurements of stream cross-sections and lake threshold levels in the Forsmark area.*

Table 2-3. Specific yield for different types of QD /Domenico and Schwartz 1998/.

Material	Specific yield (%)
Gravel, coarse	23
Gravel, medium	24
Gravel, fine	25
Sand, coarse	27
Sand, medium	28
Sand, fine	23
Silt	8
Clay	3
Peat	44
Till, silt	6
Till, sand	16
Till, gravel	16

The Manning number, M, quantifying the surface roughness at the bottom of the water courses was set to 10 $m^{1/3} s^{-1}$. This is a low value compared to smooth channels and typical rivers, but the water courses in Forsmark are very small and therefore different from those normally considered in hydraulic modelling. The bottom shape is highly irregular and there are lots of stones and vegetation; this motivates the selection of a low Manning number.

2.2.4 Vegetation

A classification of the vegetation was made based on the tree layer obtained from the inventory of the vegetation in the model area /Boresjö Bronge and Wester 2003/. In this classification, the vegetation was divided into four vegetation groups: coniferous forest, deciduous forest, shrubs and water. In the present work, the areas where no tree layer had been identified were classified as shrubs.

The properties of each vegetation group are expressed in terms of the parameters Leaf Area Index (LAI), root depth, K_c-value, and the empirical parameters used in the Kristensen and Jensen model /Kristensen and Jensen 1975/. These parameters are used in the modelling of the interception, transpiration and evaporation processes. The values of the different parameters are taken from the vegetation database associated with the MIKE SHE program.

2.3 Summary of model updates

The MIKE SHE model used in this project is based on the previous SDM F1.2 MIKE SHE model described in /Johansson et al. 2005/. Table 2-4 summarises the main updates made in the MIKE SHE model presented in this report. In addition to the modifications listed in the table, the model area has been extended to obtain a sufficient distance between the repository and the model boundaries in the open repository simulations, see Section 3.1.1.

The modifications listed in Table 2-4 and the extended model area constitute the main changes made in the present version of the Forsmark surface hydrology/near-surface hydrogeology model. In a few cases, additional changes have been to individual parameters and computational procedures. These changes are described in the text, when relevant for understanding why the results differ from those obtained with the previous model.

Table 2-4. Main differences between the previous SDM F1.2 MIKE SHE model and the present open repository model; CA denotes catchment area.

	SDM F1.2 model	Open repository model
Hydrogeological model of bedrock	Forsmark 1.1	Forsmark 1.2
Number of geological layers in the bedrock	3	8
Effective porosity of the bedrock	Generic data	Site specific data
Storage coefficient of the bedrock	Generic data	Calculated from the hydraulic conductivity of the bedrock
Basic geological model of QD (GeoEditor model)	Forsmark 1.2	Forsmark 1.2
Thickness of layer Z1[1]	1 m	0.5 m
Hydrogeological parameters of the QD	Generic data[2]	Forsmark 1.2
Meteorological data	Regional data, Örskär	Local data, Högmasten
Water courses	Water courses in CA 2 measured in the field	Water courses in CA 1 and CA 2 measured in the field

[1] The same geological model was used as a basis for the two MIKE SHE models. The bedrock surface is the same in the two model versions. In the present model, Z1 is 0.5 m instead of 1 m as in the SDM F1.2 model. This change affects also layer Z2, which becomes 0.5 m thicker than in the SDM F1.2 model.

[2] In SDM F1.2, the numerical flow model was based on generic data from the MIKE SHE database, whereas the descriptive model contained site-specific data on the hydrogeological properties of the till materials.

3 Hydrological analysis of undisturbed conditions

This chapter describes the analysis of the "natural", undisturbed surface-hydrological and near surface-hydrogeological conditions in the Forsmark area. The analysis presented constitutes an update and extension of the previously reported SDM F1.2 modelling /Johansson et al. 2005/. The objectives of the modelling discussed in this chapter are to

- present an updated (relative to SDM F1.2) base case model that makes full use of all relevant Forsmark 1.2 data,
- investigate the sensitivity to some key parameters and conditions of the model,
- study the effects of using locally measured meteorological data instead of the "reference dataset" for Örskär that was used in SDM F1.2,
- present a first comparison between modelling results and field data,
- provide a background and reference for the open repository and solute transport applications presented in Chapter 4 and Chapter 5, respectively; in particular, the undisturbed condition results is a direct input to the calculations of groundwater drawdown in the open repository cases.

First, a base case numerical model is defined by combining the data described in Chapter 2 and in /Johansson et al. 2005/ with the numerical model setup (grid and boundary conditions) presented in Section 3.1 below. This base case is also the starting point of the identification of a set of sensitivity cases; the sensitivity analysis is presented in Section 3.2. Finally, in Section 3.3, a detailed presentation of the base case model is given.

3.1 Description of numerical model and base case

3.1.1 Boundaries and numerical grid

Most of the on-shore part of the Forsmark regional model area is included in the MIKE SHE model area considered in the present work. However, the upstream (inland) boundary follows the water divide towards the river Forsmarksån catchment, rather than the boundary of the regional model area. The MIKE SHE model area, which has a size of 37.6 km^2, is shown in Figure 3-1. It can be seen that the south-western part of the regional model area is excluded. Furthermore, the model area extends some distance into the sea. This was not the case in the previous SDM F1.2 model, which included on-shore areas only.

The increase in the size of the model area is primarily motivated by the repository layout considered in the open repository transport applications, which places the repository in the north-western part of the on-shore model area. Especially in the open repository modelling, there is a need for some "safety margin" between the repository and the boundaries to obtain a reasonably precise quantification of the groundwater drawdown and inflow. When defining the horizontal extent of the model area, the deformation zones in the rock in the area were taken into consideration. The main deformation zones affecting the extent of the model area are also shown in Figure 3-1.

The reason for using the bedrock geology as the main input to this part of the modelling is that the major deformation zones also constitute major hydrogeological structures, see, e.g. /Follin et al. 2005/ that may act as boundaries for horizontal flow and transport, and for the hydrological/hydrogeological effects occurring during the open repository phase. In addition, the field-controlled catchment area boundaries identified in the surface-hydrological modelling were used to determine the position of the on-shore part of the north-western boundary.

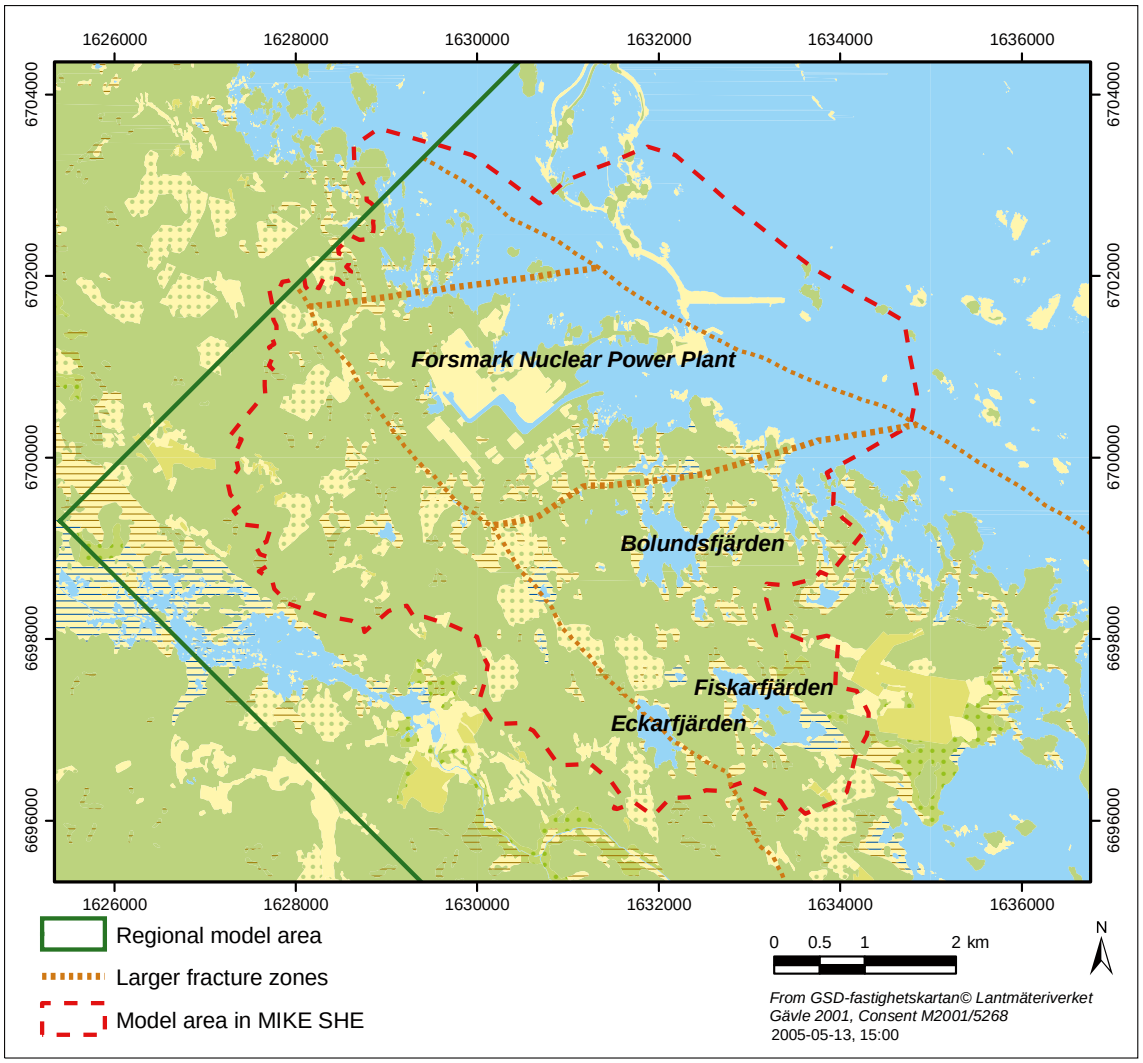

Figure 3-1. *The model area considered in the present MIKE SHE flow and transport modelling of Forsmark.*

The horizontal resolution of the calculation grid is 40 m by 40 m in the whole model area, whereas the vertical resolution varies with depth. The ground surface, as given by the topographic model, is the upper model boundary, and the bottom boundary of the model is at 135 m below sea level. MIKE SHE distinguishes between geological layers and calculation layers. The geological layers (cf. Section 2.2) are the basis for the model parameterisation, which means that the hydrogeological parameters are assigned to the different geological layers. The calculation layers are the units considered in the numerical flow model. In cases where several geological layers are included in one calculations layer, the properties of the latter are obtained by averaging of the properties of the former. The present model consists of 12 calculation layers, see Figure 3-2.

In general, the calculation layers follow the geological layers (cf. Section 2.2). However, one exception illustrated in Figure 3-2 is that the lower boundary of the uppermost calculation Z1 layer is placed at 1.0 m below the ground surface (the corresponding geological layer boundary is at 0.5 below ground). As described in Section 2.2, the stratigraphy below the lakes is different from that in the rest of the area. Specifically, the lakes are underlain by a sequence of three layers. Below the lakes, the uppermost calculation layer follows the lower boundary of the deepest of these three layers; all the lakes are underlain by two metres of till, and the Z1 boundary follows this till layer. In the sea, the lower boundary of the uppermost calculation layer follows the sea bottom (the sea itself is described as part of the Z1 layer), see Figure 3-2.

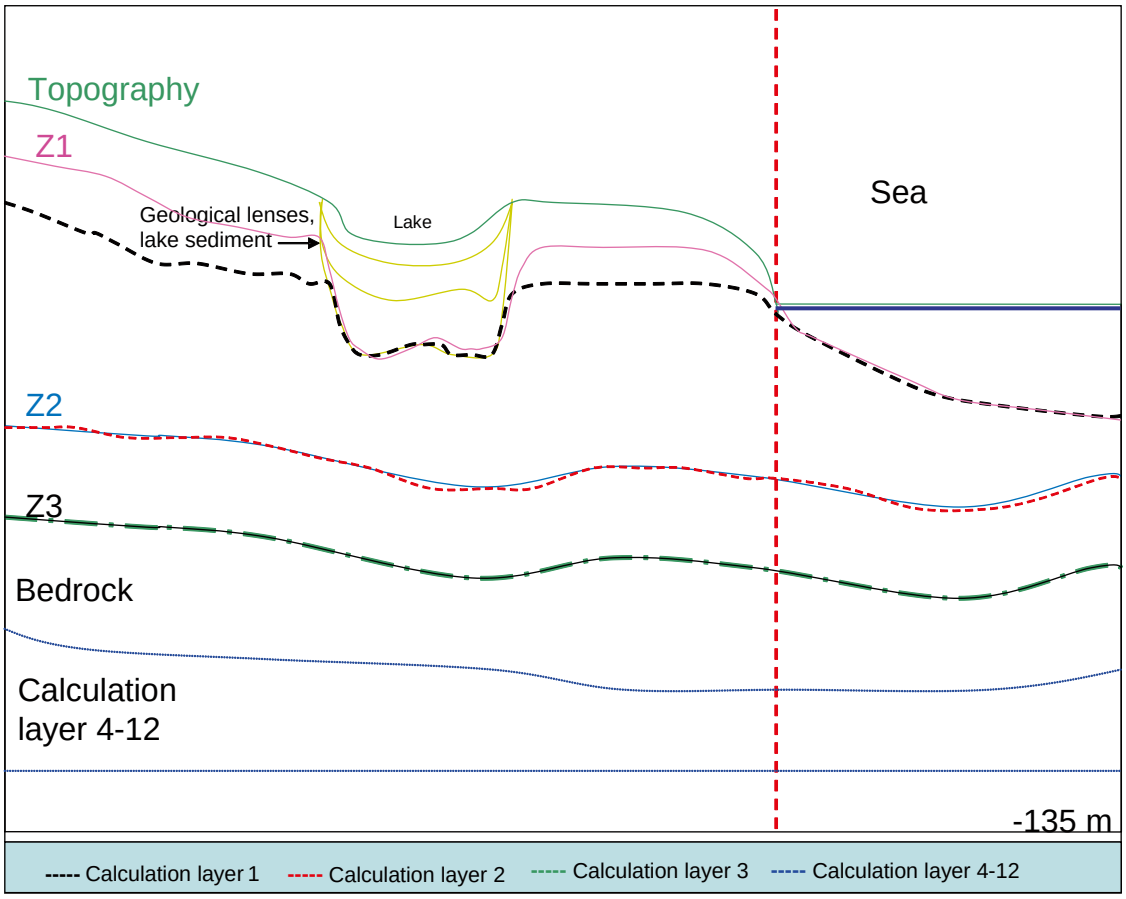

Figure 3-2. *Cross-section showing the geological layers (full lines) and calculation layers (broken lines) in the MIKE SHE model. The uppermost calculation layer is thicker than the corresponding geological layer, and integrates the three layers in the more detailed stratigraphy below the lakes.*

The groundwater divides are assumed to coincide with the surface water divides; the latter are reported in /Brunberg et al. 2004/. Thus, a no-flow boundary condition is used for the on-shore part of the model boundary. The sea forms the uppermost calculation layer in the off-shore parts of the model. Since large volumes of overland water can cause numerical instabilities, the sea is described as a geological layer consisting of highly permeable material. The hydraulic conductivity of this material is set to 0.001 ms^{-1}. The sea part of the uppermost calculation layer has a fixed head boundary condition, with the head set to 0 metre below sea level.

The top boundary condition is expressed in terms of the precipitation and potential evapo-transpiration. The precipitation is assumed to be uniformly distributed over the model area, and is given as a time series. The boundary condition for the saturated zone is described by the processes in the unsaturated zone. Water is extracted from the model volume by the “river network” modelled by the MIKE SHE channel flow compartment. The amount of water flowing to the channel flow compartment depends on the conditions in the other compartments of the model. Water is transported to the water courses via overland flow, and from the saturated zone.

The bottom boundary condition is a fixed-head condition. Model results from the Forsmark 1.2 DarcyTools groundwater flow modelling /Follin et al. 2005, SKB 2005/ are used as input data when setting the bottom boundary condition. The calculated hydraulic head from 135 m below sea level is imported to the MIKE SHE model. The time step used in the Darcy Tools simulations (one year) is much longer than that in the MIKE SHE modelling, which implies that short-term temporal variations cannot be captured. Thus, the bottom boundary condition in the MIKE SHE model is assumed to be constant with time.

3.1.2 Initial condition and handling of temporal variations

The simulations have been performed using meteorological input data for the one-year period from May 2003 to May 2004. Locally measured data on the meteorological parameters, and also groundwater level data, are available for this period; this is the main reason for the choice of simulation period.

A so-called “hot start” was used to generate the initial conditions of the model. In the base case simulation, the model was run until semi steady-state conditions were reached. This means that the model was run, with the time-dependent boundary conditions given by the meteorological data, until the variations during the year had stabilised (e.g. the pressure at a certain point shows more or less the same variation from one year to the next). The results from this simulation were used as initial conditions for the one-year simulation used to generate the final simulation results.

In the simulations of the sensitivity cases, the initial conditions for the simulations were given by a “hot-start” from the base case simulation, which means that the initial conditions were taken from the output of a long-term simulation where the hydrological conditions were allowed to stabilise using the base case input data. The simulations of the sensitivity cases were run for a single year only, i.e. without the cycling of the meteorological input that was performed for the base case.

The length of the time step in MIKE SHE is varying with time during the simulation. A maximum time step is specified. This time step can be reduced depending on the meteorological conditions and the water flow or head changes in the calculation cells. In the present simulations, the maximum time step for the saturated zone was set to three hours and the maximum time step for the unsaturated zone, the overland flow compartment and the evapotranspiration calculations was set to one hour.

3.2 Sensitivity analysis

3.2.1 Description of sensitivity cases

Model discretisation and bottom boundary condition

The purpose of this part of the sensitivity analysis is to investigate the impact on the model output of

i) the vertical discretisation of the model,

ii) the position of the bottom boundary,

iii) the type of bottom boundary condition.

In the base case, the horizontal discretisation is 40 m, whereas the vertical discretisation, except for as described above, follows the definition of the geological layers. Moreover, in the base case, a fixed pressure is assumed at the bottom boundary of the model (at a depth of 135 m below sea level). Similar to the hydrogeological properties of the rock, the horizontal pressure distribution at this depth is obtained from the hydrogeological modelling of the rock (i.e. the DarcyTools version 1.2 modelling).

In order to investigate the sensitivities to the parameter types listed above, the following simulation cases (sensitivity cases SA1_1–SA1_6) are defined:

- SA1_1: The thickness of the uppermost calculation layer is changed from 1 m to 0.5 m.
- SA1_3: A no-flow condition is applied at the bottom boundary.

- SA1_4: The vertical extent of the model is changed such that the bottom of the model is placed at 450 m below sea level. As in the base case, the bottom boundary condition is a head boundary condition; in this case, the calculated head from DarcyTools at the level of 450 m below sea level is imported to the MIKE SHE model. Five new geological and computational layers, between 135 m below sea level and 450 m below sea level were introduced to cover the increased depth of the model.
- SA1_5: The vertical extent of the model is reduced such that the bottom boundary is placed at 20 m below sea level. The calculated head at this elevation in the Forsmark 1.2 DarcyTools model is used as boundary condition.
- SA1_6: The bottom boundary is placed at 20 m below sea level using a no-flow condition at the boundary.

One parameter/condition is changed in each sensitivity case, whereas all other parameters are kept as in the base case. The sensitivity cases SA1_1 to SA1_6 are summarised in Table 3-1 below.

Hydraulic properties of QD

In near-surface groundwater flow modelling, the hydraulic properties (hydraulic conductivity, specific yield, and specific storage coefficient) of Quaternary deposits (QD) are generally subject to a large degree of uncertainty. In the present case, the interaction between groundwater and surface water is also taken into account, which implies that the quantification of surface water flow may also be influenced by the uncertainty associated with the hydraulic properties of the QD.

The sensitivity cases defined in this section are used to investigate the sensitivity of the model output to the assigned hydraulic properties of QD. It should be noted that there are site investigation data (slug tests and grain-size distribution curves) on the hydraulic conductivity of the sandy till, whereas there is scarce or no site investigation data for other hydraulic parameters and soil types. For the sensitivity analysis, the following simulation cases are defined:

- SA2_1a–c: The vertical hydraulic conductivity (K_v) of QD layers Z1, Z2 or Z3 is reduced by a factor of 10; K_v is changed in one layer in each sensitivity case.
- SA2_2a–b: The vertical hydraulic conductivity (K_v) of all QD layers Z1, Z2 and Z3 is reduced (2a) or increased (2b) by a factor of 10; K_v is changed in all layers in each case.
- SA2_3a–b: The horizontal hydraulic conductivity (K_h) of all QD layers Z1, Z2 and Z3 is reduced (3a) or increased (3b) by a factor of 10; K_h is changed in all layers in each case.
- SA2_4: The horizontal hydraulic conductivity (K_h) of the uppermost QD layer Z1 is increased by a factor of 10.

Table 3-1. Definition of simulation cases for investigating the impact of model discretisation and bottom boundary condition. In all cases, the remaining parameters and conditions are unchanged compared to the base case.

Case	Vertical disctretisation	Bottom boundary condition
SA1_1	Calculation layer 1 = 0.5 m	Base case[1]
SA1_3	Base case	No-flow boundary at 135 m below sea level
SA1_4	Base case	Head boundary from DT[1] at 450 m below sea level
SA1_5	Base case	Head boundary from DT[1] at 20 m below sea level
SA1_6	Base case	No-flow boundary at 20 m below sea level

[1]Head distribution delivered from the DarcyTools modelling team /Follin et al. 2005/.

- SA2_5a–b: The specific yield (S_y) of all QD layers Z1, Z2 and Z3 is increased (5a) or decreased (5b) by 50%; S_y is changed in all layers in each case.
- SA2_6a–b: The storage coefficient (S) of all QD layers Z1, Z2 and Z3 is increased (6a) or decreased (6b) by 50%; S is changed in all layers in each case.

All parameters not subject to changes have the same values as in the base case. The definitions of cases SA1_1 to SA2_6 are summarised in Table 3-2 below.

3.2.2 Results of the sensitivity analysis

The results of the sensitivity analysis have been analysed in terms of different components of the water balance (total evapotranspiration, transpiration and runoff) and the depth to the groundwater table.

Model discretisation and bottom boundary condition

The first sensitivity case, SA1_1, where the thickness of the uppermost calculation layer was set to 0.5 m, showed a large effect on the total evapotranspiration when compared to the base case (Table 3-3). The calculated total evapotranspiration decreases when the thickness of the uppermost calculation layer is reduced. In Mike SHE, the evapotranspiration calculations are activated in the uppermost calculation layer only. This is probably the reason why the evapotranspiration decreases when a thinner uppermost layer is considered; the groundwater table is more likely to be below the uppermost layer, and hence part of the unsaturated zone processes are inactivated when this layer is thin.

Table 3-2. Definitions of simulation cases for investigating the impact of the hydraulic properties of the QD; Kv, Kh, Sy and S denote vertical and horizontal hydraulic conductivity, specific yield and storage coefficient, respectively, index "BC" stands for base case, and "–" indicates that the base case parameter value is used for the parameter.

Case	K_h (ms^{-1})	Layer	K_v (ms^{-1})	Layer	S_y (–)	Layer	S (m^{-1})	Layer
SA2_1a	–		$K_{v,BC}$·0.1	Z1	–		–	
SA2_1b	–		$K_{v,BC}$·0.1	Z2	–		–	
SA2_1c	–		$K_{v,BC}$·0.1	Z3	–		–	
SA2_2a	–		$K_{v,BC}$·0.1	Z1, Z2, Z3	–		–	
SA2_2b	–		$K_{v,BC}$·10	Z1, Z2, Z3	–		–	
SA2_3a	$K_{h,BC}$·0.1	Z1, Z2, Z3	–		–		–	
SA2_3b	$K_{h,BC}$·10	Z1, Z2, Z3	–		–		–	
SA2_4	$K_{h,BC}$·10	Z1	–		–		–	
SA2_5a	–		–		$S_{y,BC}$+50%	Z1, Z2, Z3	–	
SA2_5b	–		–		$S_{y,BC}$–50%	Z1, Z2, Z3	–	
SA2_6a	–		–		–		S_{BC}+50%	Z1, Z2, Z3
SA2_6b	–		–		–		S_{BC}–50%	Z1, Z2, Z3

Table 3-3. Results from sensitivity case SA1_1.

	Total evapotranspiration ($mm \cdot year^{-1}$)	Total transpiration ($mm \cdot year^{-1}$)
Base case	455	197
SA1_1	290	51

As shown in Table 3-3, the difference in the calculated annual transpiration (146 mm) is almost the same as the corresponding difference in the evapotranspiration (165 mm), which indicates that most of the decrease in the evapotranspiration can be attributed to the transpiration process. Furthermore, the total potential evapotranspiration during the modelled period is 435 mm, which implies that the calculated evapotranspiration in case SA1_1, 290 mm, is not realistic. Since the geological layers and the calculation layers are separate units in MIKE SHE, the use of an uppermost calculation of larger thickness than the corresponding geological layer causes no larger problems. The thickness of geological layer Z1 is still 0.5 m, but the minimum thickness of the uppermost calculation layer is 1 m in the base case and the rest of the sensitivity cases.

Figure 3-3 and 3-4 illustrate how the groundwater levels are changing during the modelled year for the base case and the sensitivity cases SA1_3–SA1_6, i.e. the cases testing different positions of and conditions at the bottom boundary of the model. Calculated time series are taken from two different points, a topographic height and a low point in the topography. The results from cases SA1_3–SA1_4 indicate that the vertical extent of the model is sufficient; the water balance and the position of the groundwater table do not change significantly when the boundary condition at the bottom boundary at 135 m below sea level is changed. If the vertical extent of the model is increased to 450 m below sea level only small effects on the surface/near-surface system can be observed.

If, on the other hand, the vertical extent of the model is reduced such that the bottom boundary is placed at 20 m below sea level, then responses in terms of changes in both the water balance and the groundwater level are evident. When the calculated head from DarcyTools (at 20 m below sea level) is used as bottom boundary condition, case SA1_4, the water balance is strongly affected. The annual runoff increases to 563 mm, as compared to 151 mm in the base case, the annual evapotranspiration decreases to 376 mm (base case: 455 mm), and the groundwater table rises.

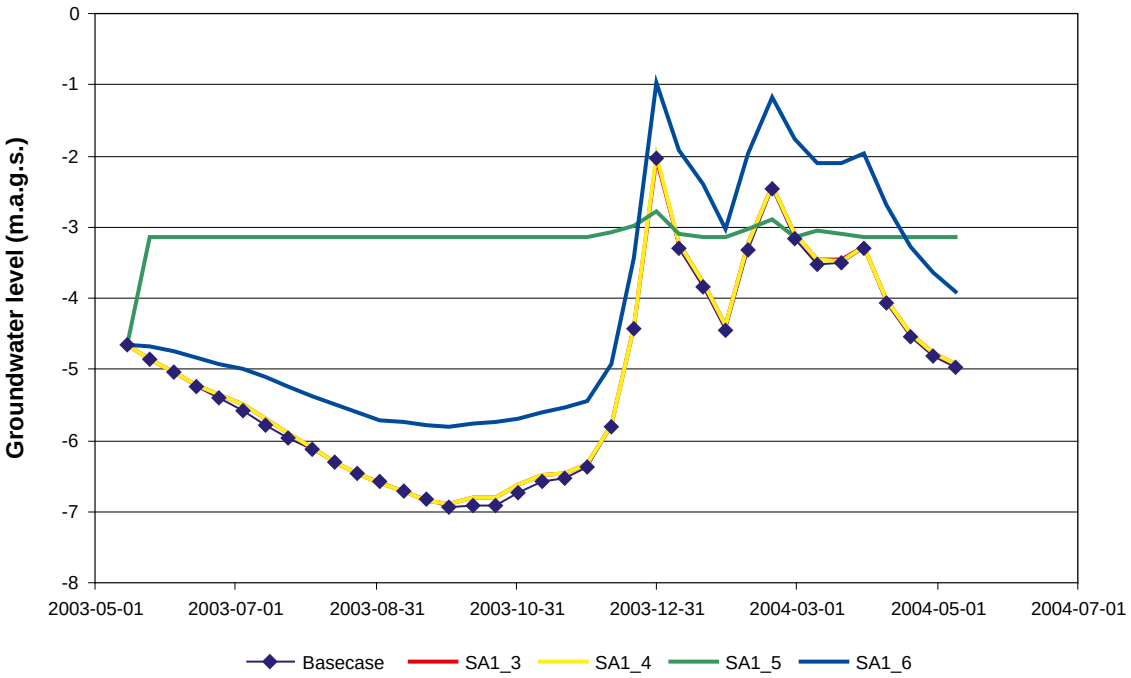

Figure 3-3. *Groundwater levels at a topographic height, expressed in metres above ground surface (m.a.g.s.), for the base case and the sensitivity cases SA1_3 to SA1_6; note that the SA1_3 and SA1_4 results are identical (the yellow line covers the red one).*

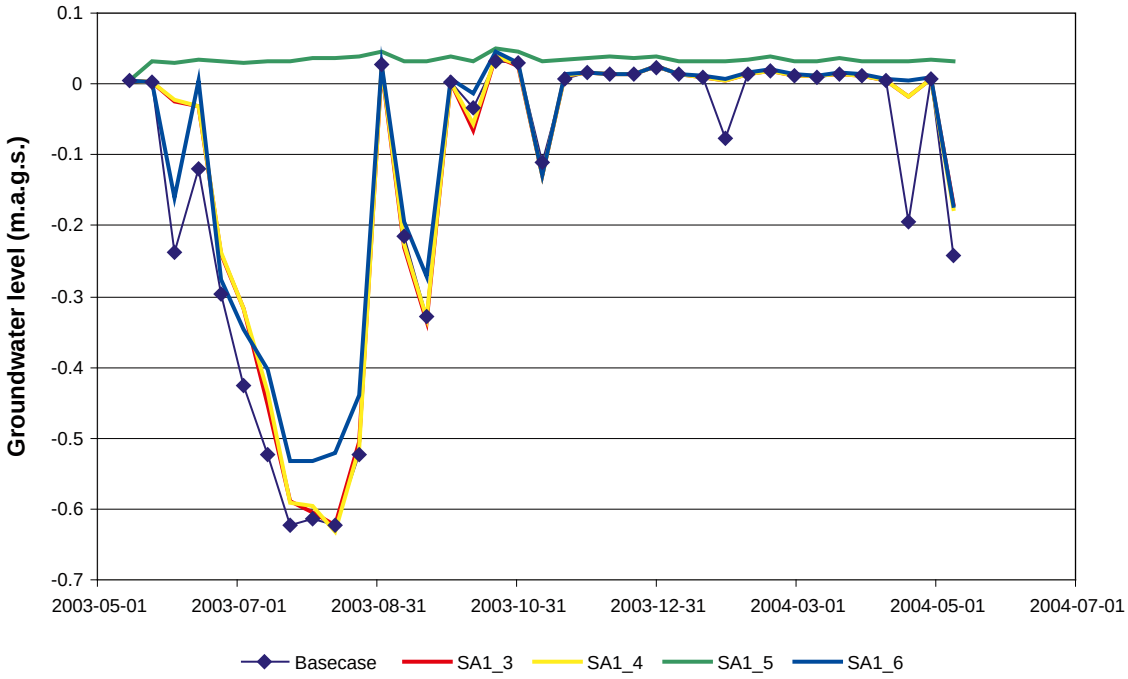

Figure 3-4. *Groundwater levels at a topographic low, expressed in metres above ground surface (m.a.g.s.), for the base case and the sensitivity cases SA1_3 to SA1_6.*

It seems to be a mismatch between the DarcyTools and MIKE SHE models making the calculated head at 20 m below sea level in DarcyTools "too high", such that water is generated at the bottom boundary to maintain the head. This inflow leads to a large decrease in the infiltration in the MIKE SHE model, which causes almost the whole precipitation to become surface run-off. In sensitivity case SA1_5, where the bottom boundary is at 20 m below sea level but a no-flow boundary condition is used, the groundwater table is rised compared to the base case. However, the different components of the water balance are not influenced to the same extent as in case SA1_4. The total volume where water can be stored is much smaller in case SA1_4 than in the base case, which is probably the reason for the higher groundwater levels.

It can also be seen in the figures, especially in Figure 3-4, that the cases with a bottom boundary at 450 m below sea level actually show better agreement with the case having a no-flow boundary at 135 m below sea level than with the base case (prescribed head). Assuming that the cases with the deepest boundary location are the most "correct", this may be taken as an indication that a no-flow condition should be used as base case. This would be based on the reasoning that the error introduced by attempting to model the inflow by use of the imported head boundary is larger than that introduced by not taking the inflow into account at all. However, the similarities between the sensitivity cases, and their differences relative to the base case, may also reflect the differences in the simulation procedure, i.e. the fact that the sensitivity cases were run for a single year only.

Hydraulic properties of QD

The results of the sensitivity cases testing the effects of the hydraulic properties on the surface hydrology and near-surface hydrogeology are summarised in Figure 3-5 and 3-6. Note that different vertical scales are used in the two figures. As expected, the depth to the groundwater table and the temporal groundwater level variations are larger at the topographic height than in the point of lower elevation; the difference between the calculated maximum and minimum levels for the base case are approximately 5 m (Figure 3-5) and 0.6 m (Figure 3-6), respectively. Similarly, the maximum absolute differences between the sensitivity cases are larger at the

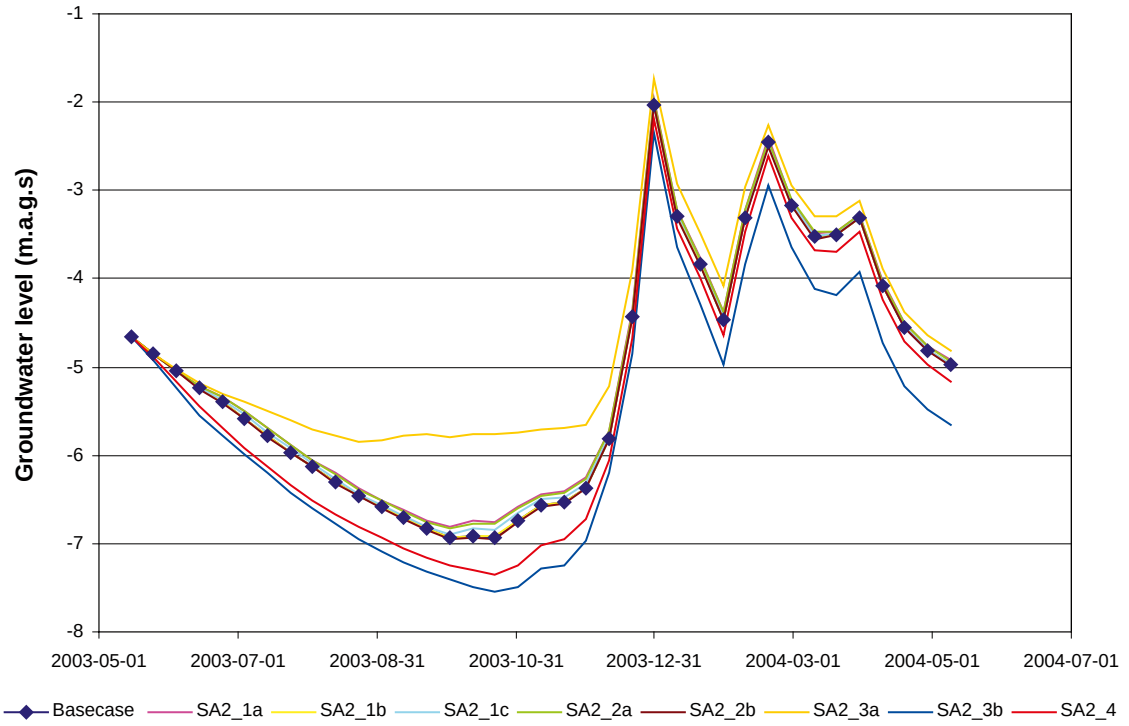

Figure 3-5. *Groundwater levels at a topographic height, expressed in metres above ground surface (m.a.g.s.), for the base case and the sensitivity cases SA2_1 to SA2_4.*

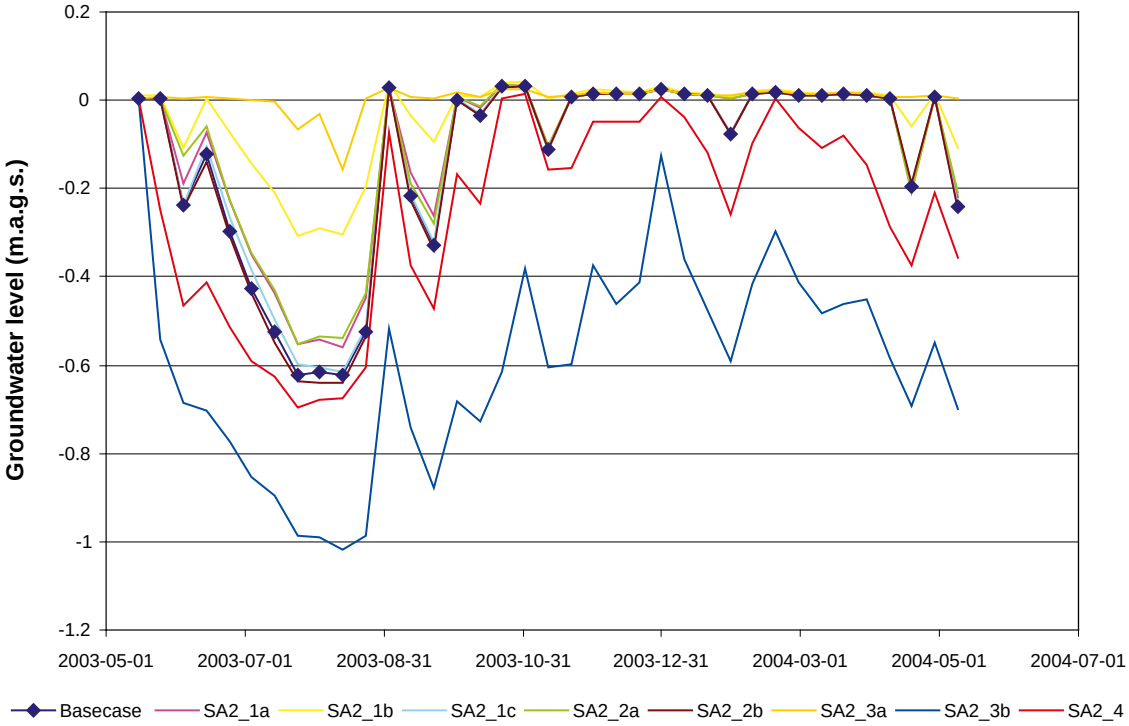

Figure 3-6. *Groundwater levels at a topographic low, expressed in metres above ground surface (m.a.g.s.), for the base case and the sensitivity cases SA2_1 to SA2_4.*

topographic height (almost 2 m, in October) than in the low-lying point (1 m, in July). However, the relative differences between the sensitivity cases (i.e. differences relative to the groundwater depth) are larger in the topographic low point.

A general observation from the results of the base case and the sensitivity cases SA2_1 to SA2_4 is that the groundwater levels are sensitive to changes in the hydraulic conductivity values assigned to the Quaternary deposits (even though the effects can be regarded as small in the topographic low point). However, the overall water balance, as expressed in terms of precipitation, total evapotranspiration and total runoff from the area, was not affected by the parameter changes tested in the sensitivity analysis. The total calculated transpiration changed 0.5–1 mm between the different cases, whereas the total calculated runoff from the area differed only ± 1 mm between sensitivity cases SA2_1 to SA2_4.

The results show that variations in the horizontal hydraulic conductivity, K_h, have the largest impact on the calculated groundwater levels. Specifically, the case in which the K_h-values of all QD layers are increased by a factor of ten, SA2_3b, shows the largest lowering of the groundwater level relative to the base case, whereas the corresponding case with a reduction of K_h by a factor of ten in all QD layers, SA2_3a, leads to the largest rise in groundwater level. This holds for both observation points considered, see Figure 3-5 and 3-6. Furthermore, a relatively large lowering of the groundwater level is obtained for the case where the K_h-value is increased in the uppermost layer only (case SA2_4). This case results in a groundwater level between the base case and case SA2_3b in both observation points.

In Figure 3-6, it is also interesting to note that cases SA2_3b and SA2_4 predict groundwater levels that lie at least a couple of decimetres below ground during (almost) the whole year, whereas the other cases indicate ponding on the ground surface for at least some six months during the simulated year. This means that when K_h is increased by an order of magnitude relative to the base case, the capacity for horizontal flow in this particular point becomes sufficient for transferring the groundwater to the surface water system without ponding and overland flow. However, it seems that this effect, if occurring in other/larger parts of the model area, has only negligible effects on the overall water balance.

The effects of variations in the vertical hydraulic conductivity, K_v, are generally much smaller than those related to K_h. The only K_v case that shows significant deviations from the base case is case SA2_1b, in which K_v is reduced by a factor of ten in layer Z2 only. This case results in a higher groundwater level than the base case, but the effect is observable in the low-lying point only (Figure 3-6).

The present sensitivity study also shows that the surface/near-surface system is insensitive to the tested changes in the specific yield and the storage coefficient of the QD (results not shown). It should, however, be noted that the sensitivity analysis with respect to the storage coefficient and the specific yield was not as detailed as the analysis of the hydraulic conductivity, and that the ranges in parameter values were smaller. Case SA2_5, in which the specific yield was modified, shows only a very small groundwater level response. Since the storage coefficient is used under confined conditions only, the head in the lowest QD layer was studied. It was found that the variation in the head was not affected by the changes in the storage coefficient.

3.2.3 Evaluation of the sensitivity analysis

The results of the first part of the sensitivity analysis indicate that the vertical extent of the base case model (from the ground surface to 135 m below sea level) is sufficiently large, and that it may constitute a reasonable compromise between the “extreme” alternatives tested. The model with the largest vertical extent, in which the bottom boundary was placed at 450 m below sea level showed only very small differences compared to the base case. Conversely, it appeared difficult to obtain a working coupling between groundwater in QD and rock when using a model with its bottom boundary as shallow as 20 m below sea level. For the two deeper boundary locations tested, it was also found that the type of boundary condition used (prescribed head or no-flow) had only very small effects on the results. This is probably due to the low hydraulic conductivity assigned to the fractured rock in the model, which implies very small groundwater flow rates in the rock.

The second part of the sensitivity analysis concerned the hydraulic parameters of the QD, primarily the horizontal and vertical hydraulic conductivities. The results showed that some of the parameter variations had relatively large effects on the groundwater levels, especially the sensitivity cases involving the horizontal hydraulic conductivity. However, only very small effects on the overall water balance of the model volume were observed. An evaluation of the various types of model outputs obtained shows that the parameters assigned to the base case model generated reasonable results. In particular, surface water levels in the lakes are in the right ranges, water balance components are in agreement with regional values, and the water-saturated areas in the model coincide with lakes and wetlands observed in the field.

Based on this evaluation it is decided not to change the hydraulic parameters from their values in the base case. Another argument in favour of keeping the base case parameters is that these are based on the available site data (at least the parameters assigned to the till, which is the dominant QD in the area). Thus, the conclusion of the sensitivity analysis is that no modifications of the initial base case model setup are needed, neither in terms of the bottom boundary condition nor concerning the hydraulic parameters. A detailed presentation of the results from the base case simulation is given in the next section.

3.3 Detailed presentation of the base case results

Having concluded that the initial base case parameterisation that provided the starting point of the sensitivity analysis can be used as base case also in the remaining part of this study, i.e. as a reference case for the open repository analysis (Chapter 4) and as input to the transport modelling (Chapter 5), we present in this section the results of the base case simulation. The presentation includes calculated water balances, surface water discharges, and groundwater levels. It should be noted that no calibration has been performed. However, a limited comparison between measured and calculated groundwater levels is reported in Section 3.3.4.

3.3.1 Water balance

The water balance presented here represents a sub-volume within the total model volume. In the model, the sea is represented as a highly conductive geological layer with a fixed head. Since the on-shore part of the model area is the main focus of the water balance calculation, the model volume overlain by the sea is excluded when calculating the water balance components. As indicated in Figure 3-7, this implies that the water exchange across the internal boundary along the coastline must be considered in the balance calculation. For simplicity, this internal boundary is assumed to be vertical from the coastline down to the bottom boundary.

The water balance components presented in the following are spatially averaged values, expressed in terms of mm·year^{-1}, representing the whole on-shore part of the model area. This means that the volumetric flow associated with a certain component is distributed evenly over the land area in the model. For some components, such as the evapotranspiration components that are inactive in where there is surface water, this implies that the values presented here are lower than they would have been if such areas had been excluded. Furthermore, these results obviously do not give any information about the spatial variability in the various components.

The calculated water balance components are presented in Figure 3-8. The figure shows the flow of water between the different compartments in the land part of the model, and the flows across the boundaries where boundary conditions other than no-flow were prescribed. The accumulated precipitation (P) during the modelled one-year period is 597 mm, and the total evapotranspiration (E_{tot}) is calculated to 455 mm; this implies that $P–E_{tot}$ = 142 mm. The total evapotranspiration is the sum of the evaporation from snow (12 mm) and intercepted water (123 mm), from ponded water on the soil surface (overland water; 36 mm), the upper soil layers (unsaturated zone; 64 mm) and the saturated zone (23 mm), and the transpiration from plants (197 mm); thus, E_{tot} is obtained by summation of all evapotranspiration components in Figure 3-8.

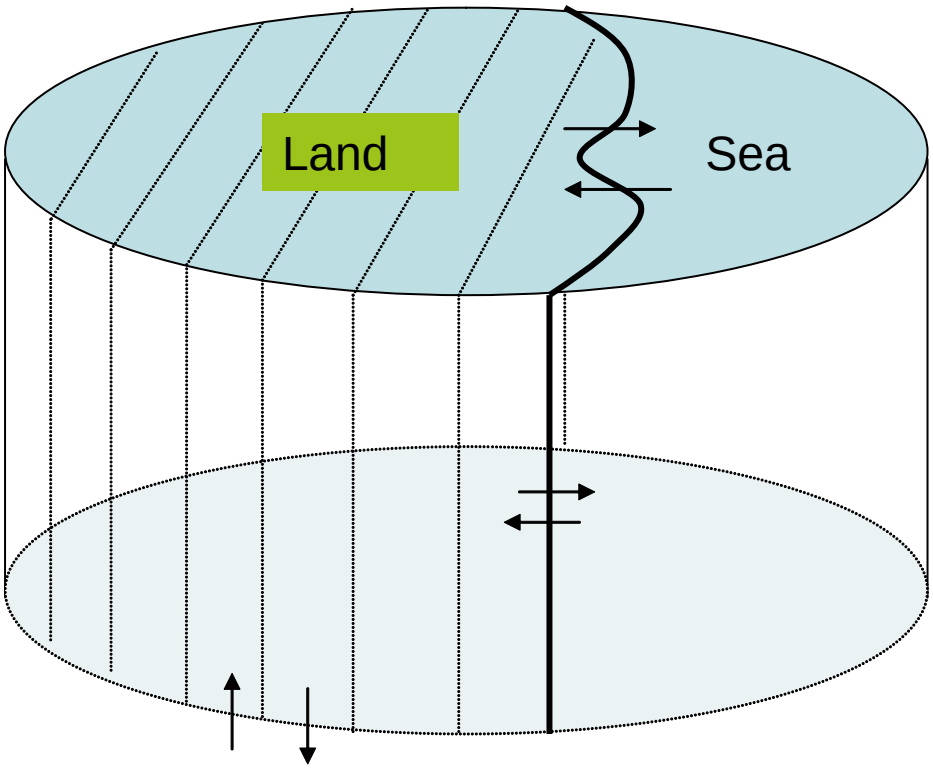

Figure 3-7. *Sub-volume considered in the water balance calculations. The water balance is calculated for the part of the model volume where there is land at the surface only.*

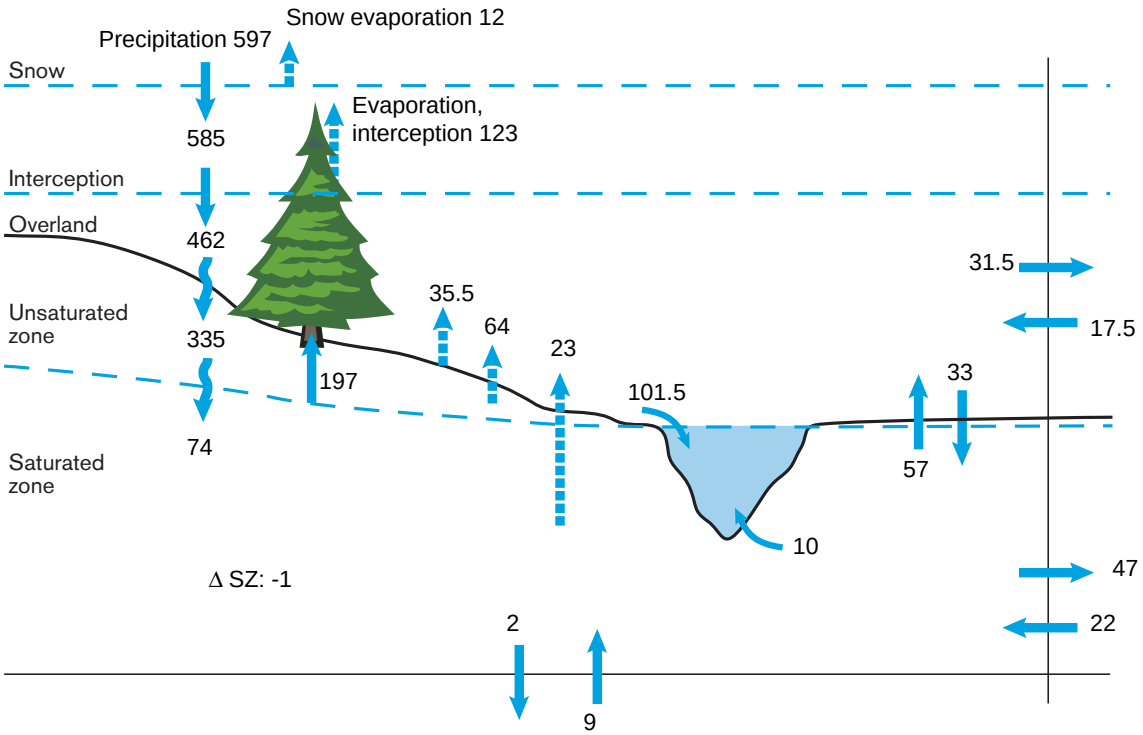

Figure 3-8. *Calculated water balance for the Forsmark area; all results are expressed in mm for the modelled one-year period (i.e. mm·year^{-1}). The arrows crossing the vertical boundary indicate the exchanges across the boundary at the coastline; the upper ones are the overland inflow and outflow, and lower ones the corresponding groundwater flows.*

The average specific runoff from water courses and overland flow is 126 mm (calculated as 102+10+32–18 = 126). During the simulation period, there is a net outflow of 25 mm of groundwater from the saturated zone to the saturated zone below the sea. There is also a net inflow of 7 mm across the bottom boundary. Including also the groundwater boundary flows in the calculation, the total runoff from the area is calculated to 144 mm (126+25–7 = 144; note that $P–E_{tot}$ = 142). It can be noted that the total evapotranspiration corresponds to about three times the runoff, implying that uncertainties in the evapotranspiration modelling may have a large effect on the calculated runoff.

Most of the water turnover takes place in the upper part of the model volume, whereas the (groundwater) flow rates at depth are small. Figure 3-8 shows that the (net) groundwater recharge from the unsaturated zone to the saturated zone is 74 mm; only 2 mm of this water percolates down into the deep bedrock. The results also show that 92% of the total groundwater flow over the boundary to the sea occurs in the uppermost calculation layer. As mentioned above, the evapotranspiration processes are modelled in the uppermost calculation layer only. Concerning the overland flow at the sea boundary, the inflow component can be explained by temporal and spatial variations in the flow combined with the use of a fixed position of the boundary.

The groundwater flow in the bedrock is dominated by the larger deformation zones; the flow of water in the rock mass in between them is very small. The discharge of the groundwater that has reached the saturated zone takes place mainly via the water courses and the overland flow parts of the model. The net groundwater runoff across the model boundary is approximately 12% of the total runoff (cf. above), which means that most of the groundwater discharges locally to the surface water system before it flows across the model boundary.

A comparison between the present water balance results and those presented in SDM F1.2 /Johansson et al. 2005/ shows relatively large differences, both in some components of the overall water balance (precipitation, total evapotranspiration and total runoff) and in the distribution between different “sub components”. Table 3-4 summarises some of the main water balance components and also selected “sub components” obtained in the two modelling exercises. It can be seen in the table that the total runoff is much lower in the present model than in the previous SDM F1.2 model. Most of the decrease in the total runoff can be explained by the lower precipitation during the 2003–2004 period (597 mm) compared to SDM F1.2 (674 mm). However, the runoff is also reduced by the slightly higher E_{tot} obtained in the present model (455 mm compared to 441 mm; all mm figures refer to one-year periods).

Table 3-4. Comparison of water balance calculations in the present work and in the previous SDM F1.2 modelling; UZ and SZ denote unsaturated and saturated zones, respectively. All figures are for one-year periods (i.e. mm year^{-1}). A negative value in the difference column indicates a lower value in the present model than in SDM F1.2.

	Present model (mm)	SDM F1.2 (mm)	Difference (mm)
Main components			
Precipitation, P	597	674	–77
Total evapotranspiration, E_{tot}	455	441	+14
Total runoff	144	226	–82
Selected sub components			
Evaporation from interception	123	163	–40
Evaporation from ponded water	36	144	–108
Evaporation from UZ and SZ	87	29	+58
Transpiration	197	70	+127
Overland → water courses	102	113	–11
Groundwater → water courses	10	66	–56

Thus, the differences in the overall water balance are to large extent caused by the differences in the meteorological input data; SDM F1.2 used data from the SMHI station Örskär for the "reference year" 1988, whereas the present modelling is based on locally measured data from 2003–2004. Thus, the two modelling exercises use meteorological datasets from two different individual years (actual time series) from two different stations. Whereas the Örskär dataset was selected to represent a "reference year" (precipitation and other variables corresponded to long-term averages), the dataset considered in the present work represents a "randomly selected" year.

As shown in Table 3-4, there are also large differences in some of the "sub components" of the water balance. Even though E_{tot} is almost the same, its distribution upon different components has changed considerably. In particular, the annual transpiration has increased from 70 mm in the SDM F1.2 model /Johansson et al. 2005, Table 5-8/ to 197 mm in the present work, which almost corresponds to the decrease in the evaporation from ponded water (from 144 mm to 36 mm). The main reason for these changes is that the SDM F1.2 model included an unrealistically large proportion of areas covered with ponded water. Most of these "excess ponded areas" outside the mapped lakes and wetlands are not observed in the present modelling results.

The main reasons for the decrease in ponded areas are improvements in the evaporation/unsaturated flow calculations and that the surface resistance governing the overland flow has been reduced. These modifications lead to an increase in the transpiration (no transpiration takes place in areas with ponded water), and a decrease in the evaporation from ponded water. Also the increase in evaporation from the unsaturated and saturated zones is probably a result of the decrease in water-covered areas.

Whereas the SDM F1.2 model had a boundary along the coastline, the corresponding boundary in the present model is placed some distance away from the coastline (in the sea). A comparison with the results in /Johansson et al. 2005/ shows that the present model has a smaller overland flow and a larger groundwater flow to the sea. However, the total outflow across the boundary does not change dramatically; it decreases with almost 30% compared to SDM F1.2. Thus it can be concluded that the main differences in comparison with the previous model are due to the smaller precipitation in the present one, whereas the main reason for the redistribution among the evapotranspiration terms is the lower flow resistance in the overland flow component.

3.3.2 Discharge in water courses

As described above, the surface runoff is calculated as the net flow of water to the MIKE 11 model plus the water that leaves the model area as overland flow. MIKE 11 calculates the discharges and water levels in the water courses. The calculated discharge in a water course varies during the year. This is illustrated in Figure 3-9, which shows the hydrograph calculated for the water course that goes into Lake Bolundsfjärden (i.e. one of the measured water courses in Figure 2-7), in a cross-section point just upstream of the inlet to the lake. It is seen that the calculated hydrograph in the water course is highly transient during the year, i.e. it has several marked peaks and periods of zero or very low flow rates between the peaks.

These results indicate that the flow is highly dependent on the weather conditions. However, it can also be seen in Figure 3-9 that there is not a perfect correlation between the discharge peaks and those in the precipitation time series (the highest precipitation peaks do not necessarily correspond to the highest discharge peaks). The maximum discharge occurs in the end of December, during a longer period of intensive rain. It should be noted that Figure 3-9 is just one example of the results from the MIKE 11 model; discharges and water levels in all points along the water courses are available as outputs from the modelling.

At the time of the present modelling, no time series of measured discharges in the water courses were available. Therefore, no comparison or calibration against measured values has been made. The total accumulated discharge in the water courses from the three main lakes in the area (Lake Bolundsfjärden, Lake Fiskarfjärden and Lake Eckarfjärden) are listed in Table 3-5. This

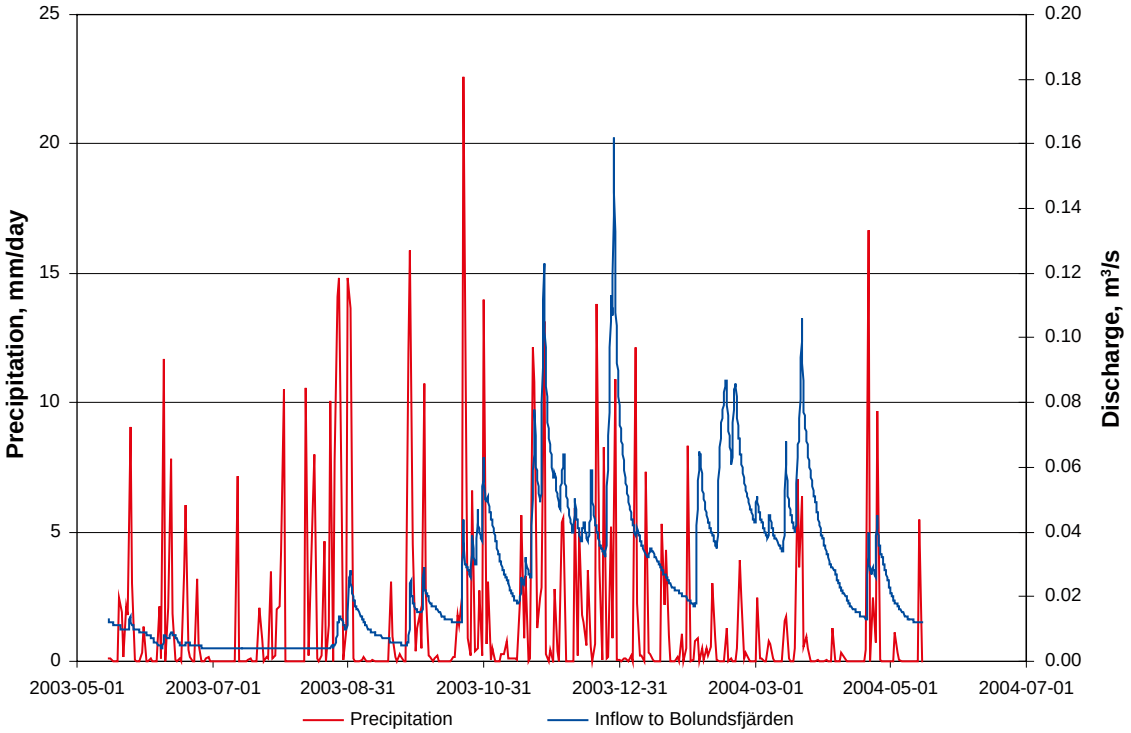

Figure 3-9. *Calculated discharge in the water course just upstream of the inlet to Lake Bolundsfjärden and the precipitation time series used in the modelling.*

Table 3-5. Calculated total and specific runoff from three lakes in the model area.

Lake	Total average runoff, Ls^{-1}	Specific runoff, $Ls^{-1}\ km^{-2}$
Bolundsfjärden	45	5.6
Fiskarfjärden	19	6.5
Eckarfjärden	7	5.4

table also shows the corresponding specific (area-normalised) discharges. It can be seen that these show relatively small differences. The largest specific runoff is calculated for the catchment of Lake Fiskarfjärden and the smallest for the Lake Eckarfjärden catchment; the difference is approximately 20%.

3.3.3 Groundwater table

Generally, the calculated groundwater level within the model area was found to be close to the ground surface, see Figure 3-10. The mean groundwater level during the simulated year May 2003–May 2004 (i.e. spatially averaged over the model area and temporally averaged over the simulation period) was calculated to 1.1 m below the ground surface. The maximum calculated depth to the groundwater table was approximately 8 m below the ground surface, which was obtained in the area of relatively higher elevation in the south-western part of the model area.

The contours of mapped lakes, wetlands and water courses in the model area are indicated in Figure 3-10 (the lake contours and water courses are marked with black lines and the wetland areas are indicated by a pattern of diagonal lines). Areas where the model results show ponded water on the ground surface are indicated by different blue colours. In the areas with ponded water, the different shades of blue indicate the calculated hydraulic head in the uppermost

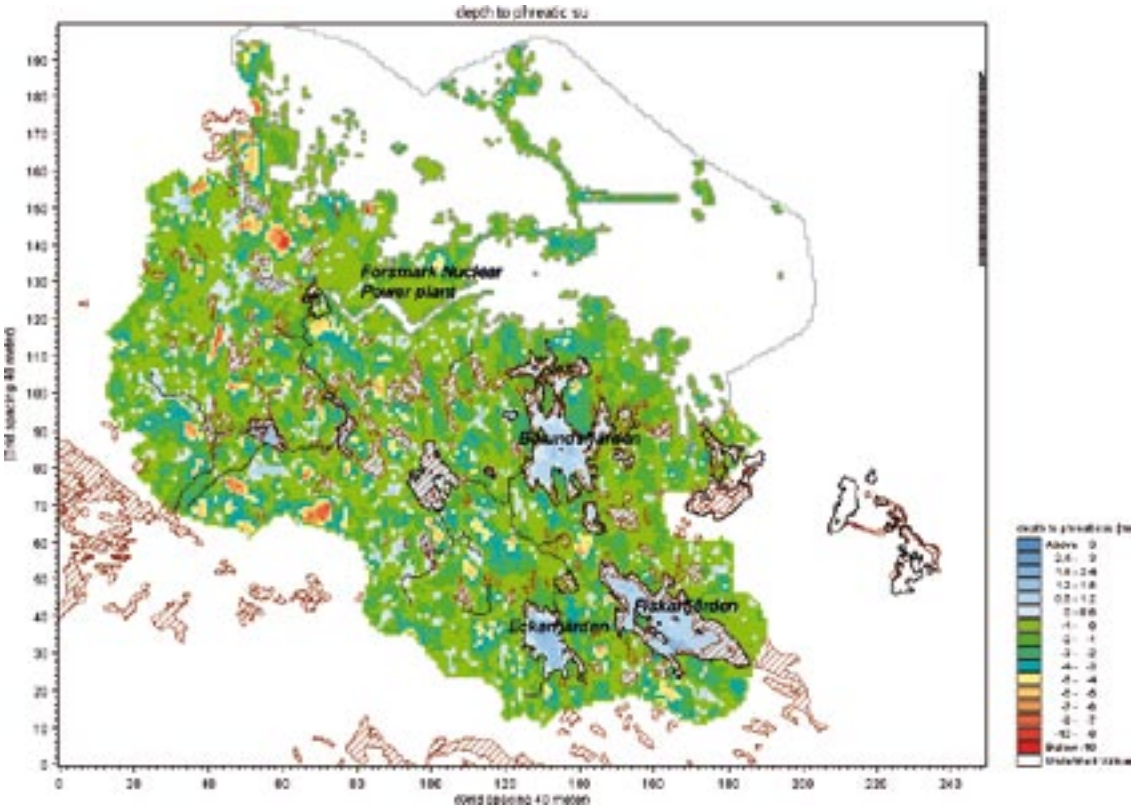

Figure 3-10. *Annual mean value of the depth to the groundwater table, i.e. mean groundwater level expressed in metres above ground surface. Positive values, indicated by blue colours, indicate water above the ground surface given by the DEM, i.e. various types of surface water, whereas negative values indicate areas with (ground)water levels below ground.*

calculation layer. It was found that the simulated water depths in the lakes were in accordance with measured depths. The water depths in some wetlands were 0.5–1 m, implying that shallow lakes, rather than wetlands, were obtained in the model.

3.3.4 Comparison between calculated and measured groundwater levels

The flow model presented above can be regarded as essentially uncalibrated, although some modifications of the surface runoff parameters were made compared to the SDM F1.2 model in order to better reproduce the extent of areas with water above ground. As described above, the general picture provided by this uncalibrated model is acceptable in terms of water-covered areas and the overall position of the groundwater table in different types of areas (i.e. typical recharge and discharge areas).

However, more detailed comparisons between calculation results and measured data are required to judge the performance of the model, and to improve it by applying some kind of calibration procedure. Among the hydrological and hydrogeological data measured at the Forsmark site, discharges in streams and groundwater levels are particularly useful for these purposes. At the time for the Forsmark open repository modelling, no discharge data was available. Therefore, the present comparison between modelling results and field data is focused on groundwater levels, even though it is recognised that discharge data will probably be more important for the assessment and calibration of future model versions.

In the following, measured and calculated hydraulic heads at a few selected groundwater monitoring well locations are compared. The monitoring wells included in the analysis are shown on the map in Figure 3-11. A detailed or complete assessment of the model is not attempted at this stage. The objective of this part of the study is to present a few comparisons that demonstrate

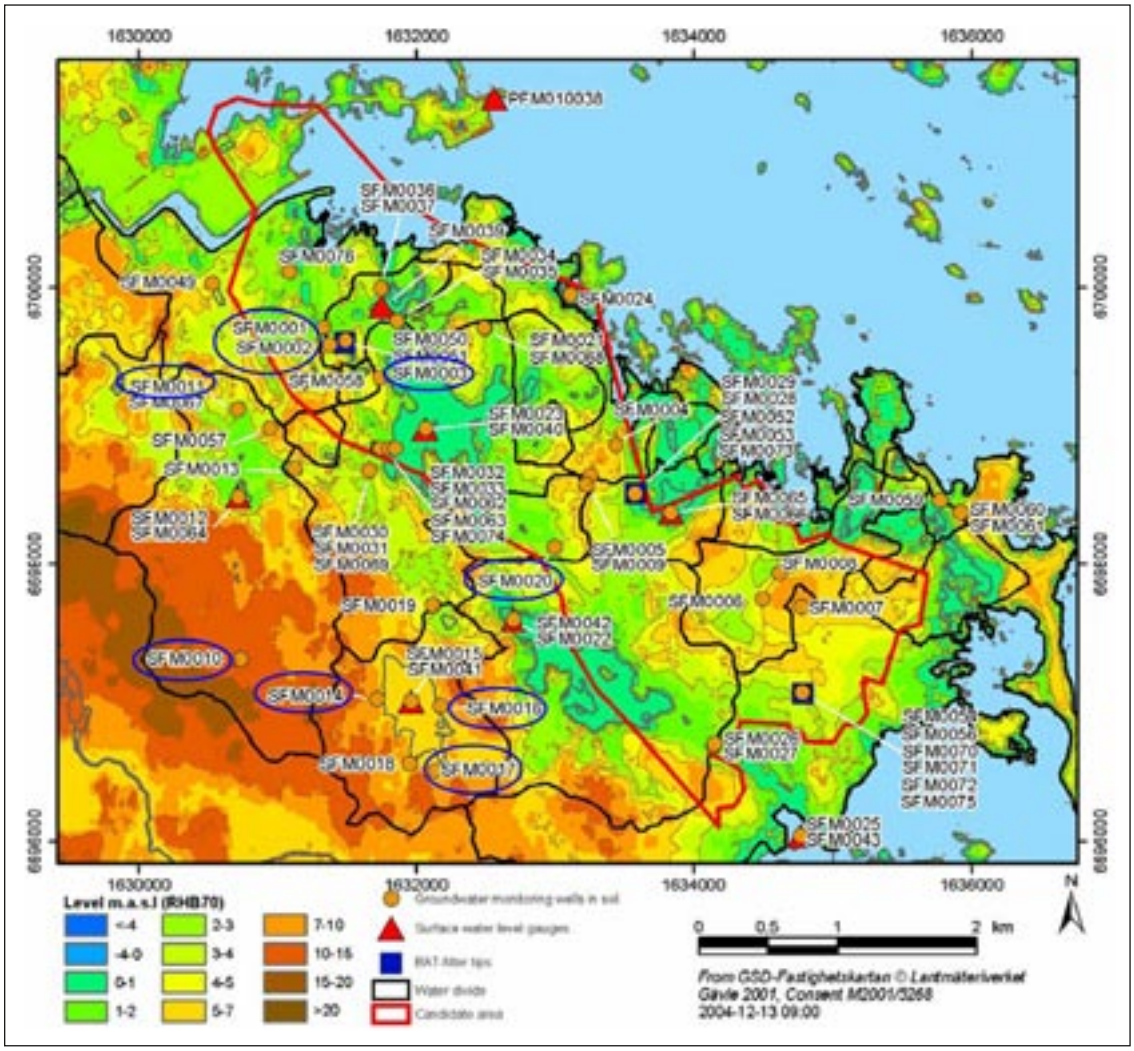

Figure 3-11. *Groundwater monitoring wells and other water level monitoring and sampling devices in Forsmark, map modified from /Johansson et al. 2005/. Encircled monitoring wells are studied in the present comparison.*

different types of deviations between calculation results and measured data, and to provide some guidance for the formulation of a calibration strategy. A specific study with the objective of presenting such a strategy will soon be initiated.

Differences between calculations and field data arise because the model constitutes a simplified description of the real system, and because the inputs to this simplified description are subject to various uncertainties. Specifically, data uncertainties and the fact that the system is modelled by use of discrete elements (i.e. the MIKE SHE grid cells) are two major causes of such differences. Below, an attempt is made to associate some of these factors with different patterns of deviations between calculated and measured heads. In the comparison of modelling results and field data, calculated heads have been taken from the calculation layers corresponding to the levels of the screens in the monitoring wells.

In the present study, results from point measurements in groundwater monitoring wells are compared with head time series calculated using a numerical model with a resolution of 40 m by 40 m. Since the groundwater table can be expected to follow the surface topography, deviations between the DEM and the actual topography is a potential cause of differences between calculated and measured heads. The groundwater monitoring wells are in many cases located at low points in the topography, see /Johansson et al. 2005/. As illustrated in Figure 3-12, this implies that the model tends to overestimate the heads at these monitoring locations.

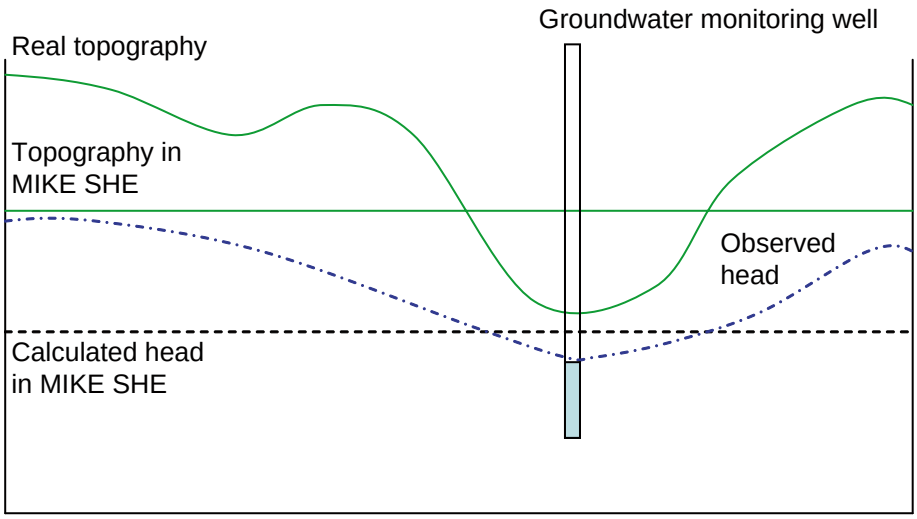

Figure 3-12. *Illustration of a groundwater monitoring well location at a topographic low and the differences between modelled and actual surface topography and groundwater table; the higher ground level at the well location in the model causes an overestimation of the groundwater level.*

Figure 3-13 shows a comparison between measured and calculated heads in the monitoring well SFM0011 (see Figure 3-11). A more or less systematic difference can be seen; the two time series display similar variations in time, but the measured curve is consistently c. 0.5 m below the calculated one. It seems likely that a geometric effect of the type discussed above affects the modelling results. The real ground elevation at SFM0011 is 0.22 m below the corresponding elevation in MIKE SHE, which indicates that at least a part of the deviation can be explained by deviations in the surface topography.

This brings up the question if groundwater levels should be expressed in terms of absolute levels (as in Figure 3-13) or relative to the ground surface. The geometry-related errors illustrated in Figure 3-12 would be reduced if the comparison was made in terms of heads relative to

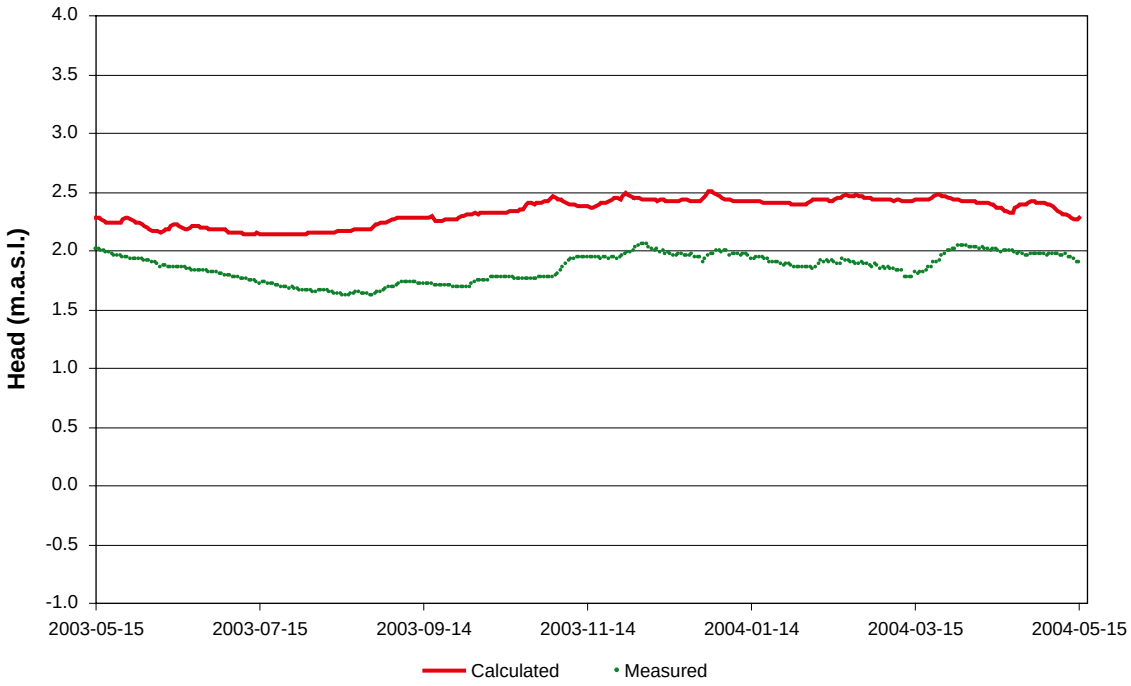

Figure 3-13. *Comparison of measured and calculated hydraulic head in SFM0011.*

the ground surface. On the other hand, absolute levels are the most relevant levels to consider with respect to the overall driving forces in the system (i.e. the head difference between the groundwater and the sea boundary). Thus, both descriptions are probably needed.

The assignment of parameters describing the various hydrological and hydrogeological properties of the system is another potential major source of discrepancies between calculated and measured heads. Again, the fact that point measurements are compared with calculated grid scale head values affects the comparison; the measured heads are to some extent determined by local properties that are spatially variable at scales much smaller than the grid scale. This means that even if the parameter values are correct in an average sense, there may still be differences between calculation results and field data due to local variations in the properties.

In the present model, each calculation layer has constant properties throughout the model volume. This implies that the only form of spatial variability considered is that between the different layers/units in the parameterised QD model. Thus, the representativity of these assigned site-scale effective values (or lack thereof) for describing the local properties determines the outcome of model/field data comparison. Different parameters have different effects on the comparison. By studying the time series, reasons for the deviations can be hypothesised. However, it should be noted that model calculations are required to reach definite conclusions on the affecting parameters and how they should be modified.

Figure 3-14 shows calculated and measured head time series for SFM0017. It is seen that whereas the overall agreement is relatively good (the largest difference is c. 0.5 m), the model appears to react faster and stronger to temporal variations. Assuming that the errors in the meteorological boundary conditions are small (locally measured, high-resolution data are used), this indicates that the parameters determining the transient responses of the system should be modified. In this case, the calibration should therefore primarily consider the storage parameters (e.g. the storativity) and the parameters governing unsaturated flow (saturated hydraulic conductivity and water retention parameters).

In Figure 3-14, it can also be observed that there are both positive and negative differences between the time series. This means that simple averaging over the whole time series (e.g. calculating the difference as the difference between the average head values) would result in a much smaller difference than those actually observed in the data, cf. below.

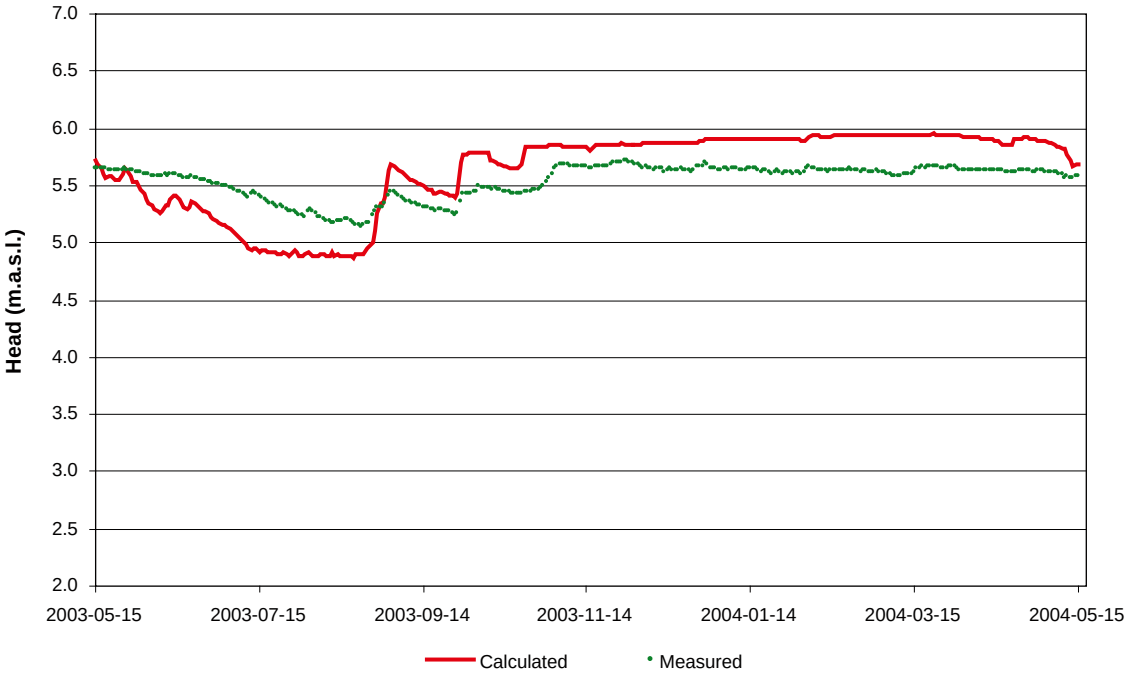

Figure 3-14. *Comparison of measured and calculated hydraulic head in SFM0017.*

Clearly, there are a multitude of other factors than those discussed above that could lead to differences between calculated and measured head values. In most cases, likely a combination of parameters must be considered in the calibration of the model. As an example of a monitoring well where many parameters probably need modification, Figure 3-15 shows calculated and measured heads in SFM0003. It is seen that the model does not reproduce the lowering of the head during the summer, and that it also shows large head variations during a period when the measured head is more or less constant.

In addition to a surface level discrepancy similar to that discussed in connection with Figure 3-13, the results indicate effects of the layering of the QD, i.e. the parameters assigned to the different layers. Specifically, it can be hypothesised that the contrast in properties between the two upper till layers in the model is too large, which makes the response to temporal variations too large in the uppermost layer and practically non-existent in second layer. Another possible reason for the discrepancy during the first half of the time series is that the rock surface is too high in the model, implying that the material where groundwater flow takes place is rock instead of till below a level of c. 1.7 m.

Table 3-4 summarises the comparison between calculated (H_c) and measured (H_m) heads. Different measures of the deviations are reported, i.e. the mean of $H_c–H_m$, (equal to the difference between the mean values of H_c and H_m), the mean of the absolute values of the differences (mean difference, irrespective of sign), and the maximum absolute difference. It can be seen that the mean values differ for three monitoring wells, i.e. those that display both positive and negative deviations during the simulation period (cf. underlined values in Table 3-4). This shows that the selection of the quantity used in the model calibration must be made with care. In particular, for SFM0010 the mean difference increases from 0.02 m to 0.40 m when considering the absolute differences. The increase in the mean difference is smaller for SFM0017 (see Figure 3-14), from 0.10 m to 0.26 m.

The mean differences are in the interval 0.3–0.9 m, except for SFM0014 where it is 1.4 m. Differences between mean values based on actual (with sign) and absolute deviations are observed for SFM0010, SFM0016 and SFM0017. The maximum absolute deviations range from 0.5 m to 2.0 m. Relative to the measured heads, the largest deviations are obtained for SFM0001-03, which are located north-west of Lake Bolundsfjärden. The smallest relative deviations are obtained for SFM0010 (south of Lake Gällsboträsket) and SFM0016-17 (near Lake Eckarfjärden).

Table 3-4. Comparison of calculated (H_c) and measured (H_m) hydraulic heads in selected groundwater monitoring wells, see Figure 3-11 for locations; ($H_c–H_m$) can be both positive and negative, whereas $|H_c–H_m|$ are the corresponding absolute values. Monitoring wells with underlined values show differences between the two mean values.

Monitoring well	Mean (H_c)	Mean (H_m)	Mean ($H_c–H_m$)	Mean $\lvert H_c–H_m \rvert$	Max $\lvert H_c–H_m \rvert$
SFM0001	1.43	0.52	0.91	0.91	1.59
SFM0002	1.76	1.24	0.53	0.53	1.50
SFM0003	2.02	1.27	0.75	0.75	1.50
SFM0010	12.76	12.74	0.02	0.40	0.93
SFM0011	2.33	1.86	0.48	0.48	0.68
SFM0014	6.72	5.30	1.43	1.43	1.98
SFM0016	5.50	5.21	0.29	0.31	0.60
SFM0017	5.64	5.54	0.10	0.26	0.49
SFM0020	1.86	1.39	0.47	0.47	0.89

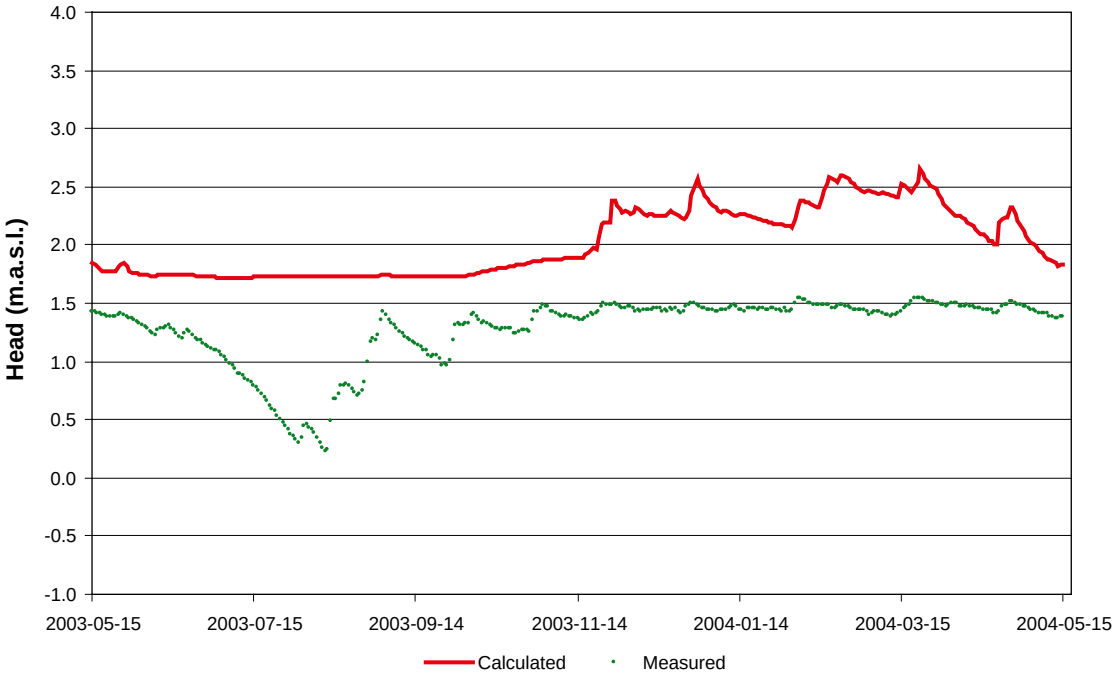

Figure 3-15. *Comparison of measured and calculated hydraulic head in SFM0003.*

The results of the present comparison of calculated and measured head values give some guidance on how future models could be calibrated. First, it can be stated, although not a conclusion of this study, that discharge data should be used in an initial calibration stage focusing on (large-scale) mean values of different layers and/or areas in the model. Time series of head measurements could be used in a second stage directed towards specific "problem areas".

Referring to the issues related to scales that are discussed above, averaging of heads from several monitoring wells should be considered (e.g. all wells within a catchment or sub-catchment). It can also be concluded that it is important to investigate whether the modelled heads show systematic deviations, possibly associated with interpolations in the DEM in combination with a bias in well locations in favour of topographic lows. As mentioned above, the calibration procedure will be further developed in a separate study.

3.4 Summary of results for undisturbed conditions

Apart from the extended model area, the main updates relative to the previous SDM F1.2 MIKE SHE model concern the hydraulic properties of the QD and the bedrock (where also the number of calculation layers has increased), and the meteorological input data. The precipitation in the updated model, which uses locally measured meteorological data from 2003–2004, is 597 mm, which is 77 mm less than in the SDM F1.2 model. This resulted in a significant decrease in the calculated runoff; the average specific runoff from the land part of the model area was calculated to 144 mm/year (c. 4.6 $Ls^{-1}km^{-2}$) in the present model.

A sensitivity analysis was performed with the main objective of investigating the sensitivity to the vertical extent of the model and the hydraulic properties of the QD. The first part, the investigation of the sensitivity to the vertical extent, showed small differences in the modelling results if the model was extended to a depth of 450 m. Similarly, only small effects were obtained when the bottom boundary condition was changed at these depths, from a head boundary condition to a no-flow boundary condition. This can probably be explained by the very low hydraulic conductivities of the bedrock at these depths.

However, the modelling results are highly sensitive to a decrease in the vertical extent of the model. The consistency between the DarcyTools bedrock model /Svensson 2005/ and the present MIKE SHE model seems to decrease the closer to the ground surface the bottom boundary is set. A prescribed head from DarcyTools generates an inflow of water over the bottom boundary, which generates a vertical flow directed upwards in the model volume. The higher the bottom boundary is placed, the more affected is the calculated water balance. If the bottom boundary is set at 20 m below sea level instead of at 135 m below sea level as in the base case, almost all precipitation leaves the model volume as surface runoff. The discrepancy between the calculated head in DarcyTools at a certain level and the head in MIKE SHE is probably due to differences in the spatial resolutions of the original models (DarcyTools data are interpolated to fit with the MIKE SHE grid).

For the sensitivity cases testing the hydraulic properties of the QD, a comparison of the results for topographic high and low points show that the largest absolute differences between the sensitivity cases are obtained for the topographic high, which also shows the largest temporal variations. Among the parameters tested, the model is most sensitive to changes in the horizontal hydraulic conductivity. The overall water balance is not affected by the investigated changes in the hydraulic parameters of the QD.

The updated model has much smaller runoff and specific discharge than the previous SDM F1.2 model. This is consistent with the much smaller precipitation (2003–2004 data from Forsmark compared to the Örskär reference data from 1988) and a somewhat larger total evapotranspiration. Thus, the changes in the overall water balance can be explained by changes in the meteorological data. However, there are also large changes in the distribution of the total evapotranspiration upon its different components. Specifically, the transpiration has increased considerably, whereas the evaporation from ponded water decreased by almost the same amount.

The changes in the evapotranspiration components are caused by modifications in the surface runoff model; less surface resistance resulted in smaller areas with ponded water. Since the transpiration is automatically set to zero in ponded areas, the decrease in the extent of such areas leads to an increased transpiration (and, of course, to a smaller evaporation from ponded water). The specific discharge is in the same range within the model area; the discharge from the catchments containing the three largest lakes in the model area is varying between 5.4 and 6.5 $Ls^{-1} km^{-2}$. The discharge in the studied water course is highly transient during the year, i.e. there are several peaks and periods of zero or very low flow rates between the peaks.

A first comparison between calculated and measured hydraulic heads was performed as a part of the present work. The results for the nine monitoring wells included in the study show that the mean differences between the results obtained with the present, uncalibrated model and the field data varied between 0.3 m and 1.4 m. In terms of mean differences, the model consistently over-predicted the measured heads. However, in three of the wells periods of alternating positive and negative deviations could be observed. Discharge data from measurements in the water courses are currently not available, but will constitute the basis for the calibration of forthcoming hydrological-hydrogeological models; also the measured head data will be used in the calibration procedure.

4 Hydrological analysis of open repository conditions

This chapter presents the modelling of the surface hydrology and near-surface hydrogeology in Forsmark under disturbed, open repository conditions. This means that the modelling considers the operational phase during which the repository, i.e. the ramp and shafts as well as the tunnels and deposition holes at depth, are open and air-filled, thereby causing inflow of groundwater and associated effects on the groundwater conditions in the surroundings. The objectives of the open repository modelling are to

- predict the inflows to the tunnel and shafts for different levels of grouting,
- quantify the near-surface groundwater drawdown caused by tunnel and shafts,
- describe the impact of tunnel and shafts on surface water levels and discharges in water courses.

The modelling discussed in this report deals with the surface hydrology and the upper part of the groundwater flow system. Thus, the model contains only the upper parts of the ramp and the shafts. The relation between the present MIKE SHE model and the DarcyTools open repository model presented in /Svensson 2005/ is illustrated in Figure 1-2. The undisturbed conditions analysed in Chapter 3 serve as a reference in the open repository modelling; most importantly, the results for the undisturbed conditions are used as a basis for calculating the drawdown of the groundwater table and the changes in hydraulic head at different depths in the model volume.

4.1 Geometry of access ramp and shafts

The “Stage D1” repository design for Forsmark, which is based on the Forsmark 1.2 site description, is described in /Brantberger et al. 2006/. A cross-section of the access ramp and the shafts is shown in Figure 4-1. The value displayed at each change of direction along the tunnel is the elevation of the tunnel in metres above sea level (i.e. negative values). The radius of each shaft is also given in the figure. The circumference of the access ramp is approximately 20 m. The ramp is described as a number of links in the modelling tool MOUSE. The modelling approach is described in Section 2.1.2. The four shafts are described as cells with atmospheric pressure in MIKE SHE; also in this case, the modelling methodology is described in Section 2.1.2.

As explained above (see also Section 1.4), only the upper parts of the underground constructions are described explicitly in the MOUSE-SHE model. The vertical extent of the access ramp is the same as the extent of the model itself, which means that the ramp ends at 135 m below sea level. The deeper parts of the repository are taken into account by the application of a bottom boundary condition obtained from the DarcyTools open repository modelling /Svensson 2005/. The DarcyTools model includes the deep parts of the repository, which means that the pressure fields obtained in these simulations can be used to transfer the effects of the deep parts to the shallower boundary of the MIKE SHE model. The different bottom boundary condition cases are described in more detail below.

4.2 Development of numerical model

The MIKE SHE model developed in the modelling of the undisturbed conditions, see Chapter 3, is the basis for the model used in the open repository simulations. Essentially, the geometrical and hydrogeological descriptions of the access ramp and the shafts are introduced in the MIKE

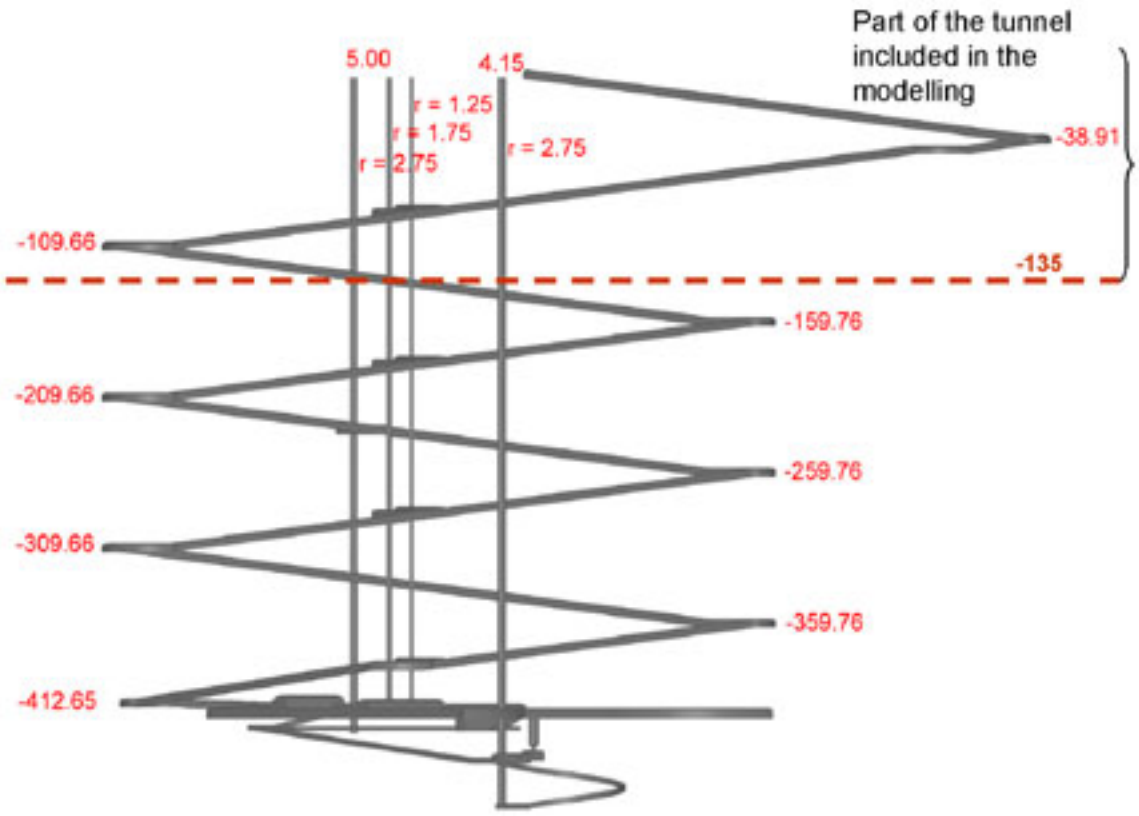

Figure 4-1. *Cross-section of the access ramp and the shafts showing the bottom boundary of the MIKE SHE model (broken line marked "–135") and the elevations (expressed in metres above sea level) along the tunnel; the "Stage D1" Forsmark repository layout is described in /Brantberger et al. 2006/.*

SHE model for undisturbed conditions. In one of the considered simulation cases, a bottom boundary condition is used that accounts for parts of the repository located below the MIKE SHE bottom boundary. These further developments are described below.

4.2.1 Hydraulic properties of access ramp and shafts

The access tunnel, the shafts and other constructions in rock will be grouted in order to reduce the inflow of groundwater. The present simulations consider different levels of grouting, expressed as different hydraulic conductivities, K_g, of the grouted zone in the rock. Specifically, three grouting levels have been defined and described in terms of the hydraulic properties of the grouted zone, as follows:

1. No grouting.
2. $K_g = 1 \cdot 10^{-7}$ m·s^{-1} → $LC_p = 1.25 \cdot 10^{-8}$ s^{-1}.
3. $K_g = 1 \cdot 10^{-9}$ m·s^{-1} → $LC_p = 1.25 \cdot 10^{-10}$ s^{-1}.

The factor LC_p above denotes the leakage coefficient of the ramp wall (see Section 2.1.2), and is calculated as $LC_p = K_g/d_g$, where d_g (= the thickness of the grouted zone), is set to 8 m in all grouting cases.

As described in Section 2.1.2, the leakage coefficients of the ramp wall and the surrounding geological medium are combined when calculating the (total) inflow to the ramp. Since the hydraulic properties of the rock are spatially variable, the leakage coefficient of the rock, LC_{aq}, (where "aq" simply denotes aquifer) differs between calculation layers. As a result, LC_{aq} varies

with depth and is calculated using the hydraulic conductivity in each calculation layer. In addition, the inflow from the surrounding rock to the ramp depends on the hydraulic head difference between them.

The only input data needed for the MOUSE-SHE simulations, except from the geometry of the ramp and the shafts, are the leakage coefficients of the ramp wall and the elevation at the lower end of the ramp. This "downsteam" end is in MOUSE described as a free outlet of a water pipe, with the hydraulic head set to 135 m below sea level (i.e. pressure head = 0 plus elevation head = –135 m above sea level). The present application of the MOUSE-SHE coupling is illustrated in Figure 4-2. In the case without grouting, the leakage coefficient of the ramp wall is set to 0.001. Since this value represents a much smaller flow resistance than that of the surrounding rock, the hydraulic properties of the surrounding rock will limit the inflow.

The present handling of the shafts in MIKE SHE is also described in Section 2.1.2. The shafts are described as cells with atmospheric pressure (pressure head = 0). A total conductance of each grid cell in contact with a shaft is calculated based on contributions from the grouted zone and the surrounding rock. The modelling of the shafts uses the same hydraulic conductivities as in the grouting cases defined above for the ramp. The input data and the resulting conductance for each layer in the model are listed in Appendix 1.

4.2.2 Simulation cases

The MIKE SHE open repository simulations were performed with two different bottom boundary conditions. In the first case, referred to as (boundary) case 1, the bottom boundary condition was the same as in the calculations for the undisturbed conditions. Model-calculated hydraulic heads at 135 m below sea level from the F1.2 DarcyTools modelling /Follin et al. 2005/, representing undisturbed (natural) conditions, were imported as the bottom boundary condition of the MIKE SHE model. The exception was the areas (grid cells) immediately surrounding the ramp and the shafts, where a no-flow boundary was applied. This was done

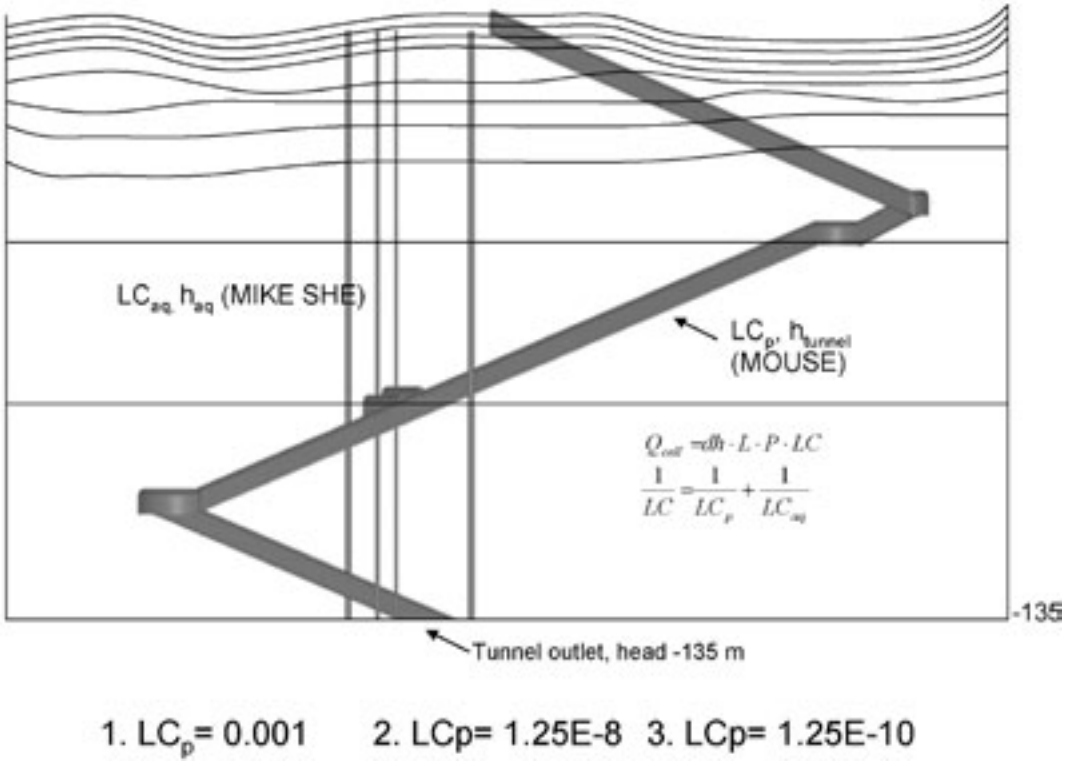

Figure 4-2. *Schematic description of the MOUSE-SHE coupling, showing the access ramp and the calculation layers in the MIKE SHE model.*

to avoid that the hydraulic head in the vicinity of the ramp and the shafts was maintained by a prescribed head boundary condition. Case 1 represents the situation when only the parts of the tunnel and shafts above 135 m below sea level have been built, i.e. before the deep parts of the repository are open. Note that the development of the construction in time is not taken into account; it is assumed that the tunnel and shafts are "installed" instantaneously at the start of the open repository part of the simulation.

In the second case, referred to as (boundary) case 2, calculated head fields at 135 m below sea level from the DarcyTools open repository simulations reported in /Svensson 2005/ were imported to the MIKE SHE model. The DarcyTools model has the whole repository and the shafts up to the level of 100 m below sea level implemented in the model. Thus, the hydro-geological effects of the repository itself and the deeper parts of the tunnel and shafts are taken into consideration, whereas those related to the upper parts of the construction are not. Also in this case, all the considered parts of the repository were assumed to be in place instantaneously at the start of the open repository simulation.

The "hot start" results for undisturbed conditions (cf. Section 3.1.2) were used as initial conditions for the open repository simulations. In these simulations, the ramp, the shafts, and the undisturbed (boundary case 1) or disturbed pressure field (boundary case 2) at 135 m below sea level were applied instantaneously at the first time step. For each of the open repository simulation cases, the model simulates a two-year period of disturbed conditions (i.e. with ramp and shafts present). Time series of the transient hydrogeological response show that the largest part of the hydrogeological response occurs during the first months of the simulation period (cf. Figure 4-8 in Section 4.3.4). This means that the simulated period (two years) is sufficiently long to provide representative output data on hydrogeological effects. Overall, it turned out that the differences between the two boundary cases were relatively small. In the following, results for both cases are presented and discussed, whereas most figures show case 1 results.

4.3 Results

4.3.1 Inflow to tunnel and shafts

The MOUSE-SHE modelling results show that the inflow to the four shafts is insignificant compared to the inflow to the access ramp; the total inflow to the four shafts is less than 0.5 L s^{-1}. It should be noted that one (air) shaft is not included in the MOUSE-SHE model, since information on this shaft was not available at time of model set up. As can be seen in Figure 4-3, the largest part of the total inflow to the ramp occurs along its upper part, from the ground surface down to 38.9 m b. s. l. (reference point P1 in Figure 4-3), and also between 38.9 and 46 m below sea level (reference point P2). Below 46 m below sea level the accumulated inflow to the tunnel is almost constant, meaning small calculated inflow below this depth.

The model-calculated average inflow to the ramp (accumulated inflow divided by the length of the simulation period) is shown in Table 4-1 for different cases. One can note that the inflow is lower in boundary case 2 compared to case 1. Case 1 includes the ramp and the shafts down to 135 m below sea level whereas case 2 includes the whole repository. Since the drawdown is slightly larger in case 2 (see Section 4.3.4), the inflow to the ramp is smaller compared to case 1. The most important observation is the influence of the hydraulic conductivity of the grouted zone (K_g) on the inflow. The case $K_g = 10^{-7}$ m·s^{-1} reduces the inflow to 50% compared to non-grouting case, and in the case $K_g = 10^{-9}$ m·s^{-1} the inflow is almost zero.

MOUSE-SHE simulates transient inflow (see Figure 4-4), whereas Figure 4-3 illustrates a "snapshot" in time. Figure 4-4 shows the temporal variation of the total inflow to the access ramp for boundary case 1 without grouting. There are two peaks in the inflow, which are attributed to numerical instabilities only; these instabilities are probably caused by the generally small inflows. Neglecting these two peaks, the total inflow to the ramp for the considered case varies in the interval 5–9 L·s^{-1}.

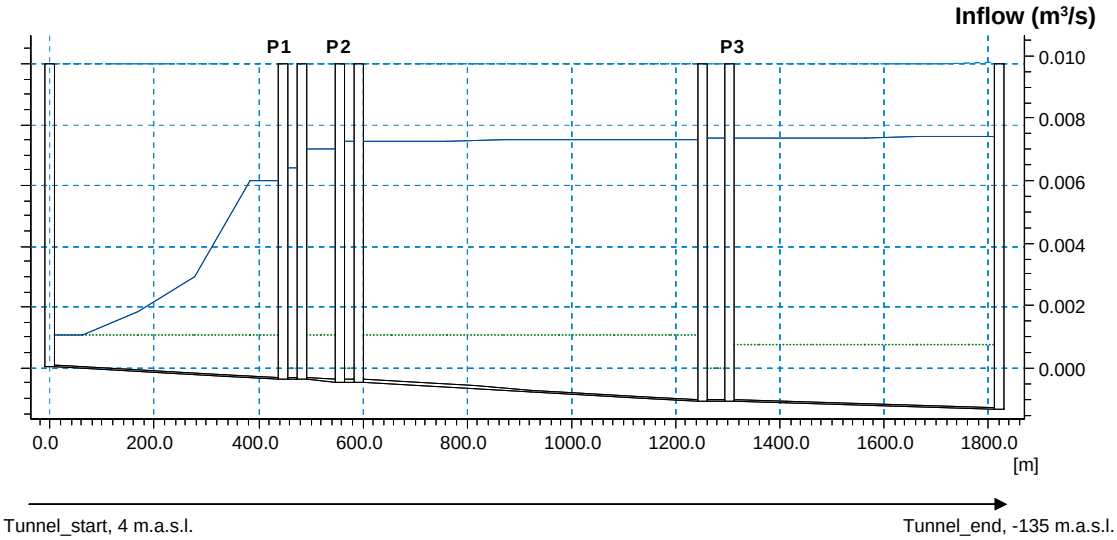

Figure 4-3. *Inflow to the access ramp (blue line; $m^{3}\cdot s^{-1}$), shown as cumulative inflow. The vertical lines indicate where the ramp changes direction. P1, P2 and P3 are reference points where the elevation of the ramp is 38.9, 46.0 and 109.7 m below sea level respectively (cf. Figure 4-1).*

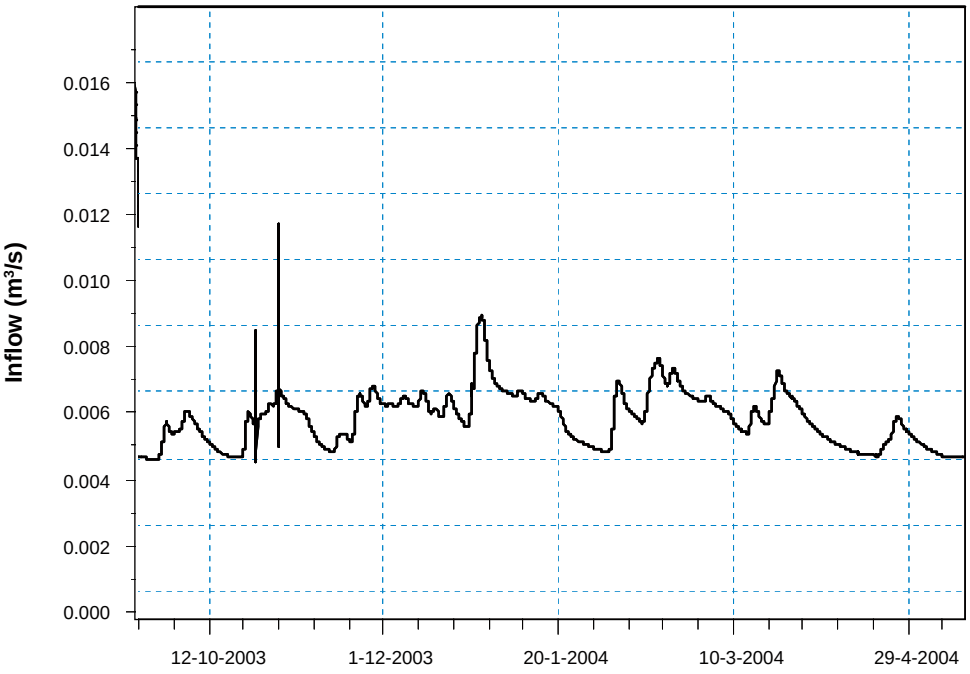

Figure 4-4. *Time series of the total inflow to the access ramp for boundary case 1 without grouting.*

Table 4-1. Calculated average inflow ($L\cdot s^{-1}$) to the access ramp in boundary cases 1 and 2 for different grouting cases.

Grouting case	Boundary case 1	Boundary case 2
No grouting	5.0	4.0
$K_g = 1\cdot10^{-7}$ m·s^{-1}	2.5	2.0
$K_g = 1\cdot10^{-9}$ m·s^{-1}	0.1	0.1

4.3.2 Groundwater drawdown

This section uses the term “influence area”, which includes the area where the model-calculated change in groundwater level or hydraulic head is 0.3 m or larger, compared to undisturbed conditions. Both for undisturbed and disturbed conditions, the comparison refers to groundwater levels or hydraulic heads at the last time step of the simulated period. Essentially, this means that two “snapshots” in time are compared, representing two different flow situations.

Table 4-2 summarizes the results of the MOUSE-SHE drawdown calculations, in terms of the largest computed groundwater level drawdown within the model area and the size of the influence area (i.e. the area with drawdown ≥ 0.3 m). The table shows that the largest drawdown and the size of the influence area are highly dependent on the hydraulic conductivity of the grouted zone. The largest drawdown (25.4 m) occurs in the case where no grouting is applied. Note that the non-grouted cases are not realistic, and are only considered here for illustrative purposes. Case 1 (only the near-surface parts of ramp and shafts are open) gives a smaller drawdown and a smaller influence area compared to case 2 (all parts of the repository are open); as discussed in the previous section, case 1 is associated with a larger inflow to the near-surface parts of the repository.

Figures 4-5 and 4-6 show maps of the groundwater level drawdown for case 1 (Figure 4-5) and case 2 (Figure 4-6) without grouting. Figure 4-5 shows that if no grouting is made, there will be a rather large drawdown (up to c. 25 m). However the influence area is limited to the areas above and immediately surrounding the access ramp and the shafts. Including also the deep parts of the repository (Figure 4-6), additional areas with a groundwater level drawdown of up to 1 m occur above the southern and eastern parts of the repository.

Figure 4-7 shows a vertical cross-section of the model area, including the upper boundaries of 11 of the 12 calculation layers, and the position of the groundwater table for boundary case 1 without grouting. Note that the deepest layer (12) associated with the bottom boundary is not shown in the figure. The access ramp intersects the section at points A, B and C, at 10, 32 and 82 m below sea level respectively. The deepest groundwater table position occurs at point A (i.e. at the shallowest cross-section/access ramp intersection), whereas the groundwater table position is higher at points B and C, having larger intersection depths. This indicates that the shallow parts of ramp and shafts cause a larger drawdown compared to the deeper parts. It is also noted that the shallowest parts of the access ramp are associated with the largest inflow (see Section 4.3.1).

Table 4-2. Summary of groundwater level drawdown results.

Hydraulic conductivity of the grouted zone (K_g)	Maximum groundwater level drawdown (m)		Influence area (km^2)	
	Case 1	Case 2	Case 1	Case 2
No grouting	25.4	25.4	0.26	0.31
10^{-7}	6.6	6.8	0.18	0.224
10^{-9}	0.14	0.7	0	0.085

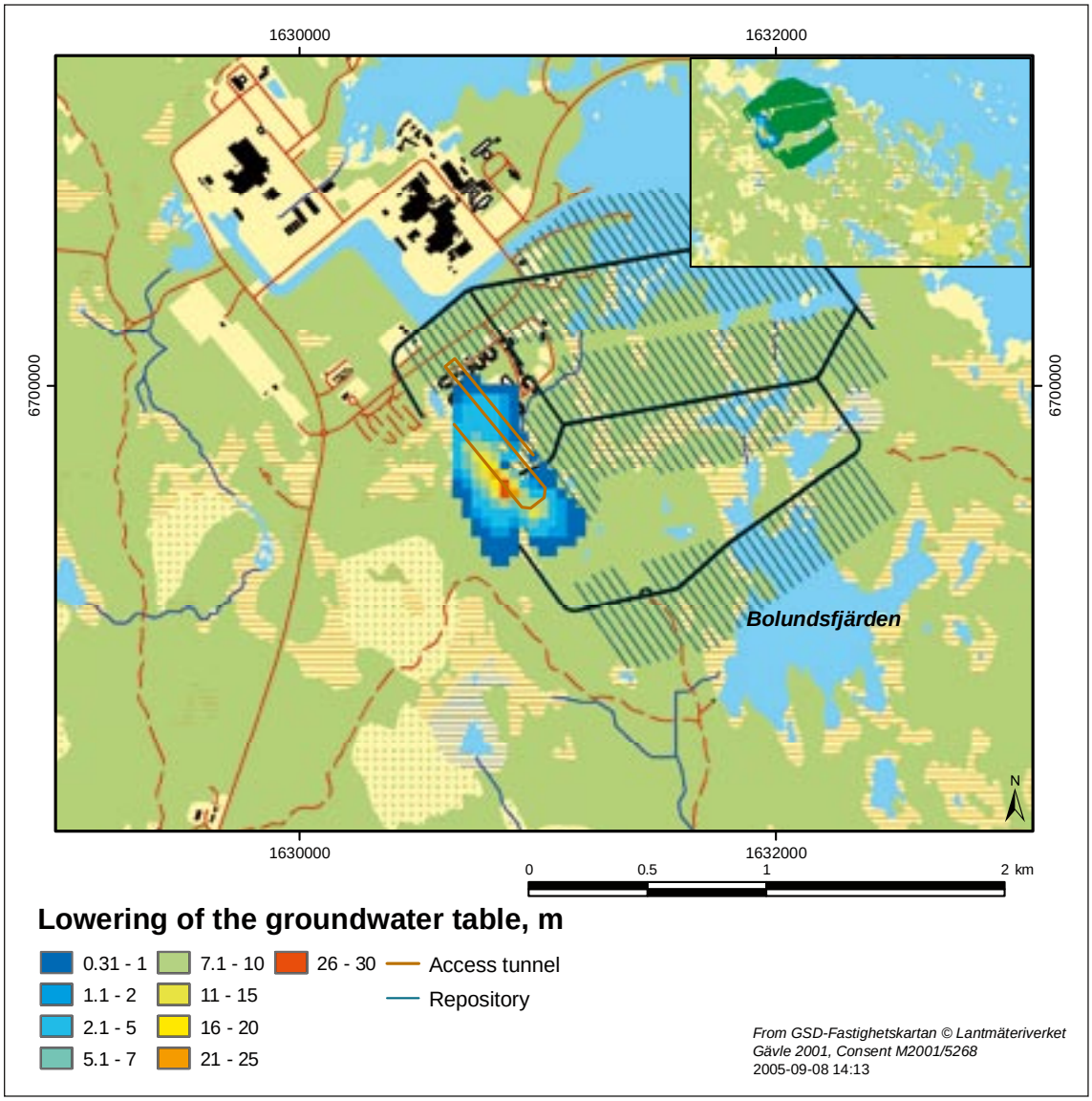

Figure 4-5. *Groundwater level drawdown for boundary case 1 without grouting. The access ramp (tunnel) and the repository tunnels are indicated in the figure.*

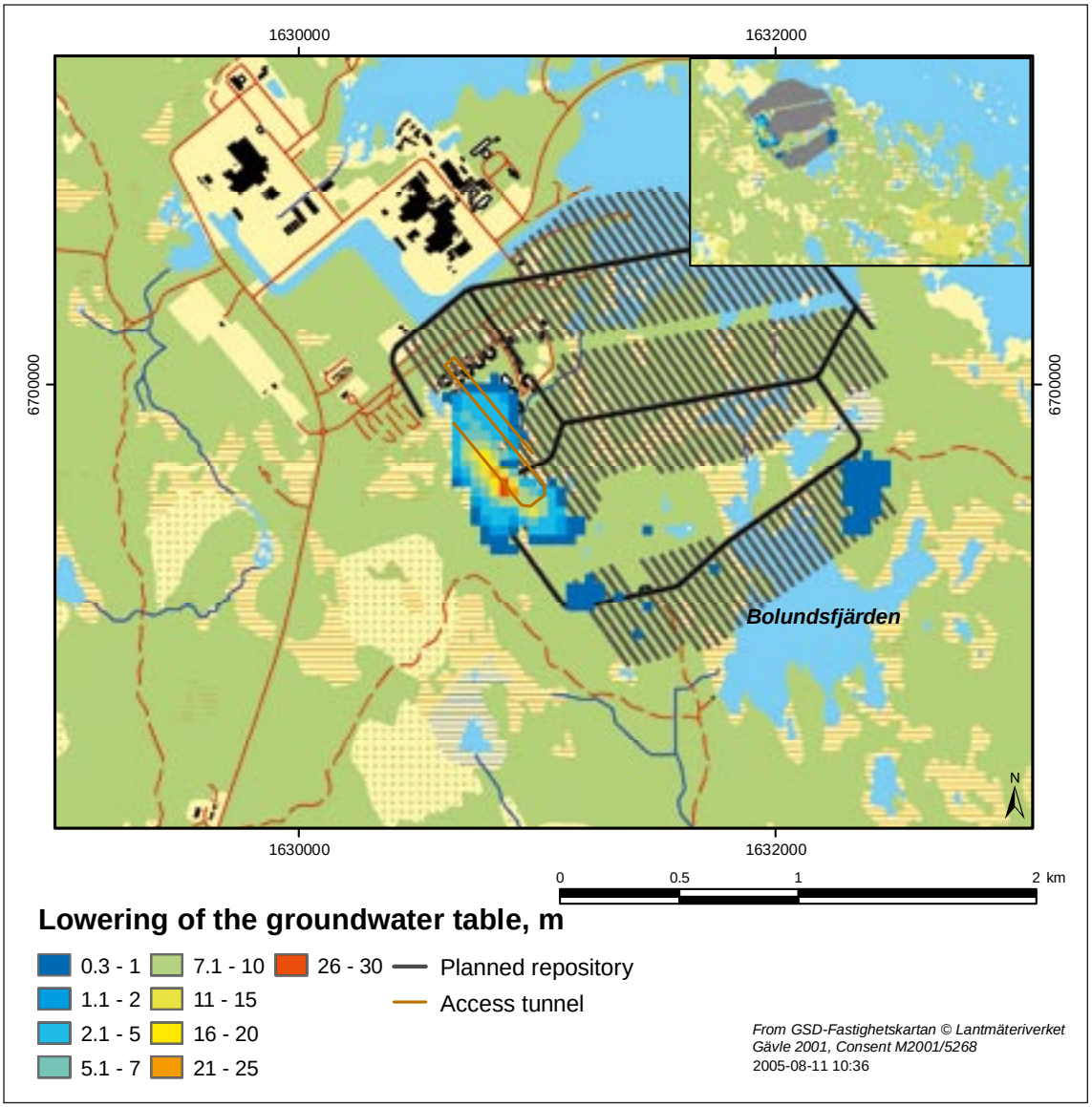

Figure 4-6. *Groundwater level drawdown for boundary case 2 without grouting. The access ramp (tunnel) and the repository tunnels are indicated in the figure.*

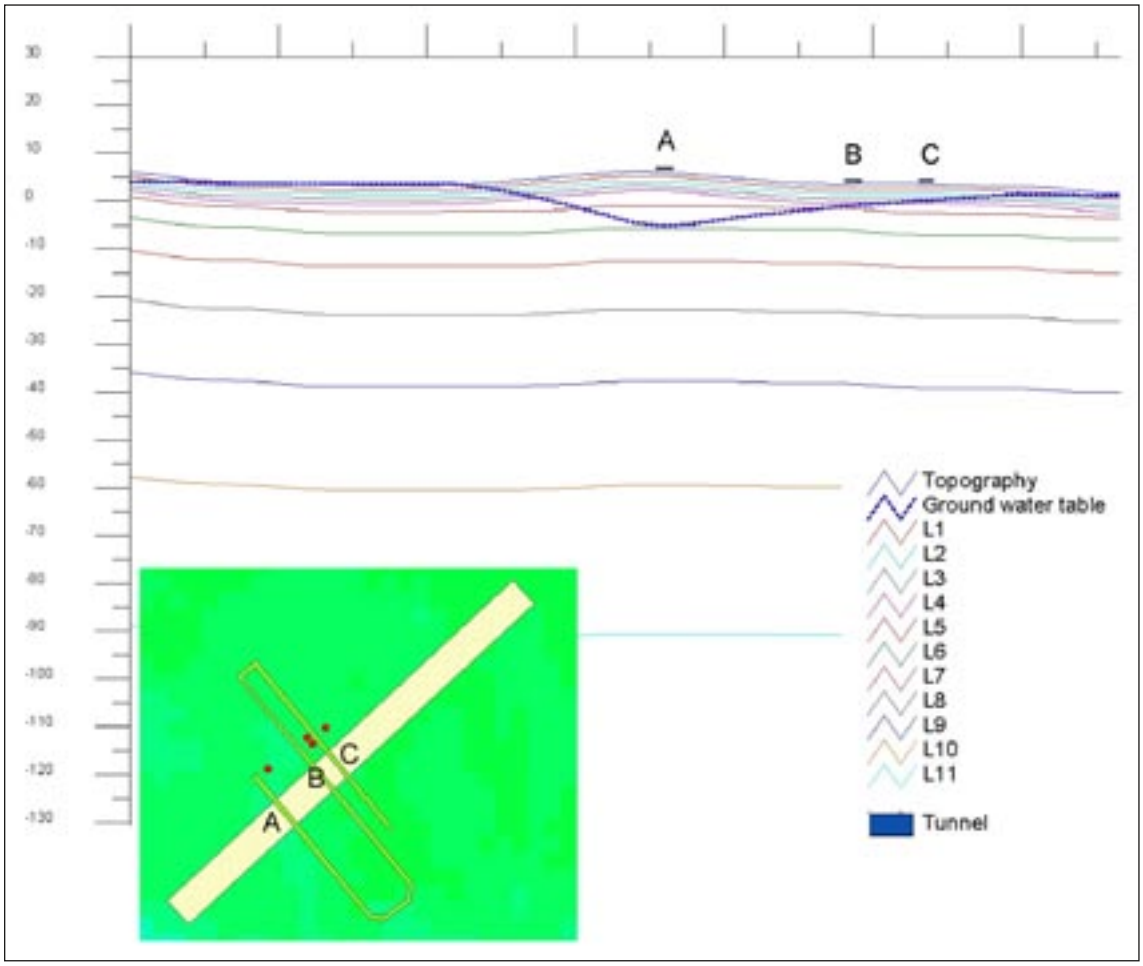

Figure 4-7. *Cross-section of the model area, illustrating the upper boundaries of 11 of the 12 calculation layers, and the position of the groundwater table for boundary case 1 without grouting. The red dots in the plane view indicate the locations of the four shafts.*

Time series of the hydraulic head during the first one-year simulation period, representing disturbed conditions, show a relatively fast hydrogeological response to these conditions. As an illustration of this, Figure 4-8 presents model-calculated time series (boundary case 1, without grouting) of the hydraulic head in calculation layer 10 (c. 60 m below sea level cf. Figure 4-7) at 6 points (A–F), located at successively larger distances from the access ramp. The location of the straight line that joins the end points A–F is shown in Figure 4-9, which also shows the computed drawdown of the hydraulic head in layer 10 within the influence area (i.e. the area with a drawdown $\geq$ 0.3 m). In the vicinity of the ramp (point A) the drawdown seizes after approximately two months, whereas it takes longer times to reach a stable drawdown farther from the ramp (e.g. 6 months at point C).

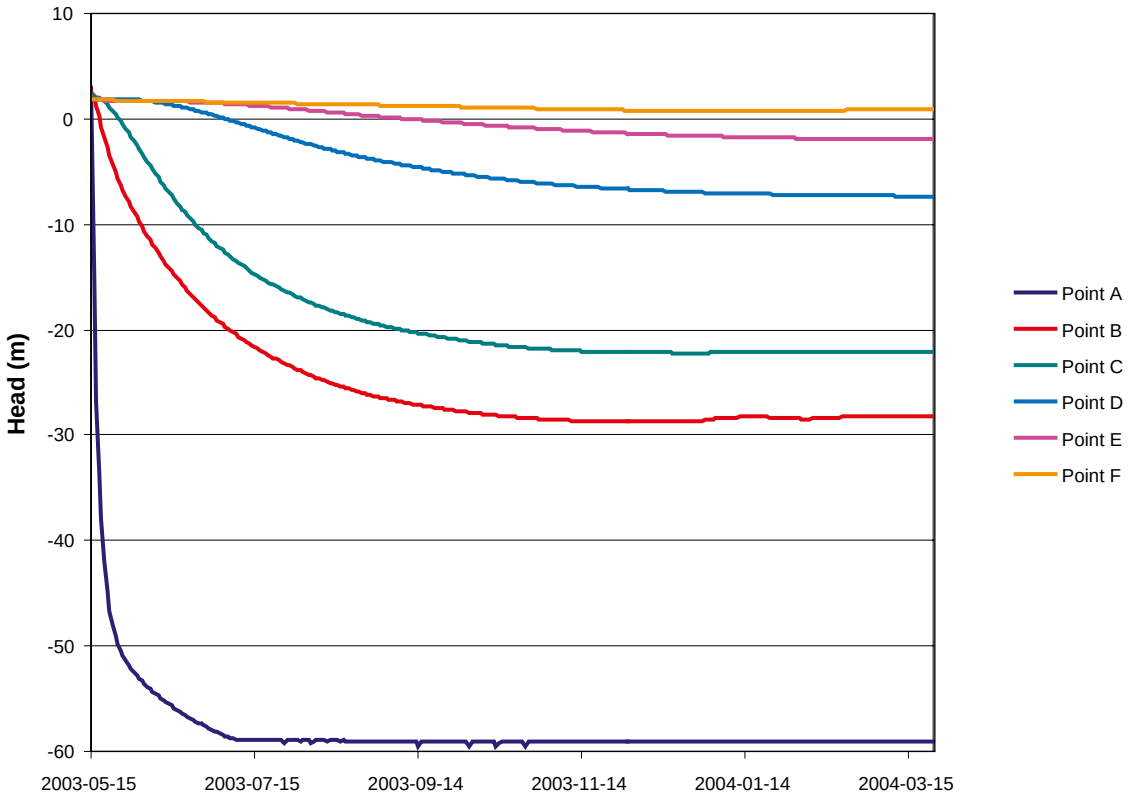

Figure 4-8. *Model-calculated time series (boundary case 1, without grouting) of the hydraulic head in calculation layer 10 (c. 60 m below sea level cf. Figure 4-7) at 6 points A–F, located at successively larger disctances from the access ramp (see Figure 4-9). Point A is located at the ramp, whereas F is at the boundary of the influence area of the head drawdown in calculation layer 10.*

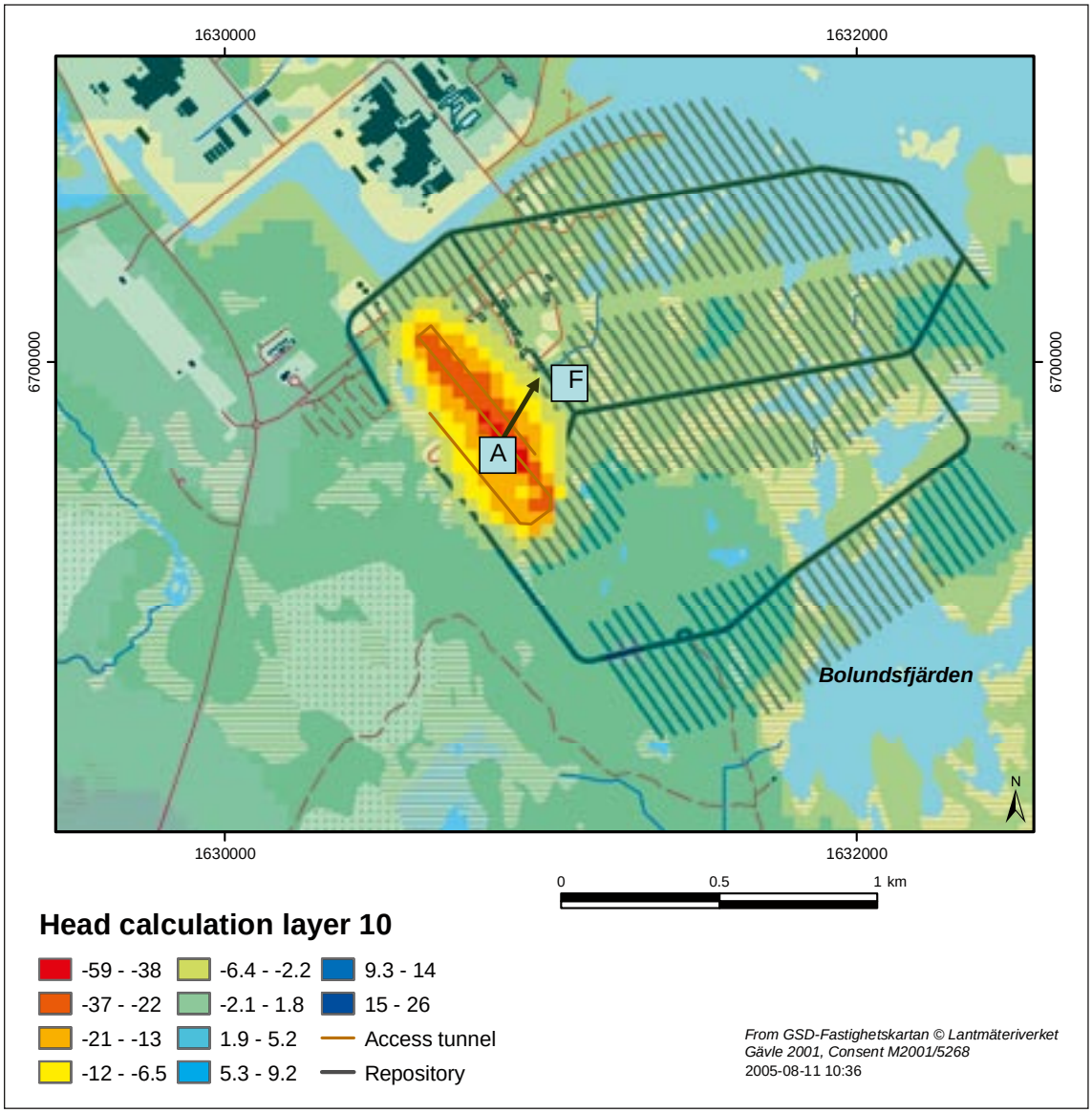

Figure 4-9. *Locations of points A–F (see Figure 4-9). For reference, the figure also shows the model-calculated hydraulic head (boundary case 1, without grouting) and its influence area in calculation layer 10.*

The hydraulic head drawdown and the associated influence area vary vertically and also during the year. The maximum influence area is seen in the second lowest calculation layer at a level of 90 m below sea level. The bedrock has a very small hydraulic conductivity at this depth; no transmissive fracture zones cross the access ramp. Considering the (hypothetical) case without grouting (boundary case 1), Figures 4-11 to 4-14 show the hydraulic head drawdown, comparing the last time step of the simulated period for undisturbed and disturbed conditions, respectively, in a selection of calculation layers (1, 3, 7, and 11) within the area indicated in Figure 4-10. Results for all calculation layers are shown in Appendix 2. The light-green areas in these figures are outside of the influence area for the hydraulic head drawdown in the considered layers.

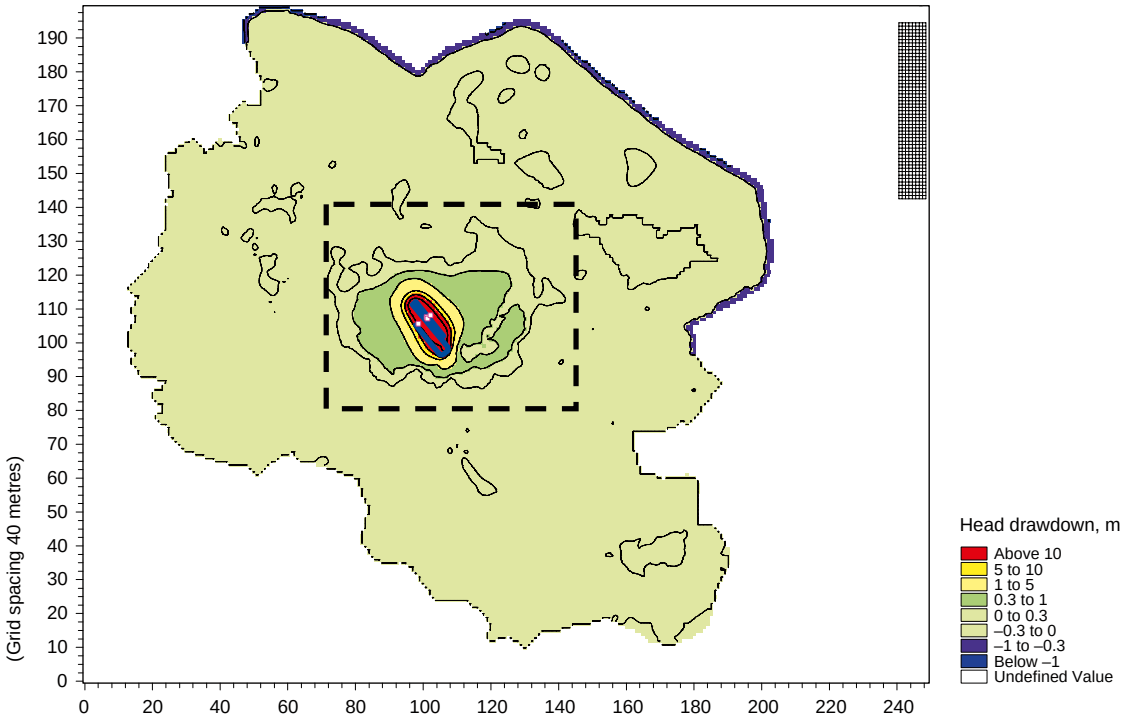

Figure 4-10. *The area (part of the MOUSE-SHE model area) in Figures 4-11 to 4-14 indicated by dashed lines. The colours indicate the hydraulic head drawdown in calculation layer 11 (cf. Figure 4-14).*

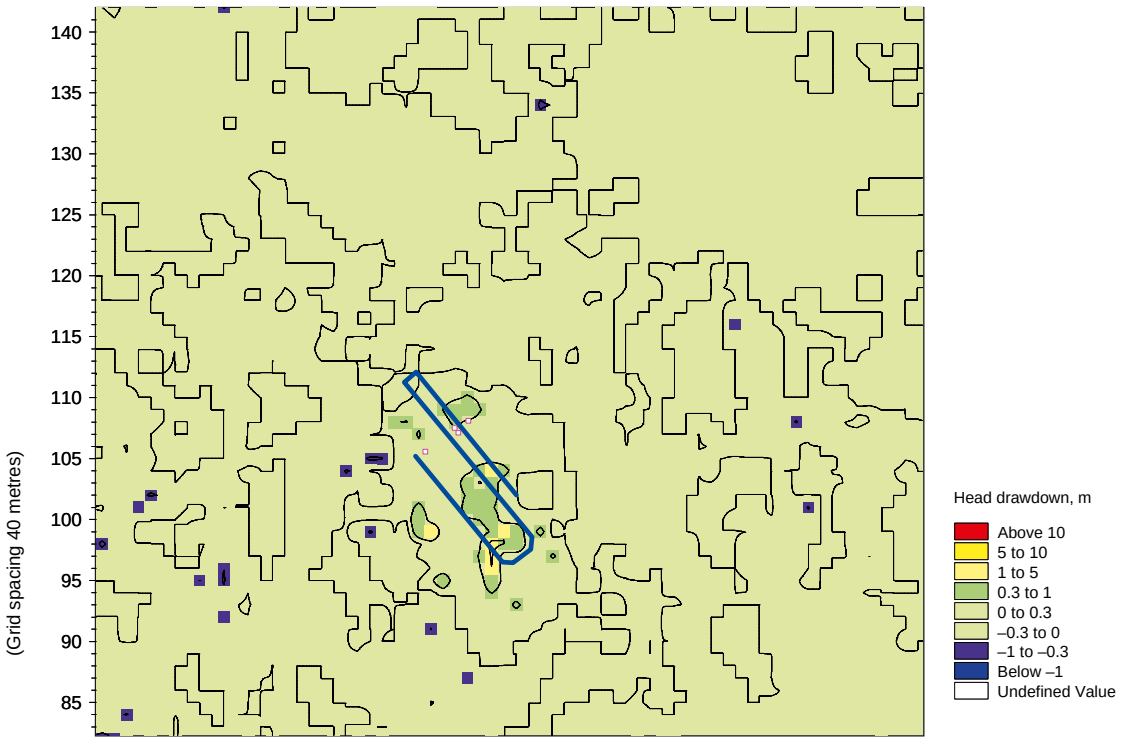

Figure 4-11. *Hydraulic head drawdown in calculation layer 1 (1 m below ground surface). The access ramp (blue line) and the four shafts (small pink squares) are indicated in the figure.*

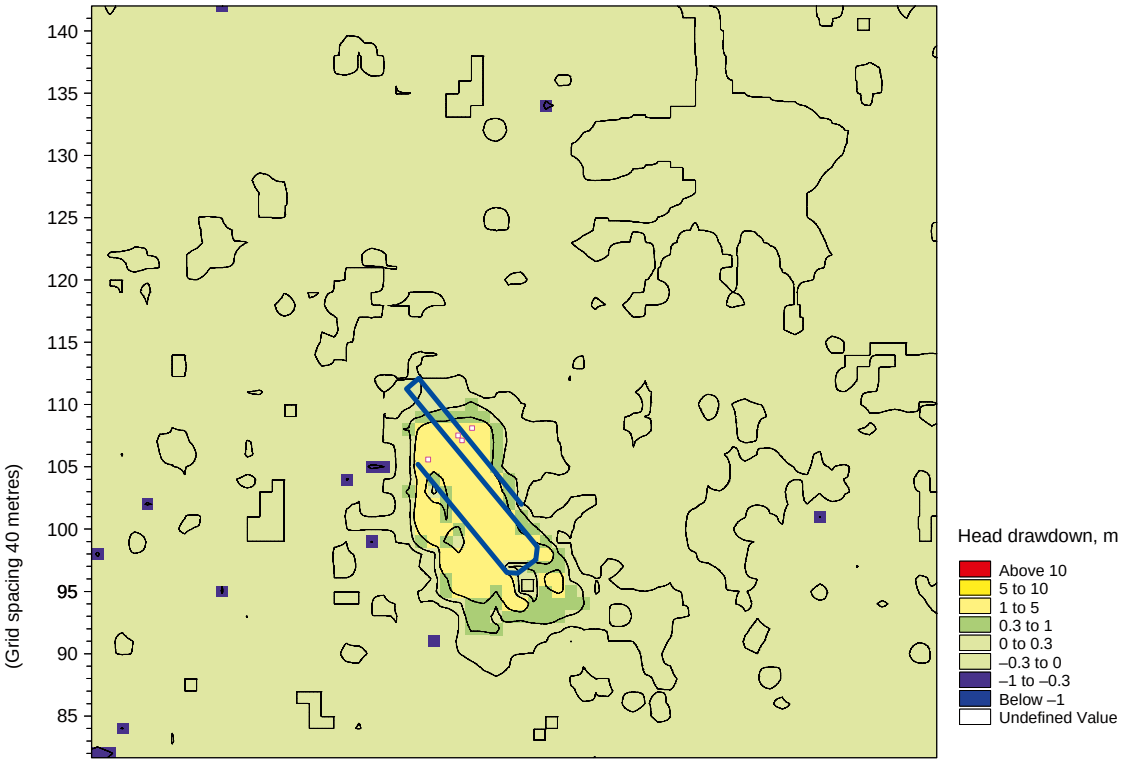

Figure 4-12. *Hydraulic head drawdown in calculation layer 3 (3 m below ground surface). The access ramp (blue line) and the four shafts (small pink squares) are indicated in the figure.*

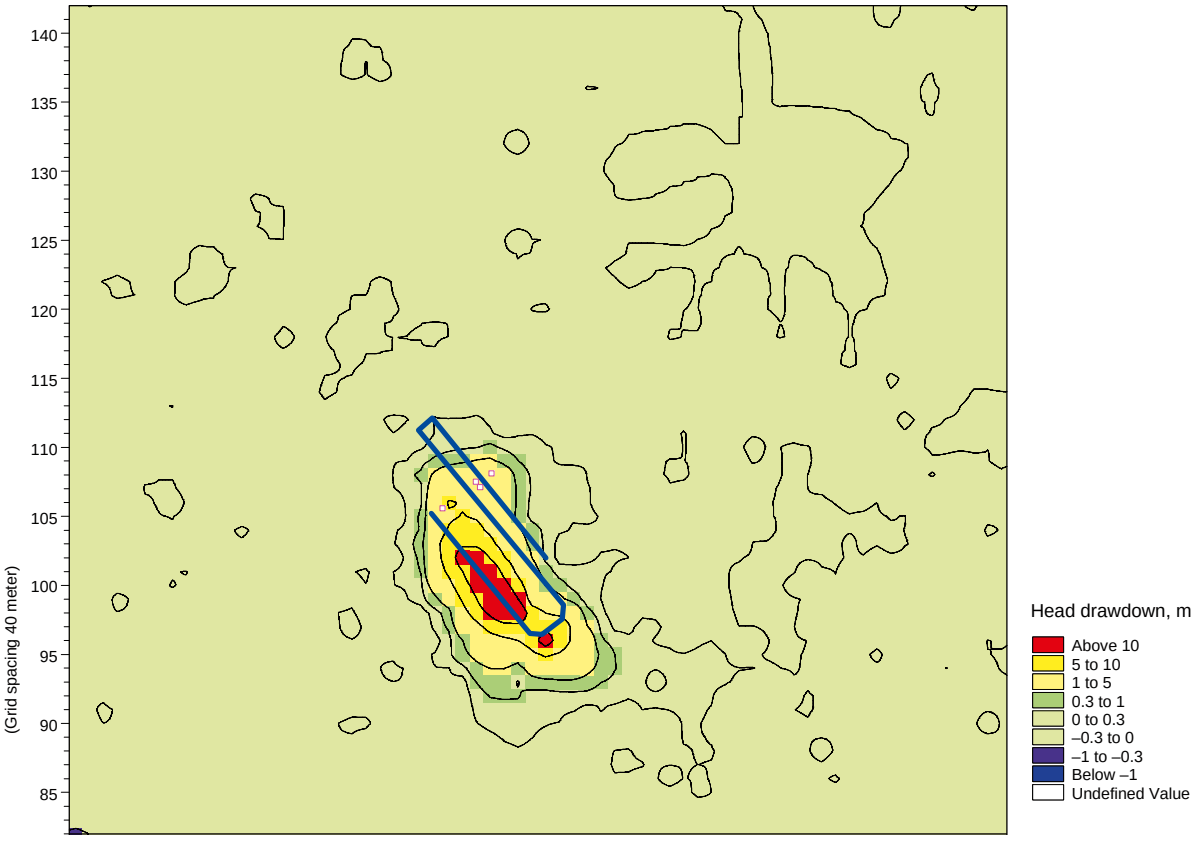

Figure 4-13. *Hydraulic head drawdown in calculation layer 7 (13 m below sea level). The access ramp (blue line) and the four shafts (small pink squares) are indicated in the figure.*

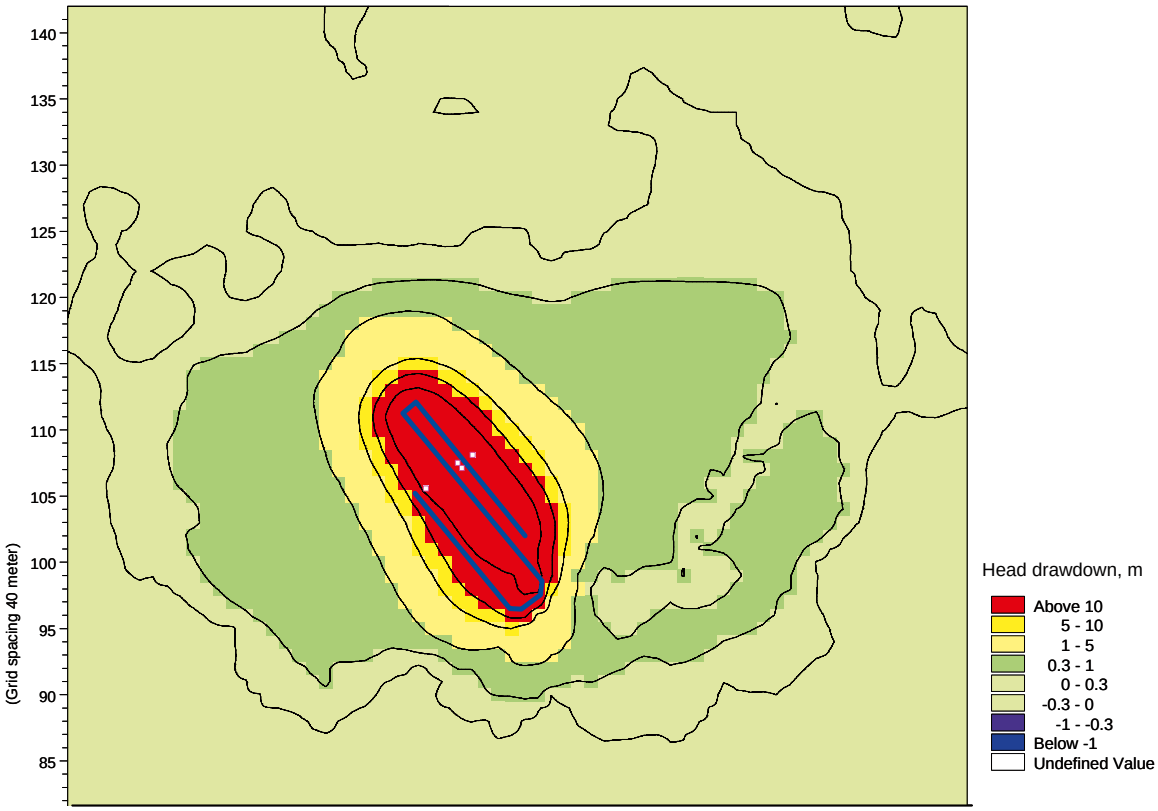

Figure 4-14. *Hydraulic head drawdown in calculation layer 11 (90 m below sea level). The access ramp (blue line) and the four shafts (small pink squares) are indicated in the figure.*

Figures 4-11 to 4-14 show that the hydraulic head drawdown occurs in the vicinity of the access ramp and the shafts. Comparing the figures, one can also note that the hydraulic head drawdown and the size of the associated influence area increases with depth. For instance, the influence area of the head drawdown at 90 m below sea level (layer 11; Figure 4-14) is several times larger than the influence area at 13 m below sea level (layer 7; Figure 4-14). It is even noted that the area with drawdown > 10 m at 90 m below sea level is of the same size as the total influence area (drawdown ≥ 0.3 m) at 13 m below sea level.

The above phenomenon is further illustrated in Table 4-3, which summarizes the size of the head drawdown influence area at different depths, for the MOUSE-SHE boundary case 1 without grouting and with $K_g = 10^{-7}$ m·s^{-1} in the grouted zone. Results are shown for 11 of the totally 12 calculation layers (strictly, the shown results apply to the bottom boundary of each layer). As mentioned previously, the deepest layer (12) is associated with the bottom boundary. This means that the drawdown is simply equal to the difference between the undisturbed and the disturbed boundary conditions (i.e. the difference between case 1 and 2 at the bottom boundary). Table 4-3 also summarizes the horizontal (K_h) and vertical (K_v) hydraulic conductivity of the geological medium in contact with the access ramp and the shafts in each of the considered layers.

According to Table 4-3, grouting has relatively large impact on the size of the influence area at shallow depths, whereas the difference between the no-grouting case and the case $K_g = 10^{-7}$ m·s^{-1} is small at larger depths. This can partly be explained by the depth-dependent hydraulic conductivity (K), from layer 1 down to layer 11 implying a total difference in K of c. 4 orders of magnitude along the access ramp. Hence, the influence of the grouted zone decreases with depth; Table 4-3 shows that if $K_g = 10^{-7}$ m·s^{-1}, the grouted zone has no influence on the inflow or the drawdown below 23 m below sea level.

In order to further illustrate the groundwater level-hydraulic head drawdown relationships, Figures 4-15 and 4-16 present two cross-sections of the access ramp, showing the hydraulic head drawdown in all 12 calculation layers (the groundwater table position is also shown in Figure 4-16); layer bottom boundaries and layer-specific head drawdowns are indicated by different colours.

Table 4-3. Geometric properties, hydraulic properties, and the calculated influence area at the bottom boundary of 11 calculation layers (of totally 12); m.b.g.s. = metres below ground surface, m.a.s.l. = metres above sea level.

Calculation layer	Lower level	K_h (m·s^{-1})	K_v (m·s^{-1})	Influence area (km^2), boundary case 1 without grouting	Influence area (km^2), boundary case 1, K_g = 10^{-7} m·s^{-1}
1	–1 m.b.g.s.	$1.10 \cdot 10^{-5}$	$1.00 \cdot 10^{-5}$	0.06	0.02
2	–2 m.b.g.s.	$1.00 \cdot 10^{-5}$	$6.00 \cdot 10^{-6}$	0.19	0.10
3	–3 m.b.g.s.	$3.00 \cdot 10^{-6}$	$2.00 \cdot 10^{-6}$	0.23	0.14
4	–4 m.b.g.s.	$1.00 \cdot 10^{-6}$	$1.05 \cdot 10^{-6}$	0.25	0.15
5	–2.5 m.a.s.l.	$1.05 \cdot 10^{-6}$	$1.05 \cdot 10^{-6}$	0.25	0.16
6	–5.5 m.a.s.l.	$1.05 \cdot 10^{-6}$	$1.05 \cdot 10^{-6}$	0.25	0.16
7	–13 m.a.s.l.	$1.05 \cdot 10^{-6}$	$1.05 \cdot 10^{-6}$	0.26	0.17
8	–23 m.a.s.l.	$1.05 \cdot 10^{-6}$	$1.05 \cdot 10^{-6}$	0.27	0.17
9	–38 m.a.s.l.	$5.27 \cdot 10^{-10}$	$5.65 \cdot 10^{-9}$	0.52	0.46
10	–60 m.a.s.l.	$5.27 \cdot 10^{-10}$	$5.27 \cdot 10^{-10}$	0.97	0.93
11	–90 m.a.s.l.	$5.27 \cdot 10^{-10}$	$5.27 \cdot 10^{-10}$	1.89	1.85

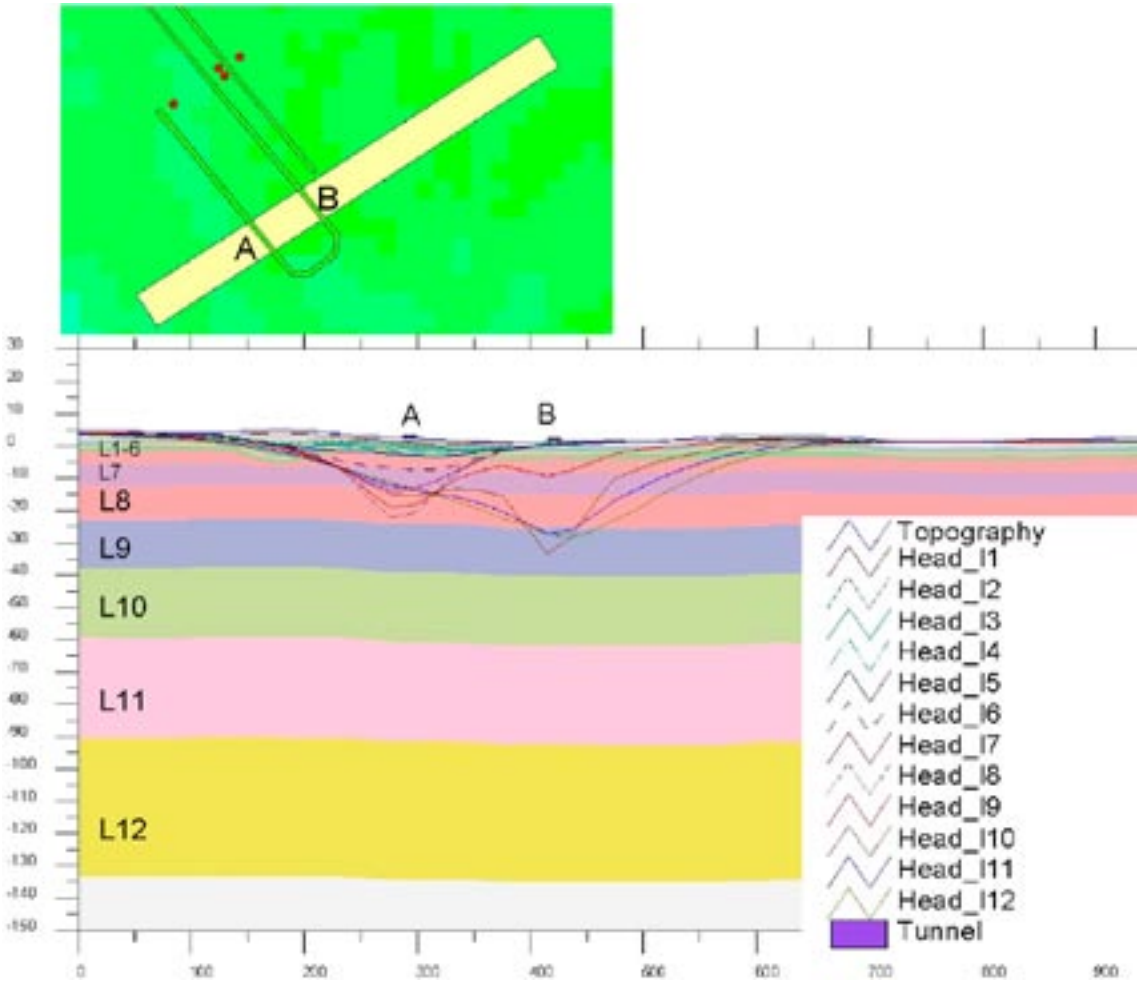

Figure 4-15. *Hydraulic head in a cross-section of the access ramp. The cross-section intersects the ramp at the points A and B. The plane view shows the locations of A and B, the ramp ("tunnel") and the shafts (red dots). Horizontal scale is metres, and vertical scale is metres above sea level.*

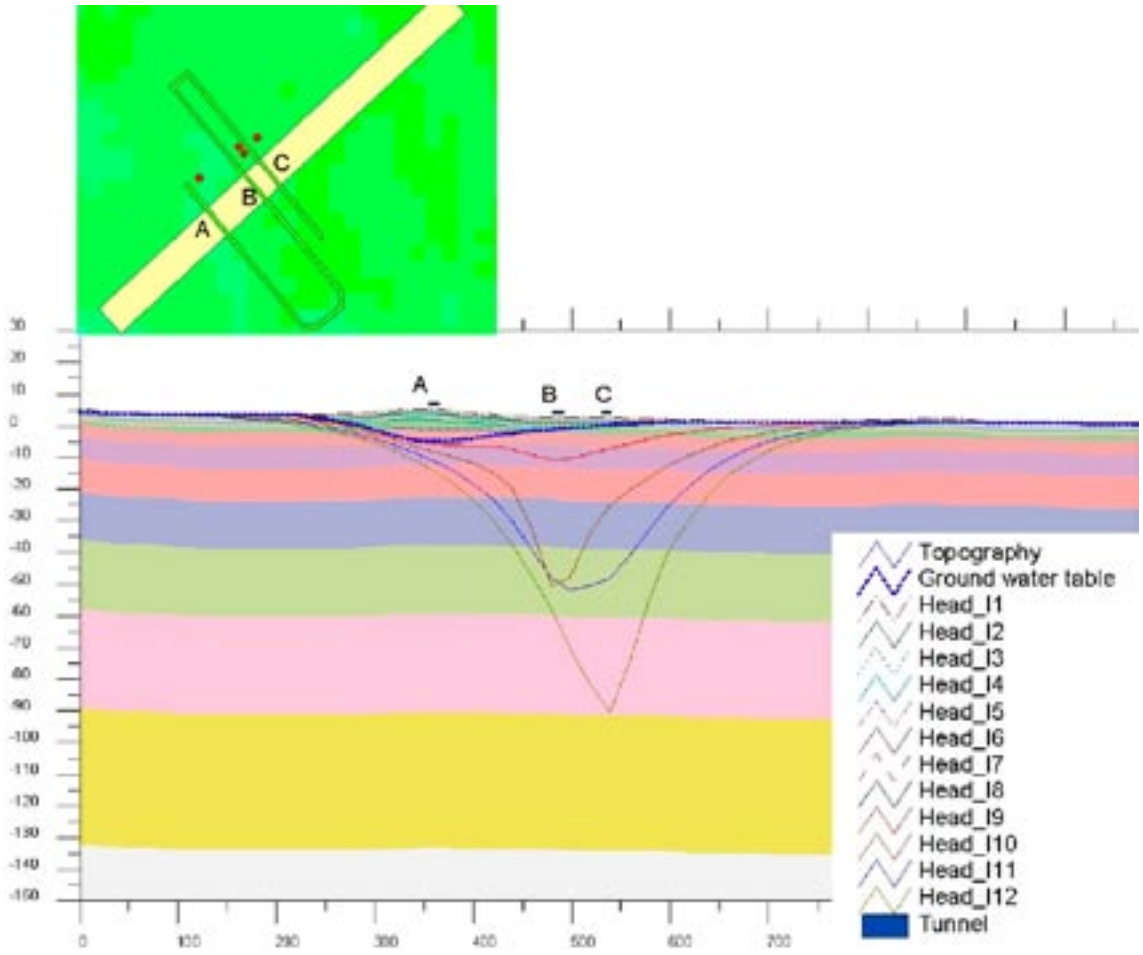

Figure 4-16. *Hydraulic head and groundwater table position in a cross-section of the access ramp. The cross-section intersects the ramp at the points A, B and C (cf. Figure 4-7). The plane view shows the locations of A–C, the ramp ("tunnel") and the shafts (red dots). For layer numbering, see Figure 4-15. Horizontal scale is metres, and vertical scale is metres above sea level.*

In Figure 4-15, the cross-section intersects the access ramp at points A and B. At point A, the ramp intersects the cross-section at 30 m below sea level (within calculation layer 9), whereas at point B the intersection is at 54 m below sea level (within calculation layer 10). In the upper calculation layers, the hydraulic head at A (shallow intersection) is influenced by the ramp, whereas there is a drawdown of the hydraulic head at B (deeper intersection) in the deeper layers, but not in layers closer to the ground surface. The last observation may be due to the low hydraulic conductivity of the bedrock at depth (see Table 4-3), reducing the transmission of the head drawdown towards the ground surface.

In Figure 4-16, the cross-section intersects the access ramp at points A, B and C (cf. Figure 4-7), at 10, 32 and 82 m below sea level (within calculations layers 7, 9 and 11, respectively). As in Figure 4-16, the shallow intersection (at A) causes head drawdown in the upper layers, and one can also see an impact on the hydraulic head in the deeper layers (10–12) from the deeper intersections (B and C). The head drawdown in the upper layers (due to the shallow intersection at A) is accompanied by groundwater level drawdown around point A, whereas no impact on the groundwater level can be noted around points B and C. Also this phenomenon is likely due to the low hydraulic conductivity of the bedrock at depth (cf. discussion on Figure 4-15); the hydraulic conductivity of the deep bedrock is too low to cause any drawdown of the groundwater level close to the ground surface.

4.3.3 Water balance

The MOUSE-SHE modelling results presented in Sections 4.3.1–4.3.2 show a relatively small inflow to the access ramp and the shafts, even in the case without grouting. Hence, the inflow has likely only a small influence on the water balance. The water balance for boundary case 1 without grouting is shown in Figure 4-17. Considering the land parts of the model area, in the no-grouting case the annual specific discharge is more or less unaffected (it is reduced from 143.5 mm to 143 mm; cf. Figure 3-8 for undisturbed conditions). The transpiration is reduced 2 mm (from 197 to 195 mm) and the total evapotranspiration 5 mm (from 454.5 to 449.5 mm).

As shown in Figure 4-17, the inflow to the access ramp and the shafts corresponds to a specific discharge of 4 mm when distributed over the whole land part of the model area (with a size of c. 26 km^2). Obviously, the inflow represents a much larger specific discharge if distributed just over the influence area of the groundwater level drawdown. For the simulation case in Figure 4-17 (boundary case 1, without grouting), according to Table 4-2 the size of the influence area is 0.26 km^2, which corresponds to 1/100 of the land parts of the model area. In turn, this implies that the inflow corresponds to a specific discharge of c. 400 mm within the influence area for the (hypothetical) non-grouting case. Even though this has not been quantified specifically, a simple area relationship indicates that the repository has large influence on the water balance within (the small) influence area of the groundwater level drawdown.

4.3.4 Surface water levels and discharges

The MOUSE-SHE modelling has neither shown any effects on surface water levels in lakes in the model area, nor on discharges in water courses. The magntitude of such effects is likely very sensitive to the assigned hydraulic properties and thickness of bottom sediments and underlying Quaternary deposits. These properties were not subject to any sensitivity analyses in the present study, but will be considered in the forthcoming version of the Forsmark MOUSE-SHE model.

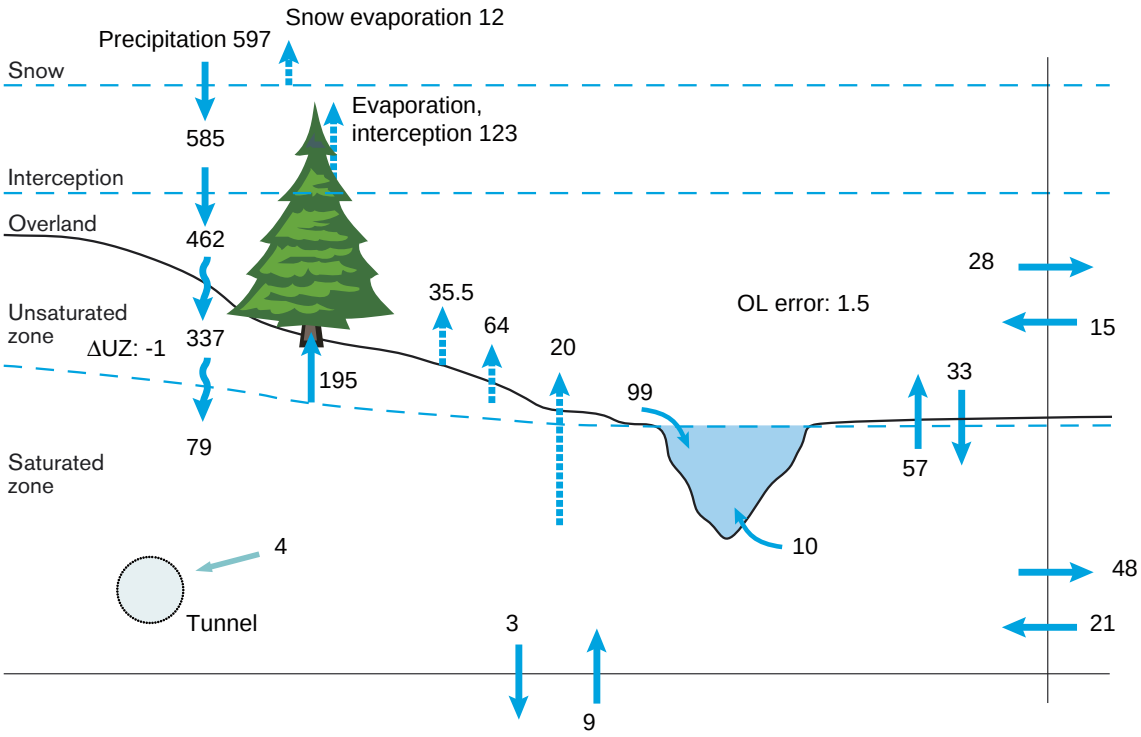

Figure 4-17. *Model-calculated water balance for the land parts of the MOUSE-SHE model area for boundary case 1 without grouting.*

4.4 Summary of open repository results

The MOUSE-SHE modelling shows that most of the inflow to the access ramp occurs in the upper c. 50 m of the ramp. Below 50 m below sea level the inflow is very small due to the low hydraulic conductivity of the bedrock. In the present modelling, the upper parts of the ramp are not intersected by high-conductive fracture zones, which overall leads to small inflow. The study shows that the model-calculated inflow is strongly dependent on the hydraulic conductivity of the bedrock in the vicinity of the access ramp, which implies that the results may be different when an updated bedrock model is used in forthcoming model versions. The modelling results also show that the inflow to the shafts is insignificant compared to the inflow to the access ramp.

The groundwater level drawdown and the size of its influence area (here defined as the area with a drawdown ≥ 0.3 m) are strongly affected by the extent of grouting applied, i.e. by the reductions of the rock hydraulic conductivity considered to represent different grouting alternatives. In a "worst case scenario" without grouting, the largest model-calculated drawdown of the groundwater level is 25 m, occurring above the access tunnel (which is shaped like a spiral that covers a certain horizontal area). Even in this (hypothetical) case, the MOUSE-SHE modelling does not show any negative effects on surface water levels or discharges. Moreover, the repository has minor impact on the water balance of the land part of the model area. However, this impact is larger if one considers the influence area of the groundwater level drawdown; in the worst case without grouting, the inflow to ramp and shafts corresponds to a specific discharge of 400 mm within the (small) influence area.

Generally, the differences in the inflow and drawdown results from boundary case 1 (deep parts of repository not included) and boundary case 2 (those parts included) were small. Case 2 produced a somewhat smaller inflow to the near-surface parts of the repository included in the MOUSE-SHE model, and a slightly larger influence area of the groundwater level drawdown. Boundary case 2 considered also the deep parts of the repository (i.e. parts located below the bottom boundary of the surface/near-surface model), by using a "disturbed" boundary condition obtained from the DarcyTools deep rock model that included the whole repository.

5 Solute transport from sources in the deep rock

This chapter presents the solute transport analyses performed using the updated Forsmark 1.2 surface hydrology/near-surface hydrogeology model described in Chapter 3. Specifically, we consider solute transport from sources in the deep rock, i.e. scenarios relevant for studying the transport from a deep geological repository. The modelling activities described below include particle tracking simulations (referred to as PT; see Section 5.1), and simulations with the MIKE SHE advection-dispersion module (abbreviated AD; see Section 5.2). In both cases, advective transport is modelled by use of the flow field for undisturbed conditions (Chapter 3). In some of the AD simulations a simple case of solute retardation, linear equilibrium sorption, is considered.

The objectives of the solute transport modelling are to:

- provide the SR-Can safety assessment with supporting, mainly qualitative information on the transport conditions in the uppermost part of the system,
- test and illustrate some of the solute transport capabilities of the MIKE SHE package,
- further develop the coupling of the partly overlapping deep rock and near-surface hydro-geological models.

The modelling uses the transient flow field from the MIKE SHE undisturbed conditions model in conjunction with the transport-specific parameters required by the PT and AD codes, respectively. In one of the PT cases considered, particles are injected along flow paths obtained from the SR-Can deep rock hydrogeology modelling reported in /Hartley et al. 2006/.

5.1 Particle tracking simulations

5.1.1 Methodology

In particle tracking simulations, hypothetical inert particles or “water parcels” are traced as they are transported by the groundwater flow field in the model volume. The resulting flow paths provide important information as such; they connect the selected starting points with groundwater discharge points or other exit points on the model boundaries. Furthermore, travel or residence times along the flow paths can be calculated.

The calculated, three-dimensional flow field is the basis for the advective transport of the particles. In MIKE SHE, the particles are transported in accordance with the local groundwater velocity calculated in the “Water movement” module. In addition to the input required for the flow modelling, the particle tracking simulations require input data on the effective porosity, the number of particles introduced, and the starting point of each particle. The effective porosity of the bedrock is imported from the DarcyTools model /Svensson 2005/, whereas the effective porosity of each QD material is assumed to be equivalent to the specific yield of that material (see Chapter 2).

In the MIKE SHE version used in the present work, particle tracking simulations can be made in the saturated groundwater zone only; particles that leave the saturated zone are not traced further. However, it is possible to identify what kind of sinks the particles have moved to, which means that it can be determined if the particles discharged into the unsaturated zone, water courses or wells, or if they left the model volume through the side or bottom boundaries. No wells are included in the present MIKE SHE modelling of the Forsmark area, but the option of using wells as registration zones could be useful in future safety assessment modelling.

Three cases, referred to as PT1, PT2 and PT3, respectively, were studied in the particle tracking simulations:

- PT1: Uniform injection below the whole land area within the model boundary (see Figure 3-1), transient flow in the MIKE SHE model.
- PT2: Injection at points given by flow paths calculated using the deep rock groundwater flow model, transient flow in the MIKE SHE model.
- PT3: Injection at points given by flow paths calculated using the deep rock groundwater flow model, steady flow in the MIKE SHE model.

In all particle tracking simulations, the particles were introduced in the second lowest layer in the model; it is not possible to introduce particles in boundary cells. Since particle injection points should be some distance into the rock to allow sufficient overlap with the deep rock hydrogeology model (cf. below), the MIKE SHE model was extended with an additional calculation layer such that the new bottom boundary was placed at 150 m below sea level. By extending the model to a larger depth, particles could be introduced at 135 m below sea level despite the fact that particles cannot be placed in boundary cells.

The simulation time was 1,500 years in all simulation cases, using the calculated transient flow modelling results obtained for the simulated one-year period during 2003–2004 as input. This means that the model results from the MIKE SHE Water movement calculation for this one-year period were cycled 1,500 times. In one of the cases, PT3, the transient model results were compared with those obtained from a steady state flow field in MIKE SHE.

A number of “registration zones” in the second uppermost calculation layer were defined. These zones make it possible for the user to study where in the model volume each particle emerges, i.e. the arrival of the particle in each pre-defined registration zone can be monitored. It is also possible to calculate the travel times for a particle to each specific registration zone. Thus, we have used two ways of observing the particles in these simulations: (i) to monitor their arrival in the various selected registration zones in calculation layer 2 (including a calculation of the associated travel times), and (ii) to determine where (to which other compartment or boundary) they left the saturated zone (cf. above).

In the present modelling of the Forsmark area, each sub-catchment, each lake and a set of marine basins were defined as registration zones. The registration zones in the sea are presented in Figure 5-1, where it can be noted that there are a number of smaller land areas within or between the sea basins that are not included in the registration zones (e.g. a number of islands and the area where the SFR facility is situated). Figure 5-2 shows the sub-catchment areas and lakes considered as registration zones in the on-shore part of the model area, also displaying the catchment numbers and lake names used in the presentation of results below.

Also in this case, it is seen that there are areas not included in the registration zones. Some of these are areas with direct runoff to the sea located between the identified catchments and the shoreline, i.e. areas that lack water courses and therefore are not part of the catchment hierarchy. However, a comparison of the registration zones in Figure 5-2 and the model area in Figure 3-1 shows that there are additional land areas north of the identified catchments where particles are introduced.

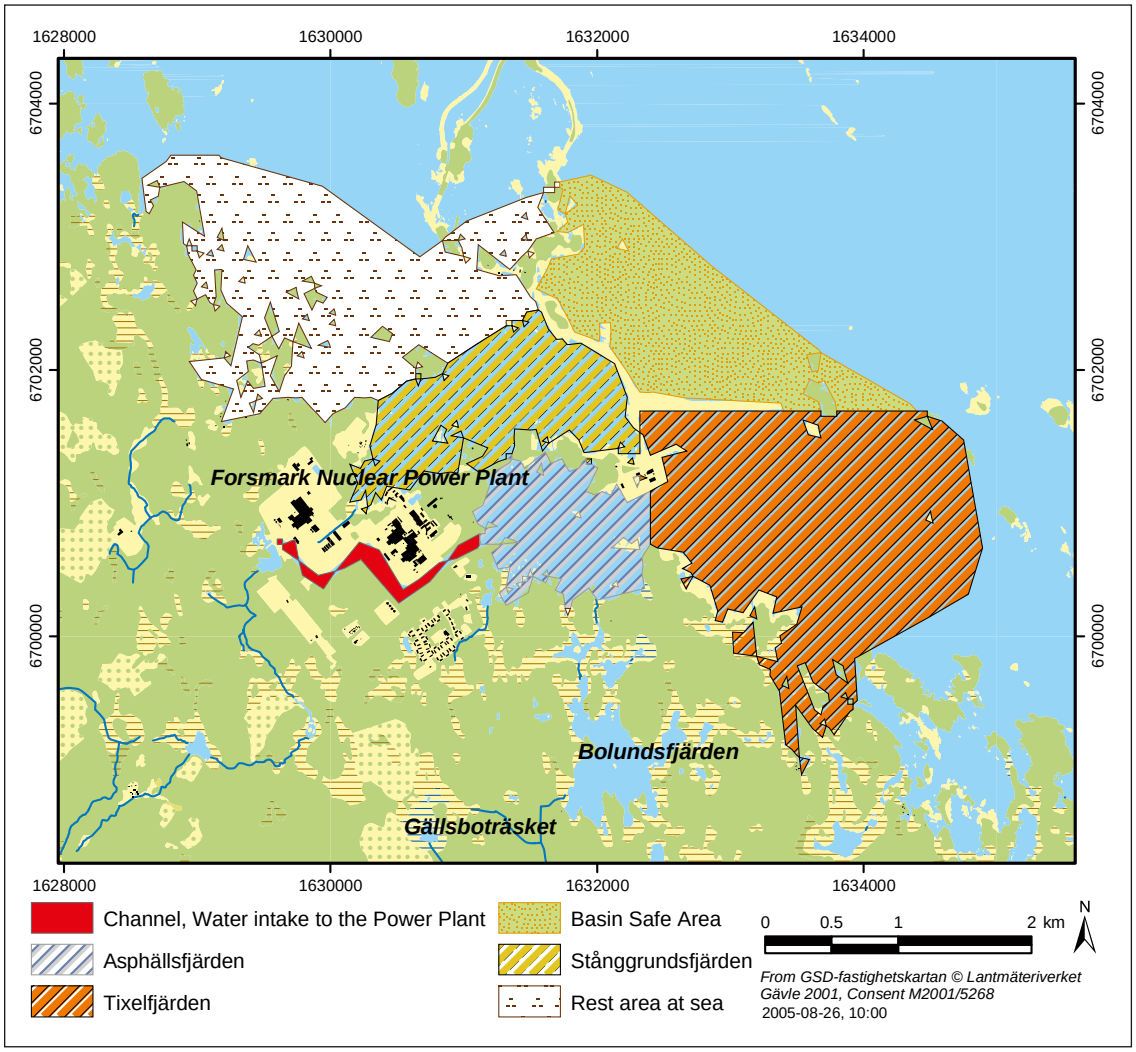

Figure 5-1. *Off-shore registration zones in the particle tracking simulations, including a number of marine basins and the intake channel to the nuclear power plant.*

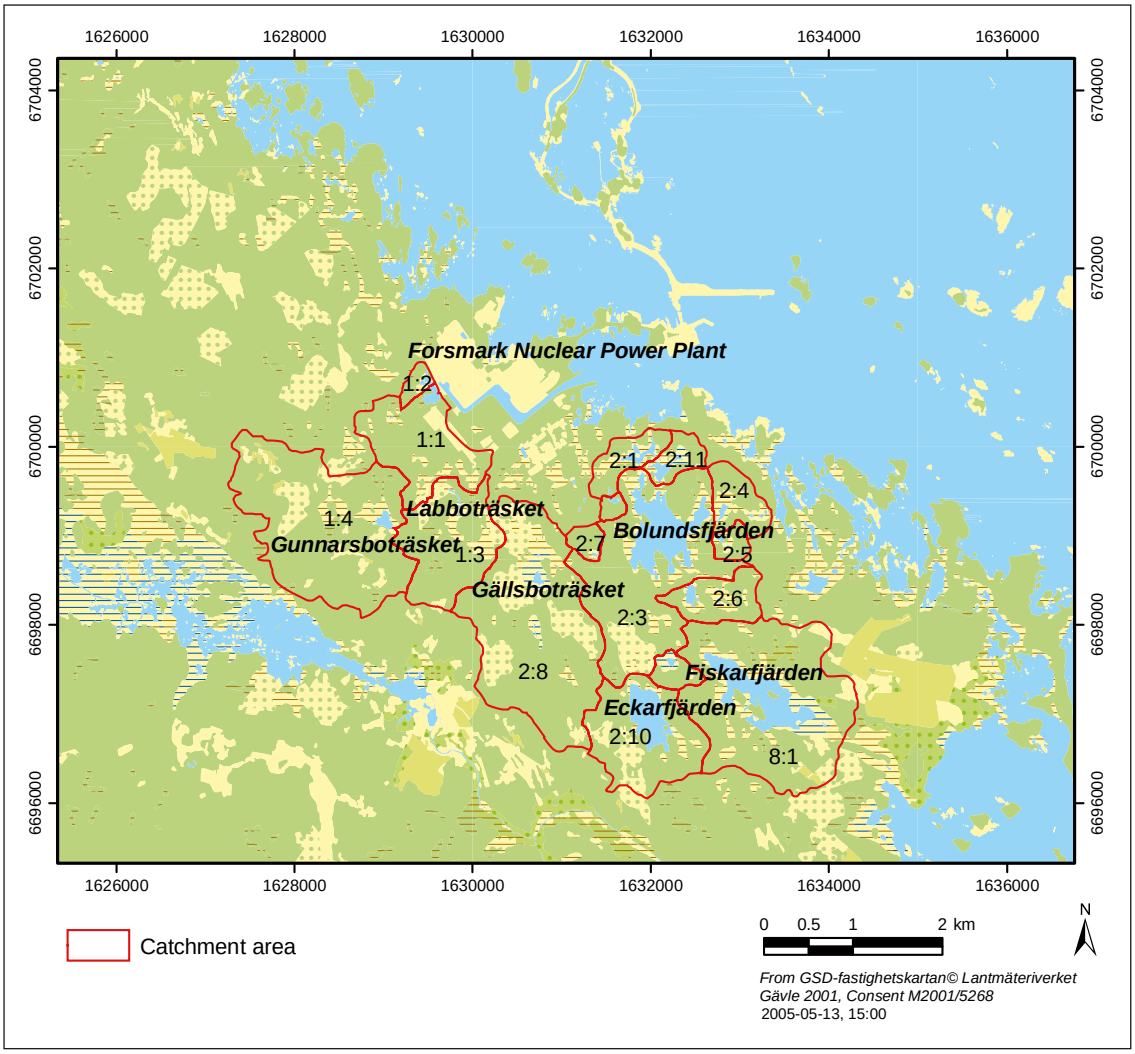

Figure 5-2. *Registration zones on land. Each catchment and lake marked in the figure corresponds to a registration zone in the particle tracking simulations.*

5.1.2 Uniform injection below the land area

The first particle tracking case, PT1, considered a uniform injection, in which three particles were introduced in each grid cell below the land part of the model area (Figure 3-1); no particles were introduced in cells overlain by the sea. In total, 49 962 particles were introduced in case PT1. The overall results, expressed in terms of where the particles left the saturated zone, i.e. to which other model compartments or boundaries they went, are summarised in Table 5-1.

Table 5-1. Results of particle tracking case PT1 showing where the particles went from the saturated zone.

	Number of particles	Fraction
Particles to the unsaturated zone	32,101	64.2%
Particles to the sea	11,159	22.3%
Particles to MIKE 11	5,401	10.8%
Particles crossing the bottom boundary	939	1.9%
Particles left in the model volume	362	0.7%
Total number of particles injected	49,962	100.0%

It is seen in the table that most of the particles, c. 64% of all particles introduced, left the saturated zone to enter the unsaturated zone. The second largest sink is the sea, which is particularly interesting to note given the fact that no particles were injected below the sea. The MIKE 11 surface water compartment is the destination for 11% of the particles. Approximately 2% of the particles left the model volume through the bottom boundary, whereas less than 1% of the particles were left in the model volume at the end of the simulation period (after 1,500 years).

As explained above, the particle tracking was also monitored by means of a collection of specific registration zones in the second uppermost calculation layer. This implies monitoring of the arrivals of particles in layer 2 within, for example, the area which at the ground surface is occupied by a specific lake. It should be noted that this does not necessarily mean that all particles registered in layer 2 within the "footprint" of the lake go directly from the saturated zone to the lake water. They may also, to some extent, discharge to the unsaturated zone in the vicinity of the lake perimeter.

With this remark in mind, the results still demonstrate that the lakes attract particles from surrounding areas. Table 5-2 shows a comparison of the number of particles released and registered, respectively, within the "footprint" of each lake within the model area. The results clearly demonstrate that the particles travel towards the lakes. The relative increase in the number of particles is larger for the small lakes than for the large lakes; Lake Labboträsket attracts five times as many particles from the surroundings as released below the lake, whereas the "imports" of particles to Lake Bolundsfjärden and Lake Fiskarfjärden correspond to 1.6 and 1.3 times the number of particles injected below the lake, respectively.

Figure 5-3 shows the starting positions of the particles registered in the lakes, using different colours for the particles associated with the different lakes. It is clear that the particles registered in the lakes originate from their immediate surroundings, and that no evidence of long-range transport to the lakes can be found. Thus, the results show that most particles released at 135 m below sea level remain within the sub-catchments where they were released; this, in turn, indicates that the horizontal transport distances are relatively small in the upper part of the rock and in the QD.

The observation of relatively small inter-catchment transport is further substantiated by the results shown in Table 5-3, where a comparison of the total numbers of particles released and registered (i.e. including both lakes and land areas) within some of the sub-catchments is presented. The larger sub-catchments receive or lose amounts corresponding to about 10% of the particles released there. Note that both increases and decreases relative to the injected amounts of particles are observed. For the smaller sub-catchments, here exemplified by 2:6 and 2:11, the relative differences can be much larger.

Table 5-2. Comparison of the number of particles released (at 135 m below sea level) and registered (in calculation layer 2) below the lakes, case PT1 (CA = catchment area).

Registration zone (lake)	CA	Released particles	Registered particles	Absolute increase	Relative increase
Labboträsket	1:3	99	601	502	507%
Gunnarsboträsket	1:4	135	560	425	315%
Bolundsfjärden	2:3	1,122	2,900	1,778	158%
Gällsboträsket	2:8	339	1,386	1,047	309%
Eckarfjärden	2:10	531	1,947	1,416	267%
Fiskarfjärden	8:1	1,473	3,406	1,933	131%

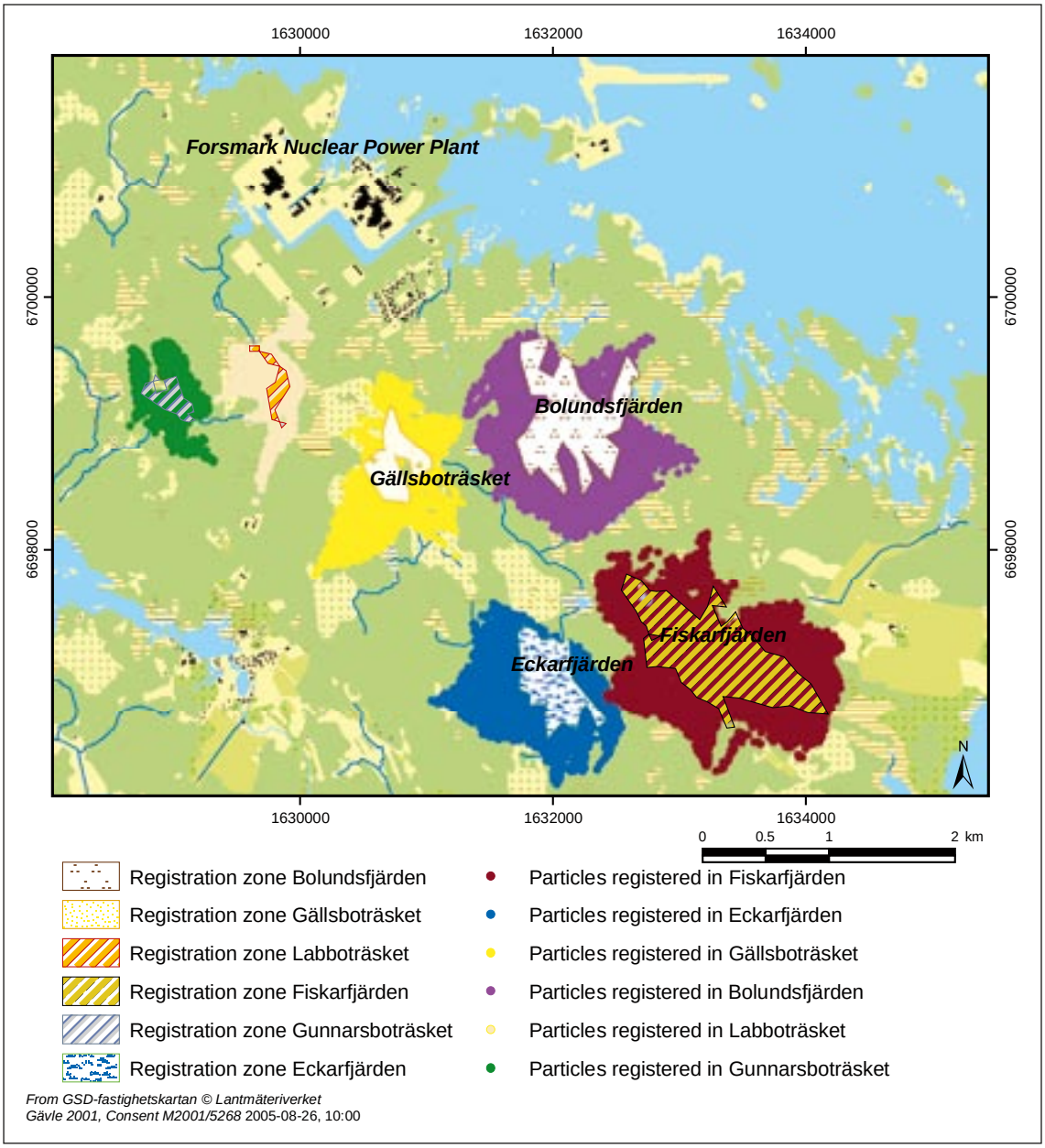

Figure 5-3. *Starting positions of particles registered in the lakes. Different colours are used to indicate particles associated with different lakes. For example, the whole blue area, including the area below the lake, generated particles to Lake Eckarfjärden.*

The areas with direct runoff to the sea ("DRO areas" in Table 5-3) lose about 50% of the particles released there. This, of course, is because the sea acts as a sink, which has its largest effect on the land areas next to it. Also other areas lose particles to the registration zones below the sea. This tendency of transport from the land areas to the sea, which implies a negative average particle balance for the land areas, is the main reason for transport across sub-catchment boundaries.

The results for the registration zones below the sea are summarised in Table 5-4. Since no particles were introduced below the sea, all particles are "imported" from the below-land injection areas. Thus, a comparison between released and registered particles is not of much interest, and therefore only the distribution among the different basins/zones is shown in the table. The results show that the largest number of particles (c. 24%) was registered below the

Table 5-3. Comparison of the number of particles released (at 135 m below sea level) and registered (in calculation layer 2) below some of the sub-catchment areas, case PT1 (CA = catchment area, DRO = direct runoff (to the sea)).

Registration zone (catchment area)	Released particles	Registered particles	Absolute difference	Relative difference
CA 1:4[1]	5,361	4,615	–746	–13.9%
CA 2:3[1]	4,677	5,070	+393	+8.4%
CA 2:6	930	681	–249	–26.8%
CA 2:10[1]	2,541	2,344	–197	–7.8%
CA 2:11	447	712	+265	+59.3%
CA 8:1[1]	5,850	5,240	–610	–10.4%
DRO areas	17,706	9,229	–8,477	–47.9%

[1] The lake in the catchment is included.

Table 5-4. Particles registered in zones below the sea, case PT1; number of particles per zone and fractions of the total number of particles in all sea zones.

Registration zone (sea basin)	Registered particles	Fraction
Intake channel	1,989	23.7%
Tixelfjärden	1,717	20.5%
Asphällsfjärden	1,265	15.1%
Stånggrundsfjärden	1,188	14.1%
Basin SAFE area	409	4.9%
Rest area at sea	1,825	21.7%
Total number of particles	8,393	100.0%

intake channel to the nuclear power plant. As shown in Figure 5-1, this zone covers only a small area. However, the channel is a deep excavation in the rock, and therefore constitutes a strong sink.

Among the other off-shore registration zones, it can be noted that Asphällsfjärden and Tixelfjärden, located just north and north-east of the candidate area, received about 35% of the particles that went to the sea registration zones. The basins further to the north, i.e. Stånggrundfjärden, the SAFE basin, and the “rest area” along the coastline, receive more than 40% of the particles. Most of these particles probably come from the adjacent (northern) land areas, and not from within the candidate area.

As mentioned in Section 5.1.1, the flow paths obtained in particle tracking simulations can be characterised in terms of travel times (also other quantities, such as path lengths, are commonly calculated in this type of simulations). Travel time statistics for the particles registered in the lakes within the model area are summarised in Table 5-5. The mean travel times from 135 m below sea level are in the range 6–25 years, with the smallest and largest mean travel times observed for Lake Gällsboträsket and Lake Fiskarfjärden, respectively. The minimum travel times in most of the lakes are on the order of a few months, whereas the maximum travel times are from a couple of decades to more than 700 years (Lake Fiskarfjärden).

The travel time results are visualised Figure 5-4. In this figure, the travel times of the particles are shown at each starting position; the colour at the starting position of a particle indicates the travel time of that particle to the lake where it was registered. It could be expected that the travel length (i.e. essentially distance from the injection point to the lake perimeter) is the flow path

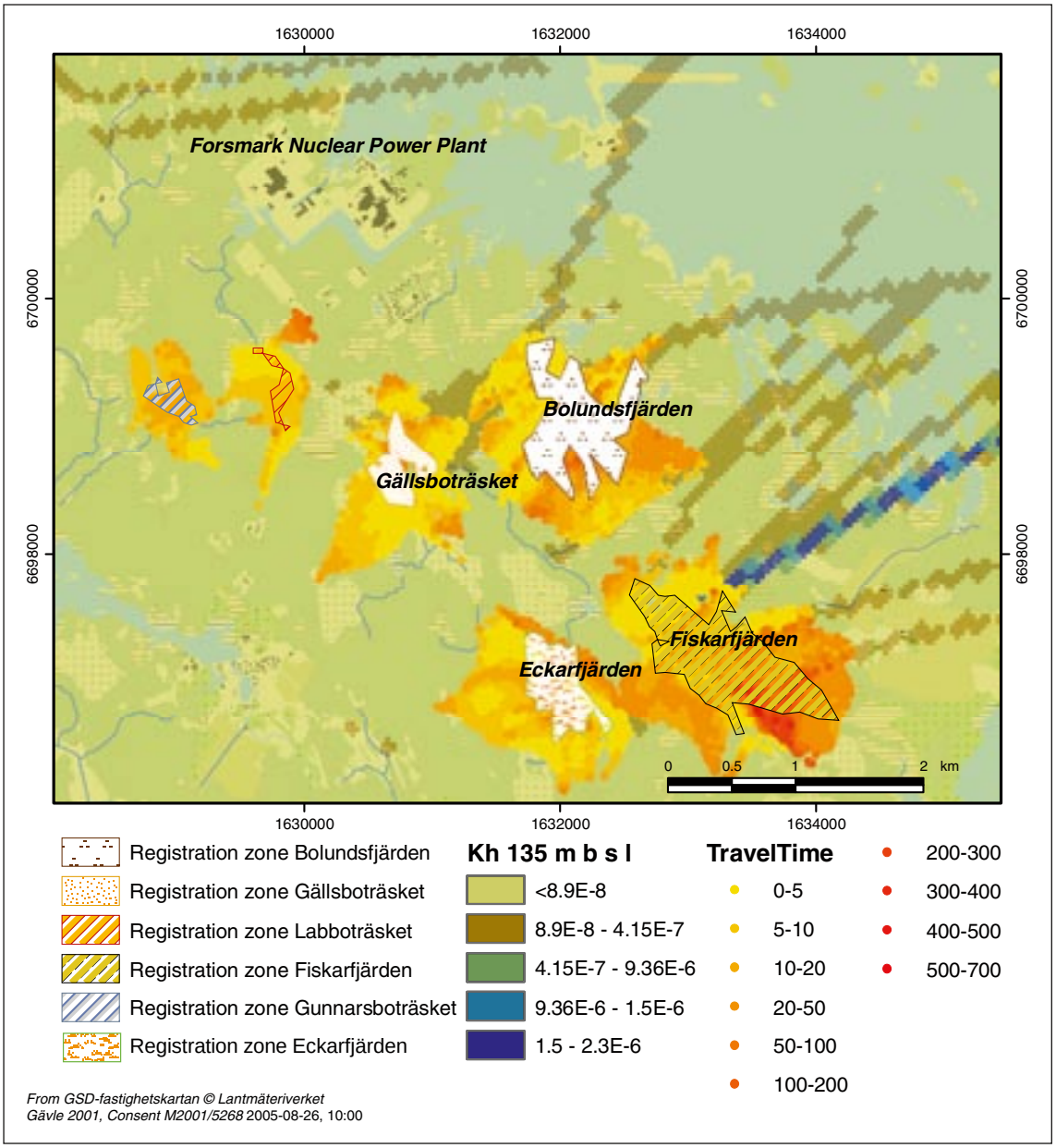

Figure 5-4. *Travel times (years) of the particles registered in the lakes in the model area; the travel time of a particle is indicated by the colour at the starting position of that particle. The hydraulic conductivity (ms^{-1}) of the bedrock at 135 m below sea level is also shown in the figure.*

Table 5-5. Calculated mean, maximum and minimum travel times from 135 m below sea level of the particles registered in each lake in the model area, case PT1 (CA = catchment area).

Registration zone (lake)	CA	Mean (years)	Max. (years)	Min. (years)
Labboträsket	1:3	8	158	0.6
Gunnarsboträsket	1:4	9	22	3.0
Bolundsfjärden	2:3	12	249	0.4
Gällsboträsket	2:8	6	63	0.3
Eckarfjärden	2:10	9	77	0.5
Fiskarfjärden	8:1	25	729	0.2

characteristic determining the travel time, thereby forming successively darker “rings” around the lakes in Figure 5-4. However, the figure indicates that the local flow conditions are spatially variable, and that the travel times rarely show this type of regular pattern. In some cases, these local variations in flow conditions and travel time can be correlated to the deformation zones indicated by higher hydraulic conductivities in the figure.

5.1.3 Injection along flow paths from the repository

In the second and third particle tracking cases, PT2 and PT3, respectively, the starting positions of the introduced particles were taken from results of particle tracking simulations with the deep rock groundwater flow model. We refer to this model as a “deep rock model” because it extends to large depth in the rock. It should be noted, however, that the deep rock model goes all the way up to the ground surface. The results utilised in the present work were obtained in the groundwater flow modelling performed for the SR-Can safety assessment using the ConnectFlow tool, see /Hartley et al. 2006/ for details. Specifically, results from the case labelled “SC_HCD3_BC_HRD3EC_HSD1_BC1_local50” are used here.

The ConnectFlow deep rock groundwater flow model is based on an Equivalent Continuum Porous Medium (ECPM) representation of the larger deformation zones and the fractured rock between them, in which the small deformation zones and the fractures are modelled stochastically using a Discrete Fracture Network (DFN) description of the rock. The hydraulic data used to develop the ConnectFlow model in /Hartley et al. 2006/ are the same as those used in the DarcyTools model in /Svensson 2005/ providing rock properties and boundary conditions for the present MIKE SHE model. However, it would obviously be preferable to take all deep rock input from the same model in future modelling efforts combining deep rock and near-surface hydrogeological models.

The ConnectFlow model considers transient, variable-density groundwater flow, where the transients are caused by shoreline displacement and salinity variations during a period of many thousand years before and after present. Thus, the transients are related to long-term changes/processes compared with the seasonal variations studied in the MIKE SHE model. However, the particle tracking in the deep rock model was performed in “frozen” flow fields representing “snap shots” of the transient flow at specific times. In the present modelling, we use flow paths generated using the modelled present-day flow field.

In the deep hydrogeological model, particles were released at each canister position specified in the repository layout /Brantberger et al. 2006/; this implies that the particles were introduced at about 410 m below sea level. The particles were traced in the “frozen” flow field from repository depth up to the ground surface. For the purpose of the present work, the locations of the particles at 135 m below sea level were exported from the ConnectFlow model to obtain input data on the starting positions of the particles in the MIKE SHE particle tracking cases PT2 and PT3. The resulting “birth locations” of the MIKE SHE particles are shown in Figure 5-5. It is noted that most of these locations are situated below the sea, especially in the Asphällsfjärden sea basin.

The starting positions and the number of particles introduced were the same in the two MIKE SHE particle tracking simulation cases PT2 and PT3; a total number of 6,676 particles were introduced in each simulation. The difference between the cases was that PT2 was based on the same transient flow field as PT1, whereas PT3 was performed in a steady flow field obtained from a selected time step in the transient simulation; the results were taken from the month of May during the year cycled in the transient case. This implies that the comparison between PT2 and PT3 indicates whether the seasonal variations in flow affect the flow paths.

The results of the PT2 and PT3 cases indicate that most particles travel more or less vertically up to the sea basins, and that the effects of seasonal variations in flow are small. The overall picture of where the particles exit the saturated zone shows that c. 90% of the particles discharge into the sea. Clearly, this is strongly related to the fact that most of the particles were injected

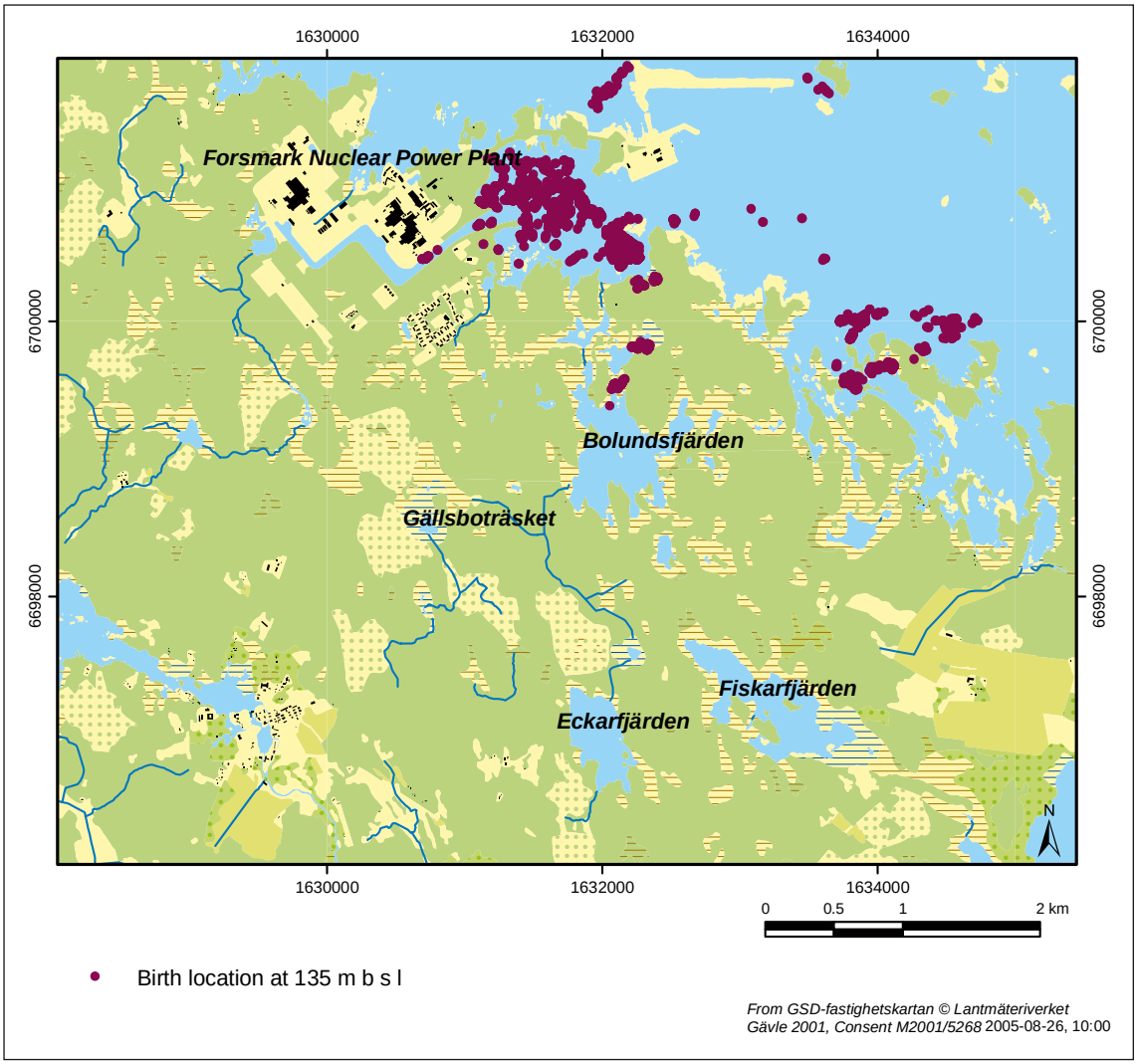

Figure 5-5. *Starting positions ("birth locations") of the particles in cases PT2 and PT3 obtained from the ConnectFlow particle tracking results in /Hartley et al. 2006/.*

below the sea (Figure 5-5). Most of the other particles, i.e. about 10%, went from the saturated to the unsaturated zone, whereas other sinks were found negligible. The amounts of particles left in the model volume at the end of the simulation were small, 1% in PT2 and 0.5% in PT3; this is the only result that shows large (relative) differences between the cases.

Similar to what was done in PT1 (cf. above), particle tracking results have also been obtained for the off- and on-shore registration zones in calculation layer 2, see Figure 5-1 (sea) and Figure 5-2 (land). The PT2 results for the different registration zones are shown in Figure 5-6. Specifically, the figure shows the starting positions of the particles registered in the various sea and land zones. The general observation made in the comparison between the starting positions at 135 m below sea level and the arrival points in the registration zones in layer 2 is that the particles stay within the zones where they were injected. This implies essentially vertical transport in the considered depth interval. In the few cases where particles have moved to a different zone, the horizontal transport distances appear to be small.

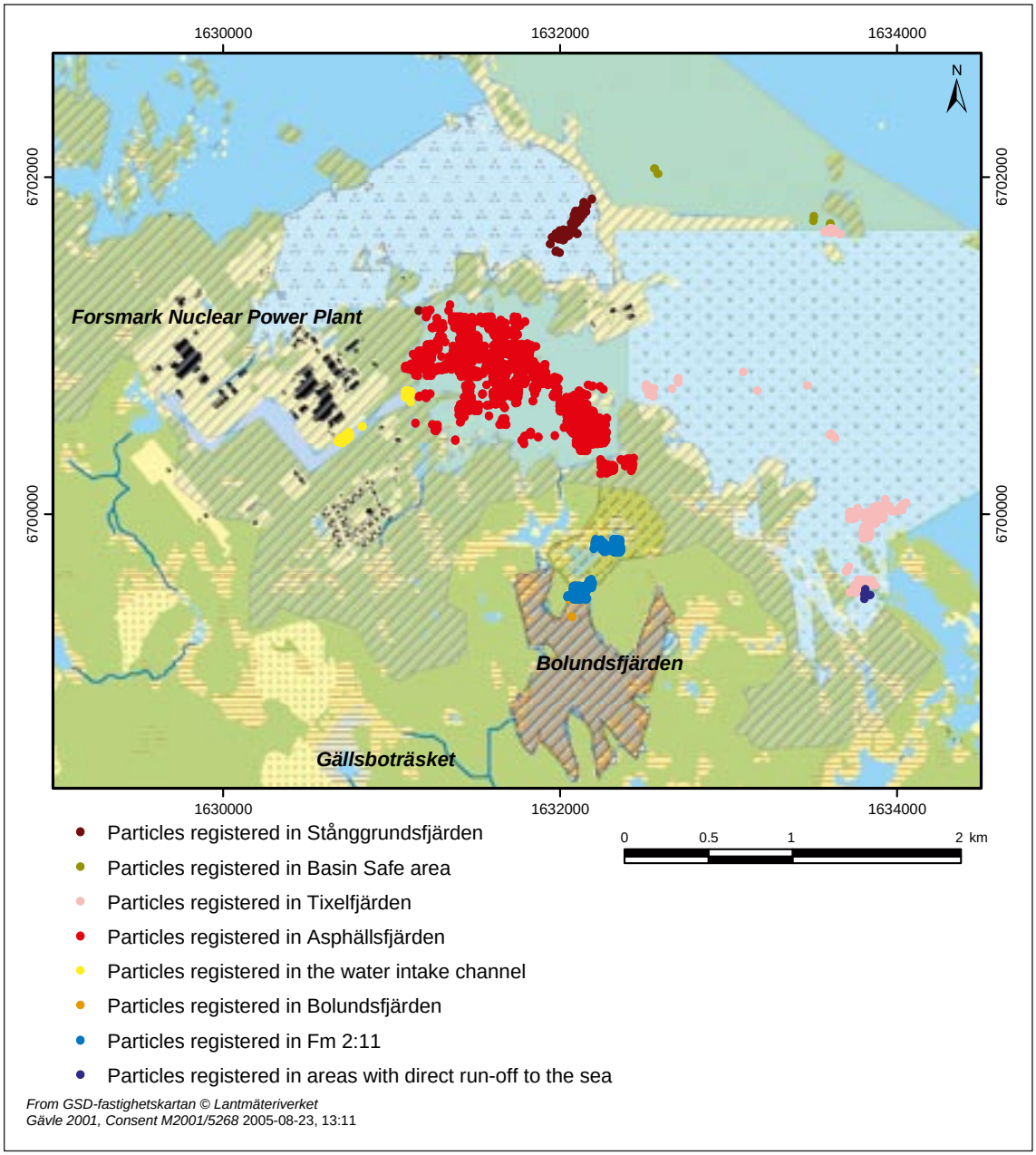

Figure 5-6. *Results of particle tracking case PT2. The figure shows the registration zones, and the "birth locations" of the particles registered in different registration zones.*

The results for the registration zones in calculation layer 2 are summarised in Table 5-6. These results lend further support to the observations of the dominance of the sea registration zones and the small differences between PT2 and PT3. Approximately 80% of the particles are registered below Asphällsfjärden, whereas the other sea zones received c. 10% combined. Among the registration zones on land, sub-catchment 2:11 received by far the largest amounts of particles; the particles registered there correspond to almost 10% of all injected particles. This sub-catchment contains Lake Puttan, which, however, is not treated as a separate registration zone in this work.

Table 5-6. Particles registered in different land (catchments and lakes) and sea registration zones (DRO areas = direct runoff areas), cases PT2 and PT3. Results are reported as numbers of particles, with fractions of the total number of particles injected within parenthesis; PT2 is used as reference when comparing the two cases.

	PT2	PT3	Absolute difference	Relative difference
Off-shore registration zones:				
Asphällsfjärden	5,315 (79.6%)	5,326 (79.8%)	–11	–0.2%
Tixelfjärden	525 (7.9%)	527 (7.9%)	–2	–0.4%
Water intake channel	67 (1.0%)	68 (1.0%)	–1	–1.5%
Stånggrundsfjärden	59 (0.9%)	58 (0.9%)	+1	+1.7%
Basin SAFE area	5 (0.1%)	7 (0.1%)	–2	–40.0%
On-shore registration zones:				
Catchment 2:11 (Puttan)	629 (9.4%)	635 (9.5%)	–6	–1.0%
Lake Bolundsfjärden	5 (0.1%)	1 (0.0%)	+4	+80.0%
DRO areas	4 (0.1%)	0 (0.0%)	+4	+100.0%
Not registered	67 (1.0%)	54 (0.8%)	+13	+19.4%
Total particles injected	6,676	6,676		

The reason for the concentrated discharge of particles below and around Lake Puttan is that a large water-bearing deformation zone reaches the near-surface groundwater system in this area. Concerning the other registration zones on land, i.e. Lake Bolundsfjärden and the areas with direct runoff to the sea, it can be noted that only very few particles are registered there. These areas also display the largest relative differences between the PT2 and PT3 cases. However, the general impression from the comparison between the two cases is that the differences are very small, which means that the effects on the flow paths of neglecting the seasonal variations, as tested here, also are small.

As shown in Table 5-7, the mean travel times of the particles registered in case PT2 vary between 4 and 230 years. Interestingly, the longest mean travel time is obtained for the Asphällsfjärden registration zone where most of the particles are registered. The shortest mean travel times are observed in catchment 2:11 and in Lake Bolundsfjärden, indicating fast transport in deformation zones connecting the deep rock and the QD. The minimum and maximum travel times of all registered particles fall within a range from less than one year (catchment 2:11) to more than 900 years (the Asphällsfjärden basin). The travel times are visualised on a particle-by-particle basis in Figure 5-7.

Table 5-7. Calculated mean, maximum and minimum travel times from 135 m below sea level of the particles registered in each registration zone in the model area, case PT2.

Registration zone	Mean (years)	Max. (years)	Min. (years)
Asphällsfjärden	230	910	6.1
Tixelfjärden	26	780	3.8
Basin SAFE area	12	18	6.4
Stånggrundsfjärden	17	51	6.1
Water intake channel	14	20	5.8
Catchment 2:11	4.0	9.9	0.9
DRO areas	8.8	10	7.1
Lake Bolundsfjärden	3.9	6.3	1.9

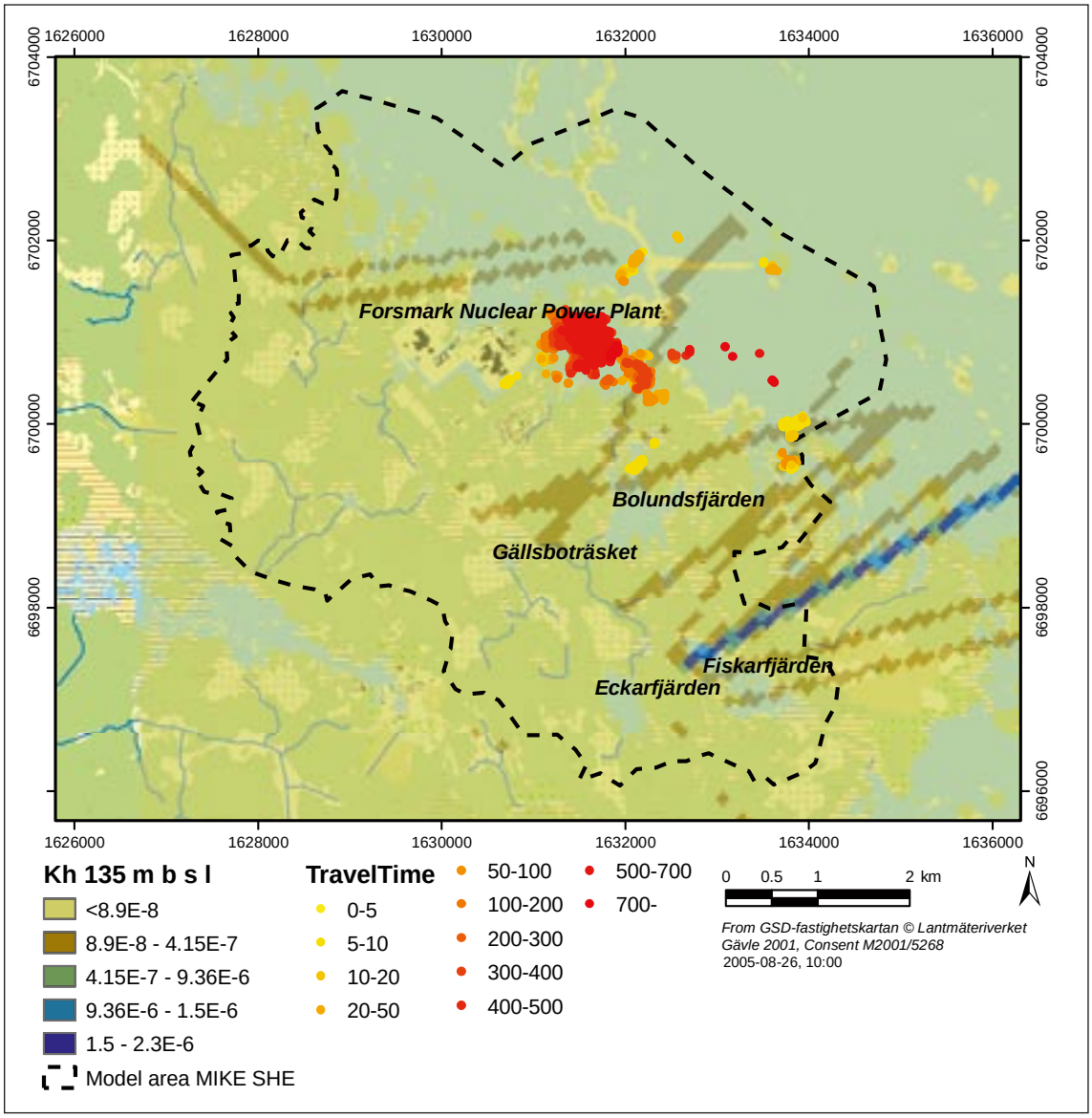

Figure 5-7. *Travel times (years) of the particles registered in case PT2. The hydraulic conductivity at 135 m below sea level (ms^{-1}) is also shown in the figure.*

It should be noted that the travel times are recorded along flow paths from the injection depth (135 m below sea level) to calculation layer 2 in the saturated zone. This means that they do not represent flow paths through the whole surface system. Further transport that would increase the travel times could take place both by groundwater and by surface water.

5.1.4 Comparison between MIKE SHE and ConnectFlow results

As mentioned above, the particles released in the ConnectFlow deep rock model are traced all the way up to the ground surface, whereas the particle tracking in MIKE SHE (cases PT2 and PT3) uses the ConnectFlow particle locations at 135 m below sea level as starting points. Thus, the effects of using the more detailed description of the upper part of the system provided by the MIKE SHE model can be evaluated by comparing the results from the two models. Specifically, a comparison is here made between the points where the particles leave the saturated zone, referred to as “exit points”, in each model. Depending on where these exit points are located, they can indicate points of discharge to the sea, to a lake, or to the unsaturated zone.

The MIKE SHE and ConnectFlow exit points comparison is illustrated in Figure 5-8, showing all particles, and Figure 5-9, which is a close-up of the area where most of the particles discharged. Blue dots indicate ConnectFlow exit points, whereas the MIKE SHE exit points are coloured on a pink-to-red scale in proportion to the number of particles recorded per cell. The results from the two models show very similar patterns. The detailed exit points differ in some cases, but the overall impression is that particles do not travel very far to "new areas" when a more detailed description of the near-surface hydrogeology is introduced. The main difference between the results from the two models is that there are no particles registered in terrestrial areas in the MIKE SHE model. Furthermore, the spreading of the particles appears to be slightly larger in the ConnectFlow results.

It follows that the present MIKE SHE-ConnectFlow comparison indicates that the more detailed treatment of the processes in the near-surface system offered by MIKE SHE has relatively small effects on the exit points. To some extent, this is probably due to the fact that most of the particles in the present analysis discharge to the sea. Vertical flow and transport are expected to dominate below the sea. Further studies of the agreement between different modelling approaches, or the lack thereof, are required to justify the safety assessment modelling approach and, if needed, provide a more detailed analysis of the near-surface flow paths. This type of modelling will be performed in connection with future model versions.

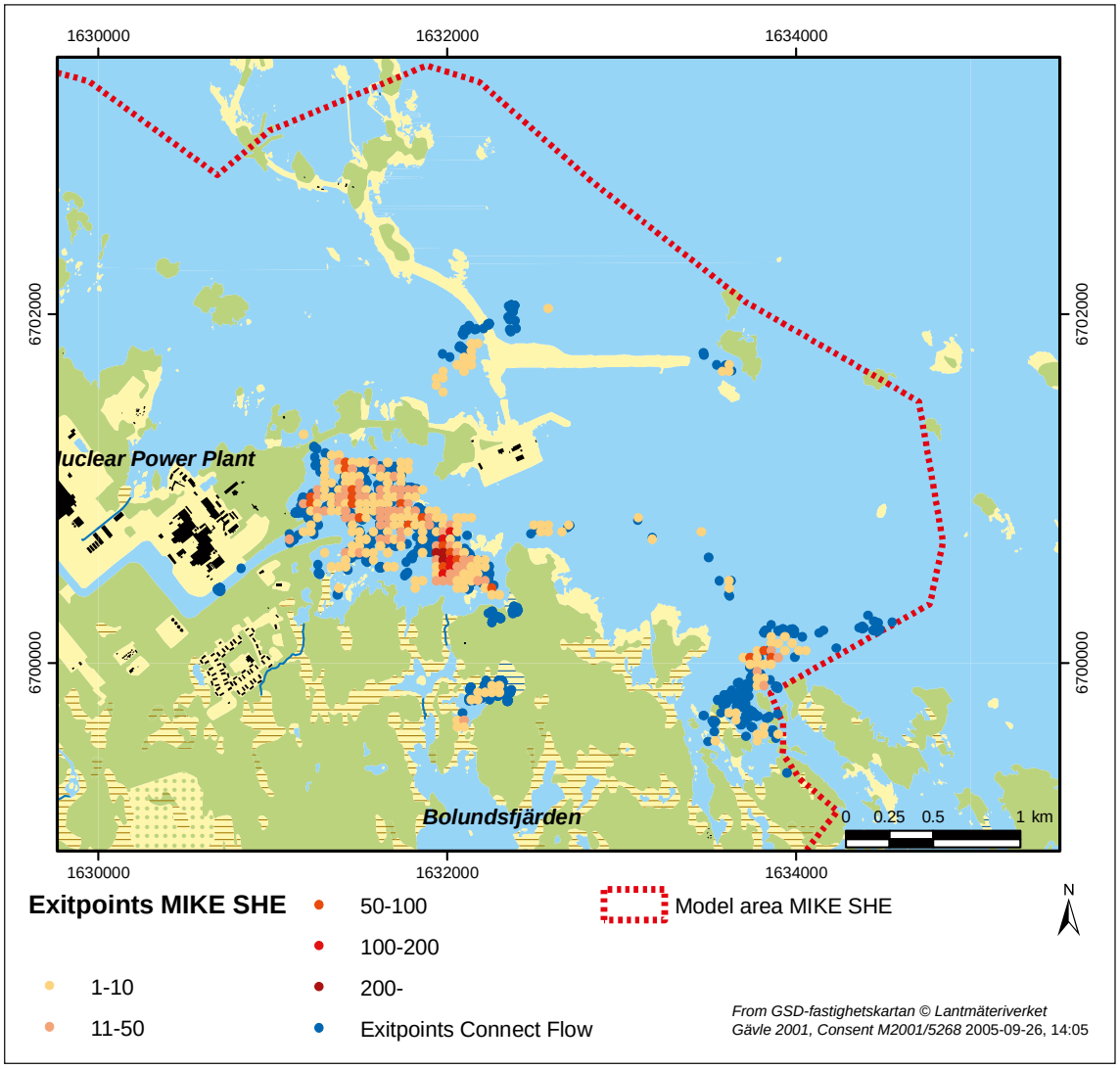

Figure 5-8. *Exit points of particles calculated with MIKE SHE (case PT2; pink to red dots, depending on the recorded number of particles per cell in the MIKE SHE model), and ConnectFlow (blue dots).*

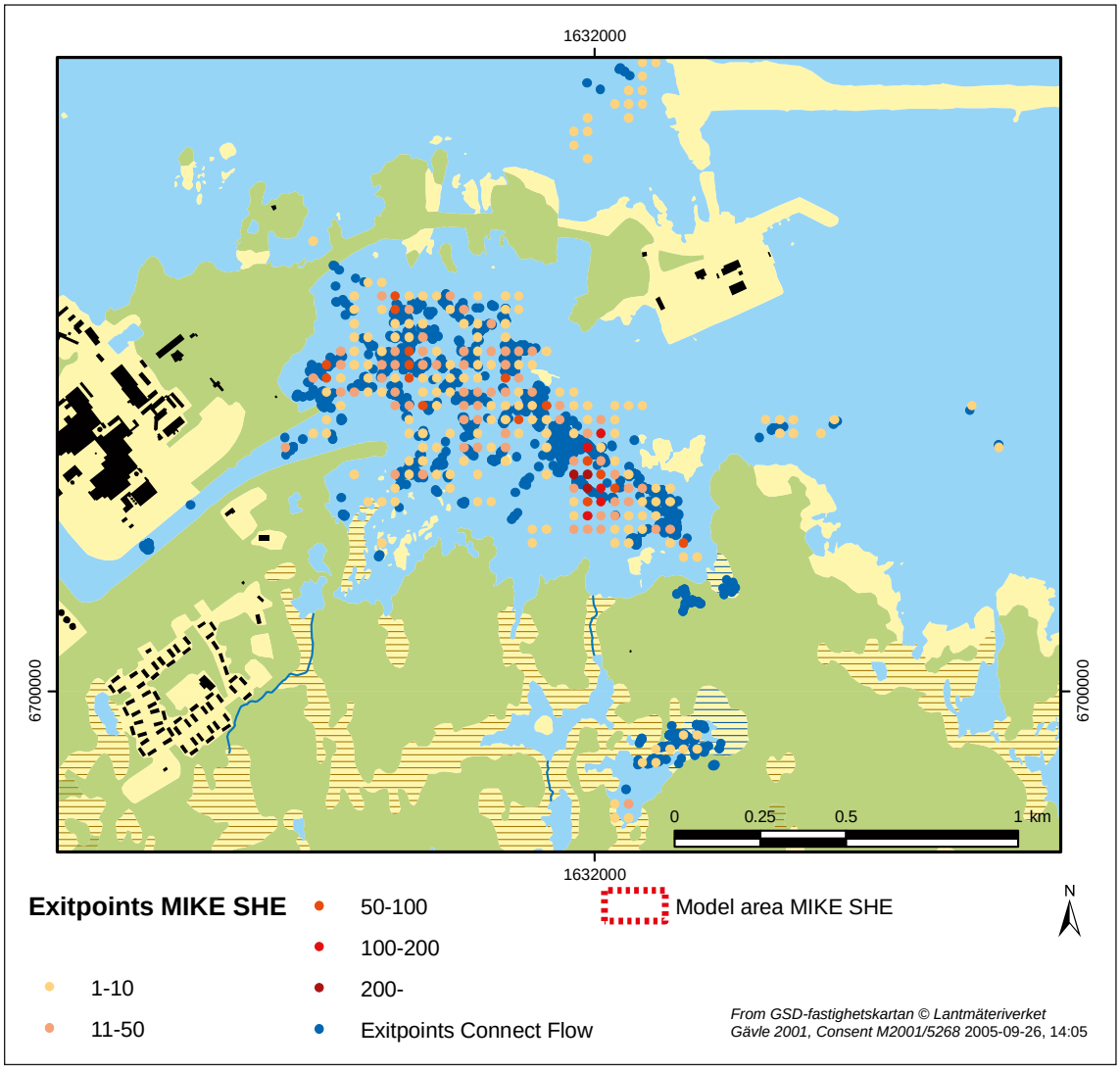

Figure 5-9. *Close-up of MIKE SHE (case PT2; pink to red dots) and ConnectFlow (blue dots) exit points in Asphällsfjärden and adjacent areas, and on land.*

5.2 Advection-dispersion calculations

5.2.1 Methodology

The advection-dispersion (AD, for short) module in MIKE SHE makes it possible for the user to consider a wider range of transport processes than the purely advective transport that can be analysed in the particle tracking simulations. In addition to advection and "classical" dispersion, i.e. dispersion modelled as a diffusive process, "simple" sorption processes, primarily linear equilibrium sorption, can be handled directly in the AD module. The AD modelling can also be used as a basis for analysing other, more complex processes (e.g. non-linear sorption and biodegradation). However, this requires that additional model components are also utilised.

Similar to the particle tracking calculations presented in Section 5.1, the calculated, three-dimensional flow field is the basis for the AD solute transport calculations. Additional input parameters required for the AD simulations are the effective porosity, the longitudinal and transverse dispersivities, and a description of the source(s) in terms of location(s) and strength(s). In the present modelling, the same effective porosity as in the particle tracking simulation was used, and the dispersivities were set to zero in all cases. Thus, "local dispersion" was neglected, which implies that numerical dispersion and "large-scale dispersion" due

differences in hydraulic conductivity between different grid cells were the only sources of solute spreading in the modelling of non-sorbing solutes.

The AD module consists of four components, each describing the transport processes in one part of the hydrological cycle /DHI Software 2005/. The four components are Overland flow transport, Channel flow transport, Unsaturated flow transport and Saturated flow transport. In the present application, solute transport has been modelled in the saturated zone only. However, it should be noted that it already in the present version of the code is possible to model the further transport in the surface water system and the unsaturated zone. The main objective of the AD calculations is to illustrate how sorption and dilution processes affect the transport from sources in the rock to and within the QD. These processes cannot be handled in the particle tracking calculations. The simulations performed in this project are also a test to investigate the capabilities of the MIKE SHE AD module.

Two different source locations were studied in the AD simulations. In the first case, referred to as case S_{SZ}, the AD source was placed in a cell from which the particles injected in the PT simulations went to the sea. The second case, denoted S_{UZ}, considered a source location where the particles injected in the PT modelling discharged to the unsaturated zone. In both source location cases, both non-sorbing and sorbing solutes were studied; sorption was modelled as a linear equilibrium process, which is the simplest possible process description (and also the most commonly used in transport models).

Linear equilibrium sorption implies that sorption is instantaneous and that the ratio of the sorbed concentration (i.e. the concentration of the substance attached to the surfaces of the solid material) to the aqueous concentration (i.e. the concentration of the same substance in the water) is given by a constant factor of proportionality. This parameter is commonly referred to as the K_d value and expressed in units of sorbed mass per unit mass of solid divided by dissolved mass per unit volume of water, i.e. in dimensions of volume per mass. In transport modelling involving linear equilibrium sorption, a parameter usually termed “retardation factor” is often used. The retardation factor, R, is a dimensionless representation of the sorption process, which is related to the K_d value and the other parameters specified in the model as

$$R = 1 + \frac{K_d \cdot \rho}{\eta}$$

where

R: retardation factor [–]

K_d: linear equilibrium distribution coefficient [L^3M^{-1}]

η: porosity of the bedrock or Quaternary deposit

ρ: density of the bedrock or Quaternary deposit [ML^{-3}]

R can, for example, be interpreted as the ratio of the (local) transport velocity of a non-sorbing substance to that of a sorbing one; hence, it quantifies how much the sorbing substance is retarded relative to the non-sorbing one.

Concerning the sorption process, three different cases representing different types of solutes are considered in the present study. These cases and solutes are referred to as non-sorbing (NS, for brevity), weakly sorbing (WS) and strongly sorbing (SS), respectively; NS implies $K_d = 0$, whereas in WS and SS the $K_d \cdot \rho$ parameter group was selected such that R was approximately 10 (WS case) and 100 (SS case) in the rock. For the QD a different value of the $K_d \cdot \rho$ parameter group was chosen, in order to obtain R values of about 10 (WS case) and 100 (SS case) for a typical porosity of the QD layers.

It should be noted that since the porosity varies within the model domain, so do the actual retardation factors (as shown in the equation defining R above). Thus, when using one constant $K_d \cdot \rho$ value in each main unit of the system (i.e. one value in the the rock and one in the QD), the effective solute retardation within these units varies from layer to layer in proportion to the layer-specific porosity. It is also emphasised that the sorption parameter values are not based on site data. The different parameter sets used here were selected for illustrative purposes only.

At both source locations, i.e. in both the S_{SZ} and the S_{UZ} source cases, continuous, constant concentration sources were applied. The constant input concentration was 1,000 mgL^{-1} in both sources. However, since the groundwater velocity differs between the source locations the injected mass fluxes and total amounts of solute injected were not the same. The sources were placed in the second lowest calculation layer in the model, layer 12. Similar to the particle tracking simulations, sources cannot be placed in the boundary layer in the AD simulations. In the following, the resulting solute concentrations in layers 9, 5 and 2 are presented.

The simulation time was 200 years in all simulation cases, using the calculated transient flow results during the modelled single year 2003–2004. Thus, the model results from the MIKE SHE Water movement calculation for this single year were cycled 200 times. Stable concentrations corresponding to the injected constant concentration were reached in all calculation layers in the NS (non-sorbing) results, but not in all WS and SS (sorbing) simulation results. The reason for still limiting the simulated time period to 200 years, i.e. much shorter than the 1,500 year-period in the PT calculations, was that the AD calculations turned out to be highly time-consuming.

5.2.2 Source discharging to the sea – case S_{SZ}

Non-sorbing solute

In the S_{SZ} case, the source was placed in a cell that in the PT simulation generated particles that left the model volume through the boundary towards the sea. The source location, which in the nomenclature of the PT sea basins discussed in Section 5.1 is below Asphällsfjärden, is shown in Figure 5-10. The vertical hydraulic conductivity in the bedrock at the source location in calculation layer 12 is $7.7 \cdot 10^{-8}$ ms^{-1}, and the horizontal hydraulic conductivity is $7.4 \cdot 10^{-8}$ ms^{-1}. These numbers indicate that the source is neither within any of the more high-permeable deformation zones in the area, nor in the most low-permeable parts of the rock.

Figure 5-11 shows the concentration distribution in calculation layer 2 after 200 years. The uppermost calculation layer, the sea, is a layer with a fixed head boundary condition. Results cannot be presented for this type of boundary layers, which is why layer 2 is the uppermost "observation layer" in this work. Essentially, the figure shows the spatial distribution of the solute in the sediment layer that constitutes the sea bottom. The area of non-zero solute concentrations, the "contaminated" area, in the sediments is 0.14 km^2, whereas the source was placed in a cell with an area of only 0.0016 km^2 (a single 40 m by 40 m cell). Thus, the solute has spread to an area almost 100 times larger than the source area. The maximum calculated concentration in the sediment layer is 350 mgL^{-1}, which is about 1/3 of the injected concentration (1,000 mgL^{-1}).

The results also show that the contaminated area is smaller in the upper bedrock than in the QD. For example, the contaminated area in the bedrock at a level of 40 m below sea level is 0.083 km^2, which is about 50 times the size of the source area. Thus, the size of the contaminated area increases along the transport path from depth towards the surface. Horizontal flow components, possibly in combination with flow transients, are the main reasons for the horizontal spread leading to this increase. As noted above, numerical dispersion may also contribute.

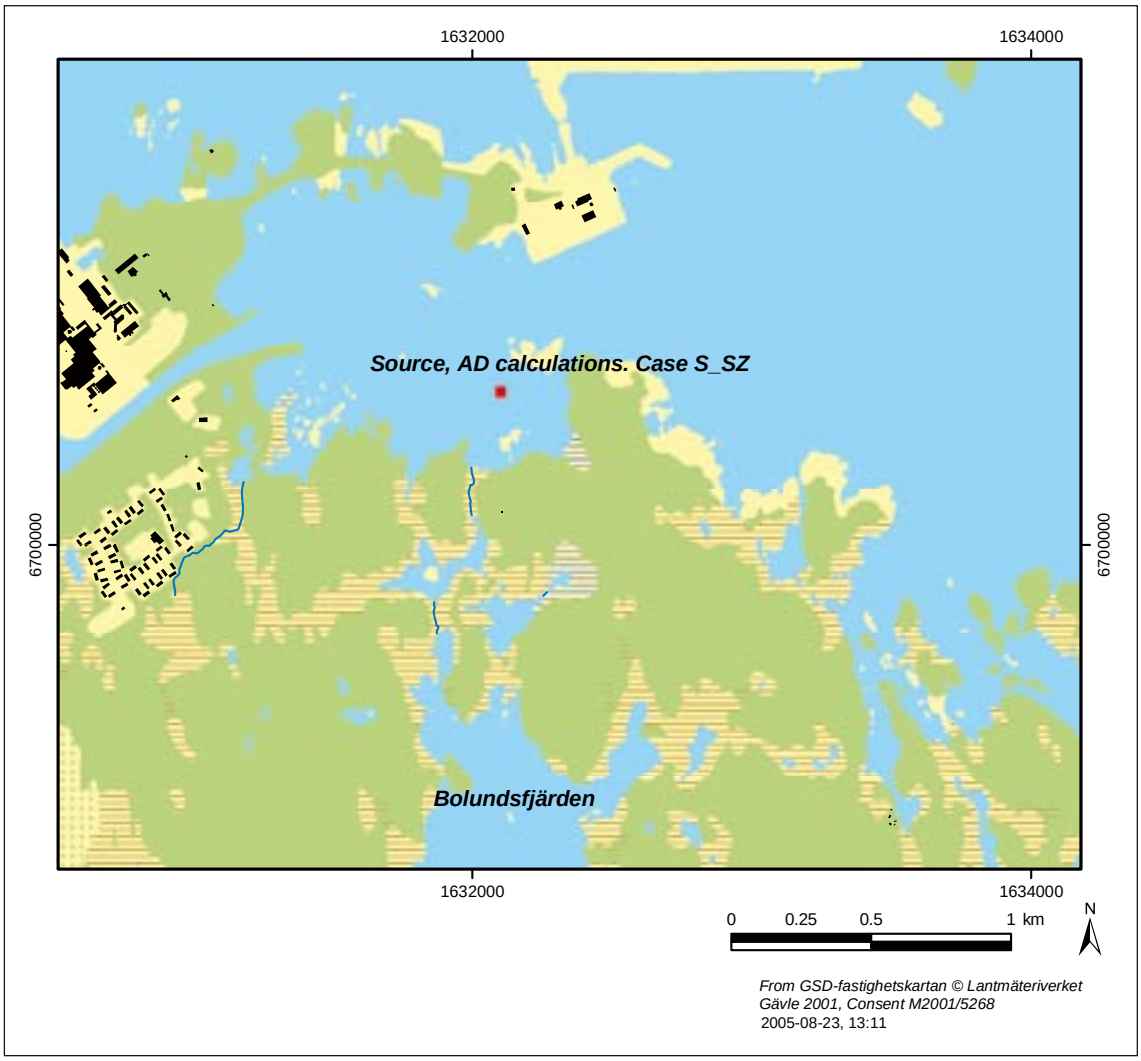

Figure 5-10. *Source location in AD simulation case S_{SZ}. The source is located in a single cell in calculation layer 12 and has a constant injected concentration of 1,000 mgL^{-1}.*

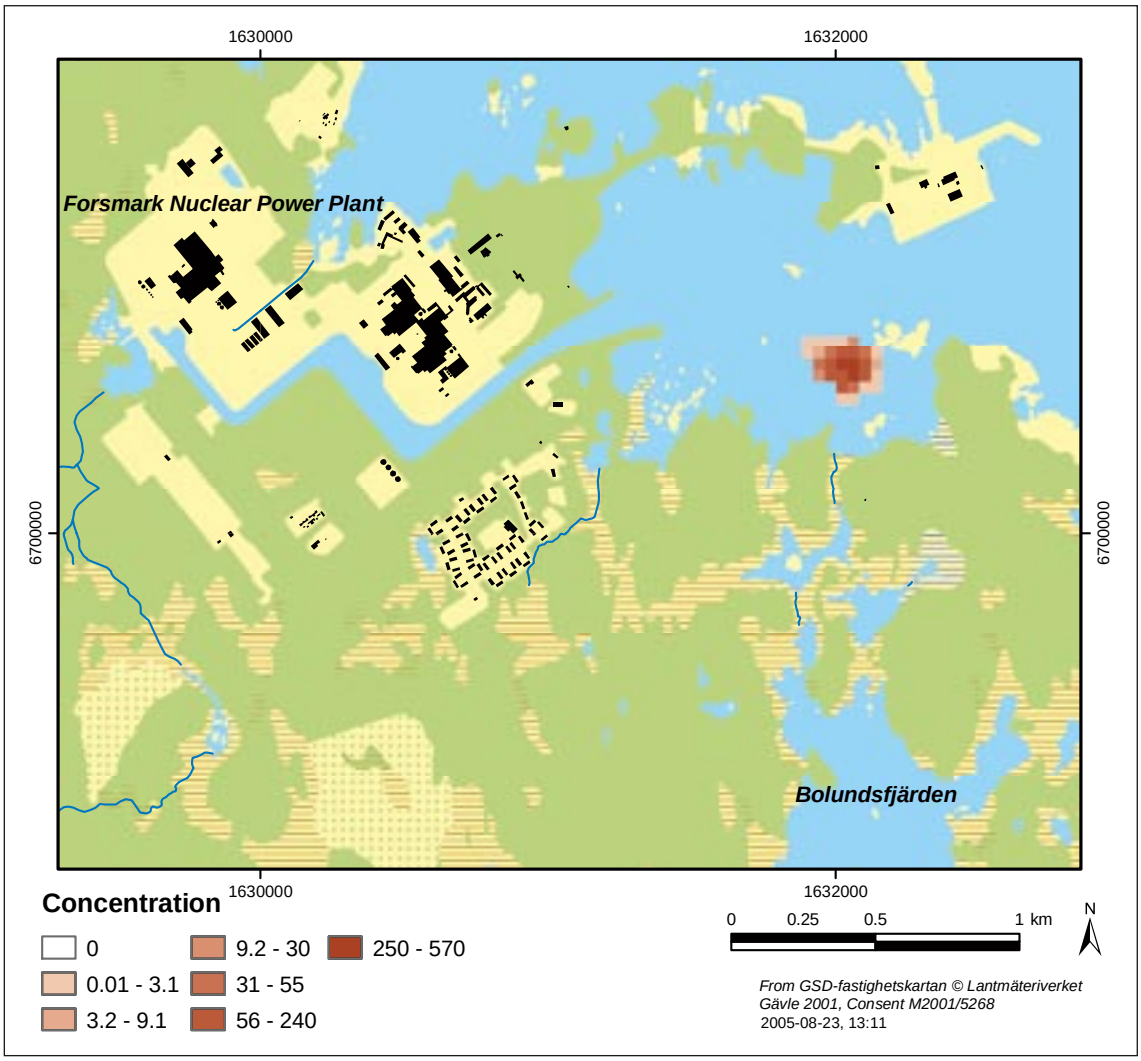

Figure 5-11. *Concentration distribution (mgL^{-1}) in calculation layer 2 after 200 years, case S_{SZ} NS (non-sorbing solute).*

Figure 5-12 shows breakthrough curves (solute concentration as a function of time) in calculation layers 2, 5 and 9 along a vertical column situated c. 80 west of the source. It is seen that the maximum concentration, i.e. the stable concentration corresponding to the constant-concentration injection, in calculation layer 2 is reached after c. 40 years. For comparison, the maximum concentration is reached after 4 years in layer 9, which is at 40 m below sea level and after 16 years in layer 5 at c. 5 m below sea level.

The maximum concentration in layer 2, the sea bottom sediment layer, is observed in the column 80 m west of the source cell. However, as shown in Figure 5-13 the cells in layers 2 and 5 along the column standing on the source cell had not reached stable concentrations after 200 years. The maximum concentration in layer 9 in the source cell column is 570 mgL^{-1}, which is obtained after about 10 years. This means that solute transport in the vertical direction from the source is relatively fast and shows a relatively small effect of dilution up to layer 9. From layer 9 the purely vertical transport appears to be slow; transport is faster some distance away from the source cell column. However, the maximum concentration in the source column is higher, indicating a smaller effect of dilution. Furthermore, a horizontal distance of 80 m between the source and the cell showing the highest concentration in layer 2 implies that horizontal transport distances in the upper part of the system are small.

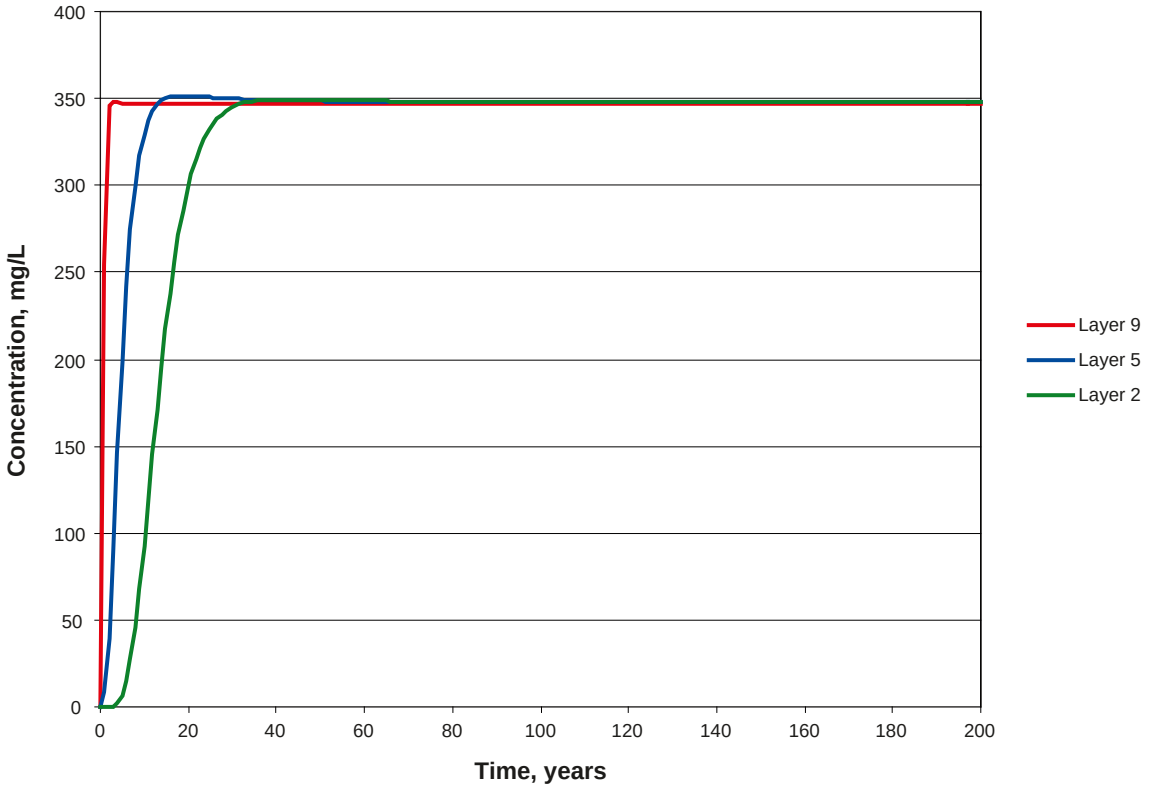

Figure 5-12. *Breakthrough curves in calculation layers 2, 5 and 9 (concentrations in mgL^{-1}) in a vertical column 80 m west of the source cell, case S_{SZ} NS (non-sorbing solute); the source is in layer 12.*

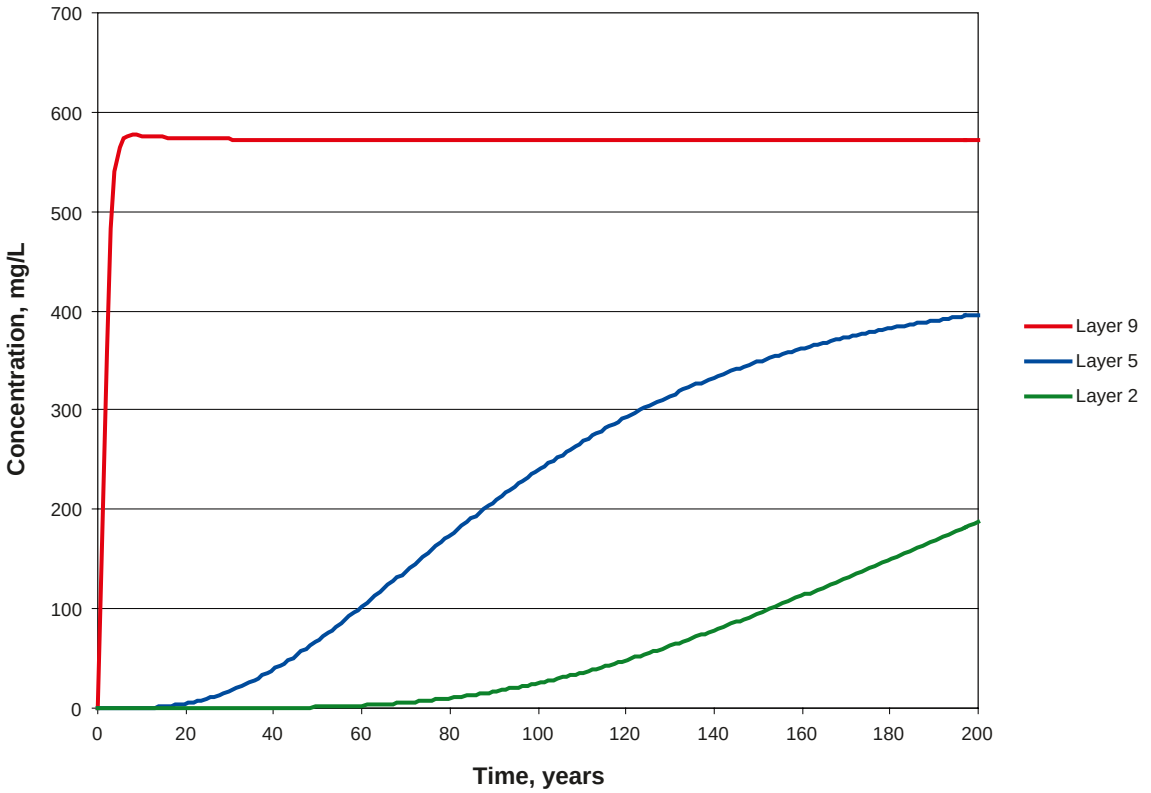

Figure 5-13. *Breakthrough curves in calculation layers 2, 5 and 9 (concentrations in mgL^{-1}) in a vertical column above the source cell, case S_{SZ} NS (non-sorbing solute); the source is in layer 12.*

The mass balance of the studied system can be obtained as an output from the MIKE SHE simulations. In this case, the cumulative mass fluxes between the various compartments of the model were monitored during the simulation. The results show that the total solute mass injected during the simulation period (200 years) was 5,360 kg. Most of the injected mass passed through the saturated zone during the simulation; the cumulative mass that had left the saturated zone compartment at the end of the simulation was 4,620 kg, corresponding to 86% of the injected mass, whereas 740 kg (14%) remained in the saturated zone. All solute that left the saturated zone went to the sea, i.e. no solute discharged to the unsaturated zone or water courses (MIKE 11) on land.

Sorbing solute

As explained above, the effects of sorption were investigated by comparing the non-sorbing solute discussed in the preceding subsection (case NS, for non-sorbing) with two cases of sorbing solutes characterised by different K_d values (case WS, weakly sorbing, and case SS, strongly sorbing). Calculated maximum concentrations in layer 2, 5 and 9 are summarised in Table 5-8. It can be seen that the maximum concentrations are fairly similar in the three cases (NS, WS and SS), except for the SS concentration in layer 2. As illustrated below, the low concentration there is due to the strong retardation, which leads to an incomplete breakthrough in the upper part of the saturated zone during the simulation period.

The breakthrough curves obtained for the three alternative sorption parameter sets considered in the S_{SZ} source case are presented for the same three "observation cells" along the column 80 m from the source as in Figure 5-12. Keeping in mind that the source is in calculation layer 12, results are shown in the upward transport direction in Figure 5-14 (layer 9), Figure 5-15 (layer 5), and Figure 5-16 (layer 2). Figure 5-14 and 5-15 show that a constant maximum concentration of almost 350 mgL^{-1} is reached in all sorption cases in both layer 9 and layer 5. As expected, the concentration breakthroughs of the sorbing solutes are delayed relative to the non-sorbing solute (NS), with the strongly sorbing solute (SS) arriving much later than the weakly sorbing one (WS). It is also seen that the breakthrough curves in layer 5 are delayed relative to the corresponding breakthroughs in layer 9.

As shown in Figure 5-16, the simulation period was too short for the sorbing solutes to reach constant concentrations in layer 2. Thus, "incomplete" breakthrough curves were obtained in the WS and SS cases. Whereas the WS curve is fairly close to the (projected) maximum level, only the very first stages of the breakthrough are observed in the SS case (note that a separate concentration scale is used for SS in Figure 5-16). This implies that a considerably longer simulation period than the 200 years used in the present study would be needed to capture the whole breakthrough in the SS case.

In the discussion of non-sorbing solutes in connection with Figure 5-12 and Figure 5-13 above, it was found that upward solute transport was faster in the column a short distance away from the source than in the actual source cell column. Of course, this observation can also be made in the results for the sorbing solutes. Figure 5-17 shows the NS, WS and SS results for calculation layer 5. A comparison with the corresponding results from the column 80 m west of the source (Figure 5-15) makes it clear that the breakthrough is much slower directly above the source.

Table 5-8. Maximum concentrations (mg L^{-1}) after 200 years in layers 2, 5 and 9 for source S_{sz} in the three sorption cases NS, WS and SS (no sorption, weak and strong sorption, respectively).

	Case NS	Case WS	Case SS
Layer 2	348	330	18
Layer 5	399	408	349
Layer 9	572	572	518

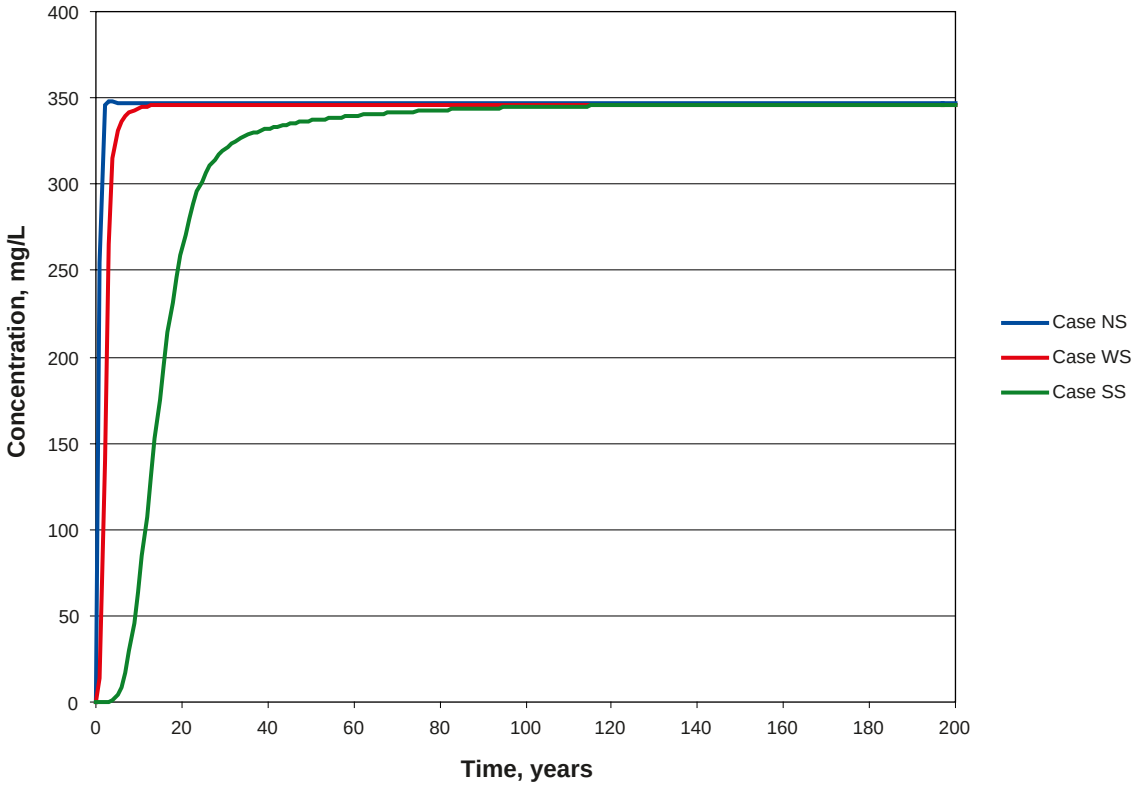

Figure 5-14. *Breakthrough curves in calculation layer 9 for non-sorbing (NS), weakly sorbing (WS) and strongly sorbing (SS) solutes (concentrations in mgL^{-1}) in a cell 80 m west of the source cell; the source is in layer 12.*

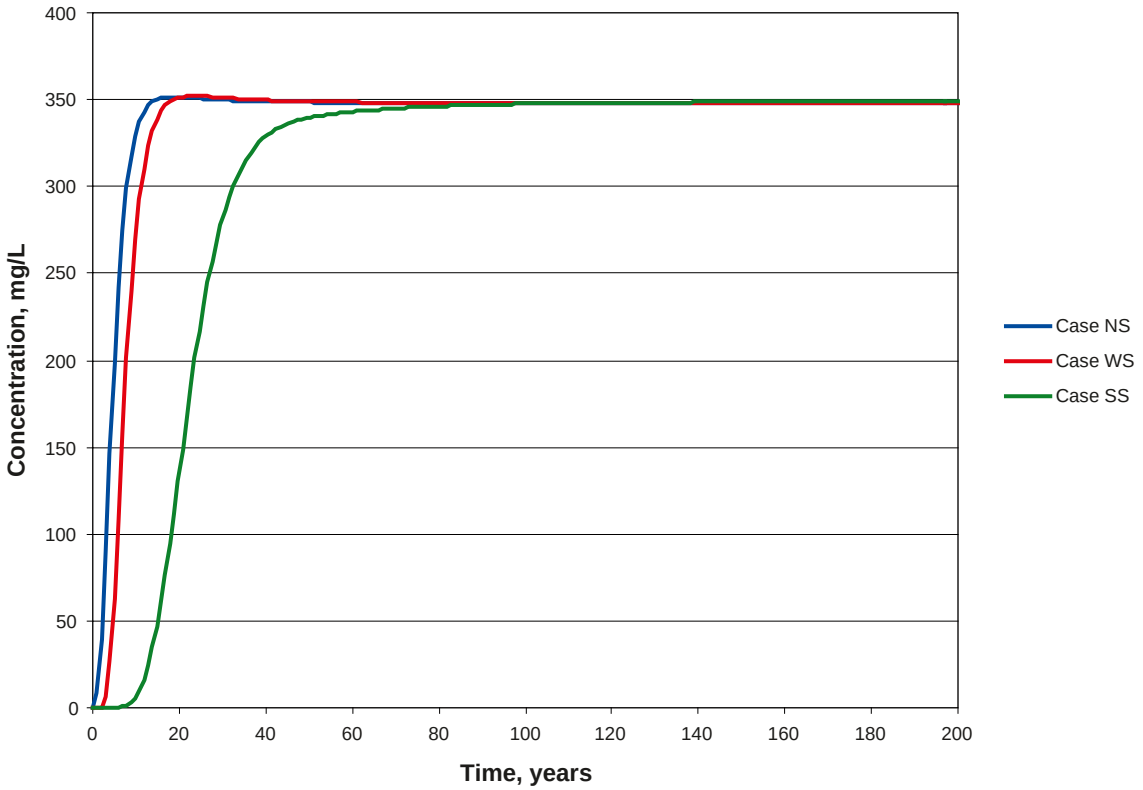

Figure 5-15. *Breakthrough curves in calculation layer 5 for non-sorbing (NS), weakly sorbing (WS) and strongly sorbing (SS) solutes (concentrations in mgL^{-1}) in a cell 80 m west of the source cell; the source is in layer 12.*

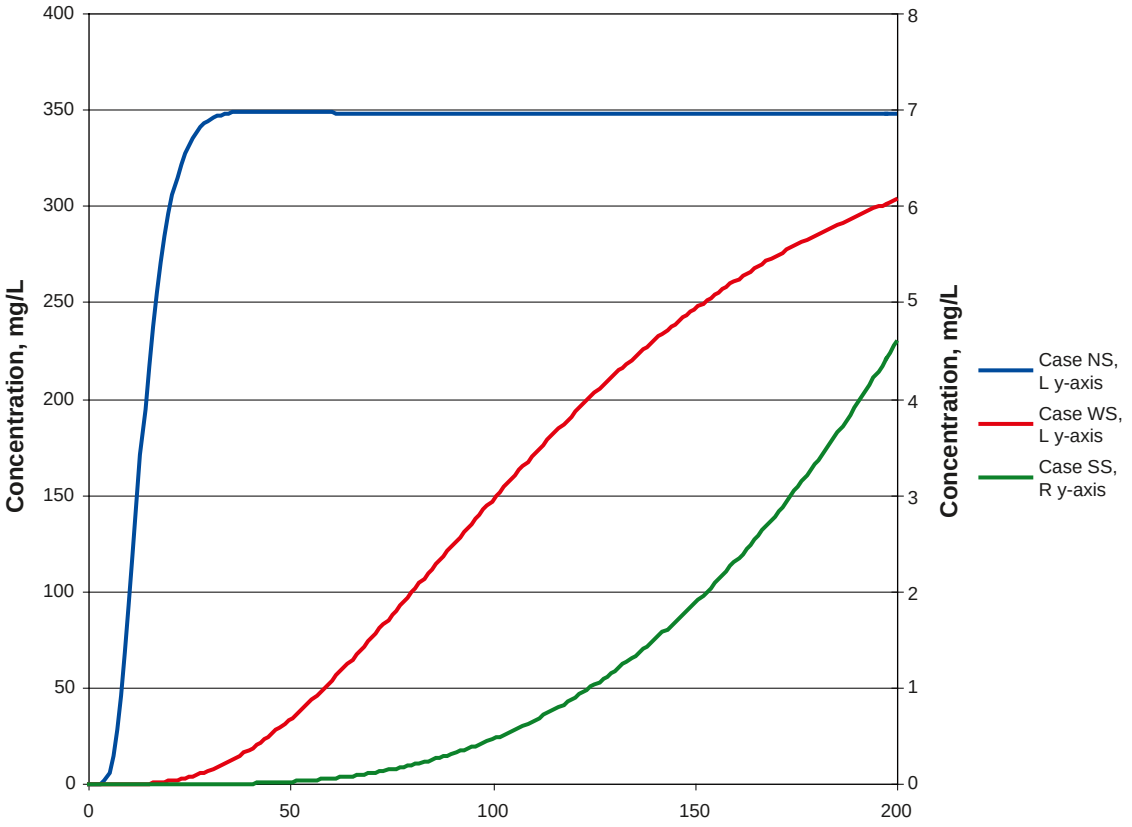

Figure 5-16. *Breakthrough curves in calculation layer 2 for non-sorbing (NS; left y-axis), weakly sorbing (WS; left y-axis) and strongly sorbing (SS; right y-axis) solutes (concentrations in mgL^{-1}) in a cell 80 m west of the source cell; the source is in layer 12.*

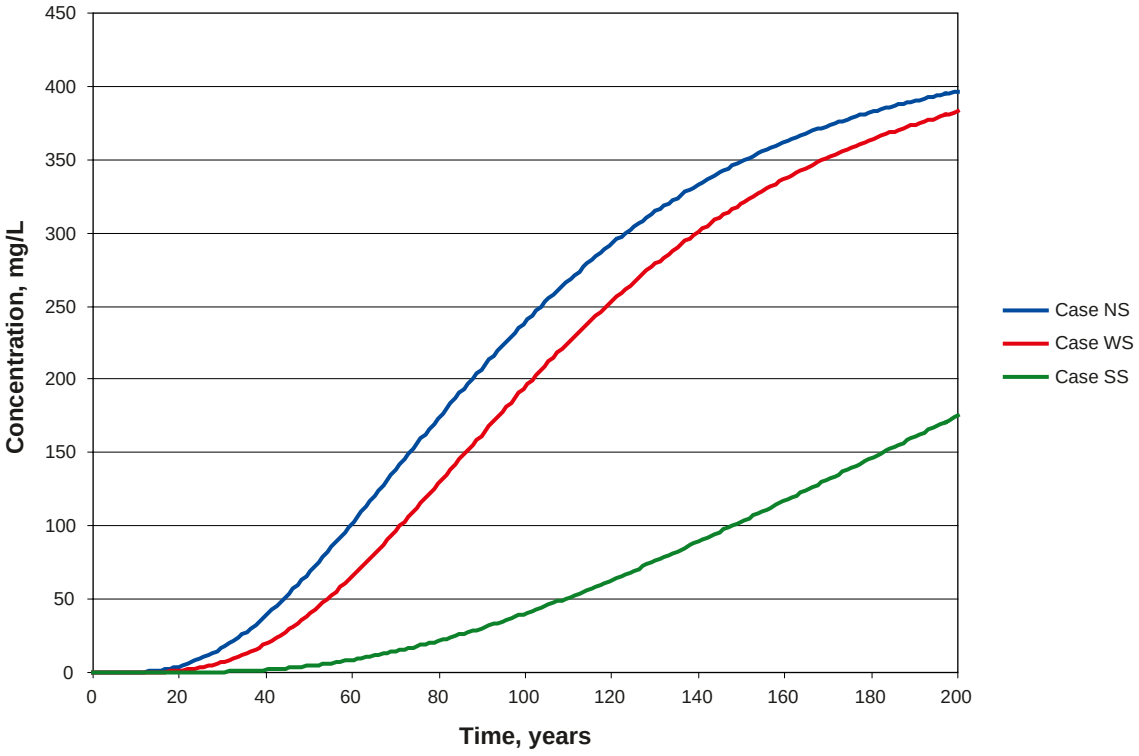

Figure 5-17. *Breakthrough curves in calculation layer 5 for non-sorbing (NS), weakly sorbing (WS) and strongly sorbing (SS) solutes (concentrations in mgL^{-1}) in the column where the source is located; the source is in layer 12.*

However, again it should be noted that the stable concentration approached just above the source is higher than the corresponding concentration in the same calculation layer west of the source.

As described above, the retardation factor, R, can be viewed as the ratio of local transport velocities of non-sorbing and sorbing solutes, which in the present parameterisation with a constant "$K_d \cdot \rho$ parameter group" depends on the porosity. As an example of the variations in the "effective retardation", porosities and retardation factors in calculation layers 12 to 5 in the column where the source is located are summarised in Table 5-9. Thus, the table shows the parameters associated with the cells from the source layer up to the upper observation layer in the rock. It is seen that the porosity in this particular column varies between $2 \cdot 10^{-5}$ and $5 \cdot 10^{-3}$, which corresponds to R-values ranging from 1.04 to 10 (WS case) and from 1.4 to 100 (SS case).

In particular, Table 5-9 shows that porosities generally are much smaller in lower parts of the modelled rock volume (layers 12 to 9) than in the upper part of the rock (layers 8 to 5). This implies that retardation is much stronger along the first part of a vertical flow path, from the source to the first observation layer (layer 9), than between the first and second (layer 5) observation layers. This explains why the ratios of the times required to reach a certain concentration in, for example, the NS and WS cases are not the same in layer 5 and 9, as they would have been in a constant-retardation model. Clearly, in illustrative simulations of the kind discussed here, the interpretation of the results would be more straight-forward if a parameterisation with a constant R was used. This would require that different K_d-values were used in each cell, with spatial variations proportional to the porosity variations; this type of parameterisation can be used in MIKE SHE.

The accumulated mass balances in the S_{SZ} source case for the different solutes considered (NS, WS and SS) are shown in Table 5-10. As expected, the results for the sorbing solutes show smaller outflows to the sea, i.e. smaller amounts of solutes that have passed through the saturated zone. Specifically, the accumulated outflow corresponds to 35% of the total inflow in the WS case and to only 0.4% in the SS case; in the NS case, 86% of the injected mass had reached the sea after 200 years.

In the WS and SS cases, the solute mass remaining in the saturated zone at the end of the simulation consists of both dissolved (aqueous) and sorbed mass. The sorbed mass is larger in the SS case, but neither the relation between the sorbed and the dissolved amounts nor the difference between the two sorbing solutes are as large as the retardation factors in the lower calculation layers indicate (i.e. corresponding to $R = 10$ and $R = 100$, see Table 5-9). The main reasons for this are that the fronts of the two sorbing solutes are at different depths in the saturated zone after 200 years, and that the solute phase distribution, as indicated by the layer-specific R-values, is spatially variable.

Table 5-9. Porosities and retardation factors in the column where the source is located; the source is in layer 12, whereas breakthrough curves are taken from layers 5 and 9.

Layer	Porosity	Retardation factor	
		Case WS	Case SS
12	$2.0 \cdot 10^{-5}$	10	100
11	$1.5 \cdot 10^{-4}$	2.2	13
10	$3.0 \cdot 10^{-5}$	7.0	61
9	$2.0 \cdot 10^{-5}$	10	100
8	$2.0 \cdot 10^{-3}$	1.09	1.9
7	$5.0 \cdot 10^{-3}$	1.04	1.4
6	$5.0 \cdot 10^{-3}$	1.04	1.4
5	$5.0 \cdot 10^{-3}$	1.04	1.4

Table 5-10. Accumulated mass balances for the saturated zone after 200 years, S_{sz} source case for non-sorbing (NS), weakly sorbing (WS) and strongly sorbing (SS) solutes. Dissolved and sorbed mass in SZ are the amounts of solute remaining in the saturated zone after 200 years.

Component	NS (kg)	WS (kg)	SS (kg)
Inflow from source	5,360	5,390	5,400
Dissolved mass in SZ	740	520	320
Sorbed mass in SZ	0	2,970	5,060
Outflow to the sea	4,620	1,900	20

Of the total mass left in the saturated zone, 85% is sorbed in the WS case and 94% in the SS case. The ratios of total mass to dissolved mass in the saturated zone are 6.7 and 17 in the WS and SS cases, respectively.

Figures 5-18 and 5-19 illustrate how the different components of the mass balance vary during the simulation period; Figure 5-18 shows the WS case results and Figure 5-19 the SS results. The values on the y-axes represent the mass transport, expressed as mass flux in units of kilograms per year, between "pools" in the model. For example, the values at the time 50 years along the x-axis represent the various mass fluxes during year 50 in the 200-year time series; note that the time scale is distorted, such that the first ten years are shown in more detail than the rest of the simulation period.

For the "pools" of dissolved and sorbed mass, the fluxes quantify the net changes in storage, i.e. the differences between inflow and outflow to/from the saturated zone and the net exchanges between the dissolved and sorbed phases. Changes in the mass distribution on dissolved and sorbed phases occur due to the variations in effective sorption properties discussed above. In both sorption cases, the inflow to the saturated zone from the source is approximately the same and constant, c. 27 kg $year^{-1}$. The sum of the changes in dissolved and sorbed mass equals the inflow from the source, as long as no outflow takes place.

The results show that almost no mass leaves the model volume to the sea during the first ten years, i.e. the "SZ to the sea" term is zero. After this initial period, the outflow increases relatively fast in the WS case (Figure 5-18), whereas it remains very small during the whole SS case simulation (Figure 5-19). In both cases, the changes in dissolved mass converge to zero during the later stages of the simulation period. If the simulation period had been sufficiently long, the grid cells that received water that had passed through the source cell would have become saturated with solute. At that point, a stable situation with constant in- and outflows, and zero changes in dissolved and sorbed mass, would have developed (neglecting the effects of numerical dispersion).

The time series of changes in sorbed mass for the two sorption cases are somewhat different, which obviously is due to the large differences in solute retardation in (parts of) the model domain. The varying porosities along the flow paths are the reason for the large changes in sorbed mass during the first fifty years. When the solute front enters a new grid cell, the amount of sorbed mass relative to dissolved mass changes if the "effective retardation factor" does. However, spatial variability in the hydraulic properties also affects the changes in the various "pools". In the hypothetical case of plug flow conditions in a domain with uniform hydraulic and sorption properties, the changes in dissolved and sorbed mass would be constant until the domain is saturated. After that, these mass balance components would be zero in that type of model.

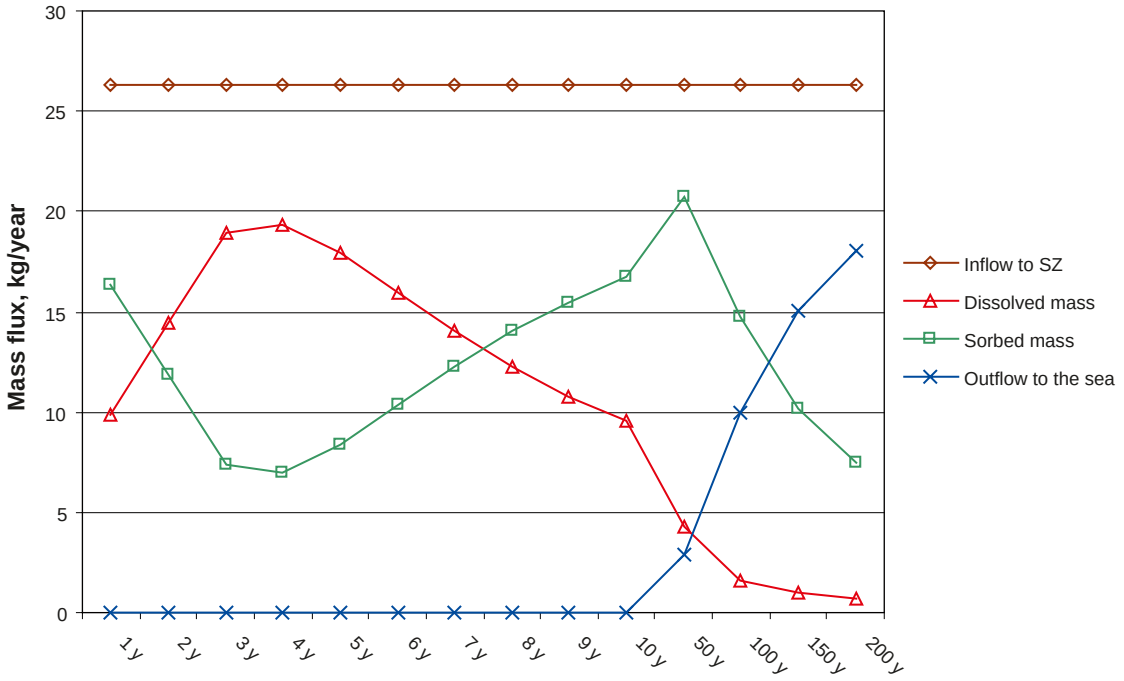

Figure 5-18. *Calculated mass fluxes to and from the saturated zone (SZ), and changes in dissolved and sorbed mass in SZ (kg year^{-1}), S_{SZ} WS case. Note that the first ten years are shown in more detail than the rest of the simulation period.*

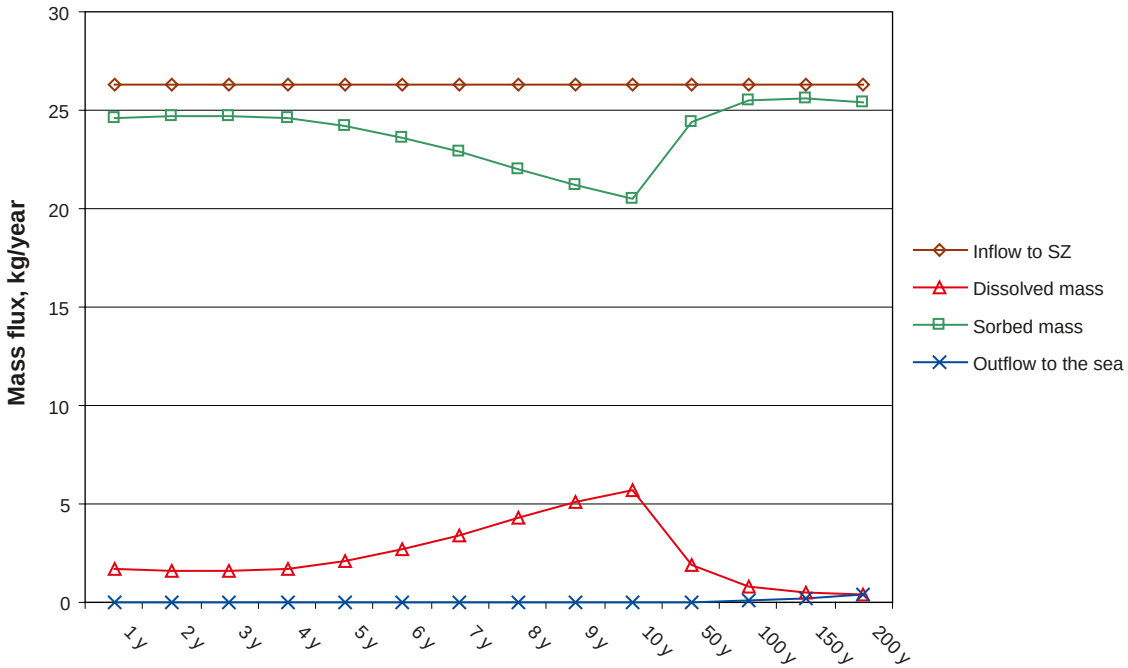

Figure 5-19. *Calculated mass fluxes to and from the saturated zone (SZ), and changes in dissolved and sorbed mass in SZ (kg year^{-1}), S_{SZ} SS case. Note that the first ten years are shown in more detail than the rest of the simulation period.*

5.2.3 Source discharging to the unsaturated zone – case S_{UZ}

Non-sorbing solute

In the second case investigated in the AD simulations, referred to as case S_{UZ}, the source was located in a cell from which the particles injected there in the PT simulations went to the unsaturated zone. The location of the source is shown in Figure 5-20. It is seen that the source is situated just north of Lake Bolundsfjärden, below the narrow strip of land between this lake and the one just north of it (Lake Puttan). As indicated on the map, this is an open area covered by reed, which relatively recently constituted a strait between the lakes. This means that the unsaturated zone most likely is very shallow.

The vertical and horizontal hydraulic conductivities in the bedrock at the source location were $8.2 \cdot 10^{-10}$ ms^{-1} and $2.1 \cdot 10^{-9}$ ms^{-1}, respectively. Thus, the conductivities in the source cell are much lower than in the S_{SZ} case (see Section 5.2.2); the S_{SZ} vertical conductivity is almost 100 times larger than that in the S_{UZ} source cell, and the ratio of horizontal conductivities is c. 35. Since the sources are specified in terms of concentrations and the concentrations are the same in the two cases, this implies that the amount of solute mass injected is much smaller in case S_{UZ} than in case S_{SZ}.

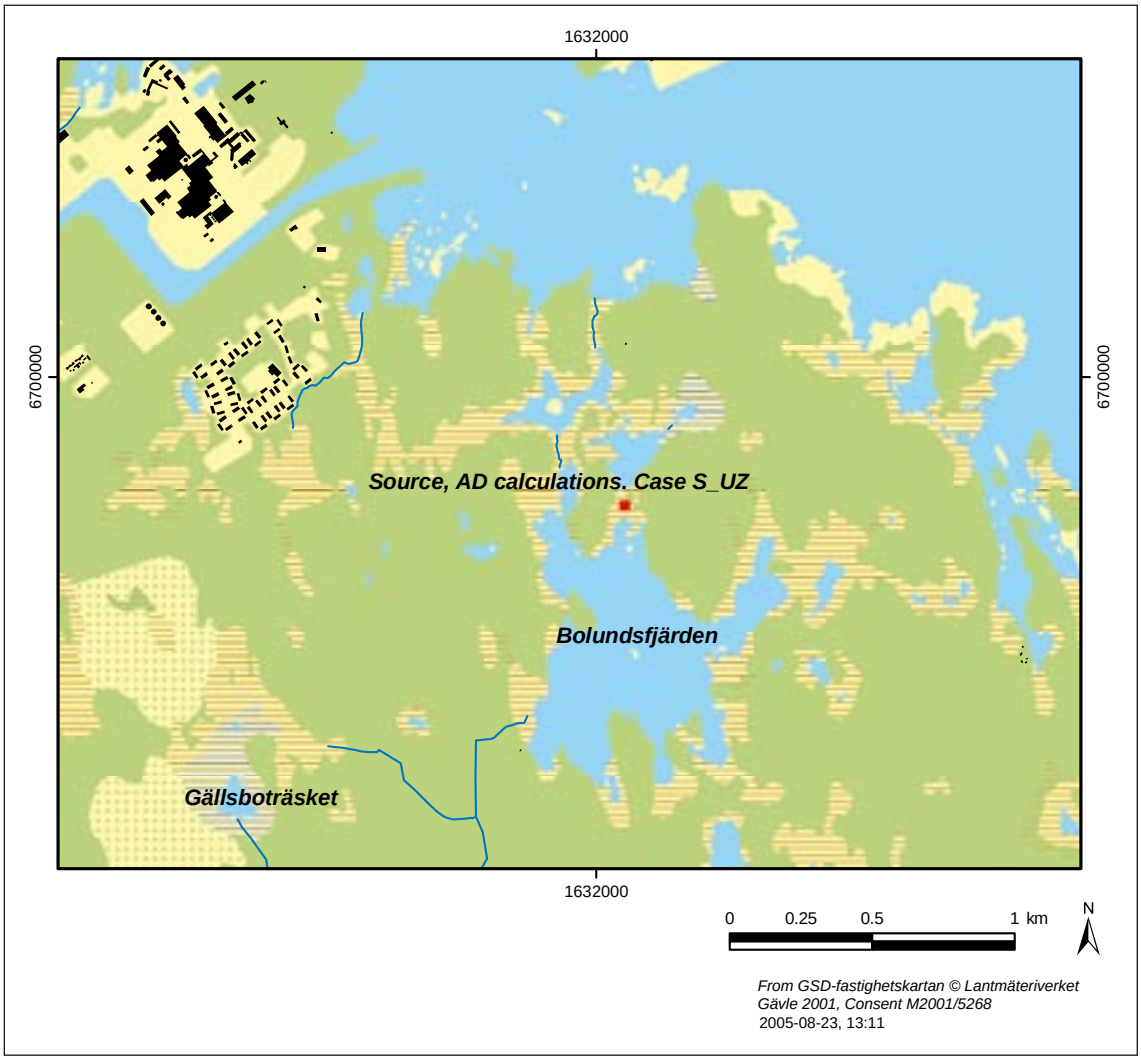

Figure 5-20. *Source location in AD simulation case S_{UZ}. The source is located in a single cell in calculation layer 12 and has a constant injected concentration of 1,000 mgL^{-1}.*

Similar to what was done for the S_{SZ} source discussed above, three sorption cases representing no sorption (case NS), weak sorption (case WS) and strong sorption (case SS), respectively, were studied. The S_{UZ} simulations were performed with the same sorption parameter fields as the S_{SZ} simulations described above; thus, case definitions and the handling of K_d-values are the same. Figure 5-21 shows the solute concentrations in calculation layer 2 for non-sorbing solute (NS case) after 200 years. The area within which solute is found in layer 2 is 0.024 km^2, whereas the area of the source (a single cell) is 0.0016 km^2. In this case, the affected area is somewhat smaller in the QD than in the upper bedrock. For example, the area with non-zero solute concentrations is 0.035 km^2 at a level of 40 m below sea level in the bedrock.

The solute concentrations are generally lower and the affected areas smaller in case S_{UZ} than in case S_{SZ}. As described above, the vertical hydraulic conductivity at the S_{UZ} source location is c. 100 times smaller than the corresponding conductivity in case S_{SZ}. This leads to a smaller groundwater velocity in the source cell and, since the same constant-concentration injection is considered in both cases, to a smaller injected mass in case S_{UZ}. The maximum concentration in calculation layer 2 is 0.5 mgL^{-1} and the maximum concentration in the bedrock at 40 m below sea level is 4 mgL^{-1}. These concentrations are much lower than that injected in the source (1,000 mgL^{-1}), which indicates that injection takes place in a cell where the velocity is lower than in the surrounding cells such that dilution is strong.

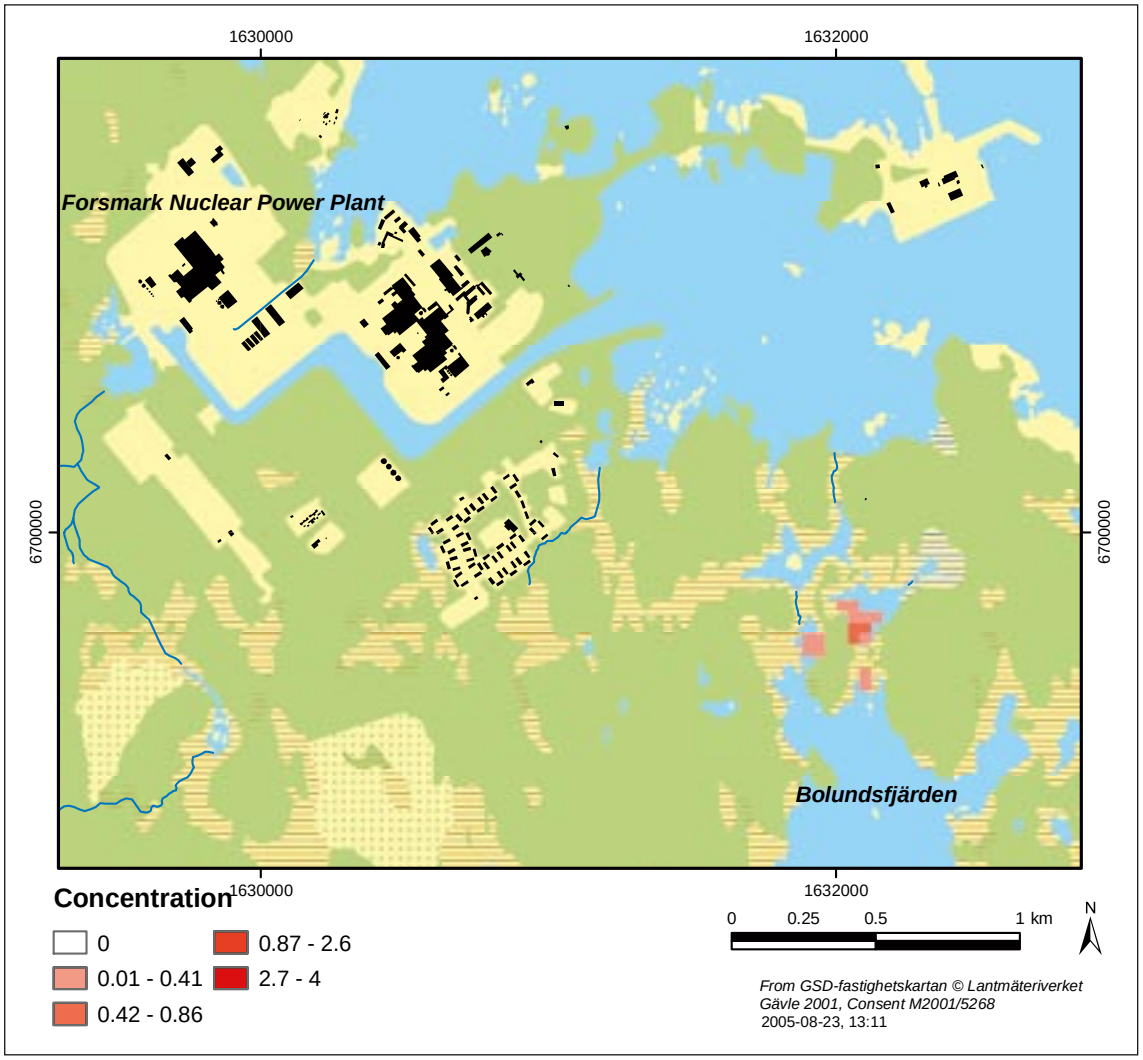

Figure 5-21. *Concentration distribution (mgL^{-1}) in calculation layer 2 after 200 years, case S_{UZ} NS (non-sorbing solute).*

Figure 5-22 shows breakthrough curves (concentration time series) from calculation layers 2, 5 and 9 in the column where the source cell is located (in layer 12). It is seen that concentration levels are very low compared to the S_{SZ} results (see Figure 5-12 and Figure 5-13), but also that the stable maximum concentrations are reached faster than in most S_{SZ} breakthrough curves. The maximum S_{UZ} concentrations in calculation layers 2, 5 and 9 are reached after c. 20 years (Figure 5-22).

Another interesting observation that can be made by comparing the S_{UZ} results with the S_{SZ} results in Section 5.2.2 is that the stable concentrations reached in the S_{UZ} breakthrough curves show large differences among the calculation layers. Specifically, the stable concentration obtained as a result of the constant-concentration injection decreases with increasing distance from the source in the S_{UZ} case; it is 4 mgL^{-1} in layer 9, c. 0.7 mgL^{-1} in layer 5, and c. 0.5 mgL^{-1} in layer 2 (Figure 5-22). The velocity profile in the layers above the source shows higher velocities than in the source cell, which leads to dilution of the solute concentration. A large increase in groundwater velocity is noted already in the calculation layer just above the source (results not shown).

The accumulated mass balance of the saturated zone in the S_{UZ} simulation with non-sorbing solute showed that the total mass entering the saturated zone was much smaller than in the S_{SZ} case and that almost all solute was transported through the saturated zone during the 200-year simulation period. Specifically, the total mass injected in the S_{UZ} simulation was 141 kg, of which only 1.5% was left in the saturated zone at the end of the simulation period. About 98% of the injected mass (138 kg) went to the unsaturated zone, which implies that other sinks, in this case different types of surface waters, received approximately 0.5% of the total mass.

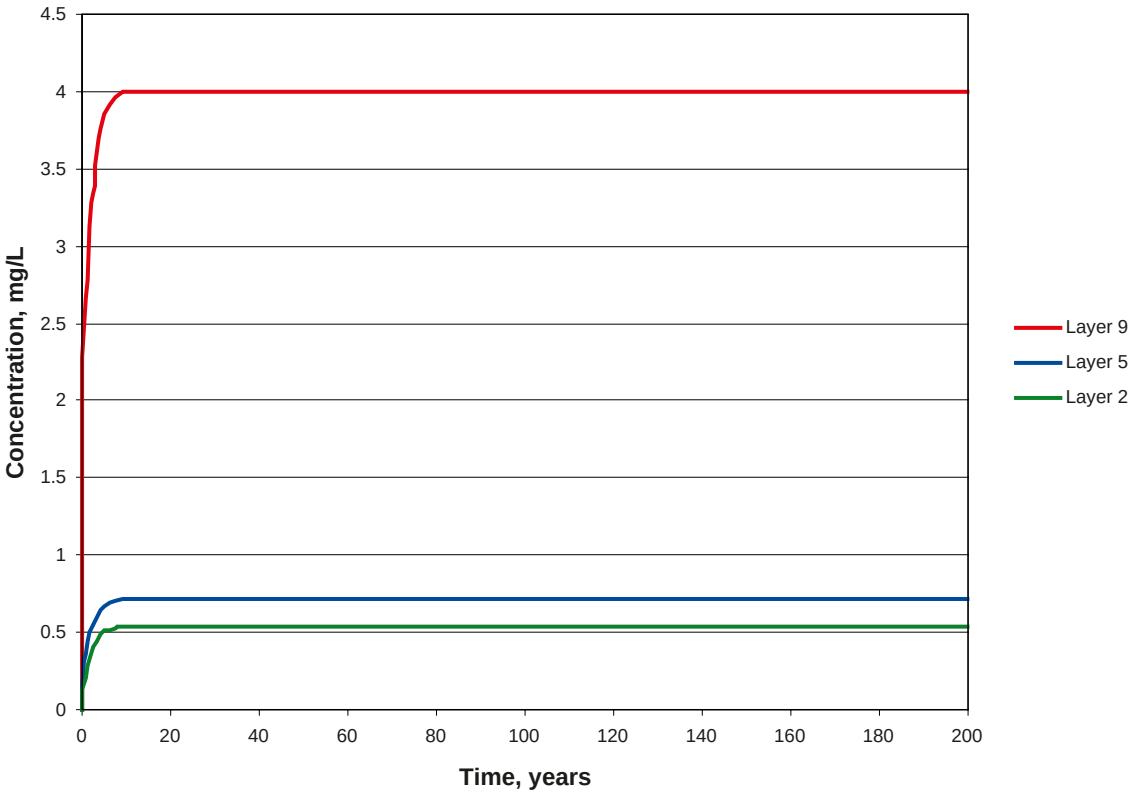

Figure 5-22. *Breakthrough curves in calculation layers 2, 5 and 9 (concentrations in mgL^{-1}) in a vertical column above the source cell, case S_{UZ} NS (non-sorbing solute); the source is in layer 12.*

Sorbing solute

Since vertical solute transport was relatively fast in the S_{UZ} case, the maximum concentrations reached in layers 2, 5 and 9 after 200 years were in all sorption cases equal to the stable concentrations corresponding to the constant-concentration source. Thus, the maximum concentrations were not influenced by the sorption parameters applied in the simulations. The calculated maximum concentrations in the source cell column are summarised in Table 5-11. The differences between the sorption cases are very small, and could most likely be attributed to minor numerical errors.

Similar to the evaluation of the S_{SZ} results (see Figure 5-18 and 5-19), the temporal variations in the various S_{UZ} mass balance components have been quantified and expressed in terms of mass fluxes. The results are shown in Figure 5-23 (case WS) and Figure 5-24 (case SS). As explained above, the results for the dissolved and sorbed mass components are the net changes in storage, i.e. the differences between inflow and outflow to/from the saturated zone and the net exchanges between the dissolved and sorbed phases. Due to the lower flow rate in the S_{UZ} source cell, the solute input flux is much smaller than in the S_{SZ} simulation, i.e. less than 0.7 kg year^{-1} compared with c. 27 kg year^{-1}.

Table 5-11. Maximum concentrations (mg L^{-1}) after 200 years in layers 2, 5 and 9 for source S_{UZ} in the three sorption cases NS, WS and SS (no sorption, weak and strong sorption, respectively).

	Case NS	Case WS	Case SS
Layer 2	0.53	0.53	0.55
Layer 5	0.70	0.70	0.70
Layer 9	4.00	4.00	4.02

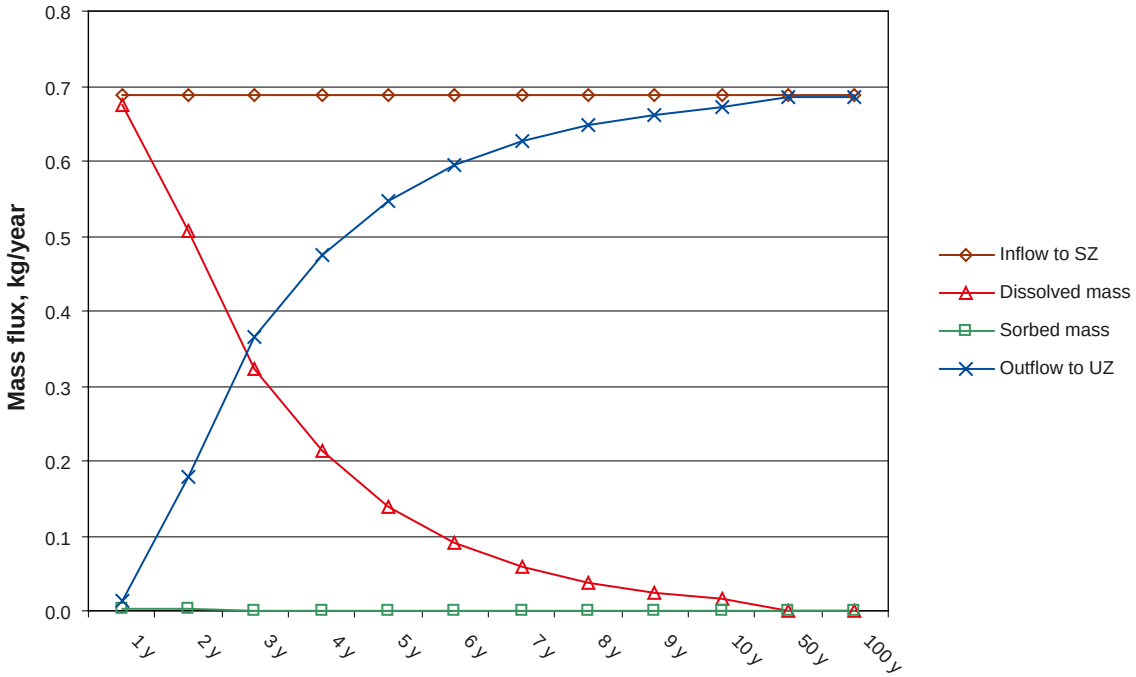

Figure 5-23. *Calculated mass fluxes from the source to the saturated zone (SZ) and from the saturated to the unsaturated zone (UZ), and changes in dissolved and sorbed mass in SZ (kg year^{-1}), S_{UZ} WS case. Note that the first ten years are shown in more detail than the rest of the simulation period.*

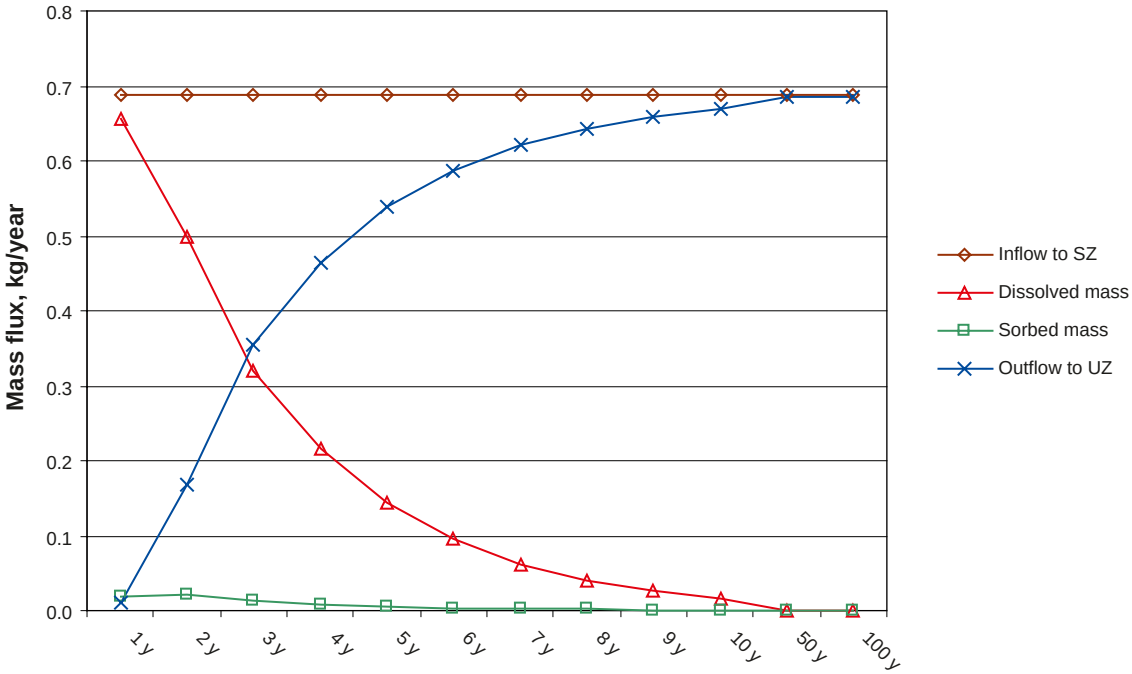

Figure 5-24. *Calculated mass fluxes from the source to the saturated zone (SZ) and from the saturated to the unsaturated zone (UZ), and changes in dissolved and sorbed mass in SZ (kg year^{-1}), S_{UZ} SS case. Note that the first ten years are shown in more detail than the rest of the simulation period.*

Since the S_{UZ} solute transport through the saturated zone was considerably faster than that in the S_{SZ} source case, the "SZ to UZ" term, quantifying the outflow from the saturated zone at its upper boundary, was non-zero already during the first year of the simulation. This means that there were flow paths with groundwater velocities large enough for the solutes to travel through the saturated zone in less than one year. As shown in Figure 5-23 and 5-24, the outflow then increased with time to become equal to the source input after about 50 years. During the rest of the simulation, the outflow was equal to the inflow from the source, and hence the amounts of dissolved and sorbed mass in the saturated zone were constant (i.e. zero net fluxes).

In both of the sorption cases studied, the net increase in solute mass in the saturated zone was almost equal to the inflow from the source during the first year. Consistent with the early solute breakthrough at the upper boundary, the mass change decreased quickly such that it after five years was only about 1/5 of the initial (first year) value. It can be noted that the S_{UZ} changes in dissolved mass within and outflow from the saturated zone were continuous decreases and increases, respectively, which indicates a smaller variability in transport properties than in the sub-volume where the S_{SZ} transport took place.

Another obvious difference between the results for the S_{SZ} and S_{UZ} source locations was the much smaller effects of sorption in the latter case. For the weakly sorbing solute (WS case, Figure 5-23) the net fluxes associated with the sorbed component were practically zero during the whole simulation, whereas somewhat larger fluxes, but still very small compared to the anticipated retardation factor, were observed for the strongly sorbing solute (SS case, Figure 5-24). As shown in the figures, the fact that only relatively small effects of sorption were observed in both cases implies that the WS and SS results are quite similar. Thus, solute retardation had no major impact on the breakthrough in the unsaturated zone or the associated change in dissolved mass in the saturated zone.

The reason for the insignificant role of sorption in the transport from the S_{UZ} source is that the porosity along the flow paths from this source was much larger than in the S_{SZ} simulation; as described in Section 5.2.1, a large porosity corresponds to a small retardation factor. In the present modelling, which is based with constant values of the "$K_d \cdot \rho$ parameter group" in

the rock and in the QD (i.e. one value for each sub-system), spatial variability in the local retardation factor is directly related to variations in the porosity. The results show that such porosity variations may cause large differences in the effects of sorption on solute transport. Finally, it can be noted that a closer inspection of the results for the sorbed phase shows that the changes in sorbed mass during the first years indeed are ten times larger in the SS case than in the WS case (i.e. proportional to the K_d-values).

5.3 Summary of solute transport results

The transport modelling presented in this chapter included particle tracking (PT) and advection-dispersion (AD) simulations. In particular, the modelling was focused on solute transport from sources at depth, i.e. from a hypothetical solute release in a nuclear waste repository in the deep rock. All simulations were performed with solute injections at 135 m below sea level, i.e. at a depth well below the thickest QD in the area but also some distance above repository depth. The main objectives of the transport modelling were to develop and illustrate model capabilities, and to provide the SR-Can safety assessment with supporting modelling results.

PT simulations were performed for two different source configurations, i.e. a uniform injection below the whole model area on land and an injection along flow paths calculated in the deep rock hydrogeology modelling. In the second case, PT calculations were performed for both transient and stationary flow fields. The results included exit points and travel times of the injected particles; in particular, the evaluation of the PT results focused on where (to which hydrological objects or boundaries) the particles went from the saturated zone (particles were tracked in the saturated zone only).

The results of the uniform injection below the on-shore part of the model area showed that most particles had their exit points within the surface water catchment below which they were injected. This indicated that the horizontal transport distances were relatively small. However, a non-negligible fraction of the particles (c. 22%) went from below land to discharge into the sea. The intake channel for water to the nuclear power plant received the largest fraction of the particles that went to the sea. Almost 50% of the particles injected below land areas with direct runoff to the sea were “lost” to other parts of the model volume; most of these particles went to the adjacent sea basins. Most of the other catchments gained or lost about 10% of the particles injected below them.

Also in the second type of PT simulation, where particles were injected along flow paths from the deep rock, particles appeared to be transported more or less vertically in the upper rock and the QD. The flow paths used to identify starting positions for the near-surface PT simulations were calculated in connection with the SR-Can safety assessment, using canister positions within the planned repository as injection points for particles in similar model calculations with a large-scale groundwater flow model /Hartley et al. 2006/.

Since most of the starting positions at 135 m below sea level extracted from the deep rock modelling results were located below the sea, the majority of the particles injected there in the near-surface model discharged into the sea. No major differences were observed when comparing the exit points calculated in the near-surface modelling with those obtained from the deep rock model (i.e. based on flow paths going all the way up to the ground surface or sea bottom in that model too). The differences between results of PT calculations in stationary and transient flow fields, comparing a constant upper boundary condition with daily variations during the single year providing the meteorological input, were also found to be small.

AD simulations were performed for two different point source locations, one from which the PT calculation generated particles to the sea (source S_{SZ}) and the other with a PT exit point in the unsaturated zone (source S_{UZ}). In both cases, a continuous, constant-concentration source was considered. The AD results emphasise the importance of the parameters describing the physical properties in the different calculation layers. Variability in porosity and hydraulic conductivity

along and among the flow paths resulted in significant differences in the spreading patterns of the solutes. These differences concerned both the advective transport and dilution, and the solute retardation associated with sorption.

Specifically, the two source locations differed in terms of the flow velocities in the source cells, implying a much larger injected mass flux in the S_{SZ} source, and those in the cells adjacent to the sources, causing the maximum concentrations in the calculation layers above the sources to be reached much more quickly in the S_{UZ} source case. Furthermore, the effects of sorption on solute transport were much larger in the S_{SZ} source case than for the S_{UZ} source. This difference was caused by the use of constant "sorption parameter groups" for the rock and the QD in combination with spatially variable porosities in each medium. With this parameterisation, solute retardation varied with the porosity, and the retardation was much smaller for the relatively large porosities of the cells in the vicinity of the S_{UZ} source.

Both the PT and the AD results clearly illustrate the importance of a proper selection of source locations (i.e. locations of individual sources or patterns of multiple sources) for the results to be representative of the transport problem studied in the modelling. If other processes than advection are to be studied, e.g. sorption as in the AD simulations presented in this report, all parameters contributing to the effect of the process should be assessed. If the modelling is performed mainly for illustrative purposes, it is probably better to adjust the parameterisation to comply with simple concepts such as constant retardation factors.

Finally, it should be emphasised that the observations summarised above should not be interpreted as final conclusions regarding, for instance, the need for a detailed representation of the surface system (cf. the comparison between near-surface and deep rock model exit points) or modelling of transient conditions (cf. the comparison between transport under stationary and daily to seasonally variable flow conditions). Further model development, including updates of the various parameters describing flow and transport properties, comparisons between calculations and data from field measurements, and more extensive numerical modelling, are required before decisive conclusions can be formulated.

6 Discussion and conclusions

This report presents modelling of surface hydrology and near-surface hydrogeology under undisturbed and open repository conditions, as well as modelling of solute transport from hypothetical sources in the deep rock. The parameterised site model describing the meteorological and hydrogeological boundary conditions and the parameters quantifying the hydrological-hydrogeological properties of vegetation, Quaternary deposits, rock and the surface water system is the common basis for these modelling activities. In this chapter, we first discuss the uncertainties associated with this basic model, and then present the overall conclusions of the work.

6.1 Description of uncertainties

The present MIKE SHE simulations of the Forsmark area are based on limited site data on the geological and hydrogeological properties of the modelled system. The dataset is that provided in the Forsmark 1.2 data freeze (July, 2004). Specifically, a simplified stratigraphic model of the Quaternary deposits is used, and the available hydraulic dataset does not include site-specific parameters for all materials represented in the flow model. Furthermore, no calibration or other comparison between simulation results and data from field measurements has been performed as a part of the modelling activities presented here.

It follows that there are a number of uncertainties associated with the application of the simulation results for describing the present surface hydrological and near-surface hydrogeological conditions within the Forsmark area, the effects of an open repository, and the transport of solutes from depth. The main uncertainties can be summarised as follows:

- Uncertainties in input data and models from other disciplines:
  - The topographical description (the DEM).
  - The geological descriptions of bedrock and Quaternary deposits (horizontal distributions and stratigraphical conditions).
  - The vegetation map.
- Uncertainties in the classification and parameterisation of different types of vegetation for use in the modelling of evapotranspiration and unsaturated flow.
- Uncertainties in the hydraulic parameters for saturated flow in Quaternary deposits and fractured rock, and in the parameters for unsaturated flow.
- Uncertainties in the delineation of catchment boundaries (the boundaries of the model) and in the description of the water courses (positions and cross-sections).
- Uncertainties related to simplifications in process models in MIKE SHE, primarily in the modelling of unsaturated flow and soil freezing/thawing.

In addition to these uncertainties related to the basic flow model, there are uncertainties related to the specific open repository and solute transport applications. The main uncertainty in connection with the open repository modelling is related to the implementation of the tunnel and the shafts in the flow model. In the transport calculations, the main uncertainties are related to transport-specific parameters such as the effective porosity, on which no site-specific information is available, and the retention parameters. Concerning retention, there are also more basic conceptual and model uncertainties, i.e. uncertainties regarding which processes to include and how to describe them in a model.

Generally, the uncertainties associated with the limited application of site data in the flow modelling are judged most important at the present stage of model development. The reasons

for these uncertainties are related both to the limited availability of site data and to limitations in the analyses performed. The present data gaps concern both basic properties of the system (e.g. hydrogeological parameters of some QD) and data needed to test the model performance (e.g. measured flow rates). Only very limited time series data that could be used for model calibration were available at the time for the Forsmark 1.2 data freeze. Longer time series will be available for the development of future model versions.

The sensitivity analysis presented in this report gives some suggestions on which parameters to vary when testing and improving the flow model. However, a more extensive sensitivity analysis is required to get the full picture of which parameters are important for model performance. For example, the sensitivities to the vegetation-related parameters used in the modelling of evapotranspiration should be further investigated. In addition, the use of water level and discharge data for model calibration should be studied to enable an efficient application of the various time series data in forthcoming model development.

A combined sensitivity analysis and calibration methodology study will be performed before the next modelling stage; the results of that study are expected to provide input on the potential for quantification and reduction of uncertainties. Whether a sufficiently fine grid resolution is used is another important aspect of the modelling that should be considered in this extended sensitivity analysis. The detailed dynamics and spatial variability of the flow cannot be captured in a model with a horizontal resolution of 40 m by 40 m, and the implications of using an enhanced resolution will be addressed. Furthermore, the open repository and solute transport applications most likely require finer grid resolutions, at least in parts of the model volumes, than the model of undisturbed flow.

The coupling of the deep rock and surface/near-surface models is another source of uncertainty. The main questions that could be answered by additional numerical modelling studies involving data exchanges between the models are related to the required depth and the selection of appropriate boundary conditions in rock in the near-surface model, and to the upper boundary condition in the deep rock model. More modelling is required to investigate and, if necessary and possible, reduce these uncertainties. It should also be noted that also the coupling of models probably requires special attention in the open repository and solute transport applications.

6.2 Conclusions

Observations and conclusions related to the specific results of the different modelling tasks considered in this study are presented in the summary sections of each modelling chapter, i.e. Section 3.4 for the modelling of flow under undisturbed conditions, Section 4.4 for the open repository modelling, and Section 5.3 for the solute transport modelling. Therefore, the present section is focused on the overall conclusions of the work, which are summarised as follows:

- An update of the MIKE SHE model of the Forsmark site was performed, such that the resulting updated numerical model consistently uses the Forsmark 1.2 dataset of hydraulic properties of rock and Quaternary deposits; this was not the case with the numerical model in the Forsmark 1.2 site description /Johansson et al. 2005/.
- The fact that the present modelling is based on the version 1.2 dataset (with a data freeze in July, 2004) implies that it does not give a representative picture of the data available when this report is published. Most importantly, much longer time series of data from meteorological, hydrological and hydrogeological measurements, primarily meteorological parameters, water levels and discharges, will be available for the next model version. This is important both for the comparison between model results and field data, and for the direct meteorological input to the model; the modelling discussed herein was performed using local meteorological data for a single year. Also the database of hydrogeological parameters has been improved by additional measurements, although to less extent than the time series dataset.

- In the present work new model applications were considered, as compared to the previous site descriptive modelling of flow under present-day, undisturbed conditions only. These applications included modelling of flow under open repository conditions and solute transport from sources in the deep rock under undisturbed condition. The open repository modelling required further development of the flow code, i.e. an integration of MIKE SHE and the MOUSE code used to model the tunnel. In the transport modelling, existing particle tracking (PT) and advection-dispersion (AD) model components were applied; this was the first time the MIKE SHE AD component was used in the SKB modelling. The application-specific model components appear to work well, but more testing is required of both the tunnel and the transport tools.
- The general impression from the relatively crude evaluations performed so far is that reasonable results were obtained in the flow and transport simulations. However, much more work is required to analyse the agreement, or lack thereof, between model and reality. For obvious reasons, this analysis must be focused on the modelling of present-day flow, whereas the open repository and solute transport models cannot be evaluated by use of presently on-going measurements at the site. Additional sensitivity studies and an efficient calibration methodology are important for improving this aspect of the modelling. Activities intended to provide these inputs have been initiated.
- In the discussion of the main uncertainties associated with the site model constituting the basis for the present modelling, the uncertainties related to the limited use of site data for testing and calibrating the flow model are judged to be the most important ones at the present stage of model development. The main reason for these uncertainties is the limited availability of site data useful for these purposes. As mentioned above, there are on-going activities intended to reduce these uncertainties in future model versions.
- The coupling of deep rock and near-surface models is important for both the flow and the transport modelling. In the present work, the near-surface flow model is coupled to a deep rock groundwater flow model of the site by import of data on rock properties and calculated pressures used to describe the boundary conditions in the rock (i.e. the horizontal bottom boundary and the vertical model boundaries). Furthermore, a coupling of transport models was tested, in which positions of particles calculated with a deep rock model were exported to the near-surface model and there used as starting positions in particle tracking simulations. These developments are promising, and should provide the basis for model integration in the next modelling stage.
- The transport modelling performed as a part of this study, both the particle tracking and the advection-dispersion simulations, were carried out for the saturated (groundwater) zone only. It would be advantageous for future transport analyses if solute transport in the whole integrated subsurface-surface water system could be modelled in the same simulations. Such modelling is already possible in the MIKE SHE advection-dispersion component, whereas some code development is required to enable integrated particle tracking simulations. The possibilities for improving the model capabilities in this direction will be investigated.

7 References

Boresjö Bronge L, Wester K, 2003. Vegetation mapping with satellite data of the Forsmark, Tierp and Oskarshamn regions. SKB P-03-83, Svensk Kärnbränslehantering AB.

Brantberger M, Zetterqvist A, Arnbjerg-Nielsen T, Olsson T, Outters N, Syrjänen P, 2006. Final repository for spent nuclear fuel. Underground design Forsmark, Layout D1. SKB R-06-34, Svensk Kärnbränslehantering AB.

Brydsten L, Strömgren M, 2005. Forsmark site investigation. Measurements of brook gradients and lake thresholds. SKB P-04-141, Svensk Kärnbränslehantering AB.

Brunberg A-K, Carlsson T, Blomqvist P, Brydsten L, Strömgren M, 2004. Forsmark site investigation. Identification of catchments, lake-related drainage parameters and lake habitats. SKB P-04-25, Svensk Kärnbränslehantering AB.

DHI Software, 2004a. MIKE SHE. An integrated hydrological modelling system. User Guide. DHI Water & Environment, Hørsholm, Denmark.

DHI Software, 2004b. MOUSE. User Guide. DHI Water & Environment, Hørsholm, Denmark.

DHI Software, 2005. MIKE SHE Advection-dispersion module. User guide. DHI Water & Environment, Hørsholm, Denmark.

DHI Sverige and VBB VIAK, 1998. Dokumentation av MIKE SHE-modellen för Kristianstadsslätten. Report to Kristianstad municipality. (In Swedish.)

Domenico P A, Schwartz F W, 1998. Physical and chemical hydrogeology (2nd ed.). John Wiley & Sons, Inc. New York, U.S.A.

Follin S, Stigsson M, Svensson U, 2005. Regional hydrogeological simulations for Forsmark – numerical modelling using DarcyTools. Preliminary site description Forsmark area – version 1.2. SKB R-05-60, Svensk Kärnbränslehantering AB.

Gustafsson D, Jansson P-E, Gärdenäs A, Eckersten H, 2006. Simulated carbon and water processes of forest ecosystems in Forsmark and Oskarshamn during a 100-year-period. SKB TR-06-45, Svensk Kärnbränslehantering AB.

Hartley L, Hoch A, Jackson P, Joyce S, McCarthy R, Rodwell W, Swift B, Marsic N, 2006. Groundwater flow and transport modelling during the temperate period for the SR-Can assessment. Forsmark area – version 1.2. SKB R-06-98, Svensk Kärnbränslehantering AB.

Johansson P-O, Werner K, Bosson E, Berglund S, Juston J, 2005. Description of climate, surface hydrology, and near-surface hydrogeology. Preliminary site description Forsmark area – version 1.2. SKB R-05-06, Svensk Kärnbränslehantering AB.

Kellner E, 2003. Wetlands – different types, their properties and functions. SKB TR-04-08, Svensk Kärnbränslehantering AB.

Kristensen K J, Jensen S E, 1975. A model for estimating actual evapotransipration from potential evapotranspiration. Royal Veterinary and Agricultural University, Nordic Hydrology 6, pp. 170–188.

Lindborg T (ed.) 2005. Description of surface systems. Preliminary site description Forsmark area – version 1.2. SKB R-05-03, Svensk Kärnbränslehantering AB.

Rhén I (ed.), Gustafson G, Stanfors R, Wikberg P, 1997. Äspö HRL – Geoscientific evaluation 1997/5. Models based on site characterization 1986–1995. SKB TR-97-06, Svensk Kärnbränslehantering AB.

SKB, 2005. Preliminary site description Forsmark area – version 1.2. SKB R-05-18, Svensk Kärnbränslehantering AB.

Sohlenius G, Hedenström A, Rudmark L, 2004. Forsmark site investigation. Mapping of unconsolidated Quaternary deposits 2002–2003. Map description. SKB R-04-39, Svensk Kärnbränslehantering AB.

Svensson U, Kuylenstierna H-O, Ferry M, 2004. Darcy Tools, Version 2.1. Concepts, methods, equations and demo simulations. SKB R-04-19, Svensk Kärnbränslehantering AB.

Svensson U, 2005. The Forsmark repository. Modelling changes in the flow, pressure and salinity fields, due to a repository for spent nuclear fuel. SKB R-05-57, Svensk Kärnbränslehantering AB.

Vikström M, 2005. Modelling of soil depth and lake sediments. An application of the GeoEditor at the Forsmark site. SKB R-05-07, Svensk Kärnbränslehantering AB.

Werner K, Bosson E, Berglund S, 2005. Description of climate, surface hydrology, and near-surface hydrogeology. Simpevarp 1.2. SKB R-05-04, Svensk Kärnbränslehantering AB.

Appendix 1

Description of shafts

Tables A1-1 through A1-4 summarise the parameters used in each calculation layer in the description of shafts S1–S4 in the MIKE SHE model. The modelling methodology is described in Section 2.1.2 of the report. The parameters and units used in the tables are the following: r (radius of shaft, m), K_h (horizontal hydraulic conductivity of the rock, ms^{-1}), Δx (horizontal grid spacing, m), Δz (height of calculation layer, m), C (conductance, m^2s^{-1}), and $K_{g,s}$ (horizontal hydraulic conductivity of grouted rock, ms^{-1}, defining the different grouting cases considered).

Table A1-1. Geometry and hydraulic parameters for shaft S1.

Calculation layer	r	K_h	Δx	Δz	C, no grouting	C, $K_{g,s}$ = 1E–7	C, $K_{g,s}$ = 1E–9
1	2.75	1.50E–05	40	1	6.48E–06	2.09E–07	2.16E–09
2	2.75	8.30E–06	40	1	3.58E–06	2.04E–07	2.16E–09
3	2.75	1.50E–06	40	1	6.48E–07	1.62E–07	2.15E–09
4	2.75	1.50E–06	40	1	6.48E–07	1.62E–07	2.15E–09
5	2.75	1.05E–06	40	2.72	1.23E–06	3.98E–07	5.84E–09
6	2.75	1.05E–06	40	4.61	2.09E–06	6.74E–07	9.90E–09
7	2.75	1.05E–06	40	6.88	3.12E–06	1.01E–06	1.48E–08
8	2.75	1.05E–06	40	10.2	4.62E–06	1.49E–06	2.19E–08
9	2.75	5.27E–10	40	14.99	3.41E–09	3.41E–09	3.09E–09
10	2.75	5.27E–10	40	21.72	4.94E–09	4.94E–09	4.47E–09
11	2.75	5.27E–10	40	30.97	7.05E–09	7.04E–09	6.37E–09
12	2.75	5.27E–10	40	42.87	9.75E–09	9.74E–09	8.82E–09

Table A1-2. Geometry and hydraulic parameters for shaft S2.

Calculation layer	r	K_h	Δx	Δz	C, no grouting	C, $K_{g,s}$ = 1E–7	C, $K_{g,s}$ = 1E–9
1	1.75	1.50E–05	40	1	4.12E–06	1.33E–07	1.37E–09
2	1.75	5.13E–06	40	1	1.41E–06	1.25E–07	1.37E–09
3	1.75	1.50E–06	40	1	4.12E–07	1.03E–07	1.37E–09
4	1.75	1.50E–06	40	1	4.12E–07	1.03E–07	1.37E–09
5	1.75	1.05E–06	40	1.15	3.32E–07	1.07E–07	1.57E–09
6	1.75	1.05E–06	40	4.61	1.33E–06	4.29E–07	6.30E–09
7	1.75	1.05E–06	40	6.88	1.98E–06	6.40E–07	9.41E–09
8	1.75	1.05E–06	40	10.2	2.94E–06	9.49E–07	1.39E–08
9	1.75	5.27E–10	40	15	2.17E–09	2.17E–09	1.96E–09
10	1.75	5.27E–10	40	21.7	3.14E–09	3.14E–09	2.85E–09
11	1.75	5.27E–10	40	31	4.48E–09	4.48E–09	4.06E–09
12	1.75	5.27E–10	40	42.9	6.21E–09	6.20E–09	5.62E–09

Table A1-3. Geometry and hydraulic parameters for shaft S3.

Calculation layer	r	K_h	∆x	∆z	C, no grouting	C, $K_{g,s}$ = 1E–7	C, $K_{g,s}$ = 1E–9
1	1.25	1.50E–05	40	1	2.94E–06	9.50E–08	9.81E–10
2	1.25	1.09E–05	40	1	2.14E–06	9.38E–08	9.81E–10
3	1.25	1.50E–06	40	1	2.94E–07	7.36E–08	9.78E–10
4	1.25	1.50E–06	40	1	2.94E–07	7.36E–08	9.78E–10
5	1.25	1.05E–06	40	2.37	4.88E–07	1.58E–07	2.31E–09
6	1.25	1.05E–06	40	4.61	9.50E–07	3.06E–07	4.50E–09
7	1.25	1.05E–06	40	6.88	1.42E–06	4.57E–07	6.72E–09
8	1.25	1.05E–06	40	10.2	2.10E–06	6.78E–07	9.96E–09
9	1.25	5.27E–10	40	14.99	1.55E–09	1.55E–09	1.40E–09
10	1.25	5.27E–10	40	21.72	2.25E–09	2.24E–09	2.03E–09
11	1.25	5.27E–10	40	30.97	3.20E–09	3.20E–09	2.90E–09
12	1.25	5.27E–10	40	42.87	4.43E–09	4.43E–09	4.01E–09

Table A1-4. Geometry and hydraulic parameters for shaft S4.

Calculation layer	r	K_h	∆x	∆z	C, no grouting	C, $K_{g,s}$ = 1E–7	C, $K_{g,s}$ = 1E–9
1	2.75	1.50E–05	40	1	6.48E–06	2.09E–07	2.16E–09
2	2.75	7.64E–06	40	1	3.30E–06	2.03E–07	2.16E–09
3	2.75	1.50E–06	40	1	6.48E–07	1.62E–07	2.15E–09
4	2.75	1.50E–06	40	1	6.48E–07	1.62E–07	2.15E–09
5	2.75	1.05E–06	40	1.33	6.03E–07	1.94E–07	2.86E–09
6	2.75	1.05E–06	40	4.61	2.09E–06	6.74E–07	9.90E–09
7	2.75	1.05E–06	40	6.88	3.12E–06	1.01E–06	1.48E–08
8	2.75	1.05E–06	40	10.2	4.62E–06	1.49E–06	2.19E–08
9	2.75	5.27E–10	40	14.99	3.41E–09	3.41E–09	3.09E–09
10	2.75	5.27E–10	40	21.72	4.94E–09	4.94E–09	4.47E–09
11	2.75	5.27E–10	40	30.97	7.05E–09	7.04E–09	6.37E–09
12	2.75	5.27E–10	40	42.87	9.75E–09	9.74E–09	8.82E–09

Appendix 2

Open repository results

Figures A2-1 through A2-11 show calculated head drawdowns in calculation layers 1–11 for boundary case 1 without grouting. Note that the elevations of the bottom boundaries are given in different units; metres below ground surface for layers 1–4, and metres below sea level for layers 5–11.

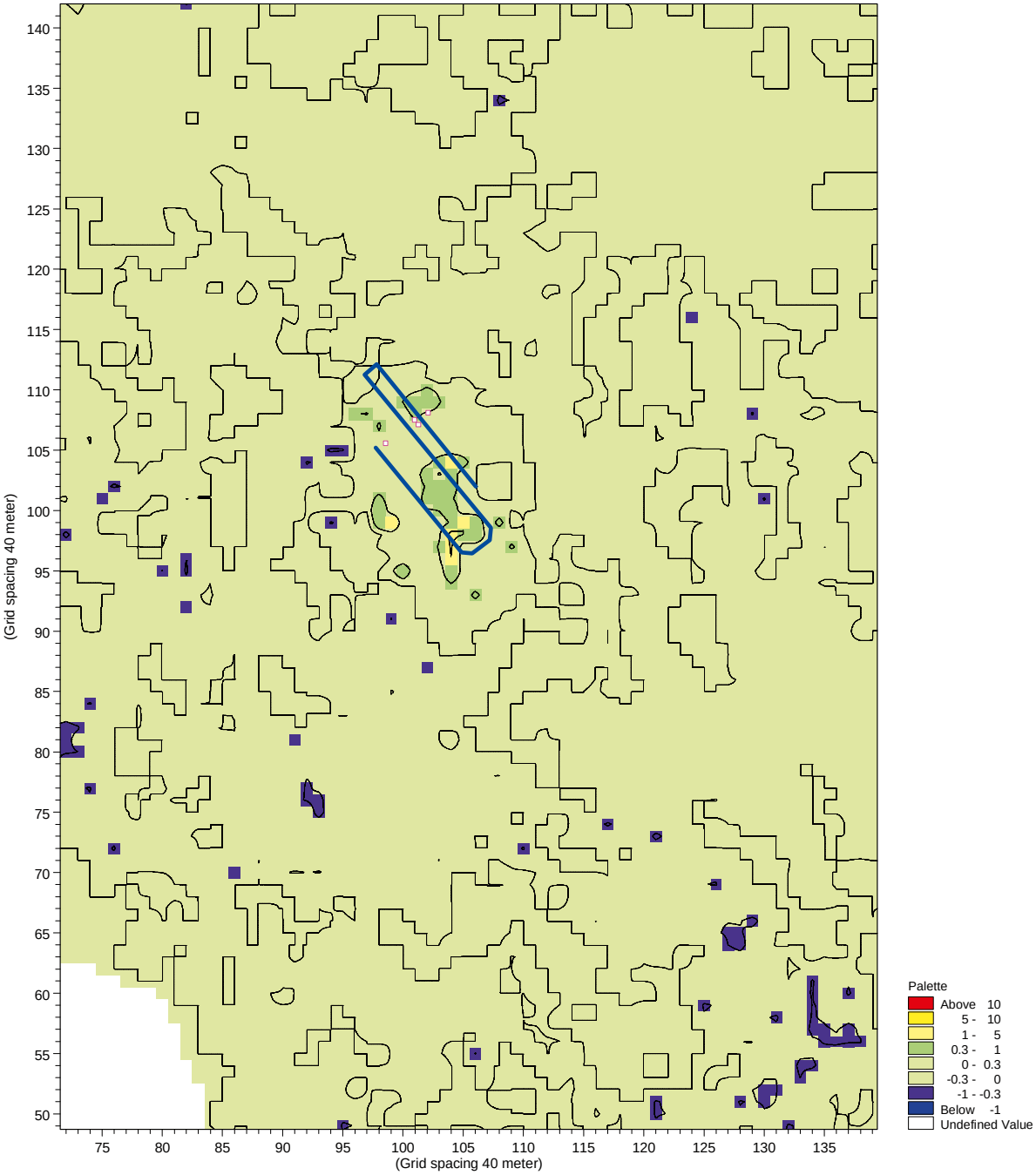

Figure A2-1. *Head drawdown in calculation layer 1 (lower boundary at 1 m below ground surface).*

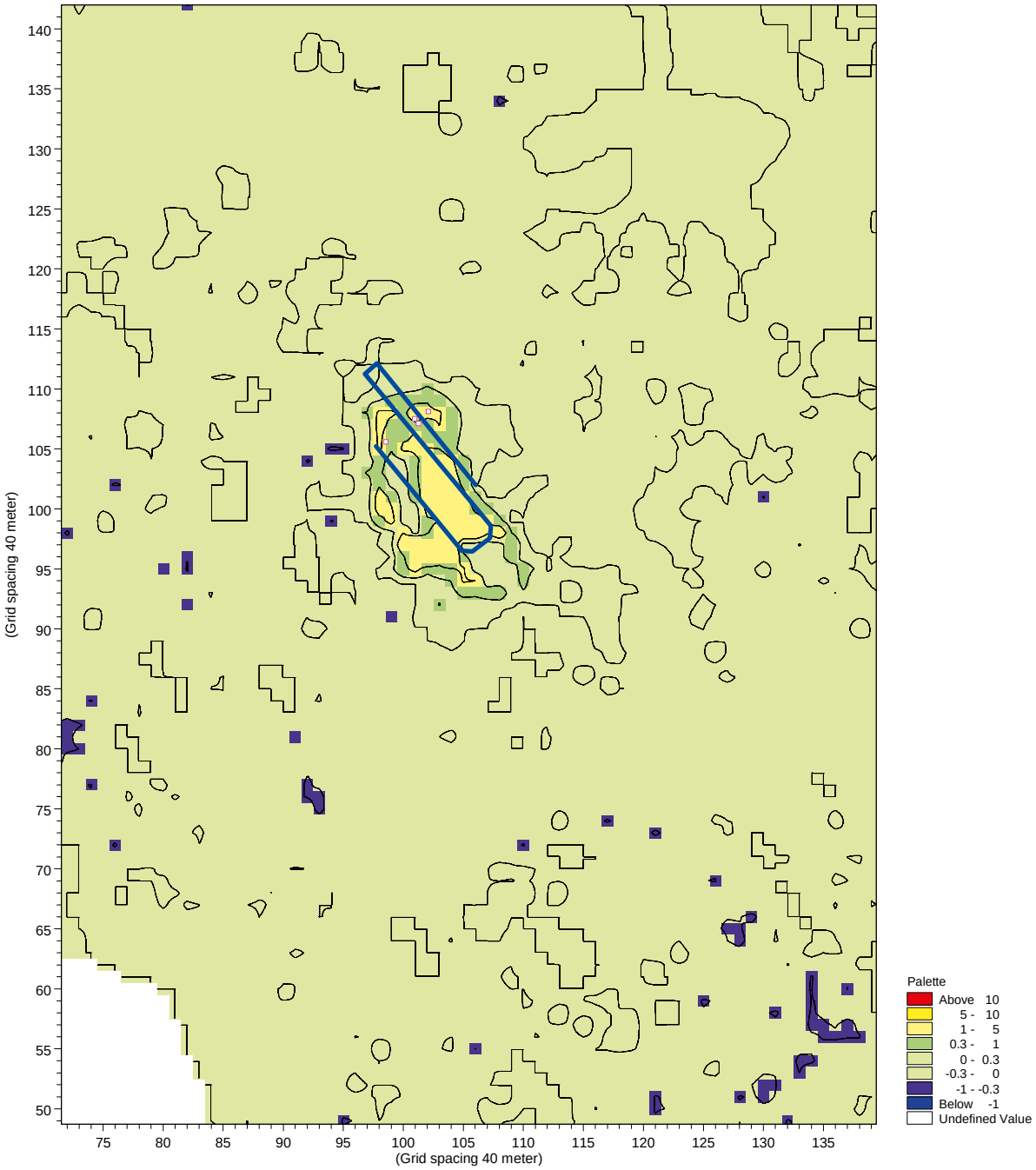

Figure A2-2. *Head drawdown in calculation layer 2 (lower boundary at 2 m below ground surface).*

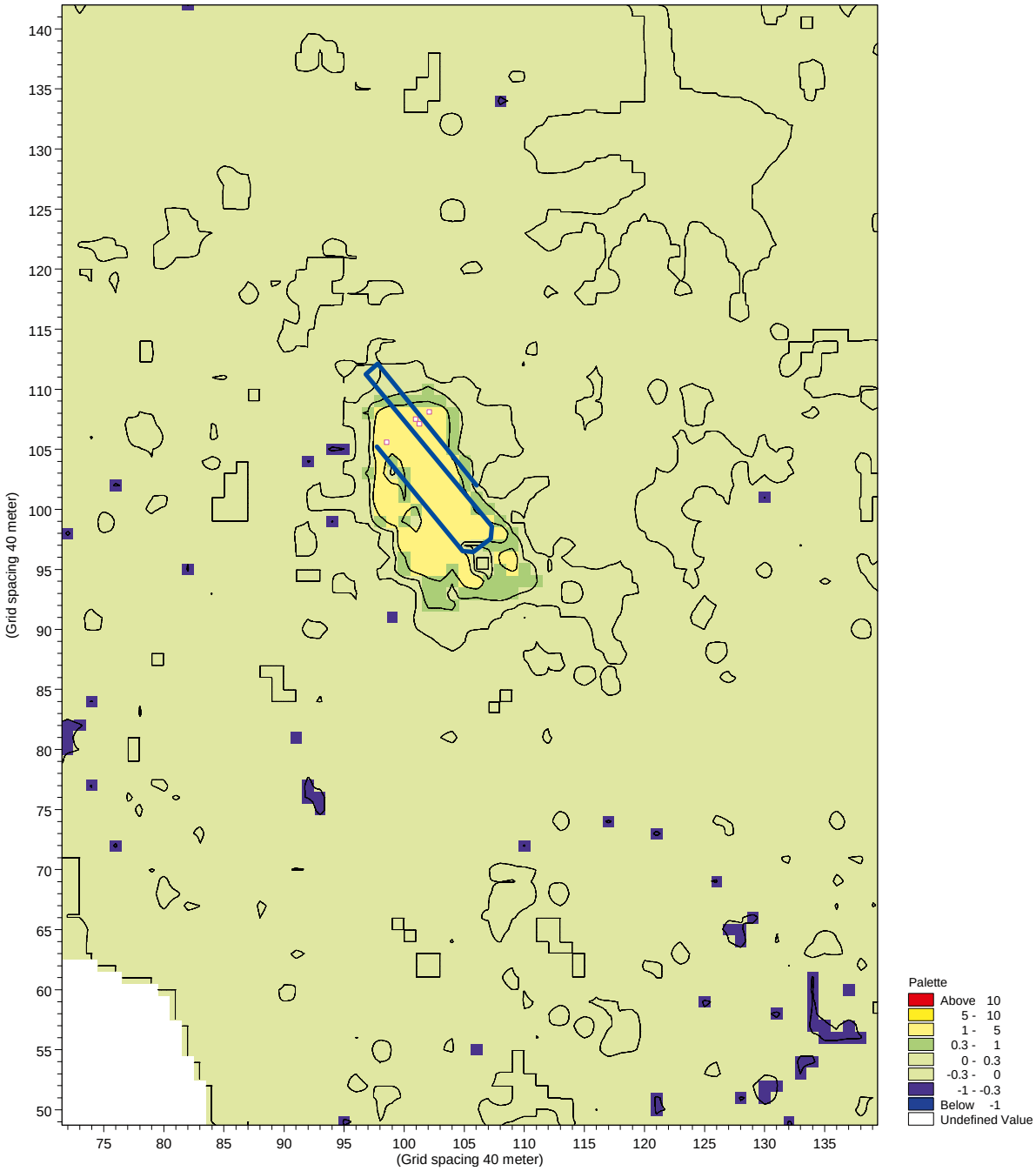

Figure A2-3. *Head drawdown in calculation layer 3 (lower boundary at 3 m below ground surface).*

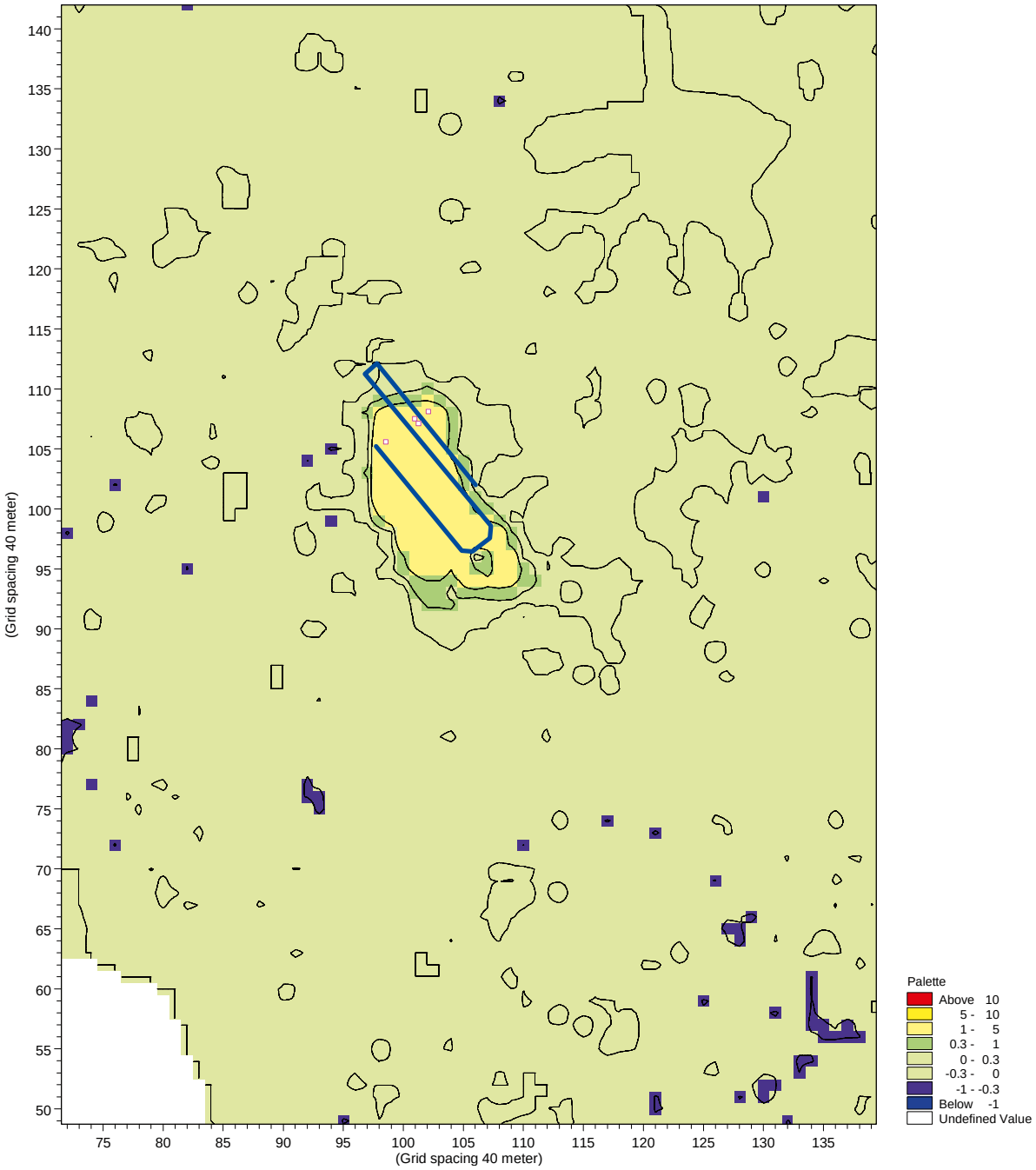

Figure A2-4. *Head drawdown in calculation layer 4 (lower boundary at 4 m below ground surface).*

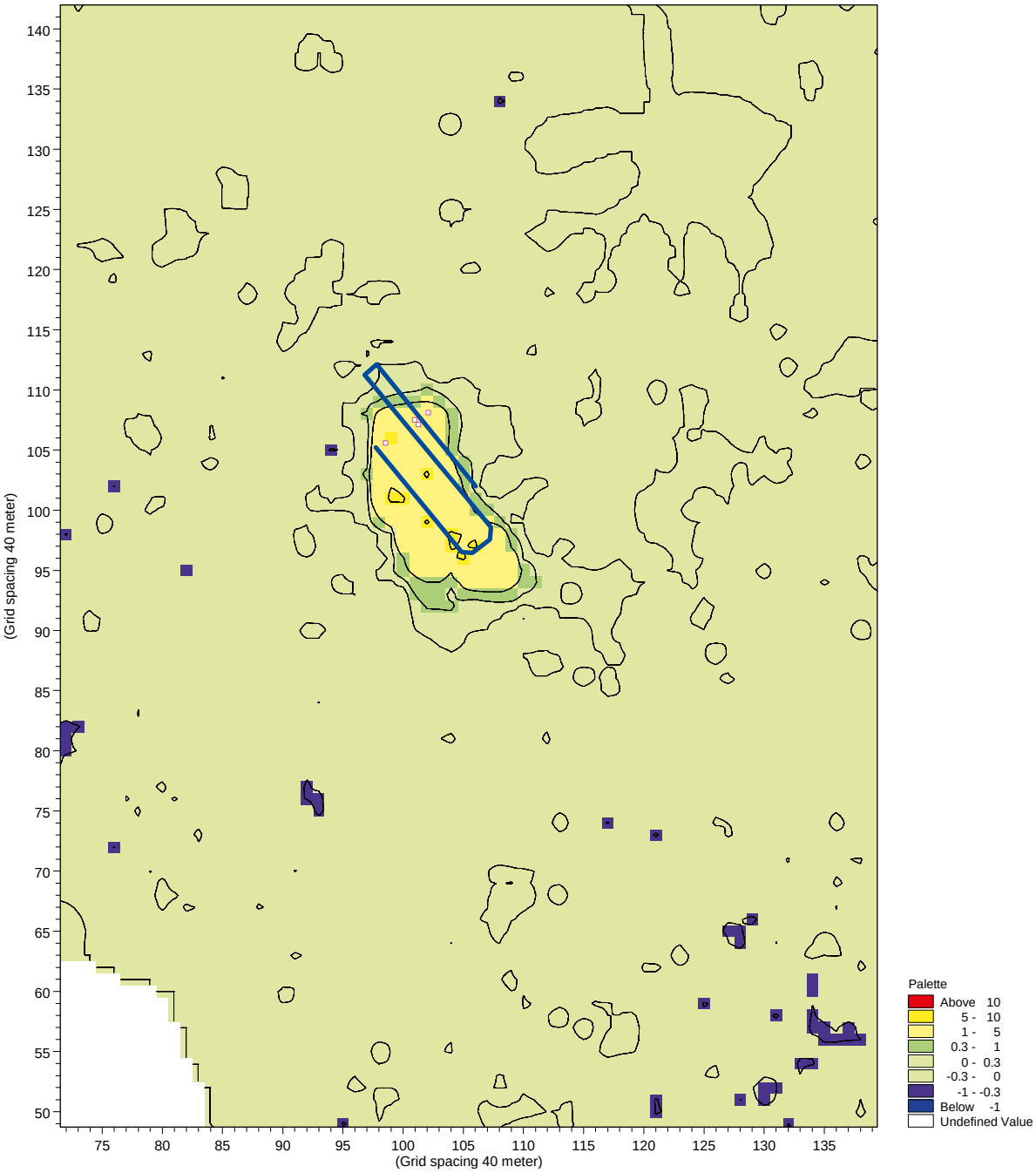

Figure A2-5. *Head drawdown in calculation layer 5 (lower boundary at 2–3 m below sea level).*

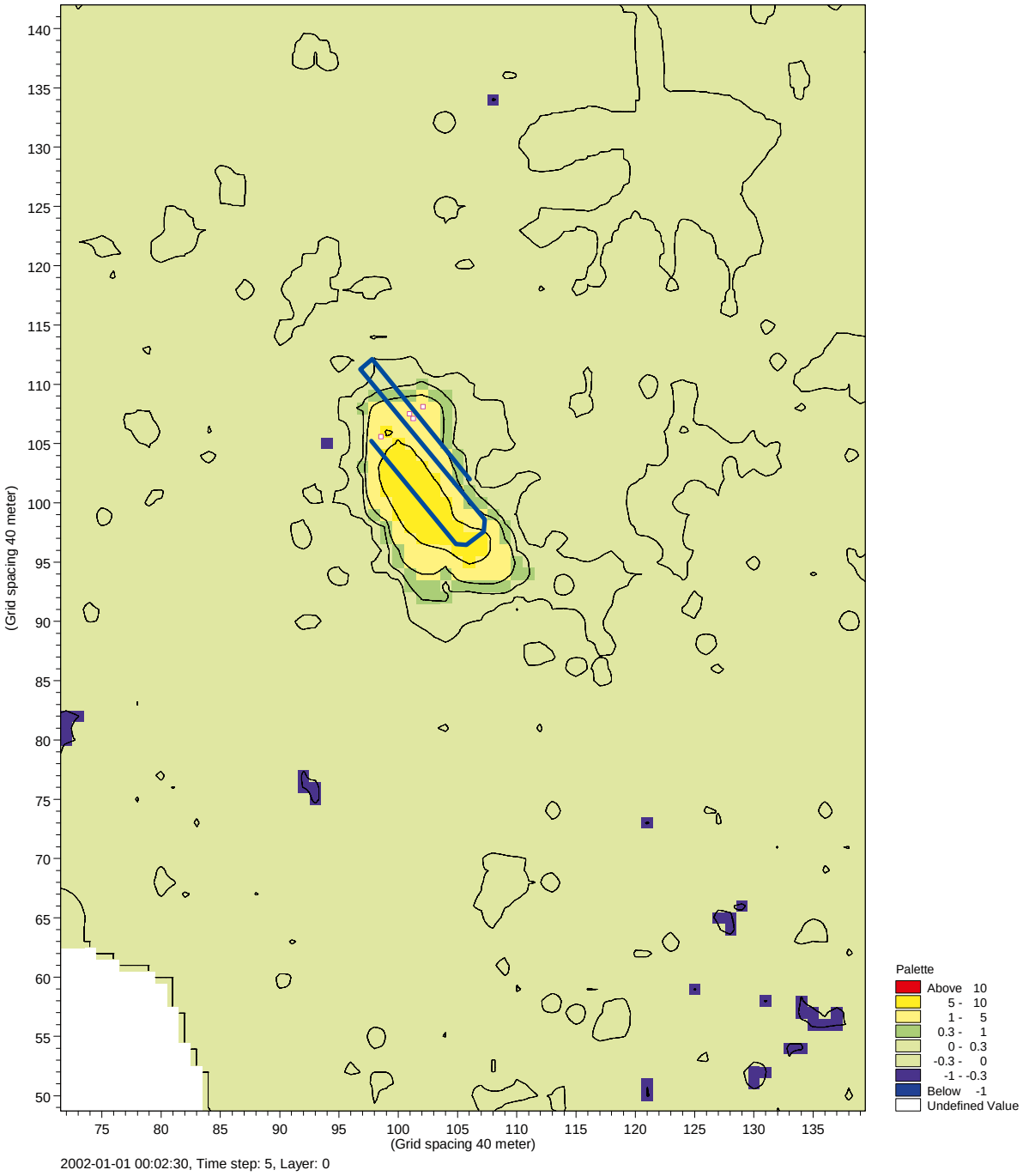

Figure A2-6. *Head drawdown in calculation layer 6 (lower boundary at 5–6 m below sea level).*

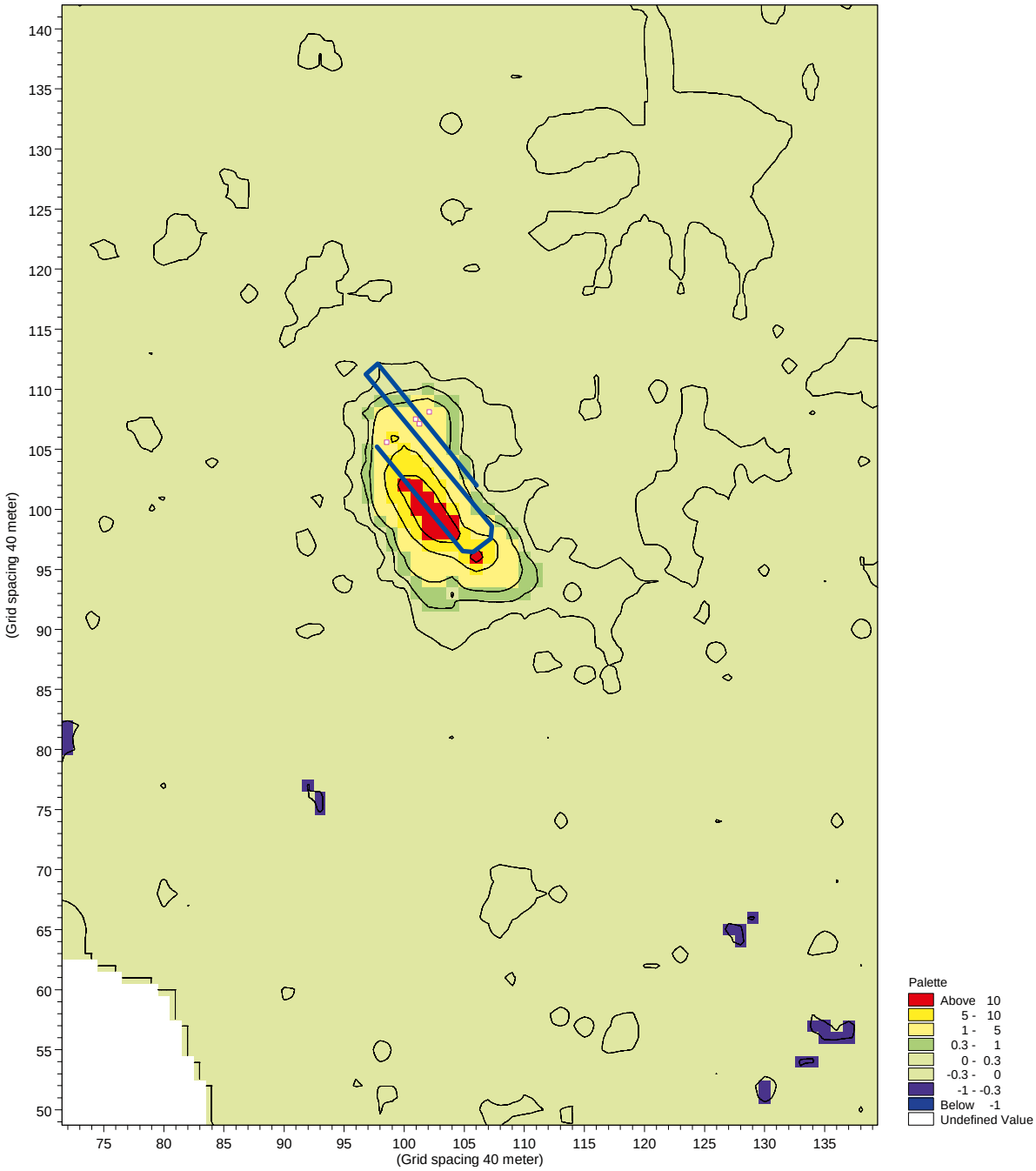

Figure A2-7. *Head drawdown in calculation layer 7 (lower boundary at 13 m below sea level).*

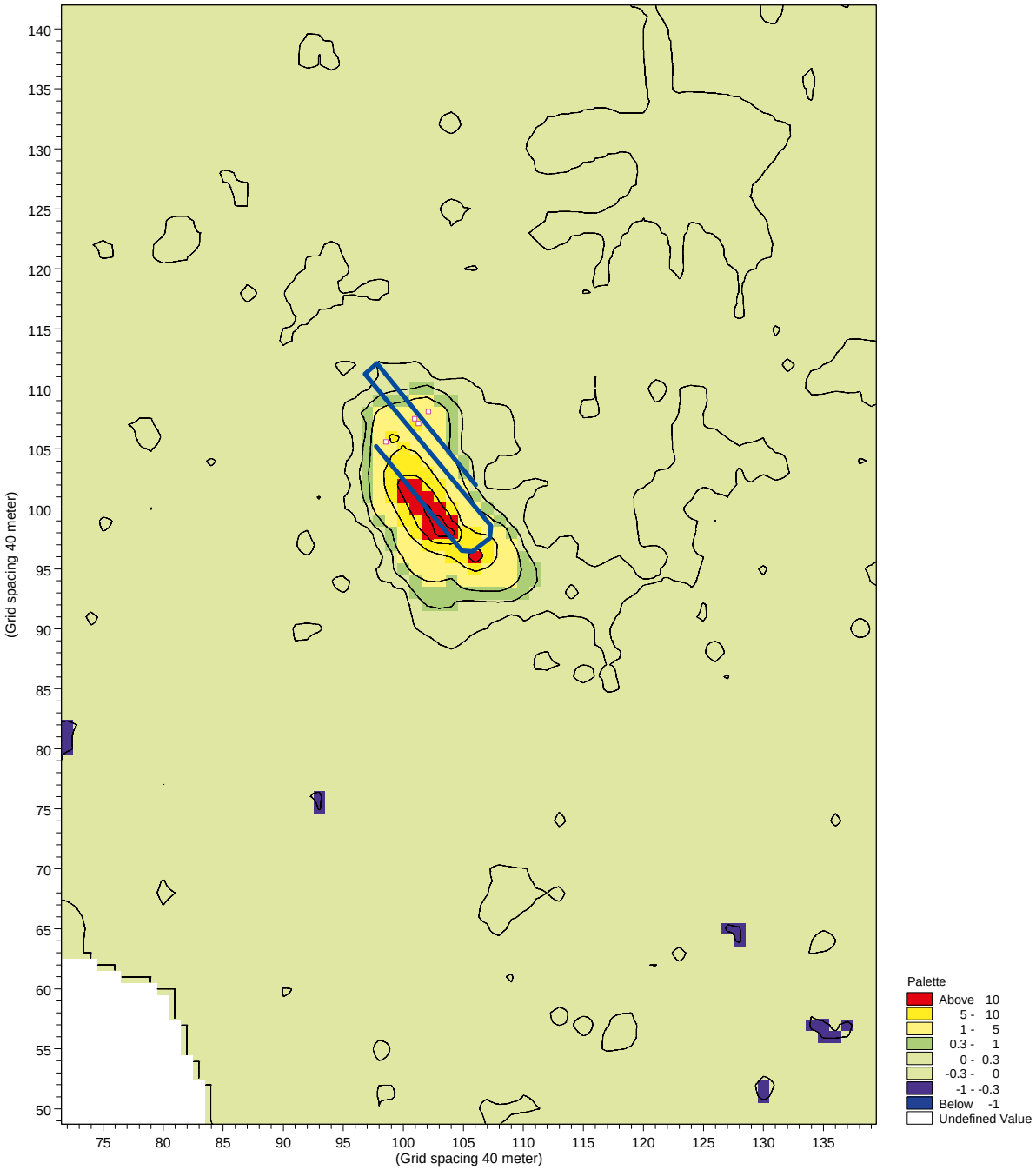

Figure A2-8. *Head drawdown in calculation layer 8 (lower boundary at 23 m below sea level).*

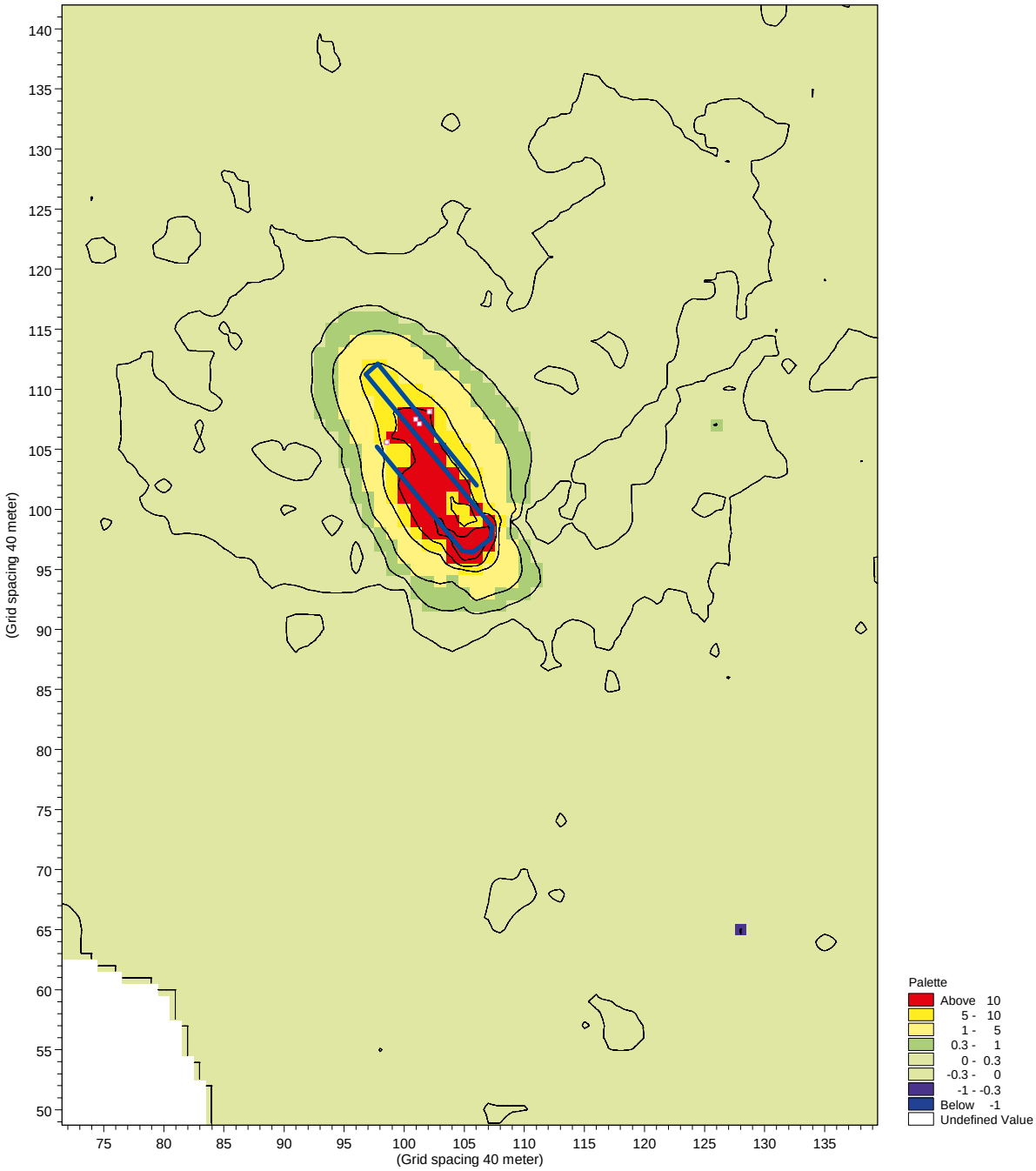

Figure A2-9. *Head drawdown in calculation layer 9 (lower boundary at 38 m below sea level).*

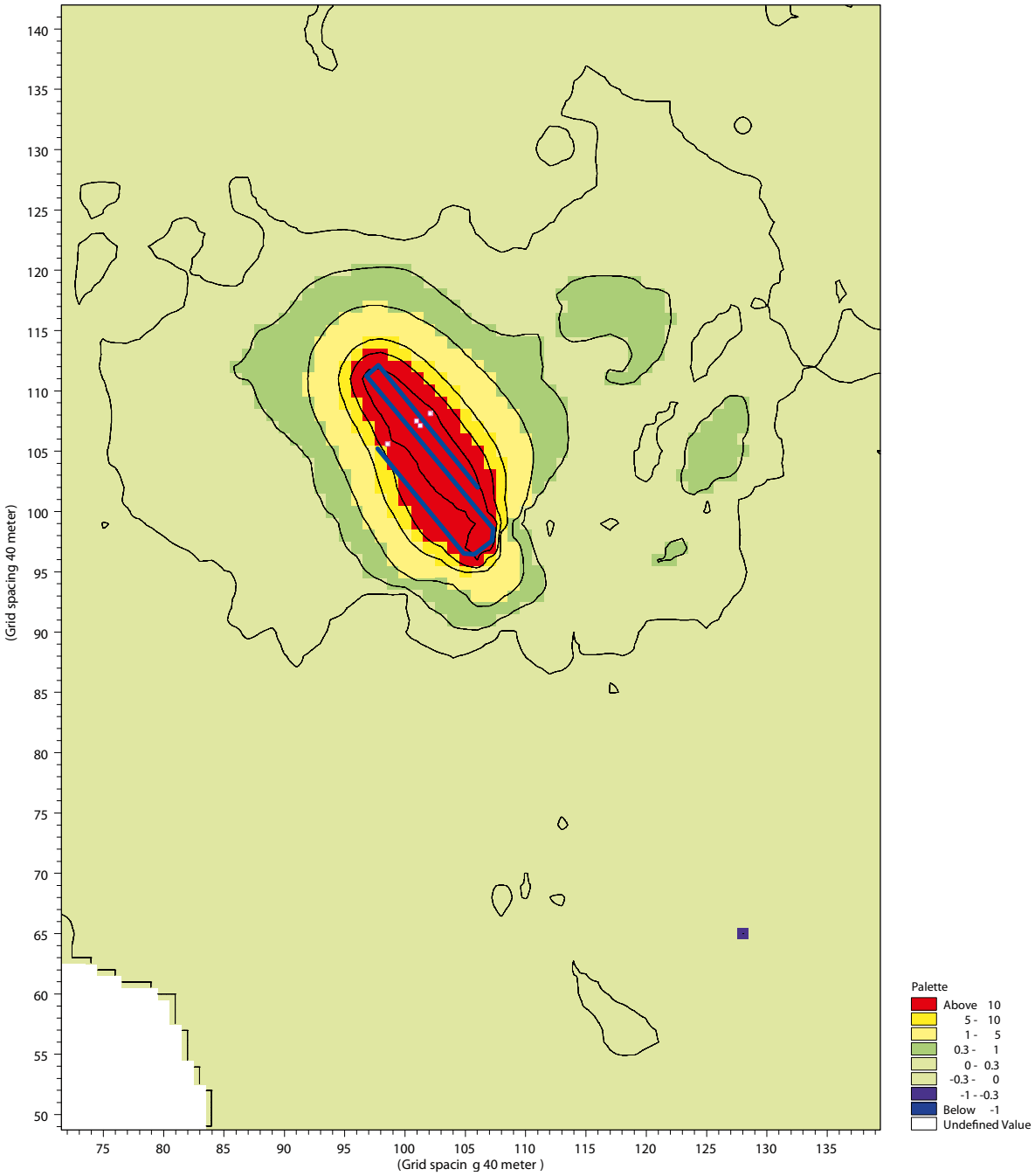

Figure A2-10. *Head drawdown in calculation layer 10 (lower boundary at 60 m below sea level).*

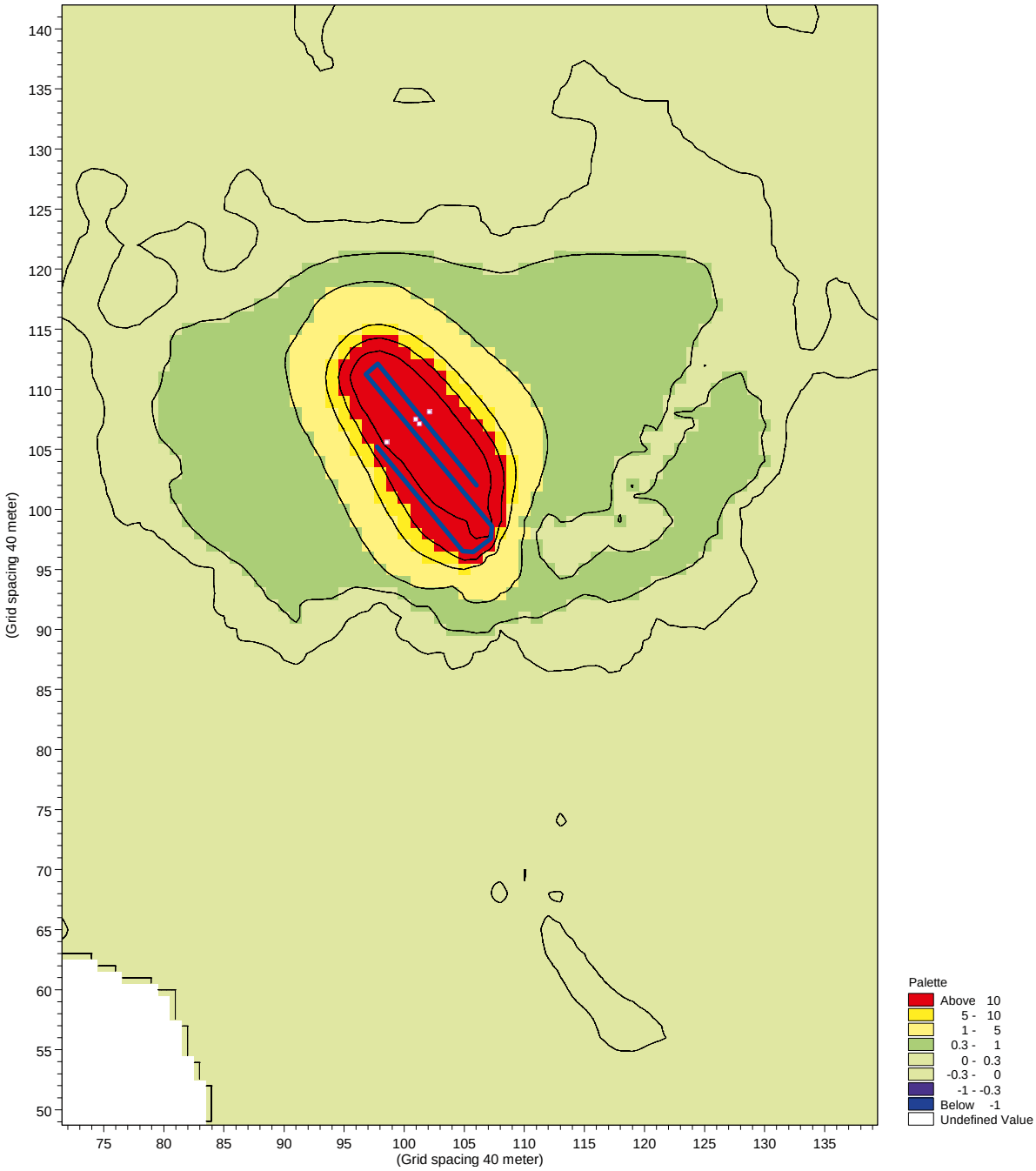

Figure A2-11. *Head drawdown in calculation layer 11 (lower boundary at 90 m below sea level).*